University of São Paulo

School of Pharmaceutical Sciences of Ribeirão Preto

Synthesis, antiurolithic activity, and biotransformation studies of galloylquinic acids from *Copaifera* species by filamentous fungi

Síntese, atividade antiurolítica, e estudos de biotransformação de ácidos galoilquínicos de espécies de *Copaifera* por fungos filamentosos

Mohamed Ahmed Mohamed Hamed Abdelsalam

Ribeirão Preto
2018

UNIVERSITY OF SÃO PAULO

SCHOOL OF PHARMACEUTICAL SCIENCES OF RIBEIRÃO PRETO

Synthesis, antiurolithic activity, and biotransformation studies of galloylquinic acids from *Copaifera* species by filamentous fungi

Síntese, atividade antiurolítica, e estudos de biotransformação de ácidos galoilquínicos de espécies de *Copaifera* por fungos filamentosos

Mohamed Ahmed Mohamed Hamed Abdelsalam

Ribeirão Preto
2018

UNIVERSITY OF SÃO PAULO

SCHOOL OF PHARMACEUTICAL SCIENCES OF RIBEIRÃO PRETO

Synthesis, antiurolithic activity, and biotransformation studies of galloylquinic acids from *Copaifera* species by filamentous fungi

Síntese, atividade antiurolítica, e estudos de biotransformação de ácidos galoilquínicos de espécies de *Copaifera* por fungos filamentosos

PhD Thesis Presented to the Graduate Program of Pharmaceutical Sciences for Obtaining Doctor of Philosophy Degree in Sciences
Area of Specialization: Natural and Synthetic Products
PhD Student: Mohamed Ahmed Mohamed Hamed Abdelsalam
Supervisors: Prof. Jairo Kenupp Bastos
Prof. John Charles Lieske, Department of Internal Medicine, Division of Nephrology and Hypertension, Mayo Clinic School of Medicine, MN, USA

Versão corrigida da Tese de Doutorado o apresentada ao Programa de Pós-Graduação em Ciências Farmacêuticas em 31/08/2018. A versão original encontra-se disponível na Faculdade de Ciências Farmacêuticas de Ribeirão Preto/USP.

Ribeirão Preto
2018

I AUTHORIZE THE REPRODUCTION AND TOTAL OR PARTIAL DISCLOSURE OF THIS WORK, FOR ANY CONVENTIONAL OR ELECTRONIC MEANS, FOR THE PURPOSE OF STUDY AND RESEARCH, SINCE THE SOURCE IS CITED.

Abdelsalam, Mohamed Ahmed Mohamed Hamed
Synthesis, antiurolithic activity, and biotransformation studies of galloylquinic acids from *Copaifera* species by filamentous fungi
Ribeirão Preto, **2018**.
149 p.; 30 cm.

PhD Thesis Presented to the Graduate Program of Pharmaceutical Sciences for Obtaining the Doctor of Philosophy Degree in Sciences
Supervisors: Prof. **Jairo Kenupp Bastos**
Prof. **John Charles Lieske**

1. Urolithiasis. 2. Total synthesis. 3. Galloylquinic acids. 4. Biotransformation. 5. Filamentous fungi

Mohamed Ahmed Mohamed Hamed Abdelsalam
Synthesis, antiurolithic activity, and biotransformation studies of galloylquinic acids from *Copaifera* species by filamentous fungi

PhD Thesis Presented to the Graduate Program of Pharmaceutical Sciences for obtaining Doctor of Philosophy Degree in Sciences
Area of Specialization: Natural and Synthetic Products
PhD Student: Mohamed Ahmed Mohamed Hamed Abdelsalam
Supervisors: Prof. Jairo Kenupp Bastos
Prof. John Charles Lieske, Department of Internal Medicine, Division of Nephrology and Hypertension, Mayo Clinic School of Medicine, MN, USA

Approved in:

Examination Committee

Prof. Dr. _____

Institution: _____ Signature:_____

Prof. Dr. _____

Institution: _____ Signature:_____

Prof. Dr. _____

Institution: _____ Signature:_____

Prof. Dr. _____

Institution: _____ Signature:_____

Prof. Dr. _____

Institution: _____ Signature:_____

Prof. Dr. _____

Institution: _____ Signature:_____

This Work is dedicated to my Beloved Mother Nadia, my two Sisters Heba and El-Shaimaa, and my Father' spirit

Dedication

First of all, I am thankful for the most merciful, omnipresent and omniscient almighty Allah with his help and blessings, making me able to achieve my mission.

I feel great honor to express my sincere gratitude to my PhD supervisor Professor Jairo Kenupp Bastos, for guiding me to the beginning of my research way and the start of my PhD journey. I am extremely thankful to him for accepting me to join his research group and for giving me the opportunity to work inside his laboratory during the period of pursuing my PhD fellowship. I feel extremely fortunate to have such a great Professor from whom I was supported a lot. I have no words to describe this massive support. His kindness always gives me new strength to face the problems of both research and my life. Whatever I need, he used to give me. His impulsive, endlessly cheerful and harmonious encouragement lifts my spirits and raises me to meet the challenges. I wish all Professors to be like him. The work presented here reflects his ingenuity and his consistent reassurance to turn failure into success.

I would like to express my sincere appreciation and thanks to TWAS-CNPq, The Academy of Sciences for the Developing World (TWAS), Italy, and the National Council for Scientific and Technological Development (CNPq), Brazil for awarding me a fully funded PhD Fellowship (190066/2014-8) that supported me during my PhD research work.

I would like to express my gratitude to my co-supervisor Prof. John Charles Lieske for his help, support and accepting me to join his lab as a visiting pre-doctoral fellow at the Department of Internal Medicine, Division of Nephrology and Hypertension, Mayo Clinic College of Medicine, Rochester, Minnesota, United States, during which I got the opportunity to acquire new biological skills.

I would like to thank Prof. Michael Romero for his supportive help with the biological experiment using Drosophila model, inside his ion transport lab at the Department of Physiology and Biomedical Engineering, Mayo Clinic College of Medicine, Rochester, Minnesota, United States. I would like to thank Prof. Niege AJC Furtado for allowing me to perform the biotransformation experiments in her microbiology lab. I would like to thank Prof. Paulo Donate for his guidance to perform the chemistry part in his lab and Daniel Previdi for his kind help. I would like to thank Prof. Antonio E. M. Crotti and Prof. Giuliano Cesar Clososki for their helpful pieces of advice.

I also would like to thank all my Professors, friends and lab-colleagues in Brazil and United States. I would like to thank Mariza, Jennifer, Victor, Carol, Ingrid, Debora, Federico, Domingos, Wesley, Simone, Marcela, Juliana, Sara, Fabio Tsuzuki, Thiago, Osman, Jacob Anderson, Amr, Kevin, Andrea, Jing Jing, Zejfa, Angelica, Mario, Pilar and Jonas.

The non-lasting prayers of my beloved mother (Nadia), my sisters (Heba and El-Shaimaa) and all my family members are the beacon of life. I have no words to acknowledge their contributions in my life, especially full support during the whole period of my academic way. I pay my respect to my family for their trust, love, insight, compassion, and prayers. I am fortunate enough to have the wonderful mother and my two sisters to share and feel what I have never courage to express to others or to face alone.

Mohamed

Acknowledgment

Italy

Ph.D. Fellowship
(190066/2014-8)

Brazil

(Grant No. 2011/13630-7)

FCFRP, USP

MN, USA

VGP
(P-3-04976)

Mayo Clinic O'Brien
Urology Research Center
(NIH DK100227)

France

Egypt

Summary

SUMMARY

Abdelsalam, Mohamed A. M. H. Synthesis, antiurolithic activity, and biotransformation studies of galloylquinic acids from *Copaifera* species by filamentous fungi. 2018. PhD Thesis. School of Pharmaceutical Sciences of Ribeirão Preto – University of Sao Paulo, Ribeirão Preto, 2018.

Renal stone disease, also known as urolithiasis, is common with a recent overall estimated prevalence rate of 14.8% that appears to be rising, with a five-year recurrence rate of up to 50%. The promising diverse bioactivities of plant extracts rich in galloylquinic acids such as *Copaifera* species leaves prompted our interest to synthesize the tri-substituted 3,4,5-tri-*O*-galloylquinic acid methyl ester (TGAME), with the goal of developing a lead compound for kidney stone prevention. The total synthesis included six steps starting from commercially available quinic and gallic acids. The key step in the synthetic pathway was through Steglich esterification of methyl quinate with 3,4,5-tribenzyloxybenzoic acid using dicyclohexylcarbodiimide and N,N-(dimethylamino) pyridine as the coupling reagents. The chemical structures of the final compound and its synthetic intermediates were elucidated by spectroscopic, spectrometric and spectrophotometric methods of analyses. The potential effect of the compound on calcium oxalate monohydrate (COM) crystal binding to the surface of Madin-Darby Canine Kidney Cells type I (MDCKI) and crystal growth in a *Drosophila melanogaster* Malpighian tubule model were investigated. Membrane, cytosolic and total Annexin A1 (ANXA1), A-enolase and HSP90 amounts were examined by Western blot analysis after subcellular fractionation, then confirmed by immunofluorescence staining of cultured cells. Pretreatment of MDCKI cells with TGAME for up to 6 h significantly diminished COM crystal-binding in a concentration-dependent manner. TGAME (50 μM) significantly inhibited ANXA1 surface expression as evident by immunofluorescence microscopy, whereas intracellular ANXA1 increased. Western blot analysis confirmed ANXA1 expression changes in the membrane and cytosolic fractions of compound-treated cells, whereas the whole cell ANXA1 remained unchanged. TGAME also significantly decreased the size, number, and growth of COM crystals induced in a *Drosophila melanogaster* Malpighian tubule model, and possessed a potent antioxidant activity in a DPPH assay. We also have performed a biotransformation study of galloylquinic acid compounds using filamentous fungi to predict their pharmacokinetic behaviors. The results showed that galloylquinic acids from *Copaifera lucens* leaves (*n*-butanolic fraction, BF) were transformed by *Aspergillus alliaceus* into one major metabolite 3-*O*-methyl gallic acid (M1), which is one of the known metabolites of gallic

acid studied in humans. The biotransformed product was identified by UPLC-DAD-MS/MS and ^{1}H NMR. Pretreatment of MDCKI cells with BF (50 μg/mL) and its transformed product M1 (5 μM) for 3 h significantly diminished COM crystal-binding to these cells. The compounds significantly reduced surface expression of ANXA1 and HSP90 (COM-binding proteins) as evidence by immunofluorescence microscopy, whereas the intracellular level increased. Western blot analysis confirmed these changes in membrane and cytosolic fractions of compound-treated cells, whereas whole cells remained unchanged. M1 also showed a promising antioxidant activity in DPPH assay.

Keywords: Urolithiasis, renal stones, calcium oxalate monohydrate crystals, galloylquinic acids, *Drosophila*, biotransformation, filamentous fungi

RESUMO

Abdelsalam, Mohamed A. M. H. Síntese, atividade antiurolítica, e estudos de biotransformação de ácidos galoilquínicos de espécies de *Copaifera* por fungos filamentosos. 2018. Tese de Doutorado. Faculdade de Ciências Farmacêuticas de Ribeirão Preto – Universidade de São Paulo, Ribeirão Preto, 2018.

Calculo renal, também conhecido como urolitíase, é comum com uma taxa de prevalência estimada global recente de 14,8%, a qual parece estar aumentando, com uma taxa de recorrência em cinco anos de até 50%. As várias atividades biológcas promissoras de extratos de plantas ricas em ácidos galolquínicos, como as folhas das espécies de *Copaifera*, levaram nosso interesse em sintetizar o éster metílico do ácido 3,4,5-tri-*O*-galoilquinico trissubstituído (TGAME), com o objetivo de desenvolver um composto com potencial para prevenção de cálculos renais. A síntese total incluiu seis etapas a partir dos ácidos quínico e gálico disponíveis comercialmente. O passo-chave na via sintética foi a esterificação de Steglich viável do quinato de metila com ácido 3,4,5-tribenziloxibenzóico usando diciclo-hexilcarbodiimida e N, N-(dimetilamino)piridina como reagentes de acoplamento. As estruturas químicas do composto final e seus intermediários sintéticos foram elucidados por métodos espectroscópicos, espectrométricos e espectrofotométricos de análises. O efeito potencial do composto sobre a ligação de cristal monoidratado de oxalato de cálcio (COM) à superfície de células de rim caninas tipo I de Madin-Darby (MDCKI) e o crescimento de cristais em modelo de túbulos Malpighi de *Drosophila melanogaster* foi investigado. As quantidades de membrana, citosólica e total de Annexina A1 (ANXA1), Alfa-enolase e HSP90 foram examinadas por análise de transferência de Western após fracionamento subcelular, as quais foram confirmadas por coloração por imunofluorescência de células cultivadas. O pré-tratamento de células MDCKI com TGAME por até 6 h diminuiu significativamente a ligação de cristal COM de uma maneira dependente da concentração. O TGAME (50 μM) inibiu significativamente a expressão superficial de ANXA1 por microscopia de imunofluorescência, enquanto o ANXA1 intracelular aumentou. A análise de Western Blot confirmou alterações de expressão de ANXA1 na membrana e frações citosólicas de células tratadas com os compostos, enquanto a ANXA1 de células inteiras permaneceu inalterada. O TGAME também diminuiu significativamente o tamanho, o número e o crescimento de cristais de COM induzidos em um modelo de túbulos Malpighi *de Drosophila melanogaster*, o qual apresentou também potente atividade antioxidante em um ensaio de DPPH. Adicionalmente, realizamos estudos de biotransformação de derivados do ácido galoilquínico, utilizando fungos filamentosos, para prever seus

comportamentos farmacocinéticos. Os resultados mostraram que os ácidos galoilquínicos das folhas de *Copaifera lucens* (fração *n*-butanólica, BF) foram transformados por *Aspergillus alliaceus* em um metabólito majoritário, o ácido 3-*O*-metil gálico (M1), que é um dos metabolitos conhecidos do ácido gálico estudado em humanos. O produto biotransformado foi identificado por UPLC-MS/MS. O pré-tratamento de células MDCKI com BF e seu produto transformado por 3 h diminuiu significativamente a ligação de cristal COM a estas células em concentrações de 50 μg/mL e 5 μM, respectivamente. Os compostos reduziram significativamente a expressão superficial das ANXA1 e HSP90 (proteínas de ligação COM) como evidenciado por microscopia de imunofluorescência, enquanto o nível intracelular aumentou. A análise por Western blot confirmou estas alterações nas frações de membrana e citosol das células tratadas com estes compostos, enquanto as células inteiras permaneceram inalteradas. M1 também apresentou atividade antioxidante promissora no ensaio DPPH.

Palavras-chave: Urolitíase, cálculos renais, cristais de oxalato de cálcio monoidratados, ácidos galoilquínicos, *Drosophila*, biotransformação, fungos filamentosos.

LIST OF FIGURES

LIST OF TABLES

LIST OF SCHEMES

APPENDICES

LIST OF ABBREVIATIONS

ATTC	American type culture collection
ANXA1	Annexin A1
BC	Before Christ
BID	Bis in die (two times a day)
BF	*n*-Butanolic fraction
BOD	Biochemical oxygen demand
CKD	Chronic kidney disease
CaOx	Calcium oxalate
CaP	Calcium phosphate
COM	Calcium oxalate monohydrate
CDM	Calcium oxalate dihydrate
CID	Collision-induced dissociation
COX-2	Cyclooxygenase-2
^{13}C NMR	Carbon nuclear magnetic resonance
DCC	N,N'-Dicyclohexylcarbodiimide
DMAP	Dimethylaminopyridine
DPPH	2,2-Diphenyl-1-picrylhydrazyl
ESRD	End-stage renal disease
EGCG	Epigallocatechin gallate
GAGs	Glycosaminoglycans
HPLC-UV	High performance liquid chromatography

HPF	High-power fields
^{1}H NMR	Hydrogen nuclear magnetic resonance
HRCs	Human renal epithelial cells
HSP90	Surface heat shock protein 90
IR	Infrared
IL-1	Interleukin-1
iPBS	Insect phosphate buffer saline composition
JL	John Lieske
LC/MS-MS	Tandem liquid chromatography mass spectroscopy
MBD	Mineral and bone disorder
MDCKI	Madin-Darby Canine Kidney Cells type I
MCP-1	Monocyte chemoattractant protein 1
MDA	Malondialdehyde
NHANES	National Health and Nutrition Examination Survey
NSAIDs	Non-steroidal anti-inflammatory drugs
NADPH	Nicotinamide adenine dinucleotide phosphate
OPN	Osteopontin
OD	Optical density
PCNL	Percutaneous nephrolithotomy
PGG	1,2,3,4,6-penta-*O*-galloyl-beta-D-glucose
PDA	Photodiode array or Potato dextrose agar
PSI	Pounds per square inch

QID	Quarter in die (four times a day)
RSS	Relative supersaturation
ROS	Reactive oxygen species
RIRS	Retrograde intrarenal surgery
RT	Room temperature
SWL	Shockwave lithotripsy
SOD	Superoxide dismutase
SD	Standard deviation
TID	Ter in die (three times a day)
TGAME	3,4,5-tri-*O*-galloylquinic acid methyl ester
TLC	Thin layer chromatography
UPTF1	Urinary prothrombin fragment 1
UPLC	Ultra-performance liquid chromatography
UV	Ultra violet

TABLE OF CONTENTS

Introduction

1 Introduction

Renal stones (calculi; *s* calculus) disease is considered to be one of the oldest and most ubiquitous diseases known to humankind. Calculi are mineral concretions (deposits) in the renal calyces and pelvis that are found to be free or attached to the renal papillae. By contrast, diffused renal parenchymal calcification is called nephrocalcinosis.

Stones that develop in the urinary tract system are known as urolithiasis or nephrolithiasis, however the later refers specifically to calculi formed inside the kidney. When the stones are formed in the ureters, in this case, it is known as ureterolithiasis, where the stones develop when the urine becomes excessively supersaturated with respect to mineral, leading to crystal nucleation, growth, aggregation and retention with the kidneys (1).

The earliest evidence of this disorder is a bladder stone, dating back to about 4800 BC, found among the pelvic bones in the tomb of a young predynastic Egyptian (2). However, other stones from that era have been reported and out of 9000 mummies examined, only four had positive evidence of calculi, so that the prevalence of the disorder must have been fairly low, at least among upper class Egyptians.

Stones have also been found in North America in the graves of early Indians (ca 1500 BC) (3, 4), but in South America stone disease appears to have been rare amongst the indigenous population until after the Spanish Conquest (5).

In India, references to stone-formation can be located in early Sanskrit documents written between 3000 and 2000 BC (6), and stones were well-recognized in Classical times by Hippocrates in Greece (7) and by Celsus in Rome (6).

Since that time the pattern of stone disease has changed with fluctuation both in the geographical distribution and in the type and composition of stones formed (8, 9). Over the centuries the incidence appears to have been generally increasing, particularly amongst the more industrially developed nations, although there are reports of "troughs" and "waves" in the incidence pattern during and after the two World Wars (8-11).

Over a lifetime, the disease can affect up to 10 -15% of the population (12). After passage of a first stone, the risk of recurrence is 40-50 % within 5 years and 75% within 20 years (13, 14). First-time stone formers do not regularly have a full urine and electrolyte evaluation due to the low incidence of a reversible metabolic cause. However, a reversible metabolic abnormality can be identified in over 90% of recurrent stone formers (12).

The costs associated with stone disease have also risen, increasing from an estimated US$2 billion in 2000 to over US$10 billion in 2006 in the United States alone (15). The

prevalence of stones has been consistently increasing over the past 50 years and further increases are expected owing to changing lifestyle, dietary habits, obesity and global warming (16, 17). Obesity (18), diabetes (18-20), hypertension (17, 20, 21) and metabolic syndrome (22) are considered risk factors for stone formation; conversely, stone formers are at risk of hypertension (21-23), chronic kidney disease (CKD) and end-stage renal disease (ESRD) (23-26).

Urolithiasis of the bladder is a well-documented risk factor for tumor development in humans and rodents and is considered the initiating event that leads to a hyperplastic response, followed by papillomas or diffuse papillomatosis, which may eventually become transitional cell carcinoma (27).

Major advances have been made in the medical and surgical management of patients with kidney stones. Stones can be fragmented using shockwave lithotripsy (SWL) to enable them to pass in the urine, or surgically removed using percutaneous nephrolithotomy (PCNL) or retrograde intrarenal surgery (RIRS). PCNL involves direct endoscopic access into the kidney through an incision in the flank, whereas RIRS is performed using a flexible fibre-optic ureteroscope to access the upper urinary tract through natural passageways. Medical therapies are being used to ease stone passage, promote expulsion and reduce stone recurrence. Important advances have also been made in our understanding of stone pathogenesis.

1.1 Epidemiology

A recent study of epidemiological data from seven countries revealed incidence rates for kidney stones of 114-720 per 100,000 individuals and prevalence rates of 1.7-14.8%, and in nearly all countries, the rates seem to be rising (28). According to data from the National Health and Nutrition Examination Survey (NHANES), the self-reported prevalence of kidney stones in the United States has increased nearly threefold, from 3.2% in the period 1976-1980 to 8.8% in 2007-2010 (16, 29). The lifetime prevalence of kidney stones in the United Kingdom increased by 63% (7.14-11.62%) between 2000 and 2010 (30).

The propensity to form stones varies according to sex, ethnicity and geography. Although historically stones have been two to three times more common in men than in women, recent data indicate that this disparity is diminishing. For example, data from the US Nationwide Inpatient Sample revealed a decline in the male to female ratio for hospital discharges for stones, from 1.7 in 1997 to 1.3 in 2002 (31). The male to female ratio of incident kidney stones also declined in Rochester, Minnesota, USA, from 3.1 to 1.3, between 1970 and 2000 (32). In Florida (USA), a study revealed that the increase in rates in women was greater than that in men

between 1998 and 2004 (33). In Canada, a 48% increase in stone treatment between 1991 and 2010 was primarily accounted for by an increase in procedures among women (34). The reason for the surge in stone disease in women is not precisely understood, but some have proposed that it might be attributable to changes in lifestyle and diet, resulting in increased obesity among women, a known risk factor for stone formation (31).

Racial and ethnic differences in stone prevalence have long been recognized. In the United States, non-Hispanic white individuals have the highest prevalence among racial and ethnic groups (10.3%), followed by Hispanics (6.4%) and non-Hispanic African Americans (4.3%) (16). Comparison of NHANES II (1988-1994) with NHANES III (2007-2010) data has shown that the rise in kidney stone prevalence among Hispanics and African Americans was nearly double that of their white counterparts (16, 29).

Geographical variation in stone disease typically reflects environmental risk factors, with higher stone prevalence in hot, arid climates. In the United States, kidney stones are most prevalent in the south and southeast regions and are lowest in the west of the country (29, 35-37). After controlling for other factors, ambient temperature and sunlight have been shown to be independently associated with stone prevalence (37).

Numerous systemic diseases and factors have been associated with an increased risk of kidney stones. Weight, weight gain, body mass index (18, 38, 39) and diabetes (18, 40) have been shown in large prospective cohort studies to correlate with the risk of incident kidney stones, with a greater effect in women than in men in some cohorts. A multivariable model based on recent NHANES data showed that obesity and diabetes were associated with a 55% and a 59% increased risk of kidney stones, respectively (16). Metabolic syndrome has also been linked to risk of kidney stones, with NHANES data indicating that the number of metabolic traits correlates with the risk of stones (41). Jeong and colleagues (42) detected a 25% higher rate of radiographically detected kidney stones among individuals with metabolic syndrome in a screened population in Asia, after adjusting for confounding variables.

The risk of cardiovascular disease has been associated with a history of kidney stones, although a cause and effect relationship has not been definitively established. Ferraro and colleagues (43) showed a modest increased risk of incident cardiovascular disease among women with a history of stones, but not in men in three large prospective cohorts. Similarly, among individuals registered in the Canadian health care system, a 63% higher risk of incident myocardial infarction was detected among stone formers, with a greater effect in women than

in men (44). A matched pair analysis revealed a 31% higher risk of myocardial infarction in stone formers than in the general population in Olmstead County, Minnesota, USA (45).

1.2 Microstructure of kidney stones

Kidney stones are solid masses, ranging in size from a grain of sand to a pearl (or larger) - a stone does not have to be symptomatic. Depending on their composition, stones are either yellow or brown in color and smooth or jagged in texture or appearance. Globally, approximately 80% of kidney stones are composed of calcium oxalate (CaOx) mixed with calcium phosphate (CaP). Stones composed of uric acid, struvite and cystine are also common and account for approximately 9%, 10% and 1% of stones, respectively (46). They are composed of crystals and a ubiquitous organic matrix, which not only coats the crystals but is also present inside the crystals and the inter-crystalline spaces (47-49). The matrix of calcific stones contains many macromolecules, including osteopontin (which also has a role in bone biomineralization), inter-α-inhibitor (a plasma protein) and urinary prothrombin fragment 1 (UPTF1) - all of which are normally present in the urine (50), albeit in small quantities (50-52). The matrix also contains various forms of lipids, which have been shown to induce crystal nucleation (53, 54). The association between the crystals and the matrix seems to start early upon crystal nucleation and continues throughout the formative and growth phases of the developing stone. Although some urinary molecules, such as UPTF1, are considered crystallization inhibitors, others such as osteopontin can act as both inhibitors and promoters of crystallization (55). These molecules seem to be produced as a protective response against mineralization. However, both CaOx and CaP crystals have been shown to induce the production of macromolecules that inhibit and/or modulate crystallization (52, 56, 57).

1.3 Calculi types

There are four main types of stones and they are named after their major constituents or compositions (Figure 1). Calcium stones are the most common and occur as CaOx and CaP crystals, alone or in combination. Most kidney stones are partially or completely composed of CaOx, which exists as a monohydrate or dihydrate. Individual crystals of CaOx monohydrate (COM) are thin and plate-like, and generally acquire a ‘dumb-bell’ shape through twinning, as seen in urinary sediments. Inside the stones, COM crystals are arranged radially into fan-shaped profiles with distinct concentric laminations, showing outward growth of the crystals and stones. CaOx dihydrate (COD) crystals have characteristic tetragonal bipyramidal envelope shape both in urinary sediment and in kidney stones. CaOx stones are small with shiny exteriors

and generally contain both COM and COD crystals. COM stones are more common than the pure COD stones (58). In mixed stones, COD crystals are predominantly present on the stone surface, which appears jagged. By contrast, pure COM stones have smooth surfaces and they appear as six sided prisms. CaOx stone formation is a multistep process. Hypercalciuria, hyperoxaluria and hypocitraturia are major risk factors.

1.3.1 Calcium Phosphate (CaP) stones

This kind of stones is mainly found as basic CaP (apatite), calcium hydrogen phosphate dihydrate (brushite) or tricalcium phosphate (whitlockite). Pure CaP stones are rare (59). Apatite is the most common crystal in kidney stones and is often a powdery mass that fills the spaces in between other types of crystals, mainly CaOx crystals. Whitlokite is very rare in both kidney stones and urinary sediments. Brushite frequently occurs in kidney stones and is present as rosettes of radially arranged thin blade-like crystals. Hypercalciuria, hypocitraturia and increased urinary pH are major risk factors for CaP stone formation (60).

1.3.2 Uric acid stones

The stones of uric acid comprise 8-10% of all kidney stones worldwide, with a disproportionate prevalence in stone formers who are obese and insulin resistant. Unlike calcium stone types, overly acidic urine (a pH of <5.5) is recognized as the main abnormality responsible for uric acid nephrolithiasis (61). In addition to the insolubility of uric acid at low urinary pH and dehydration, conditions that lead to excessive urinary uric acid excretion, known as hyperuricosuria, have also been associated with uric acid stone formation. These high levels might be due to excess dietary intake of purine-rich foods (62) or endogenous uric acid overproduction, as occurs in conditions such as gout (gouty diathesis). Increased purine catabolism (which can occur in those with myeloproliferative disorders or in those receiving chemotherapy) and the use of drugs that prevent renal reabsorption of uric acid are also contributing factors. Most uric acid stones are compact, appearing like pebbles, with a central core of loosely aggregated anhydrous uric acid crystals surrounded by radiating columnar anhydrous uric acid crystals organized in concentric laminations (58, 63). Some stones display a compact outer layer enclosing a porous friable interior consisting of anhydrous uric acid, uric acid dihydrate and COM crystals mixed with organic material.

1.3.3 Struvite stones

They are large aggregates of orthorhombic ‘coffin-lid’-shaped struvite crystals covered with spherulitic carbonate apatite crystals and mixed with cellular debris, which often included bacteria (63). They are also known as ‘infection stones’, represent 7-8% of all stones worldwide

and are typically caused by increased production of ammonia secondary to infection with urease-producing organisms, such as *Proteus* or *Klebsiella*. The subsequent alkaline urine leads to the formation of magnesium ammonium phosphate hexahydrate crystals (64). Struvite and associated carbonate apatite crystals can grow quickly into large stones referred to as "staghorn calculi", appropriately named for their horn-like projections that occupy the renal pelvis and renal calyces. Although historically feared for their association with high mortality, struvite stones and their association with urosepsis and infections are now treatable with surgical intervention and antibiotics. In the modern era, these stone types are better known for their preponderance for recurrence, particularly in immunocompromised individuals with incomplete stone removal.

1.3.4 Cystine stones

Cystine stones form as result of an autosomal recessive defect in the renal transporter of the amino acid cystine (65). The lack of cystine reabsorption leads to increased urinary cystine excretion. At normal urinary pH, cystine is insoluble and forms cystine crystals that can aggregate to form recurrent kidney and bladder stones. Cystine stones are compact, amber coloured, slightly opaque and with homogenous interiors. Higher magnification of the stone and urinary deposits reveals a unique and characteristic hexagonal structure of the cystine crystals (65).

1.3.5 Iatrogenic stones

Iatrogenic stones can be formed when the urine becomes supersaturated with certain relatively insoluble drugs or their metabolites, leading to crystallization in the renal collecting ducts. For example, patients with HIV who are treated with protease inhibitors such as indinavir and atazanavir are at risk for developing nephrolithiasis (66). Both indinavir and atazanavir are metabolized by the liver, with a considerable proportion of the drug excreted in the urine unchanged, leading to their crystallization and the formation of kidney stones (67). Even when given as part of a multiple drug regimen, atazanavir can crystallize in the urine and form kidney stones (68). Exposure to any one of five different antibiotic classes was associated with nephrolithiasis. Risks were increased 2.3-times, 1.9-times, 1.7-times, 1.7-times, and 1.3-times for sulfas, cephalosporins, fluoroquinolones, nitrofurantoin/methenamine, and broad-spectrum penicillins, respectively, taken 3-12 months before the date of diagnosis.

Poorly soluble dietary contaminants can also crystallize and form stones. For example, melamine has been implicated in the deaths of dogs and cats (69, 70) and caused a major health emergency in China in 2008. Melamine adulteration of infant formula led to the development

of stones and sand-like calculi in the urinary tracts of >294,000 infants (71, 72) >50,000 of whom were hospitalized; six patients died as a result.

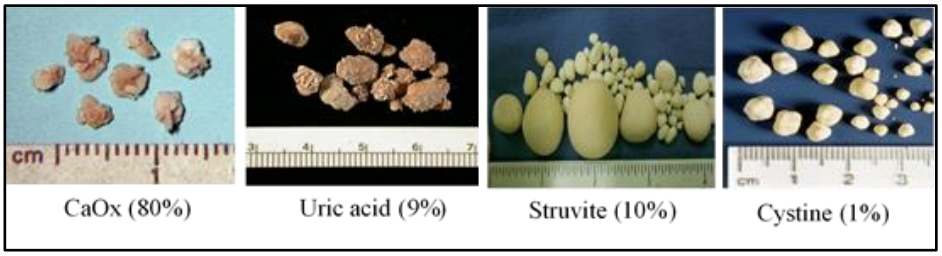

Figure 1. Renal stones types and composition.

1.4 Chemistry and mechanisms/theories of stone formation

Several models of how kidney stone is formed, have been proposed; the two dominating mechanisms for the initiation of stones are commonly described by the terms 'free particle' (in which crystals form 'Randall's plugs' in the tubule) and 'fixed particle' (in which stones grow on so-called Randall's plaques) (Figure 2). Although these models encompass all the possible hypothetical models of how stones begin, no single model can rationalize the evidence observed from all patients with stones-many factors probably contribute. Regardless of the model, the chemical processes of nucleation and crystal growth are essential for the initiation and development of all stone types (73). Stone formation is caused by an abnormal combination of factors that influence the thermodynamic driving force (supersaturation) and the (kinetic rate-controlling) processes involved in the crystallization of the various stone-forming minerals. The principal thermodynamic driving force for both stages is the degree of supersaturation of the fluid within which initiation occurs (73, 74). Whether this takes place intracellularly or extracellularly, the laws of crystallization chemistry should apply.

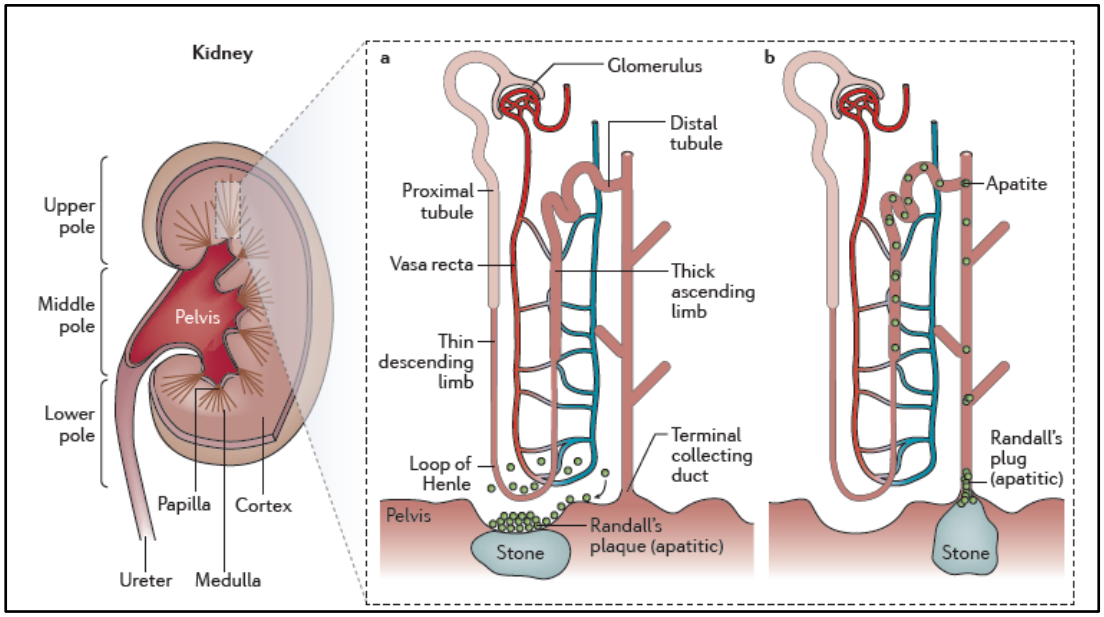

Figure 2. Macroscopic and microscopic morphology of human kidneys and location of stones. (a) According to the fixed-particle mechanism, stones begin as depositions of calcium phosphate (CaP) in the interstitium (apatite), grow outwards reaching the renal papillary surface, become exposed to the pelvic urine and establish a nucleus for the deposition of calcium oxalate (CaOx), leading to the formation of CaOx stones attached to a CaP base, known as Randall's plaques. (b) By contrast, in the free-particle mechanism, for example, CaP, uric acid or cystine crystals form in the renal tubules, move with the urine, aggregate and plug the terminal collecting ducts. These plugs, called Randall's plugs or lesions, are exposed to the pelvic urine. Deposition of CaOx crystals on the CaP plugs leads to the formation of CaOx kidney stones.

1.5 Stages of stone formation

1.5.1 Crystal nucleation

Nucleation (in which solute molecules dispersed in a solvent begin to cluster) is the first stage in crystallization. There are two types of nucleation, either homogeneous or heterogeneous. Homogeneous nucleation requires a high degree of supersaturation with respect to the mineral concerned; *in vitro* this would normally take place in a pure solution containing no particulate matter and in a receptacle that is chemically inert. By contrast, heterogeneous nucleation is the much more likely mechanism through which crystal initiation occurs in the urine (74). The process can occur in the presence of particulate matters consisting of proteins, other organic polymers or crystals of another mineral, and is contained within receptacles lined

with chemically active cell surfaces. Heterogeneous nucleation requires a lower level of supersaturation than homogeneous nucleation for crystal initiation.

1.5.2 Supersaturation of urine with ions

The relative supersaturation (RSS) level at which nucleation occurs is known as the formation product of the mineral concerned; it is not a fixed thermodynamic constant, but covers a range of supersaturation values within which *de novo* crystal nucleation can take place. Its value depends on several factors. First, the length of time of incubation affects the RSS. The longer a given supersaturated solution is left to stand, the more likely it is to precipitate crystals. The higher the initial RSS, the shorter is the nucleation time (75).

1.5.3 Crystal growth and agglomeration

Once a crystal nucleus is initiated inside the kidneys (74), exposure to the urine enables the stone to grow by encrustation (76, 77). As we previously mentioned before, there are two basic pathways (free-particle and fixed-particle mechanisms) for the establishment of a stone nucleus, both of which can be active in any stone former, although stones from idiopathic stone formers are generally formed attached to plaques (78, 79). In the free-particle mechanism (74), crystals nucleate, grow and aggregate within the urine of the renal tubules. Once crystals aggregate to form large particles, they are retained inside the kidneys either by becoming too large to pass through the tubular lumens or by attaching themselves to the tubular (80). In the presence of high supersaturation, crystal deposits occlude the collecting ducts forming Randall's type 2 lesions or plugs (81), which protrude out into the renal pelvis and become exposed to the pelvic urine. Once tubular openings are blocked, stasis can promote the formation of small stones behind the plugs. Similarly, unattached stones in the renal calyces can also form through the free-particle mechanism.

1.6 Prevention, management and current treatment

Although prevention of new calcium stones is possible, there is no effective pharmacological therapy or treatment that can dissolve existing calcium stones. In non-idiopathic calcium nephrolithiasis, the primary conditions should be addressed with specific treatments. In these cases, preventive measures are supportive. In the majority of patients with idiopathic stone disease, behavioral and nutritional interventions are potentially helpful and should be the first step of stone prevention (82). Nutritional advice for patients with calcium stones include increased water intake (>2 liter per day and >3 liter per day in the summer) to provide 24 h diuresis of >2 liter (83), and maintenance of a balanced diet with calcium intake

not <800-1,000 mg per day, reduced meat and poultry intake (≤0.8 g per kg of body weight) (84), reduced salt intake (<2 g per day, which is equivalent to 5 g of table salt (sodium chloride)), avoidance of excess food intake, increased vegetable consumption (85) and avoidance of soda beverages (86). Low calcium diets should be avoided in the majority of patients because they increase intestinal absorption and urinary excretion of oxalate, thereby increasing lithogenesis (87); furthermore, such diets can cause or worsen mineral and bone disorder (MBD) in calcium stone formers. Low oxalate diets are difficult to attain because of the presence of oxalate in many common foods. Only foods with very high oxalate content should be limited or avoided. The concomitant consumption of foods that are rich in oxalate and calcium is a possible strategy to decrease the absorption of oxalate (88). Drug treatment could be considered if stones continue to recur despite the above measures, or if the CKD and/or MBD risks are considerable, or in certain groups of people (for example, flying airline personnel) and in those who have severe urine metabolic abnormalities. For example, thiazides reduce calciuria and might improve bone mineral density (89) and should be considered in patients with high or relatively high urine calcium levels and recurrent calcium stones. However, thiazides have also been shown to decrease stone activity in individuals with normocalciuria (90). Indeed, the American Urological Association guidelines (91) suggest that lowering calciuria with thiazides might be effective regardless of the absolute rate of calcium excretion. Thiazides are appropriate for both CaOx and CaP stones when dietary measures and increased fluid intake have not been successful in preventing stone recurrence. Allopurinol or febuxostat could be useful in patients with calcium stones who are hyperuricosuric (91); the former was shown to be effective in reducing urinary uric acid and stone recurrence in hyperuricosuric CaOx stone formers without other metabolic abnormalities (91). Although no data support its use, the hypouricosuric effect of febuxostat suggests that this drug could be effective in stone formers who cannot tolerate allopurinol (92).

Citrate (generally potassium citrate) use to increase citraturia, which raises the inhibitory activity against calcium crystallization (93), has been shown to be effective in two randomized trials (94). Citrate is indicated in those with recurrent CaOx stones with decreased urinary citrate excretion; in patients with complete or incomplete distal renal tubular acidosis, chronic diarrhoeal states, drug-induced or diet-induced hypocitraturia; and in patients with MBD who form stones. In general, potassium citrate is preferred to sodium citrate because it attenuates calciuria and, therefore, is likely to be more effective in preventing calcium stones (95). However, some concern pertains to overtreatment with citrate, which in theory might

increase the risk of forming new CaP stones because it raises urinary pH (via its metabolism to bicarbonate by the liver). However, in patients with medullary sponge kidney and/or distal renal tubular acidosis and pre-existing high urinary pH, kidney stone recurrence rate is decreased rather than increased after treatment with citrate (96). To prevent frequently occurring uric acid stones, uric acid supersaturation in the urine must be decreased. This can be achieved by increasing urinary volume (>2 liter per day), increasing urinary pH to approximately 7.0, decreasing uricosuria and administering sodium bicarbonate or potassium citrate. Although not supported by data from clinical trials, allopurinol or febuxostat can be used if the patient has hyperuricosuria and dietary measures fail to normalize urinary uric acid (97). Reducing the concentration of cystine in the urine and increasing its solubility will prevent stone formation in this highly recurrent stone disease. The preventive strategy involves increasing water intake to >3 liter per day and the administration of sodium bicarbonate or potassium citrate to raise urinary pH and increase the solubility of cystine. Early in the treatment course, urinary pH should be checked multiple times per day to titrate the quantity of alkali; at a later stage of treatment, the urinary pH should be monitored less frequently. If the previous measures fail to prevent new stones, 6-mercaptopropionyl glycine can be administered, with d-penicillamine as an alternative treatment (88). Given that both drugs can cause proteinuric glomerular diseases, urine should be periodically monitored for proteinuria. Patients with cystine stones require close follow-up because of the high metabolic activity of the disease (with a very high risk of stone recurrence, the rapid growth of these stones, staghorn stone formation, need of surgical procedures and CKD occurrence) and because of the possible adverse effects of treatment.

Treatment of the pain associated with kidney stones (renal colic) is based on the use of NSAIDs as a first choice in the absence of contraindications (98) and, in case of failure in relieving pain, opioids. Intravenous paracetamol (acetaminophen) also seems to be as effective as morphine (99). The use of antispasmodics does not seem to have a significant effect (100). If analgesia cannot be achieved with the previous measures, drainage of the renal pelvis through percutaneous nephrostomy or ureteral stenting and eventually stone removal should be performed.

Surgical interventions such as shockwave lithotripsy, ureteroscopic fragmentation and retrieval and percutaneous nephrolithotomy are common procedures for stone disease. Hydration should be normal and intravenous fluids are only indicated in the case of protracted vomiting because it does not favour stone expulsion but instead increases pain and the risk of complications (renal pelvic rupture and urine extravasation) (101). α-Adrenergic receptor

antagonists (mainly tamsulosin) (102) and calcium channel blockers have been demonstrated to be an effective medical expulsive therapy, believed to be due to their ability to dilate the distal ureter and increase the probability of spontaneous stone passage. The efficacy of these agents in promoting the passage of small distal ureteral stones (<5 mm in size) has recently been decried by two well-designed, randomized, placebo-controlled trials, one of which found efficacy only for larger stones (≥5 mm in size) and the other found no efficacy for stones of any size (103).

Oral dissolution of existing stones is generally effective only with uric acid stones. Two-thirds of these stones can be at least partially dissolved by following the same rules suggested for their prevention: modulating the pH of urine to 7.0, increasing urinary volume and decreasing uricosuria with allopurinol or febuxostat (104).

1.7 Natural products and stone disease

Historically, natural products (secondary metabolites) have been used since ancient times and in folklore for the treatment of many diseases and ailments. Classical natural product chemistry methodologies enabled a vast array of bioactive secondary metabolites from plant, terrestrial and marine sources to be discovered. Many of these natural products have gone on to become current drug candidates. Natural products have been the most successful source of potential drug leads (105-108). They continue to provide unique structural diversity in comparison to standard combinatorial chemistry, which presents opportunities for discovering mainly novel low molecular weight lead compounds. Since less than 10% of the world's biodiversity has been evaluated for potential biological activity, many more useful natural lead compounds await discovery with the challenge being how to access this natural chemical diversity (109).

A number of plants have been studied for their potential use in the modulation and treatment of stone disease. *Copaifera* is a flowering plant that belongs to the family Leguminosae (Fabaceae) Juss., subfamily Caesalpinoideae Kunth (110). The scientific name means "copal-bearer" (or more accurately, copaiba-bearer), since economically important oleo-resin can be obtained from these plants that are used by indigenous Amazonian people for medicinal purposes. They are also important for production of biodiesel and wood, especially *Copaifera langsdorffii*. *Copaifera* consists of 43 species, and is largely distributed in South America (37 species, 28 species in Brazil), Central America (4 species), and Africa (4 species) (111). Several members of the genus are present in Latin America, mainly in the Amazon region (112).

Our group has studied the effect of the *Copaifera langsdorffii* Desf. leaf extract on the ethylene glycol-induced nephrolithiasis in rats, where the plant extract was able to prevent stone formation. Significantly lower oxalate levels and osteopontin (OPN) expression and increased citrate levels were observed after extract administration. Phytochemical analyses showed that the extract is rich in phenolic compounds such as galloylquinic acids that are capable of preventing stone formation (113). In another study, we observed that *C. langsdorffii* have increased levels of magnesium and decreased levels of uric acid in urinary excretions. Treated animals have a significant decrease in the mean number of calculi and a reduction in calculi mass. Calculi taken from extract treated animals were more brittle and fragile than calculi from untreated animals. Moreover, breaking calculi from untreated animals required twice the amount of pressure as calculi from treated animals (114). The anti-inflammatory and antiurolithic effects of polyphenolic compounds from *Quercus gilva* Blume were investigated in a previous study, where some isolated compounds from the plant showed potent anti-oxidative and anti-inflammatory activities. These compounds were further tested before for their inhibition of the gene expression of the inflammatory cytokines, where some other phenolic compounds in the extract showed dose-dependent inhibitory activities on gene expression of COX-2 and IL-1 (115).

Recently, epigallocatechin gallate (EGCG), a green tea polyphenol was reported to inhibit free-radical production induced by oxalate (116). It also decreases binding of calcium oxalate monohydrate crystals onto renal tubular cells via decreased surface expression of α-enolase (117).

PGG (1,2,3,4,6-penta-*O*-galloyl-beta-D-glucose), a polyphenolic and water soluble gallotannin (118) isolated from gallnut of *Rhus chinensis* MILL, is known to have several biological effects towards stone disease, including attenuation of renal cell migration, hyaluronan expression, and crystal adhesion (119). The compound also reduces renal crystallization and oxidative stress in a hyperoxaluric rat model (120).

Natural products including gallotannins found also in green teas have been studied as potentially novel treatments to prevent crystal retention and kidney stone formation. Gallotannin significantly inhibited COM crystal growth and binding to Madin-Darby Canine Kidney Cells type I (MDCKI) renal epithelial cells. It significantly attenuated oxalate-induced mRNA and protein expressions of monocyte chemoattractant protein 1 (MCP-1), OPN, nicotinamide adenine dinucleotide phosphate (NADPH) oxidase subunit p22phox and p47phox in human primary renal epithelial cells (HRCs). The molecule also reduced the levels of reactive

oxygen species (ROS) and malondialdehyde (MDA) as well as enhanced antioxidant enzyme superoxide dismutase (SOD) activity in oxalate treated HRCs (121).

Phyllanthus niruri and *Costus arabicus* L. (*C. arabicus*) are plants used in Brazilian folk medicine to treat urolithiasis. The Aqueous extract of the later inhibits calcium oxalate crystal growth and adhesion to renal epithelial cells (122). *P. niruri* is a plant belonging to the Euphorbiaceae family, which have a worldwide distribution. It is used in Brazil by patients with urolithiasis (123, 124). It was reported that the oral administration of *P. niruri* aqueous extract to rats induces an inhibitory effect on vesical CaOx crystal growth, which is associated with a reduction in the urinary excretion of glycosaminoglycans (GAGs) and with an increase in the content of these macromolecules in the calculi compared with untreated animals (125). Also, *P. niruri* significantly reduces the endocytosis of CaOx crystals in MDCK cells in culture (126). The effect of the extract of *P. niruri* on crystal deposition in experimental urolithiasis was also studied before (127). Moreover, it has an inhibitory effect on crystal growth, which is independent of citrate and Mg, but might be related to the higher incorporation of GAGs into the calculi (125).

Holarrhena antidysenterica, a plant that has a traditional use in the treatment of stone disease, where its crude extract possesses antiurolithic activity, possibly mediated through the inhibition of CaOx crystal aggregation, displaying antioxidant and renal epithelial cell protective activities (128).

In a previous study, the *in vitro* effect of lemon and orange juices on calcium oxalate crystallization has been investigated, where lemon juice was found to inhibit the rate of crystal nucleation and aggregation (128).

1.8 Herbs for prevention of urolithiasis (129)

Barberry root bark (*Berberis vulgaris*) - Barberry was found to inhibit calcium oxalate crystallization and prevent kidney damage caused by oxidative stress in animal studies. The water extract was the most effective preparation (130). **Dose:** Tea: 1 tsp. dried root bark to 300 mL water, decoct for 10-15 minutes, steep for 30 min, taken as 120 mL BID/TID.

Black cumin seed (*Nigella sativa*) - in animal studies, the use of this herb significantly protected against experimentally induced formation of CaOx stones (131). **Dose:** Tea: ½ tsp. dried seed, 240 mL hot water, steep covered 20 minutes, take 120 mL BID/TID.

***Chanca Piedra*/Stonebreaker** (*Phyllanthus niruri*) - is native to tropical regions and has a long history of use for helping to prevent and pass kidney stones. In several *in vitro* and animal studies, daily intake of this herb helped to prevent the formation of kidney stones (132).

In a human study, this herb was found to reduce urinary calcium levels in patients with hypercalciuria (132). It also slowed the growth of existing stones (127). **Dose:** Tea: 1-2 tsp. dried herb, 240 mL hot water, steep 30 min. Take 2-3 cups per day. Tincture (1:5): 3-6 mL (60-120 gtt.) TID.

Evening primrose seed oil (*Oenothera biennis*) **-** in a human study, daily ingestion of the oil (1000 mg per day) significantly increased citraturia (urinary citrate levels) while reducing urinary oxalate, calcium and the Tiselius risk index, which is a measurement of risk for forming kidney stones (133). **Dose:** Tea: 2 tsp. dried leaf, 240 mL hot water, steep for 45 min, taken as 240 mL BID, Tincture (1:5): 1.5-3 mL TID.

Fagolitas - is a Spanish herbal formula containing fluid extracts of Uva Ursi, Corn Silk, *Ricinus zanzibarensis*, tincture of Saw Palmetto, mother tincture of Buchu, glycerin and Anise essence. Animals given this formula had a significant reduction of papillary and intratubular calcification in the kidneys (134).

Fenugreek seed (*Trigonella foenum-graecum*) **-** the seeds of this herb are commonly used in northern Africa to prevent and treat kidney stones. In an animal study, it was found that Fenugreek seed significantly reduced calcification in the kidney and helped in preventing kidney stones (135, 136). **Dose:** Tea: 1-2 tsp. dried seed, 300 mL water, decoct for 15-20 minutes, steep 30 min, taken as 120-180 mL TID, Tincture (1:5): 2-4 mL (40-80 gtt.) TID.

Gokshura fruit/root (*Tribulus terrestris*) **-** this herb is an Ayurvedic rasayana, nephroprotective agent, and is commonly used in India and China to treat urinary tract disease. In animal studies, it prevented the formation of kidney stones and helped to reverse early stage urolithiasis. *In vitro* research supports the animal data and further suggest that this herb also protects against calcium oxalate-induced renal injury (137). **Dose:** Powder: 1 tsp. TID.

Hibiscus flowers (*Hibiscus sabdariffa*) **-** in animal studies, Hibiscus was able to increase urinary oxalate excretion and it significantly reduced oxalate deposition in kidneys (138). In another study, patients with previous history of kidney stones, Hibiscus tea (2 cups per day) increased oxalate and uric acid excretion and enhanced urinary citrate levels (139). **Dose:** Tea: 1-2 tsp. dried flowers, 240 mL hot water, steep for 20 min, taken as 240 mL BID/TID, Tincture (1:2 or 1:5): 2-4 mL TID.

Jin Qian Cao herb (*Desmodium styracifolium***) -** this Chinese herb inhibits urinary calcium excretion and increases urinary citrate, significantly reduces formation of renal stones (140). **Dose:** Tea: 2-3 tsp. dried herb, 240 mL hot water, steep 40 min. Taken as 2-3 cups per day.

Rose hips (*Rosa canina*) - experimental animals were given an infusion of Rose hips, Rose hips and magnesium, or magnesium alone. Both the herb and the mineral promoted an increase in urinary citrate and reduced urinary calcium excretion (141). **Dose:** Tea: 1 tsp. Rose hips, 240 mL hot water, steep for an hour. Taken as 120 mL TID.

Rupture wort herb (*Herniaria hirsuta*) - in animal studies, this herb inhibited the deposition of CaOx crystals in kidneys (142). **Dose:** Tea: 1 tsp. dried herb, 240 mL water, decoct 5-10 min, taken 1-2 cups per day.

Shatavari root (*Asparagus racemosus*) - this important Ayurvedic Rasayana (rejuvenative remedy) was found to inhibit formation of CaOx stones in animal study (143). **Dose:** Tea: 1 tsp. dried, powdered root, 240 mL water, decoct 10 min, steep for 40 min, taken as 2 cups/day. Tincture (1:5): 2-4 mL (40-80 gtt.) TID.

Varuna bark (*Crataeva nurvala*) - daily intake of this Ayurvedic herb reduced urinary calcium excretion and kidney stone formation (144). **Dose:** Tea: 2 tsp. dried bark, 350 mL water, decoct 15 min, steep for an hour. Taken as 240 mL 2-3 times per Day Tincture (1:5): 4-5 mL (80-100 gtt.) TID.

Water plantain root (*Alisma orientalis*) - the Chinese herb Ze Xie/Water Plantain root has a long history of use in traditional and complimentary medicine (TCM) for treating dysuria, edema, and cystitis. In animal studies, it was also able to inhibit experimentally induced calcium urolithiasis (145). **Dose:** 2 tsp. dried root, 300 mL water, decoct 20 min, steep for an hour, taken as 120 mL TID.

Wu Ling San - this TCM formula is comprised of aqueous lantain root (*Alisma orientalis*), *Polyporus umbellatus*, *Atractylodes macrocephala*, Fu Ling (*Wolfiporia cocos*), and Cinnamon bark. In animal studies it effectively reduced CaOx deposition in rat kidneys (146). **Dose:** Powder: 6-9 grams BID, Tablets: 4-5 tablets BID.

Herbs for treating kidney stones

Many herbs in TCM, Ayurveda, Native American medicine, Eclectic/Physiomedical medicine and European traditions have a long history of being used to help with kidney stones and urinary calculi, among them:

Couch grass rhizome (*Elymus repens*) - is a soothing diuretic that can be useful as part of a formula to make passing stones easier. It also promotes uric acid excretion. Therefore, it can help to prevent uric acid stones. **Dose:** Tea: 2-3 tsp. dried rhizome, 12 oz. water, decoct 30 min, steep for 30 min, taken as 1 cup 3 times/day Tincture: (1:4 or 1:5, 1:2.5): 3-5 mL (60-100 gtt) TID/QID.

Golden rod herb (*Solidago spp.*) - herbalists in the UK often use Solidago with Pellitory-of-the-Wall or Parsley Piert for helping to pass kidney stones. The British herbalist Christopher Hedley, AHG, says that he has seen this simple formula "cause stones to vanish". The patients never noticed the stone passing and upon a follow up with an ultrasound, they had disappeared. **Dose:** Tea : 1-2 tsp. dried herb, 240 mL hot water, steep covered, 20-30 min, take 2 cups/day Tincture (1:5): 2-3 mL (40-60 gtt.) TID/QID.

Horse Chestnut seed (*Aesculus hippocastanum*) - the specific indications for *Aesculus* are for throbbing pain with edema and inflammation. It is most often used for hemorrhoids, varicose veins and trauma injuries. The analgesic and anti-inflammatory effects also help with the intensive pain caused by kidney stones and reduce swelling of the ureter, thus allowing stones to pass more easily. **Dose:** Tincture (1:2): .25-.75 mL (5-15 gtt.) TID, Capsules: A standardized product (16-20% Escin) has been used in several studies with a dose of 300 mg of the extract every 12 h.

Horsetail herb (*Equisetum arvense*) - this herb is rich in silicic acid and helps strengthen bones, teeth, hair, skin and nails. It also helps speed healing of minor kidney damage and hematuria caused by passing stones. In the UK, Horsetail has the reputation of promoting expulsion urinary calculi. **Dose:** Tea: 1 tsp. dried herb, 240 mL water, decoct 15 min, steep 1 h, taken as 120 mL 3times/day, Tincture (1:5): 1-2 mL (20-40 gtt.) TID.

Hydrangea root bark (*Hydrangea arborescens*) is a native American shrub which is one of the most effective urinary tract analgesics. It is indicated for genito-urinary tract pain and spasm and it is used with Khella, Lobelia, Kava, Horse Chestnut, and Yucca root for acute pain caused by kidney stones. **Dose:** Tea: 1 tsp. dried bark, 240 mL cold water, steep for 1 h. Taken as 120 mL TID Tincture (1:5): 2-3 mL TID.

Jin Qian Cao herbs (*Desmodium styracifolium*) - there are three herbs known as Jin Qian Cao. Out of the three, Desmodium and *Glechoma longituba* are believed to be more effective for helping to pass kidney stones. Lysmachia (also known as Jin Qian Cao) is believed by some practitioners to be more useful for treating gallstones, but it is also commonly used in formulas for helping to pass kidney stones. **Dose:** Tea: 2-3 tsp. dried herb, 240 mL hot water, steep 40 min. Taken as 2-4 cups per day.

Kava root (*Piper methysticum*) – it was introduced to western medical practice by the British explorer Captain Cook. In the U.S.A, the Eclectic physicians primarily used it for urinary tract pain. It helps relax the ureters, allowing stones to pass more easily and diminishes colicky, spasmodic pain. **Dose:** Tea (Decoction): 1-2 tsp. dried root, 240 mL water, decoct 15 min, steep

for 1 h, then blend. Taken as 120 mL QID, Tincture (1:4, 1:5): 2-4 mL (40-80 gtt.) TID/ QID, Capsules: Standardized (60 mg Kava lactones), 2-4/day.

Khella seed (*Ammi visnaga*) – this is a northern Africa plant is an effective antispasmodic, useful for relieving spasm and pain in the urinary tract, gall bladder, respiratory tract and cardiovascular system. Khella is very useful as part of a protocol for helping to pass urinary calculi. **Dose:** Tea: 1 tsp. dried seeds, 240 mL hot water, steep covered for 30 min, taken as 120 mL TID, Tincture (1:5): 1-2 mL TID.

Lobelia seed/fresh herb (*Lobelia inflata*) is primarily known as a respiratory remedy used for asthma and spasmodic coughs. It is also an effective antispasmodic for the cardiovascular, genito-urinary and musculoskeletal systems. The tincture of lobelia seed or the tincture of the green flowering herb is highly useful for relieving acute pain caused by stones passing through the ureters. It should be used in formulas combined with Khella, Hydrangea, or Horse Chestnut. **Dose:** Tincture: fresh herb (1:2), 0.5-1 mL (10-20 gtt) TID/QID, seed (1:5), 0.25-0.75 mL (5-15 gtt) TID/QID.

Marshmallow root (*Althea officinalis*) is the most soothing and mucilaginous herbal diuretic. Consuming enough quantities of the tea can help ease passage of urinary stones and relieve inflammation and tissue damage. **Dose:** Tea: 1-2 tsp. dried herb, 240 mL hot water, steep covered 20 min, take 120-240 mL TID.

Pellitory of the Wall herb (*Parietaria diffusa*) is used in the UK as a diuretic, kidney trophorestorative and to help pass urinary calculi and stones. It is often combined with Goldenrod, Parsley or Parsley Piert to help prevent stones or assist in their passage. **Dose:** Tea: 1-2 tsp. dried herb, 240 mL hot water, steep 30 min, take 120 mL TID, Tincture (1:5): 1.5-2 mL (30-40 gtt.) QID.

Punarnava herb (*Boerhaavia diffusa*) is a common Indian weed is used as a kidney restorative and to help expel kidney stones. In an *in vitro* study it was able to inhibit formation of struvite stones, but there is no data about this effect *in vivo*. **Dose:** Powder: 1 tsp. TID.

Varuna bark (*Crateava nurvala*) is an Ayurvedic herb is used to help prevent kidney stones and is also used with banana stem (*Muse paradisiaca*) for treating kidney stones. In a recent human study. The authors state that this formula "helped to dissolve renal calculi, facilitated their passage and reduced pain." **Dose:** Tea: 2 tsp. dried bark, 350 mL water, decoct 15 minutes, steep for 1 h. Taken as 240 mL 2-3 times per day, Tincture (1:5): 4-5 mL (80-100 gtt.) TID.

Wild Carrot seed (*Daucus carota*) **-** British herbalist Anne McIntyre FNIMH used Wild Carrot seed along with Parsley Piert (Alchemilla arvensis) for helping to expel kidney stones. **Dose:** Tincture (1:5): 5 mL TID - 2.5 mL (50 gtt) of each.

Yucca root (*Yucca spp.*) - Alabama herbalist Phyllis Light, RH (AHG) uses Yucca root to help ease passage of kidney stones and relieve urinary tract pain. **Dose:** Tea: 1 tsp. dried root, 300 mL water, decoct 15 min, steep for 20 min, take 120 mL TID, Tincture: 1-2 mL (20-40 gtt.) TID.

Objectives

2 Objectives of the PhD project

2.1 General objectives

- Investigating the biological activity of galloylquinic acid compounds towards renal stone disease (urolithiasis) for the pre-clinical discovery of new therapeutic candidates as antiurolithic agents.

2.2 Specific objectives

- The total synthesis of a bioactive galloylquinic acid compound (3,4,5-tri-*O*-galloylquinic acid methyl ester, TGAME).
- Characterization of the obtained synthetic compound and its chemical intermediates by spectroscopic and spectrophotometric techniques that include: HPLC-UV, LC/MS-MS, ^{1}H NMR, ^{13}C NMR, two dimensional (2D) NMR and IR.
- Biotransformation studies of galloylquinic acid compounds from *Copaifera lucens*, by filamentous fungi, aiming to predict the pharmacokinetic profile of these compounds.
- Antiurolithic activity of TGAME, galloylquinic acid compounds and their biotransformed metabolites by performing the following assays:
  - Cytotoxicity study in Madin-Darby Canine Kidney Cells type I (MDCKI) and human renal cells (JL).
  - Cell-calcium oxalate monohydrate (COM) crystal adhesion assay.
  - Subcellular localization of potential crystals receptors [α-enolase (enolase-1), Annexin A1 and HSP90] by protein extraction followed by Western blot analysis.
  - Neutralization of a potential COM-binding proteins using a specific antibody.
  - Confocal microscopy and immunofluorescence staining.
  - The use of *Drosophila melanogaster* (fruit fly) for studying calcium oxalate crystals growth, size and number by the inhibitory effects of the synthetic compound.

Chapter 1

Total synthesis of the plant metabolite 3,4,5-tri-O-galloylquinic acid methyl ester

3 Chapter 1

3.1 Background

Natural products from medicinal plants, either as pure compounds or as standardized extracts, provide unlimited opportunities for new drug leads because of their availability and chemical diversity. Due to the fact that plant extracts usually occur as a combination of various types of bioactive compounds or phytochemicals with different or similar polarities, their isolation and purification still remain a big challenge for the process of identification and characterization of bioactive compounds with high yield. Moreover, compounds isolated are often available in minute amounts. Thus, synthesis of natural products can provide powerful tools in solving supply problems in clinical trials and marketing of potentially active natural compounds.

The science of natural product synthesis has been recognized with the Nobel Prize in chemistry with constant periodicity over the entire history of the award. Included among these prizes are those given to E. Fischer (in 1902; for his work on sugar and purine syntheses), H. Fischer (in 1930; for his research into the constitution of haemin and chlorophyll and especially for his synthesis of haemin) and R. Robinson (in 1947; for his investigations on plant products of biological importance, especially the alkaloids). Currently, the field appears as vigorous as ever, and its future looks as promising as its past has been rewarding.

Galloylquinic acids are polyphenolics, classified as hydrolysable tannins with low molecular weights. They consist of a sugar core of quinic acid (-OH) esterified with one, two or three gallic acid units to give the mono-, di- and tri-galloylquinic acids. The phenolic group of the galloyl moieties at position 3 can be found substituted with one, two or three methyl groups to give the methoxy derivatives. The –COOH of quinic acid can be esterified as found in the polyphenolic 3,4,5-tri-*O*-galloylquinic acid ethyl and methyl esters that were previously isolated from *Guiera senegalensis* leaves (147) and *Lepidobotrys staudtii* stem bark (148), respectively. Galloyquinic acids are considered to be one of the major secondary metabolites found in *Copaifera* species (149) such as *Copaifera langsdorffii* and *Copaifera lucens* (Fabaceae - Caesalpinoideae) which are native to Brazil. Our research group showed that galloylquinic compounds from the aqueous fraction of *Copaifera langsdorffii* leaves display a potential gastroprotective activity in mice model with induced ulcer and cytotoxicity against gastric adenocarcinoma cells (150). Furthermore, such compounds possess other promising biological and pharmacological activities such as antiasthmatic (151), anti-HIV (152),

leishmanicidal (153), antioxidant (154) and DNA polymerase inhibitory activities. They have the ability to bind irreversibly to HIV glycoprotein (gp120) and inactivate virus infectivity (155). They are characterized as a new class of HIV reverse transcriptase (RT) inhibitor (156).

Recently, we have reported the effect of hydroalcoholic extract from the leaves of *Copaifera langsdorffii* Desf. (Fabaceae - Caesalpinoideae) on urolithiasis and nephrolithiasis models in rats, where animals treated with the extract have increased levels of magnesium and decreased levels of uric acid in urinary excretions. Moreover, treated animals have a significant decrease in the mean number of calculi and a reduction in calculi mass (113, 114). The chromatographic analysis of *Copaifera* leaves extracts revealed that they are very rich in phenolic compounds identified mainly as galloylquinic acids (150) that might significantly contribute to their antiurolithic activity. However, the chromatographic isolation and purification of such class of compounds are costly and require specific stationary phase due to their complexity, similar polarities and chemical structures. Most of the reported methods of isolation was based on gel filtration using Sephadex LH-20 column chromatography (149, 156, 157). The previously mentioned points aroused our attention to synthesize the 3,4,5-tri-*O*-galloylquinic acid methyl ester (TGAME) (Figure 3) and investigate its activity towards urolithiasis.

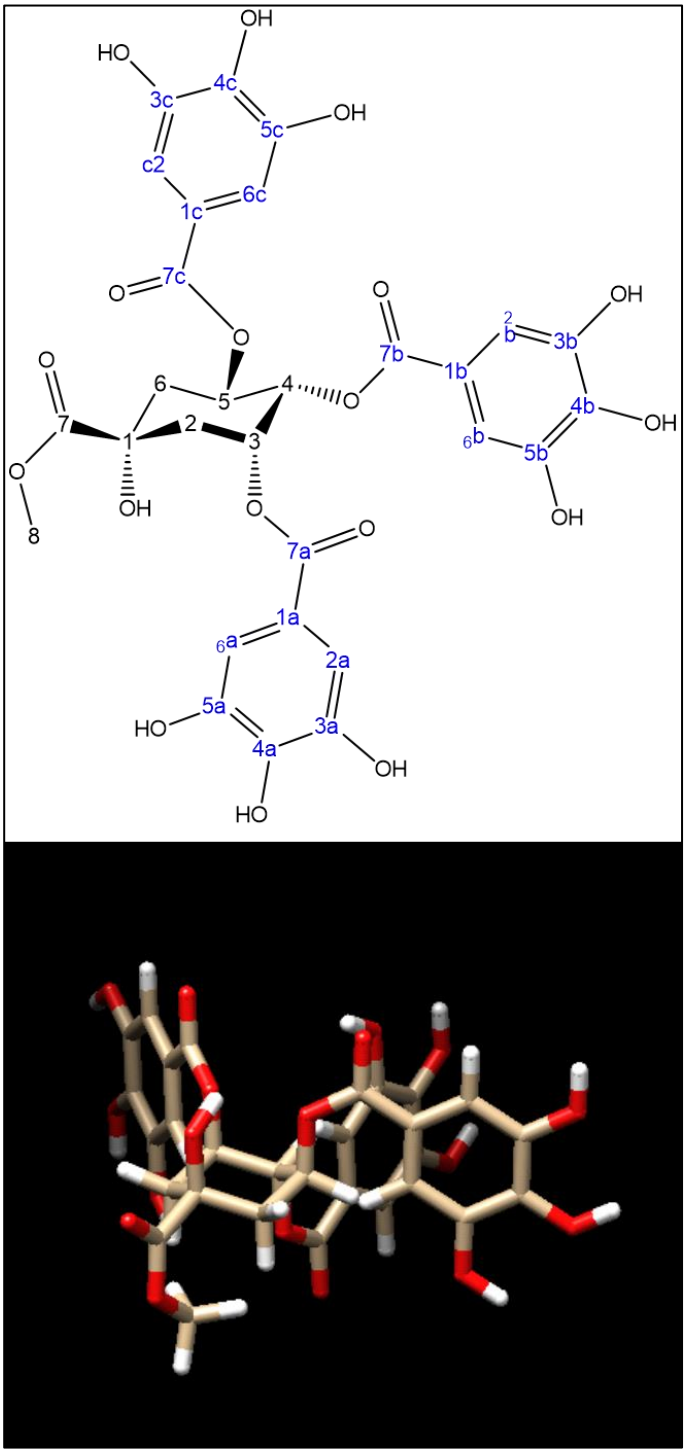

Figure 3. Chemical structure of 3,4,5-tri-*O*-galloylquinic acid methyl ester (TGAME, 6). The 3D structure was drawn by Chimera 1.11.2 software.

3.2 Materials and methods

The synthesis of 3,4,5-tri-*O*-galloylquinic acid methyl ester (TGAME, 6) is summarized in the following scheme:

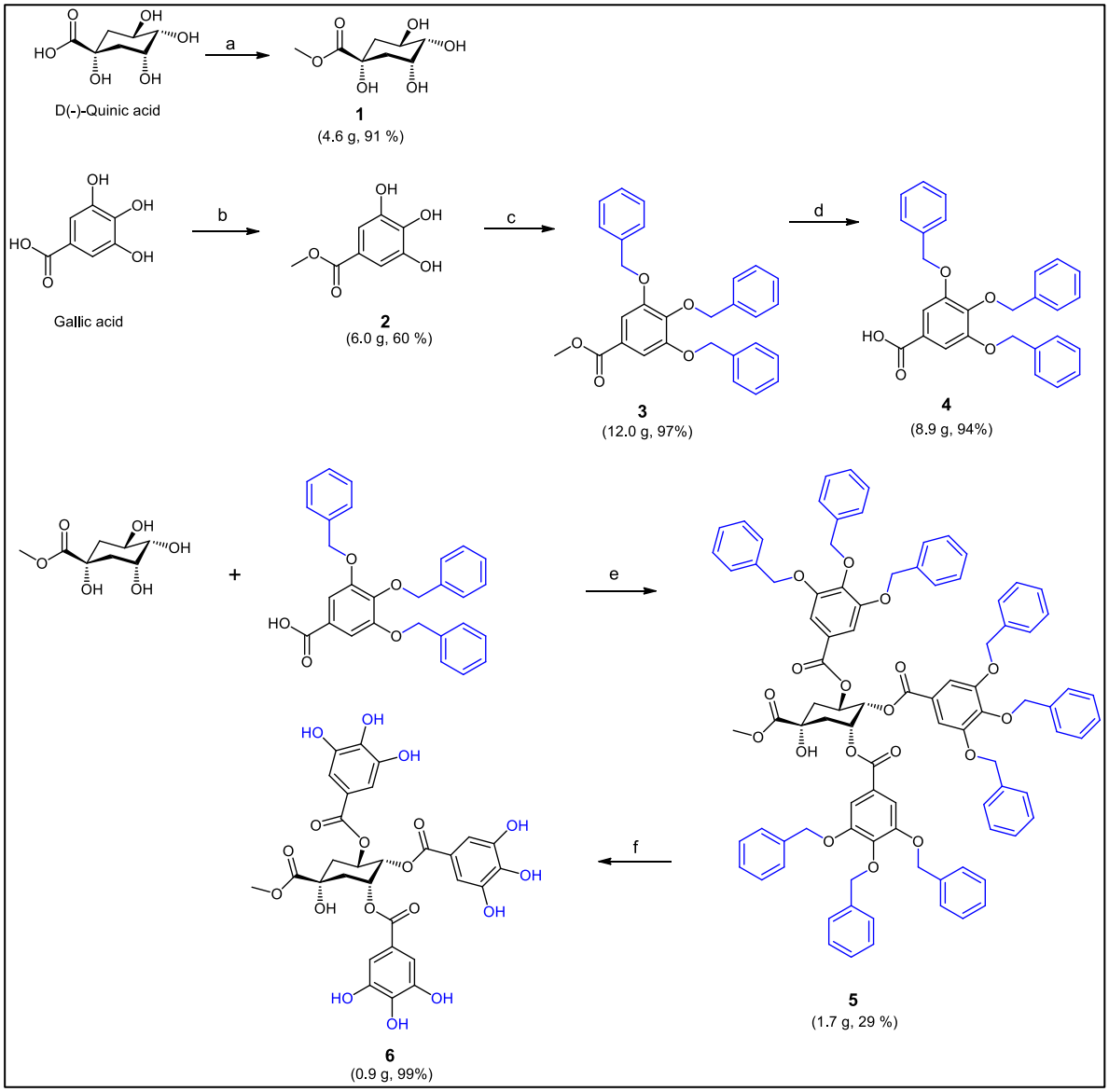

Scheme 1. Schematic representation of the synthesis of 3,4,5-tri-*O*-galloylquinic acid methyl ester (TGAME, 6). Reagents and conditions: (a) & (b) H_2SO_4, methanol, reflux for 18 h for (a) and 24 h for (b); (c) KI, K_2CO_3, benzyl chloride, acetone, reflux/21 h; (d) NaOH, ethanol, reflux/2 h then HCl; (e) DCC, DMAP, CH_2Cl_2, reflux/72 h followed by purification using silica gel column chromatography, $CHCl_3$/methanol (100:1); (f) H_2, pressure 80 psi equivalent to 6 kgf/cm^2, ethyl acetate, 10% Pd/C for 6 h.

The purity of the tested compound were determined by HPLC analysis and MS error of precision data as being ≥ 98%. All methods were performed using anhydrous solvents purchased from commercial vendors and used without further purification. Quinic and gallic acids were purchased from Sigma Adrich, Germany in addition to all other reagents. Hydrogenolysis was performed using a hydrogen reactor system (FAMABRAS, IND. BRAS. 1/8, 255046, Brazil) supported with pressure controller (CLASSE B ABNT).

All melting points (°C, uncorrected) were determined in capillary tubes using Fisatom™ melting point device (Mod. 431, Brazil, Serie 1237344).

Optical rotation $[\alpha]_D^{25}$ was done using polarimeter (Jasco P-2000), Serial No. A104161232, Japan) at 25°C and a wavelength of 589 nm. Methanol and chloroform were used as solvents. Three readings of $[\alpha]_D^{25}$ were recorded and the average was taken.

Chromatographic purification was performed based on flash chromatography using silica gel (pore size 60A°, 40-63 µm, Sigma, batch #MKBC6227) and the solvent systems indicated. Solvent systems are expressed as v/v percent ratios. All reactions were monitored by TLC using fluorescent precoated silica gel plates (Merck, Germany) at short wavelength. Molybdate/H_2SO_4 spray solution was used as the raveling reagent.

The IR spectra were recorded using FT-IR spectrophotometer (Perkin Elmer Spectrum Two) in the range of 400-4000 cm^{-1} by KBr pellet technique.

The analytical HPLC analysis was performed on a Shimadzu LC-10ADvp (Japan) operated with multisolvent delivery system, equipped with a Shimadzu SPD-MICAvp photodiode array detector (PDA). Analyses were performed using analytical reversed phase column (Polar-RP C 80 A) with dimensions of 150 mm × 4.6 mm (Shimadzu) and a particle diameter of 4 μm; the mobile phase consisted of acidified water (A) (0.1% formic acid in water) and methanol (B) in gradient conditions as follows: 15-50% of B (45 min), 50-90% of B (45-65 min) and 90-15% of B up to 75 min; flow rate, 1 mL/min, with injection volume of 20 µL. All samples were dissolved in HPLC grade methanol (2 mg/mL) and filtered through 0.45 µm filter prior to automatic injection.

Mass spectra were acquired on a high resolution MicroTOF II-Q mass Spectrometer (Bruker Daltonics, Billerica, MA, US) fitted with an ESI operating system in the positive and negative ion modes. Accurate masses were obtained using TFA-Na^+ (sodiated trifluoroacetic

acid, 10 mg/mL) as the internal standard; end plate: - 500 volts; capillary: 3500 volts; dry gas temperature: 180°C with flow rate 4L/min; nebulizer gas pressure: 0.4 bar of nitrogen gas; infusion bomb model: Cole Parmer with a flow rate 300 μL/h.

^{1}H NMR, ^{13}C NMR, and two-dimensional (2D) spectroscopic techniques were recorded on a Bruker-Avance DRX500 spectrometer operating at a frequency of 500 MHz. Samples were dissolved in Aldrich deuterated dimethyl sulfoxide (DMSO-*d*6) for compounds 1-4, 6 and chloroform ($CDCl_3$) for compound 5. Data for ^{1}H NMR are reported as follows: chemical shift (δ, ppm), multiplicity (s = singlet, d = doublet, t = triplet, m = multiplet, coupling constant (s) in Hz, integration). Data for ^{13}C NMR are recorded in terms of chemical shift (δ, ppm).

3.2.1 Synthetic steps of TGAME

3.2.1.1 Synthesis of quinic acid methyl ester. methyl-(1*S*,3*R*,4*S*,5*R*)-1,3,4,5 tetrahydroxycyclohexanecarboxylate (Compound 1)

To a stirred solution of methanol (160 mL) and sulfuric acid (2 mL), quinic acid (4 g) was added. The mixture was refluxed at 79-80°C for 18 h. TLC analysis demonstrated whole conversion of quinic acid into a single product spot (R_f = 0.56; ethyl acetate /methanol/water/formic acid = 6:3:3:0.2). The reaction mixture was then poured over solid $NaHCO_3$ until no effervescence (neutralization was detected by litmus paper), and then it was filtered. The filtrate was evaporated to give a solid crude hygroscopic residue (8.67 g) that was recrystallized in methanol to give rosette crystals (4.60 g, 91%) with undefined melting point and molecular formula of $C_8H_{14}O_6$.

3.2.1.2 Synthesis of methyl 3,4,5-trihydroxybenzoate (compound 2)

Sulfuric acid (1 mL) was added drop-wise to a stirred solution of gallic acid in methanol (10 g dissolved in 100 mL methanol). The resulting reaction mixture was refluxed for 24 h. The solvent was evaporated and an off-white precipitate was obtained which was dissolved in ethyl acetate (150 mL). The organic phase was washed with distilled water (3 X 20 mL) and sodium bicarbonate solution (3 X 20 mL), successively. The organic phase was dried over anhydrous sodium sulphate, then evaporated to furnish 8 g of a yellowish-white precipitate (R_f = 6.3; ethyl acetate /formic acid = 8:2). The product was purified by recrystallization in methanol and clusters of plate-like crystals (Figure 4) were formed (6 g, 60%); mp 200-202°C; molecular formula $C_8H_8O_5$.

Figure 4. Crystals of compound 2.

3.2.1.3 Synthesis of methyl 3,4,5-tribenzyloxybenzoic acid (compound 3)

Compound 2 (5 g (27.15 mmol)), 2 g (12 mmol) of KI and 22 g (159 mmol) of dry K_2CO_3 were mixed in 250 mL of acetone and stirred for 20 min at room temperature (RT). Next, 11 g (87 mmol) of benzyl chloride in 50 mL of acetone was added portion-wise. The suspension was refluxed for 21 h. TLC screening revealed a single spot (Figure 5) of the formed product (R_f = 0.30; hexane:ethyl acetate = 8:2). The reaction mixture was filtered, then the filtrate was concentrated under vacuum. The resulting residue was re-suspended in 200 mL of CH_2Cl_2, then filtered through Celite (Figure 6) and was concentrated under vacuum. The product was obtained as off-white solid (12 g, 97%). Molecular formula $C_{29}H_{26}O_5$.

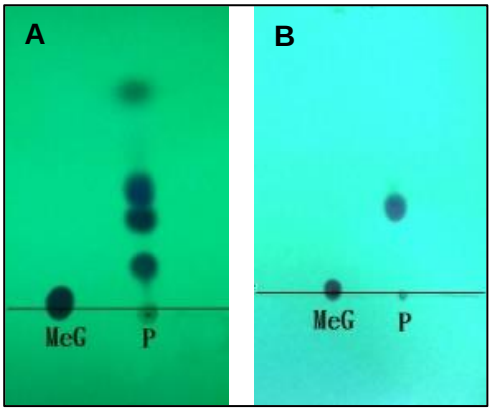

Figure 5. TLC screening of (MeG, compound 2) and its reaction product (P, compound 3). (A) After 4.5 h. (B) After 21 h. TLC mobile phase system: hexane: ethyl acetate; 8:2. Revealed under UV lamp λ_{254} nm. R_f of the product is 0.33.

Figure 6. Purification of compound 3 by filtration through celite under vacuum.

3.2.1.4 Synthesis of 3,4,5-tribenzyloxybenzoic acid (compound 4)

Compound 3 (10 g) was mixed with a solution of 1.77 g (44.25 mmol) sodium hydroxide in 250 mL of 95% ethanol. The resulting mixture was heated up for 2 h with reflux followed by immediate pouring into 260 mL of 0.6 M HCl and stirred for 10 min, and finally filtered under vacuum. The resulting polar product (Figure 7) was washed with a 1:1 mixture of 95% ethanol and water (50 mL), followed by pure water (50 mL), 95% ethanol (50 mL), methanol (2 X 25 mL), and diethyl ether (25 mL). The yield was dried under vacuum overnight to give a white solid (8.9 g, 94%); mp 192-195^{o}C with a molecular formula of $C_{28}H_{24}O_5$.

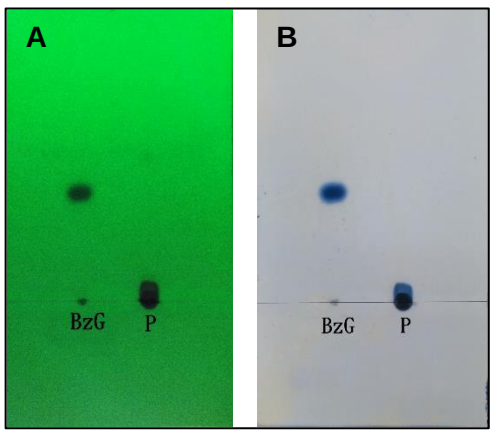

Figure 7. TLC screening of (BzG, compound 3) and its hydrolytic reaction product (P, compound 4). **(A)** Revealed under UV lamp λ_{254} nm and **(B)** Sprayed with molybdate reagent. TLC mobile phase system: hexane: ethyl acetate; 8:2.

3.2.1.5 Synthesis of (1*S*,3*R*,4*S*,5*R*)-1-hydroxy-1-(methoxycarbonyl)cyclohexane-3,4,5-triyl tris (3,4,5-tris (benzyloxy) benzoate) (compound 5)

A suspension of 7 g (16 mmol) of 3,4,5-tribenzyloxybenzoic acid, 0.82 g (4 mmol) of methyl quinate, 4 g (20 mmol) of dicyclohexylcarbodiimide (DCC), and 12.24 g (18.4 mmol) of N,N-(dimethylamino) pyridine (DMAP) in 500 mL of dry dichloromethane was refluxed for 72 h. The reaction was monitored by TLC (dichloromethane/toluene/ethyl acetate = 7.5:2.5:0.1) (Figure 8). After cooling to RT, the mixture was filtered and then concentrated using a rotary evaporator. The resulting crude residue (14.5 g) was purified by flash chromatography (two times, 97 fractions of 20 mL each were collected/per one time) (Figure 9) using a mixture of chloroform/methanol (100:1). The desired product fractions (f 71 to 81 and f 82 to 91) were combined and concentrated to give (1.74 g, 29%) of a faint yellowish-white glassy material (R_f = 0.2); mp 129-130°C; molecular formula $C_{92}H_{80}O_{18}$; $[\alpha]_D^{25}$: - 49.2 (*c* 0.15; $CHCl_3$); *m/z* $[M+H]^+$ 1473.5239, MS $[M+Na]^+$ 1496.5005, MS $[M+K]^+$ 1511.4664.

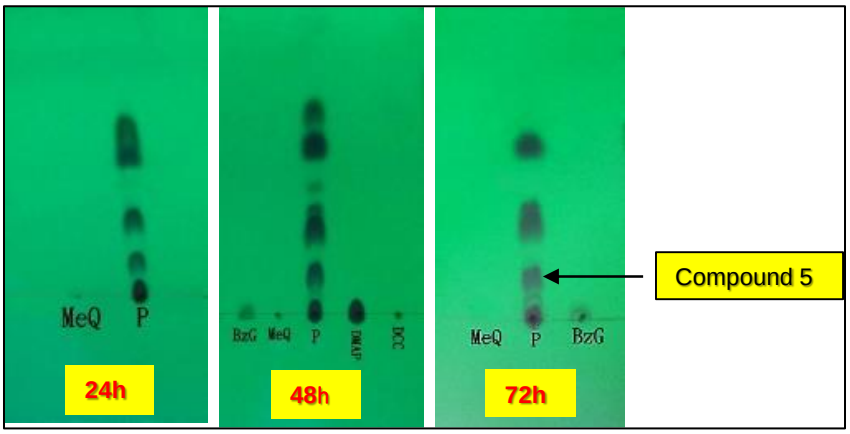

Figure 8. TLC monitoring of the coupling reaction of compound 1 (MeQ) and compound 4 (BzG) using DCC and DMAP after 24, 48 and 72 h.

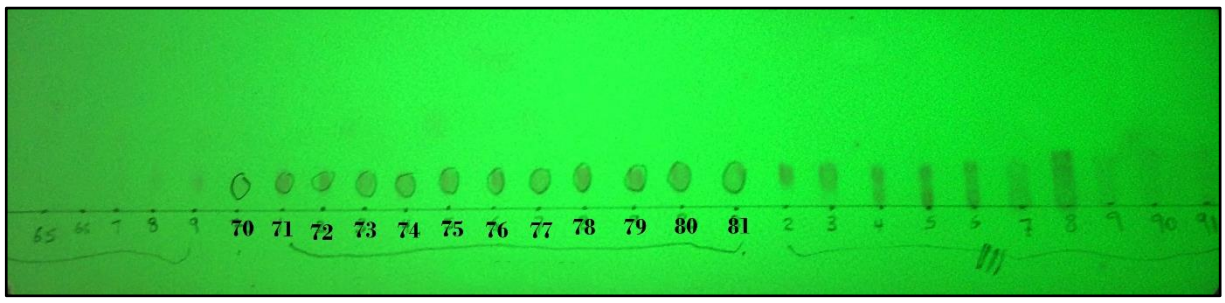

Figure 9. TLC screening of the fractions obtained by flash chromatography for the purification

of the product obtained by coupling reaction of compound 1 and compound 4. Fractions of 71-81 are of interest (compound 5). Revealed under UV lamp λ_{254} nm, (R_f = 0.2; dichloromethane: toluene: ethyl acetate = 7.5:2.5:0.1).

3.2.1.6 Synthesis of TGAME, (1*S*,3*R*,4*S*,5*R*)-1-hydroxy-3,4,5-tris ((3,4,5-trihydroxybenzoyl) oxy) cyclohexanecarboxylic acid (compound 6)

A suspension of 44 mg of palladium (10 wt % on activated carbon) and 200 mg of compound 5 in 15 mL of dry ethyl acetate was stirred at RT for 6 h inside a cell of a hydrogen reactor system (Figure 10) at RT under a hydrogen gas atmosphere with a pressure of 80 psi, equivalent to 6 kgf/cm^2. Next, the reaction mixture was filtered through Celite filter-aid using a mixture of ethyl acetate and methanol. The filtrate was concentrated under vacuun and the obtained residue was lyophilized, recrystallized in ethyl acetate to give light yellow amorphous solid (93 mg, 99%).

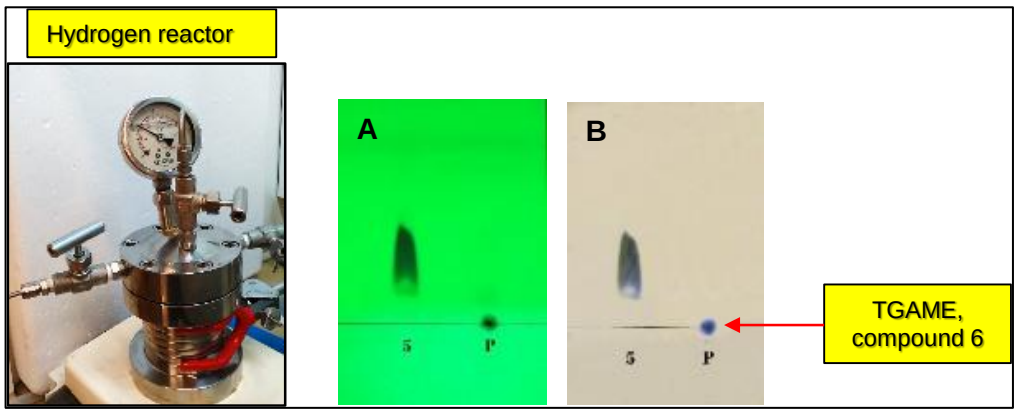

Figure 10. TLC screening of the product P (compound 6) obtained by the hydrogenolysis of compound 5 using hydrogen reactor (Pd/C 10wt %). TLC mobile phase ($CHCl_3$: CH_3OH; 100:1). (A) Revealed under UV light λ_{254} and (B) Sprayed with molybdate reagent.

3.3 Results and discussion

The biological effects of polyphenols are mostly ascribed to the antioxidant properties of their phenolic groups. The galloylation of polyphenols significantly modifies their biological properties (158). An increased activity by increasing the number of galloyl moities is usually reported, but a reduction in activity can also occur. Galloylation was previously shown to affect the physico-chemical properties of polyphenols, which is crucial for the mechanism of their antioxidant activities (159). The presence of galloyl groups affects the ability to donate electrons, chelate iron, and regenerate tocopherol (vitamin E) as well as it also affects the lipophilicity (160, 161). A previous publication documented that epigallocatechin gallate (a polyphenolic compound) strongly interacts with phospholipid bilayers due to hydrogen bond formation, and it inhibits COM crystal adhesion to renal tubular cells by decreasing α-enolase (COM-binding protein) surface expression (117). On this basis, we decided to synthesize the tri-substituted galloylquinic acid with the goal of developing a compound for kidney stone prevention.

The total synthesis included six steps starting from commercially available quinic and gallic acids as shown previously in Scheme 1. The key step in the synthetic pathway was Steglich esterification (162) of methyl quinate with 3,4,5-tribenzyloxybenzoic acid using dicyclohexylcarbodiimide (DCC) and N,N-(dimethylamino) pyridine (DMAP) as the coupling reagents. This type of esterification is a mild one, which allowed the conversion of the sterically demanding and acid labile methyl quinate, a compound with complex stereochemistry, into the triester form. A protection protocol using benzyl chloride was applied for the hydroxyl groups of gallic acid to mask their reactivity and formation of undesired side products. The proposed mechanism of the reaction is illustrated in Scheme 2. A common explanation of DMAP catalysis suggests that it is a stronger nucleophile than methyl quinate. Therefore, it reacts with the *O*-acylisourea leading to formation of a reactive amide "active ester". This intermediate cannot form intramolecular side products, but reacts rapidly with methyl quinate – OH alcohol groups. DMAP acts as an acyl transfer reagent in this way, and subsequent reaction with the aliphatic – OH gives the ester. From the broad variety of the previously-reported acylation conditions employed, using 3,4,5 tribenzyloxybenzoic acid as the reagent to acylate quinic acid in the presence of DDC and 4-dimethylaminopyridine at 60°C provided the best results (163). Interestingly, the acylation reaction was regioselective in the case of the benzyl ester and exclusively yielded the tri-acylated product. The tetra-acylated derivative was not formed. This

behavior is thought to be due to a sterically hindered hydrogen bridge that deactivated 1-hydroxy group of methyl quinate.

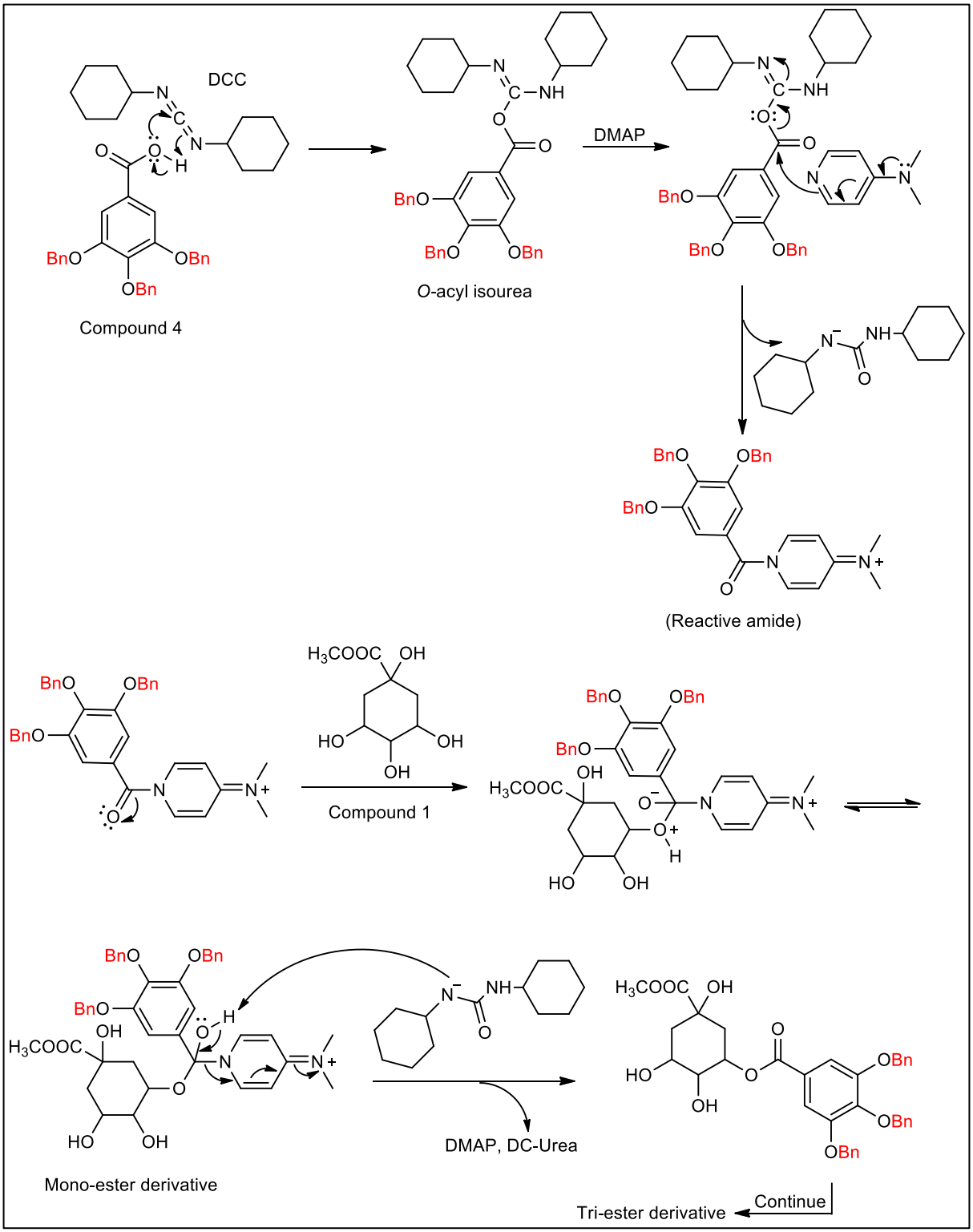

Scheme 2. The proposed mechanism of the coupling reaction between compound 1 and 4 for the synthesis of 3,4,5-tri-*O*-galloylquinic acid methyl ester (TGAME, 6).

The chemical structures of the final compound and its synthetic intermediates were elucidated by spectroscopic, spectrometric and spectrophotometric means of analyses. Compound 1 was obtained as rosette crystals after crystallization with methanol (4.60 g, 91%) with undefined melting point and a molecular of formula $C_8H_{14}O_6$. Compound 2 was obtained as clusters of plate-like crystals in methanol (6 g, 60%); mp 200-202ºC with a molecular formula of $C_8H_8O_5$. Compound 3 was obtained as an off-white solid (12 g, 97%); with a molecular formula $C_{29}H_{26}O_5$. Compound 4 was in the form of white solid (8.9 g, 94%); mp 192-195ºC; $C_{28}H_{24}O_5$. Compound 5 was obtained as a faint yellowish-white glassy material (1.74 g, 29%); mp 129-130°C with a molecular of formula $C_{92}H_{80}O_{18}$; $[\alpha]_D^{25}$: - 49.2 (*c* 0.15; $CHCl_3$). The R_f values of the TLC screening are summarized in Table 1.

Table 1. TLC screening of the desired synthetic compound 6 and its reaction intermediates.

Compound #	Mobile phase system	R_f value
Compound 1	Ethyl acetate/CH_3OH /H_2O/formic acid;6:3:3:0.2	0.56
Compound 2	Ethyl acetate /formic acid = 8:2)	6.30
Compound 3	Hexane/ethyl acetate; 8:2	0.30
Compound 4	Hexane/ethyl acetate; 8:2	-
Compound 5	CH_2Cl_2/toluene/ethyl acetate; 7.5:2.5:0.1	0.20
Compound 6	$CHCl_3$/CH_3OH; 100:1	-

The desired synthetic compound TGAME was obtained as a light yellow amorphous solid (93 mg, 99%) with mp 137-140˚C. The compound specific rotation $[\alpha]_D^{25}$ was - 42.6, which is levorotatory similar to the naturally occurring one in plants (156). The HPLC-UV (Figure 11) analysis of the product demonstrated one single peak with t_R at 33.57 min. The UV spectrum of this peak showed two characteristic bands at 225 and 275 nm, indicating that the compound belongs to the galloylquinic acids class.

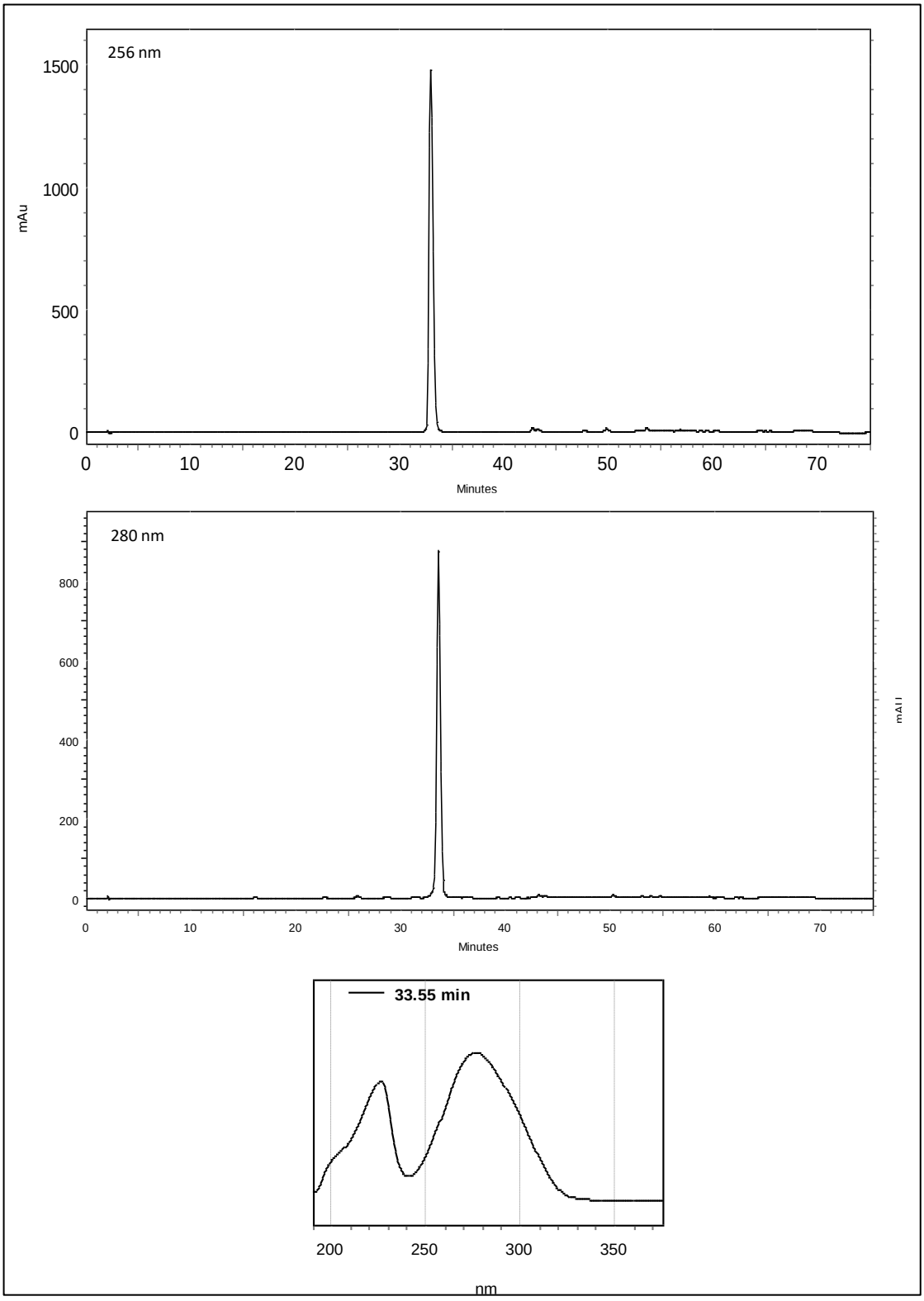

Figure 11. HPLC-UV analysis of TGAME (compound 6).

The IR spectral data of compound 6 and the synthetic intermediates are summarized in (Figure 12 and Table 2). TGAME showed a broad band at 3387 cm^{-1} indicating the presence of hydroxyl groups, which are H-bonded. A characteristic carbonyl group of the ester appeared at 1707 cm^{-1}. The bands at 1216 and 1034 indicated the presence of a C−O functional group. Two bending bands of C−H appeared at 1475 and 1338 cm^{-1} reflecting an aliphatic methyl group.

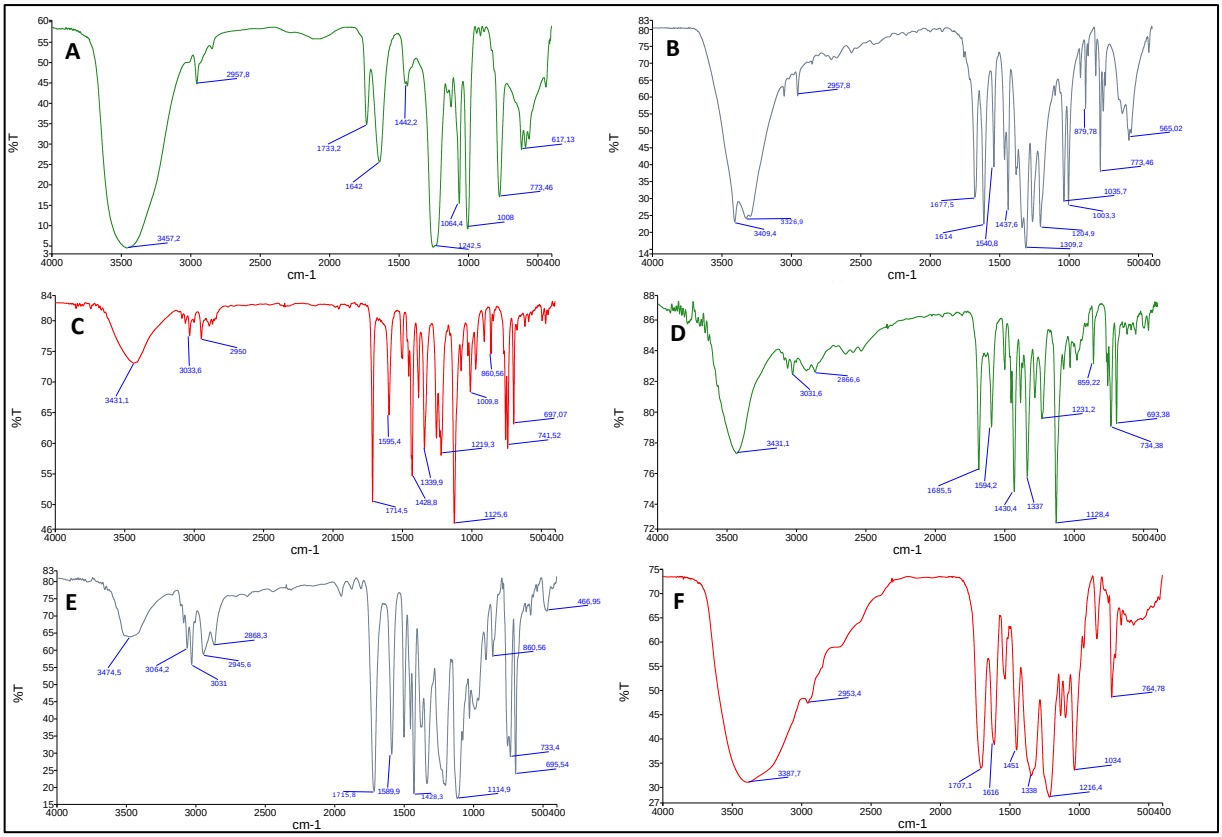

Figure 12. FTIR spectra of compounds 1-6 (A-F), respectively.

Table 2. Frequencies of the characteristic absorption bands in FTIR spectra of the formed intermediates used in the synthesis of 3,4,5-tri-*O*-galloylquinic acid methyl ester in (cm^{-1}).

Functional group	**1**	**2**	**3**	**4**	**5**
	Frequency in cm^{-1}				
υ (O−H)	3457 (H-bonded)	3326	—	3431	3474 (H-bonded)
υ C−H aromatics	—	—	3033 (stretch)	3031 (stretch)	3064 and 3031
υ (C−H) aliphatic	2957	2957	2950	2866	2945 and 2868 (stretch)
υ (C═O)	1733	1677	1714	1685	1715
υ (C−C) aromatics	—	1614, 1540 and 1473	1595 and 1428	1594 and 1430	1589
υ C−H (−CH_3)	—	—	—	—	1428
υ C−H (−CH_2−)	1442 (bend)	—	1428 (bend)	1430 (bend)	1428 (bend)
υ (C−O)	1242, 1064 and 1008	1309, 1204, 1003 and 1035	1339, 1219, 1125 and 1009	1337, 1231, 1128	1114
υ C−H aromatics	—	879 and 773 (out-of-plane bend)	860, 741 and 697	859, 734 and 693	860, 733 and 695 (out-of-plane bend)

The NMR data of TGAME and its synthetic intermediates are summarized in (Tables 3-7 and Appendix I) revealed the presence of quinic acid core substituted at the C-3, C-4 and C5 positions by galloyl moieties. The ^{13}C NMR spectrum exhibited five aliphatic signals due to two methylene carbons (C-2 and C-6) and three oxymethine carbons (C-3, C-4 and C-5), as confirmed by *DEPT*, in addition to a quaternary carbon (C-1), a carbonyl signal (C-7) and a methoxy (C-8). These NMR data are in agreement with those of quinic acid (150) which has its unique stereochemistry pre-established before from shikimate pathway and through the coupling constants of its ^1H NMR spectra. The galloyl units were indicated by the carbon signals with chemical shifts between 109 and 165 ppm (^{13}C NMR), as well as by the hydrogen signals with chemical shifts between “6.89 to 6.92” (^1H NMR).

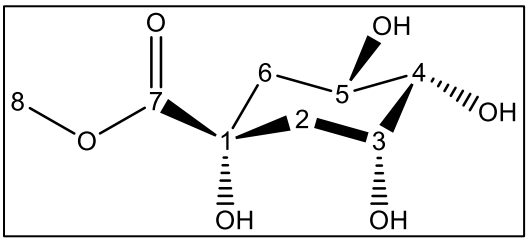

Compound 1 (quinic acid methyl ester or methyl quinate)

(Methyl-(1*S*,3*R*,4*S*,5*R*)-1,3,4,5 tetrahydroxycyclohexanecarboxylate)

Table 3. ^{1}H NMR (500 MHz) and ^{13}C NMR (125 MHz) data for compound 1 in DMSO-d_6.

Position	δ_H (ppm)	δ_C (ppm)
1	–	74.0
2	1.92 (1H, dd)	37.6
	1.71 (1H, dd)	
3	3.74 (1H, m)	51.7
4	3.31 (1H, dd)	67.1
5	3.84 (1H, m)	48.7
6	1.82 (2H, m)	37.6
7	–	174.2
8 (-CH_3)	3.50 (3H, s)	53.0
H (-OH)	4.11 (2H, s)	–
H (-OH)	4.62 (2H, s)	–

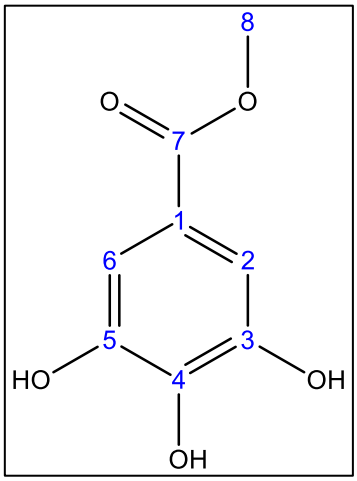

Compound 2

(Methyl 3,4,5-trihydroxybenzoate)

Table 4. ^{1}H NMR (500 MHz) and ^{13}C NMR (125 MHz) data for compound 2 in DMSO-d_6.

Position	δ_H (ppm)	δ_C (ppm)
1	–	119.3
2	6.94 (1H, s)	108.5
3	–	145.6
4	–	138.5
5	–	145.6
6	6.94 (1H, s)	108.5
7	–	166.4
8 (-CH_3)	3.74 (3H, s)	51.6

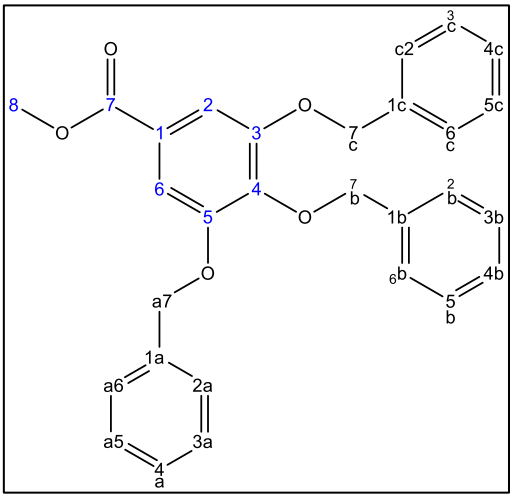

Compound 3

(Methyl 3,4,5-tribenzyloxybenzoic acid)

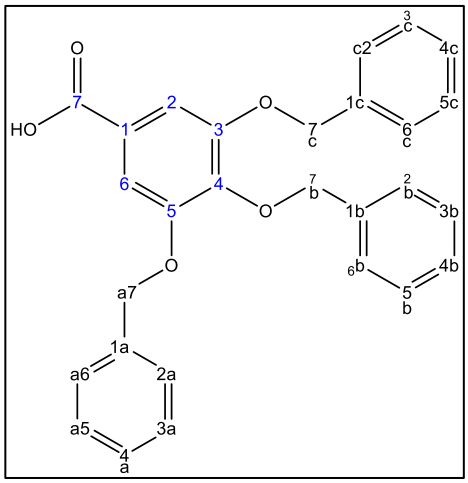

Compound 4

(3,4,5-tribenzyloxybenzoic acid)

Table 5. ^{1}H NMR (500 MHz) and ^{13}C NMR (125 MHz) data for compound 3 and 4 in DMSO-d_6.

Position	3		4	
	δ_H (ppm)	δ_C (ppm)	δ_H (ppm)	δ_C (ppm)
1	–	124.8	–	126.2
2	7.25 (1H, s)	108.1	7.25 (1H, s)	108.2
3	–	152.1	–	152.0
4	–	141.3	–	140.9
5	–	152.1	–	152.0
6	7.26 (1H, s)	108.1	7.26 (1H, s)	108.2
7	–	165.8	–	166.9
8	3.83 (3H, s)	52.3	–	
1a	–	136.7	–	136.9
2a	7.27 (1H, s)	128.4	7.28 (1H, s)	128.4
3a	7.28 (1H, s)	127.6	7.29 (1H, s)	127.6
4a	7.29 (1H, s)	128.1	7.30 (1H, s)	128.1
5a	7.30 (1H, s)	127.6	7.31 (1H, s)	127.6
6a	7.31 (1H, s)	128.4	7.32 (1H, s)	128.4
7a	5.18 (s, 2H)	70.3	5.18 (2H, s)	70.2
1b	–	137.3	–	137.4
2b	7.40 (1H, s)	128.4	7.38 (1H, s)	128.4
3b	7.41 (1H, s)	127.6	7.40 (1H, s)	127.6
4b	7.45 (1H, s)	128.2	7.43 (1H, s)	128.2
5b	7.47 (1H, s)	127.6	7.44 (1H, s)	127.6
6b	7.50 (1H, s)	128.4	7.47 (1H, s)	128.4
7b	5.05 (s, 2H)	74.2	5.04 (2H, s)	74.2
1c	–	136.7	–	136.9
2c	7.32 (1H, s)	128.4	7.33 (1H, s)	128.4
3c	7.33 (1H, s)	127.6	7.34 (1H, s)	127.6
4c	7.34 (1H, s)	127.9	7.35 (1H, s)	127.9
5c	7.35 (1H, s)	127.6	7.36 (1H, s)	127.6
6c	7.36 (1H, s)	128.4	7.37 (1H, s)	128.4
7c	5.18 (s, 2H)	70.3	5.18 (2H, s)	70.2

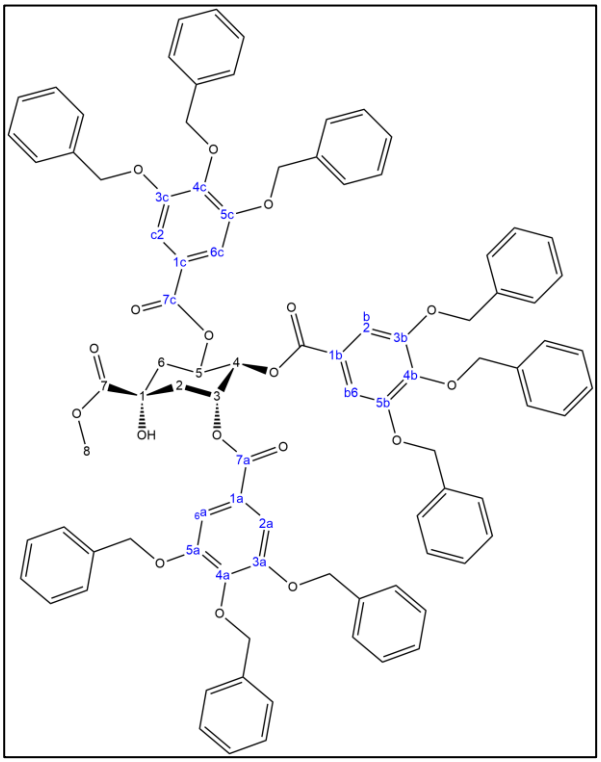

Compound 5

(1*S*,3*R*,4*S*,5*R*)-1-hydroxy-1-(methoxycarbonyl) cyclohexane-3,4,5-triyl tris (3,4,5-tris (benzyloxy) benzoate)

Table 6. ^{1}H NMR (500 MHz) and ^{13}C NMR (125 MHz) data for compound 5 in $CDCl_3$.

Position	δ_H (ppm)	δ_C (ppm)
1	–	75.20
2	2.25 (1H, dd) 2.42 (1H, dd)	39.30
3	5.86 (1H, m)	69.43
4	5.54 (1H, dd)	68.49
5	5.97 (1H, m)	73.49
6	2.52 (1H, dd) 2.27 (1H, dd)	36.13
7	–	174.96
8	3.80 (3H, s)	53.53
(-CH_2)	4.90 (18H, s)	71.10, 71.19, 71.39
C=O		165.39, 165.42, 165.50
H_{Ar}	7.15-7.45 (51H, m)	C_{Ar}:109.26, 109.39, 127.76, 127.79, 128.49, 128.58, 128.64, 128.68, 136.50, 136.75, 136.87, 152.64, 152.75, 152.79

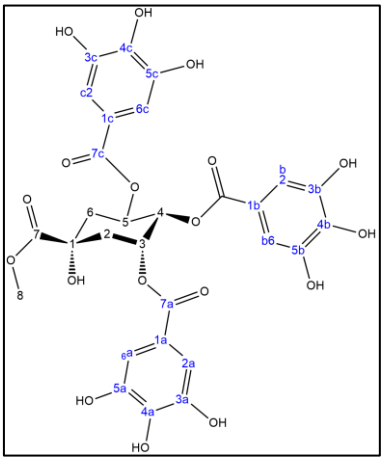

Compound 6, TGAME

(3,4,5-tri-*O*-galloylquinic acid methyl ester)

1*S*,3*R*,4*S*,5*R*)-1-hydroxy-3,4,5-tris ((3,4,5-trihydroxybenzoyl) oxy) cyclohexanecarboxylic acid

Table 7. ^{1}H NMR (500 MHz) and ^{13}C NMR (125 MHz) spectral data for 3,4,5-tri-*O*-galloylquinic acid methyl ester (compound 6) in DMSO-*d*6.

Position	δ_H (ppm)	δ_c (ppm)
Quinic acid moiety		
1	–	72.8
2	2.30 (m, 2H)	29.2
3	4.90 (m, 1H)	68.4
4	5.40 (dd, 1H)	63.3
5	5.60 (m, 1H)	68.6
6	2.40 (m, 2H)	35.5
7	–	173.9
8 (-CH_3)	3.49 (s, 3H)	52.4
-OH (aliphatic)	3.43 (s, 1H)	–
Galloyl moieties		
1a	–	119.8
2a	6.89 (s, 1H)	109.2
3a	–	145.9
4a	–	139.3
5a	–	145.9
6a	6.89 (s, 1H)	109.2
7a	–	165.2
1b	–	119.2
2b	6.92 (s, 1H)	128.1
3b	–	145.8
4b	–	139.0
5b	–	145.8
6b	6.92 (s, 1H)	128.2
7b	–	165.6
1c	–	119.8
2c	6.94 (s, 2H)	128.4
3c	–	145.9
4c	–	139.3
5c	–	145.9
6c	6.94 (s, 2H)	128.7
7c	–	165.0
-OH (phenolic)	3.75 (s, 9H)	–

The HMBC and HSQC spectra of compound 5 (Figure 13) demonstrated key correlations between protons and carbons of quinic and gallic acids units of which agreed with our previous published data (150).

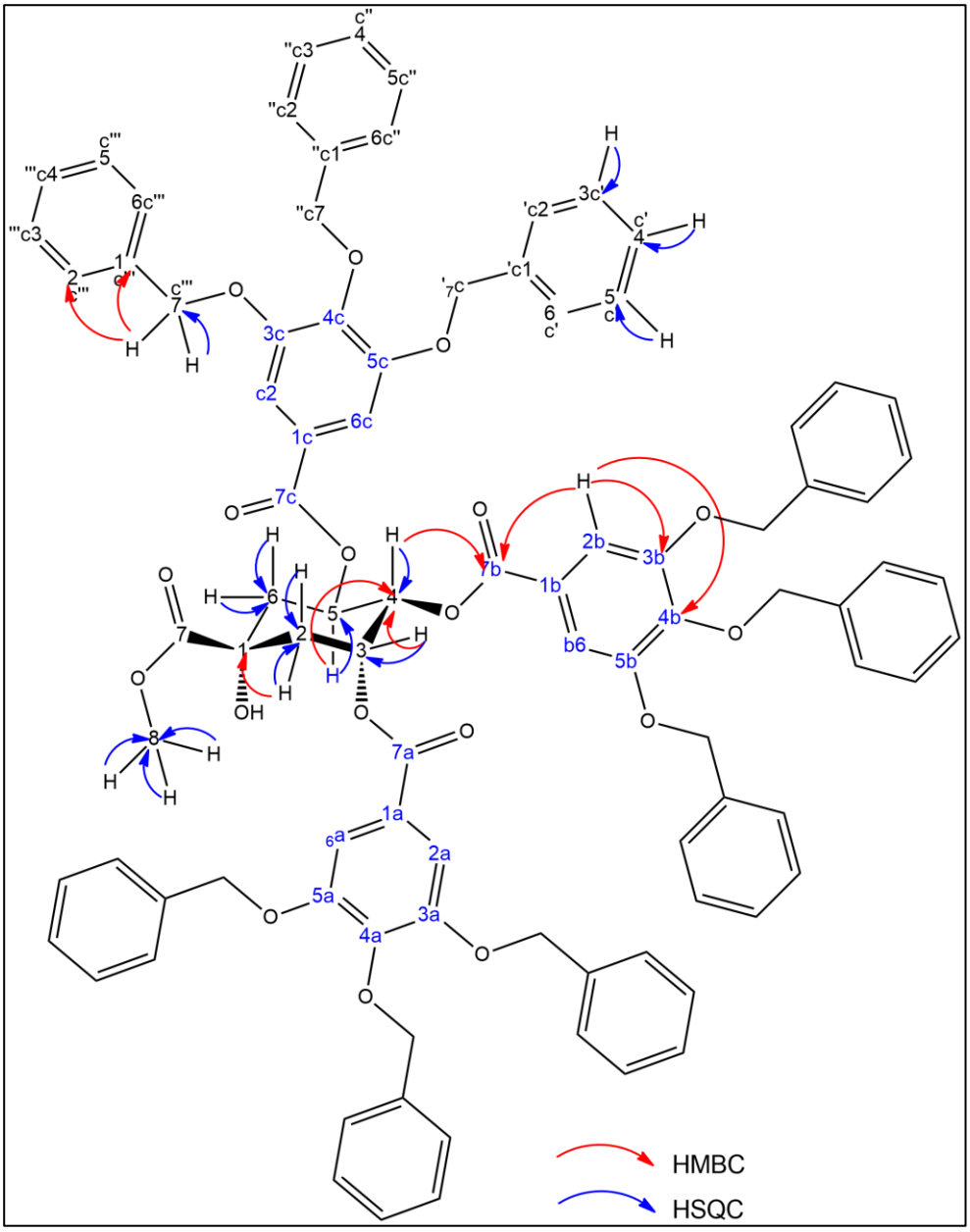

Figure 13. Two dimensional NMR (2D HMBC and HSQC) correlations necessary for identifying the positions of galloyl subunits and the methyl group linked to quinic acid in compound 5 as a pro-synthetic intermediate for compound 6.

The molecular weight of TGAME was determined by ESI-MS/MS in both negative and positive ion modes. The experimental and calculated *m/z* of the protonated molecular ion $[M+H]^+$ were 663.1190 and 663.1200, respectively (Figure 14). The proposed fragmentation pattern of the protonated molecular ion is illustrated in Scheme 3.

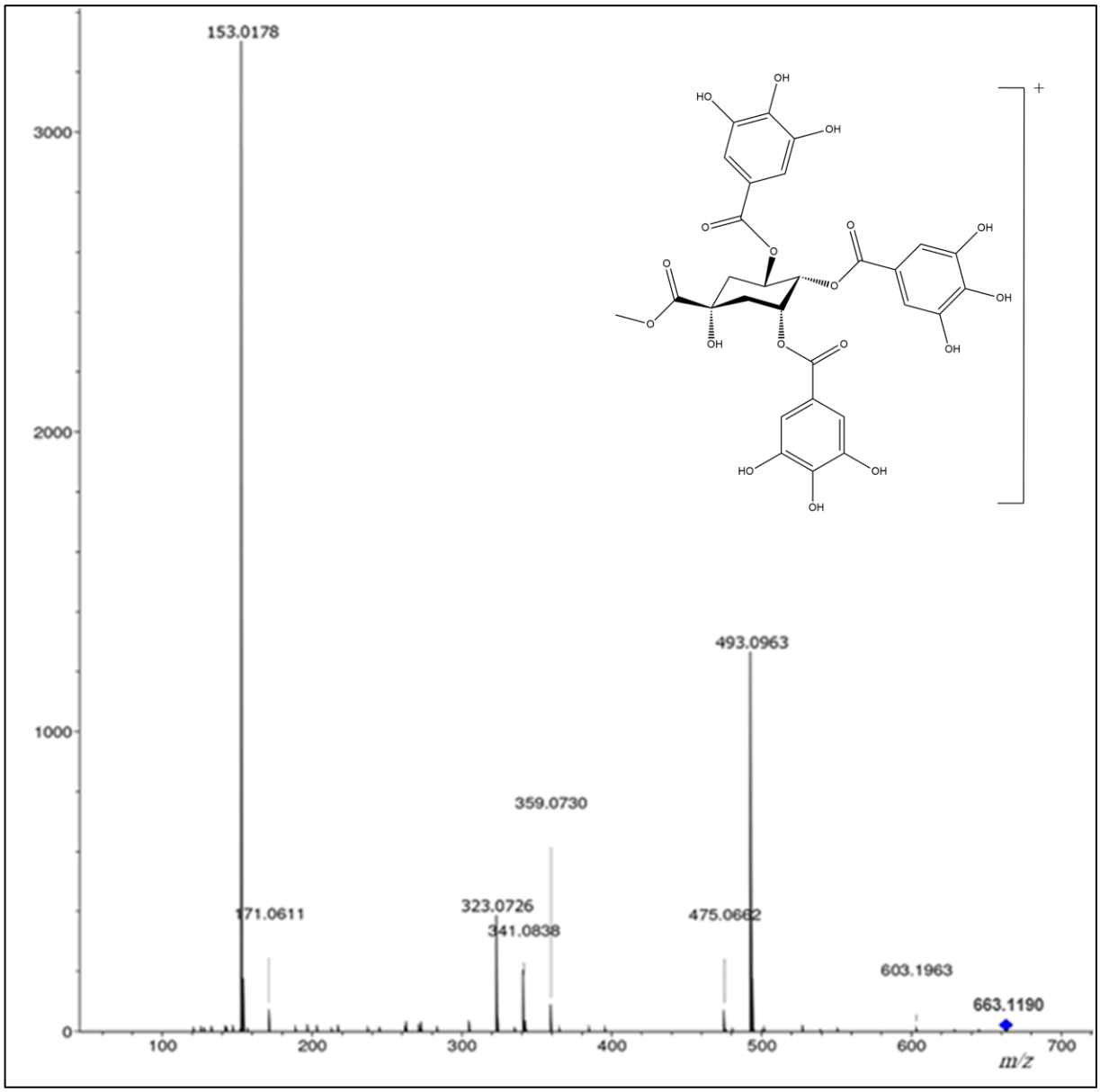

Figure 14. ESI-MS/MS spectrum of compound 6 in the positive ion mode $[M+H]^+$.

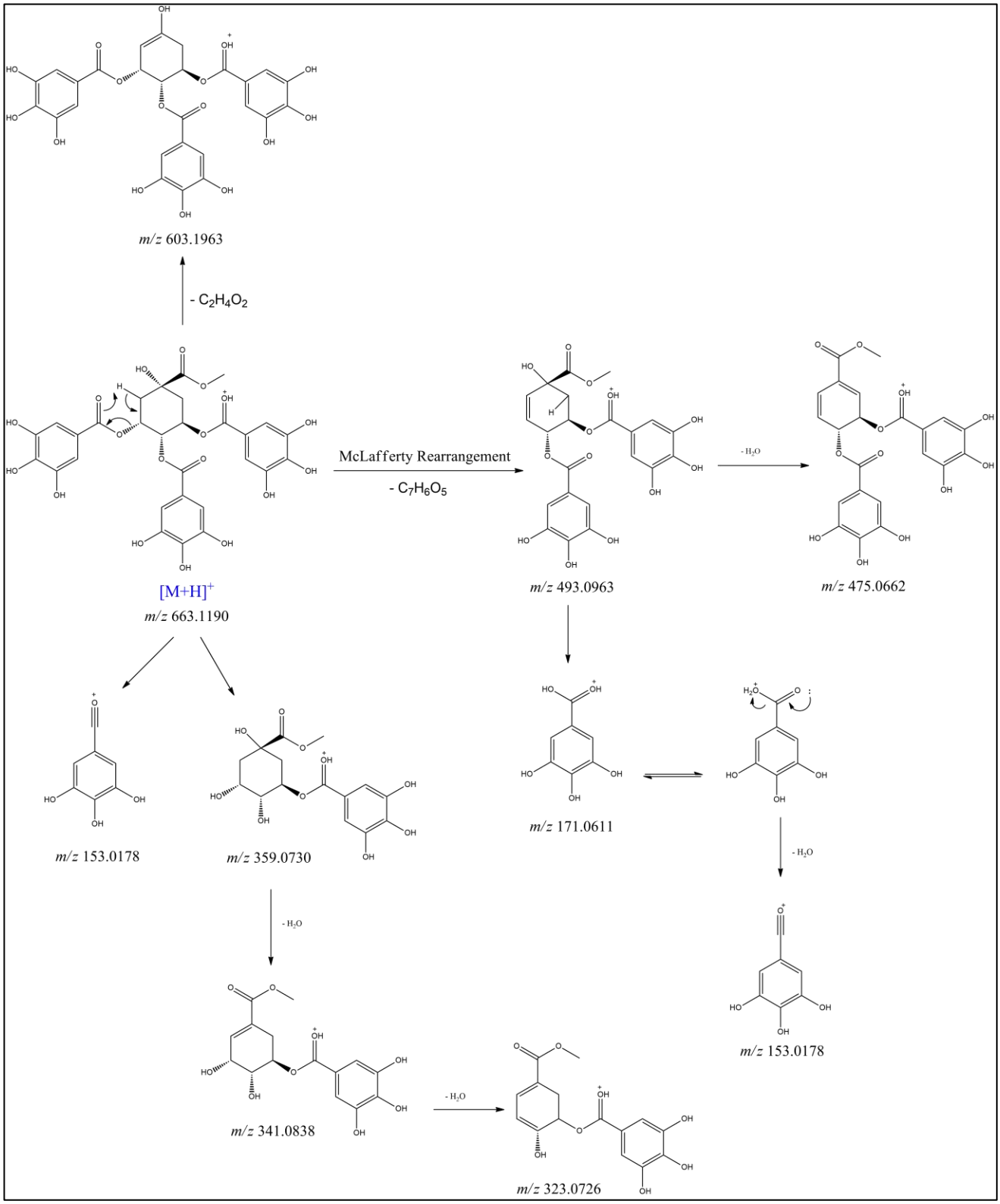

Scheme 3. ESI-MS/MS proposed fragmentation pattern of compound 6 in the positive ion mode. *m/z* $[M+H]^+$ measured 663.1190, calculated $[M+H]^+$ 663.1200.

The MS analysis in the negative ion mode revealed a molecular ion of *m/z* $[M-H]^-$ at 661.0878 (Figure 15). The base peak formed at *m/z* 169.0089 through McLafferty rearrangement pathway. Other fragments were formed through the loss of water and CO_2 as shown in the proposed fragmentation pathways (Scheme 4).

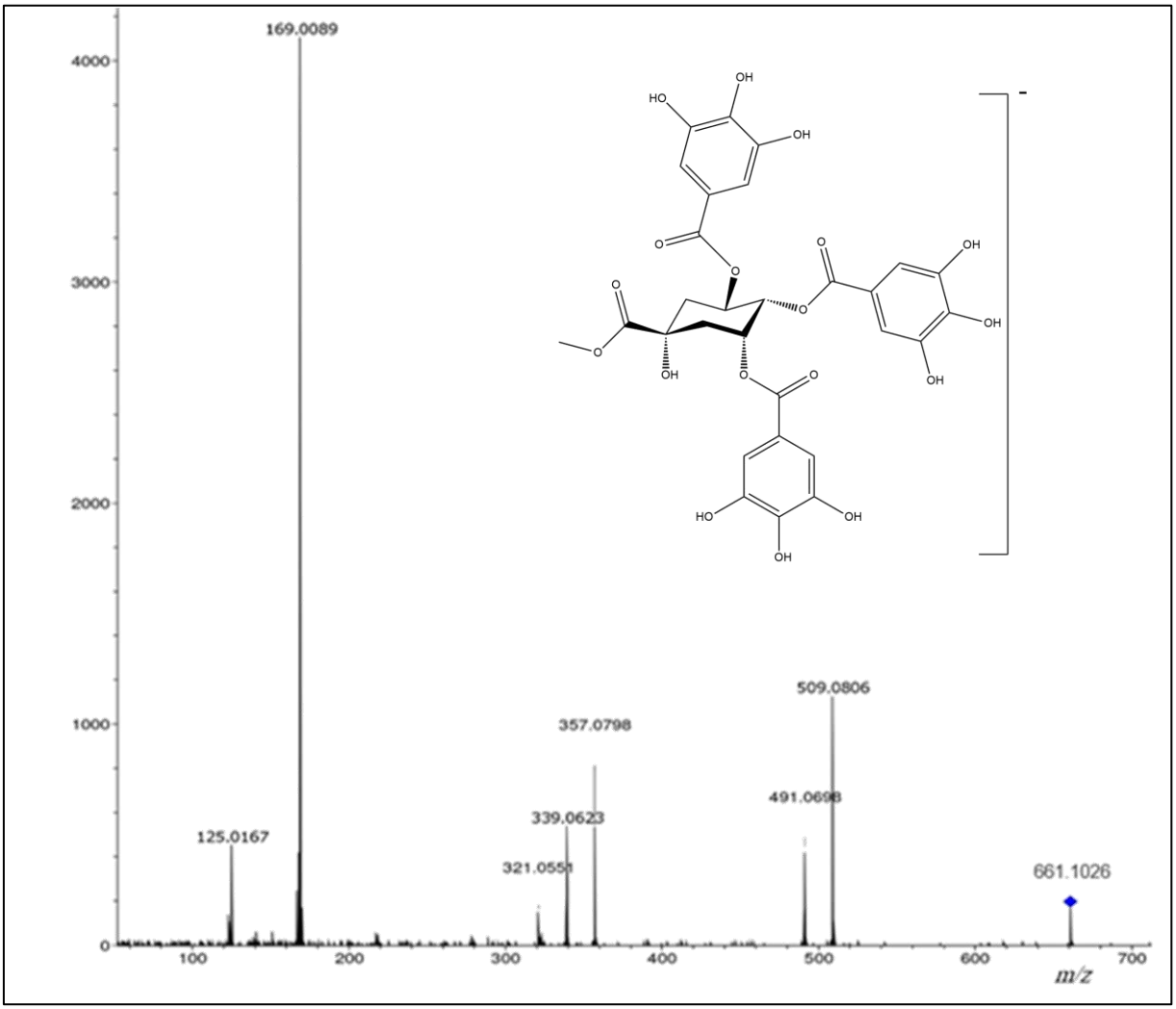

Figure 15. ESI-MS/MS spectrum of compound 6 in the negative ion mode $[M-H]^-$.

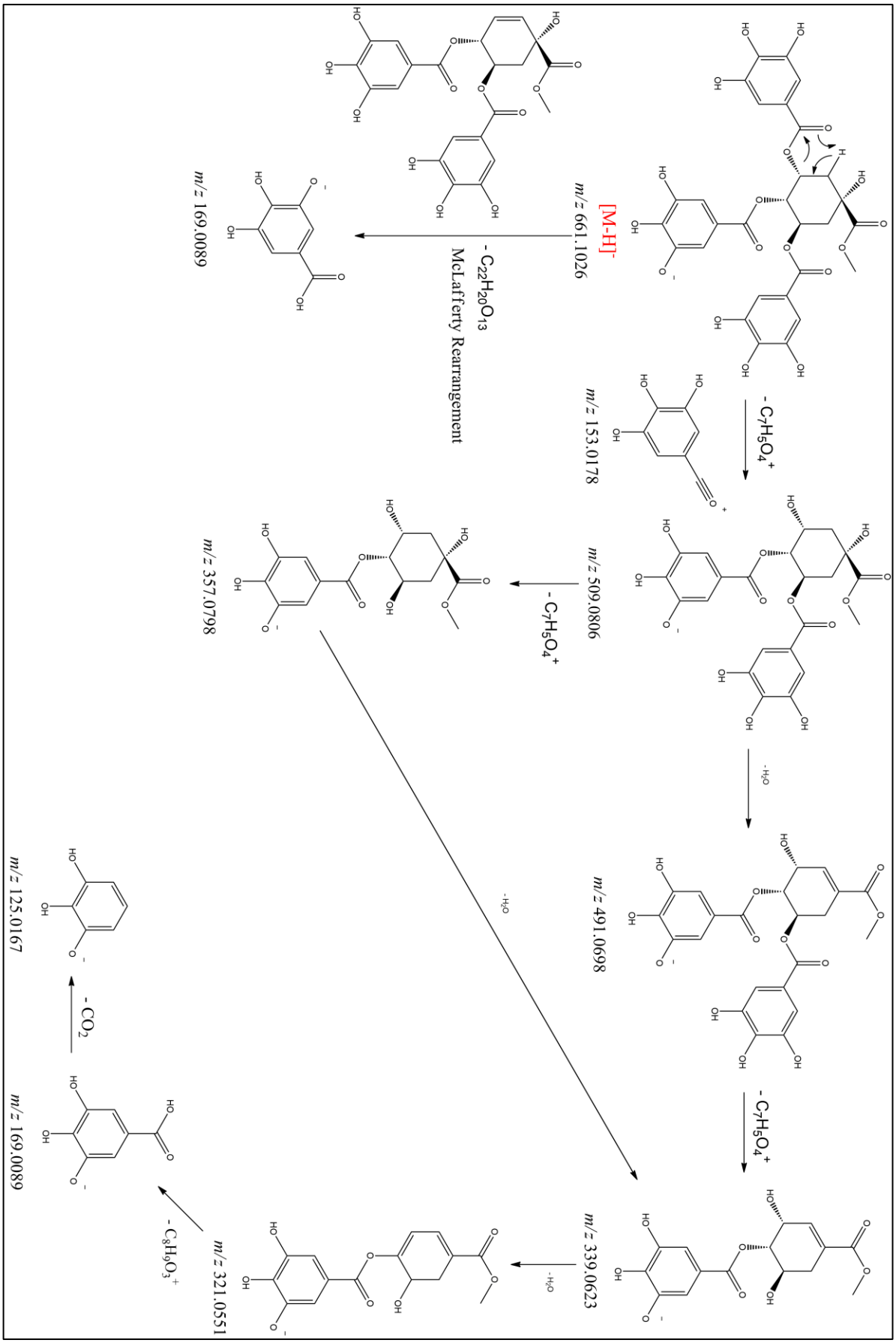

Scheme 4. ESI-MS/MS proposed fragmentation pattern of compound 6 in the negative ion mode. *m/z* measured [M-H]- 661.1026, calculated [M-H]- 661.1000.

The sodiated molecular $[M+Na]^+$ ion (Figure 16) was also observed in the positive ion mode at *m/z* 685.1012. The calculated *m/z* of this ion was 685.1000 with an error of precision of +1.75 ppm. The base peak was at *m/z* 153.0179 (Scheme 5).

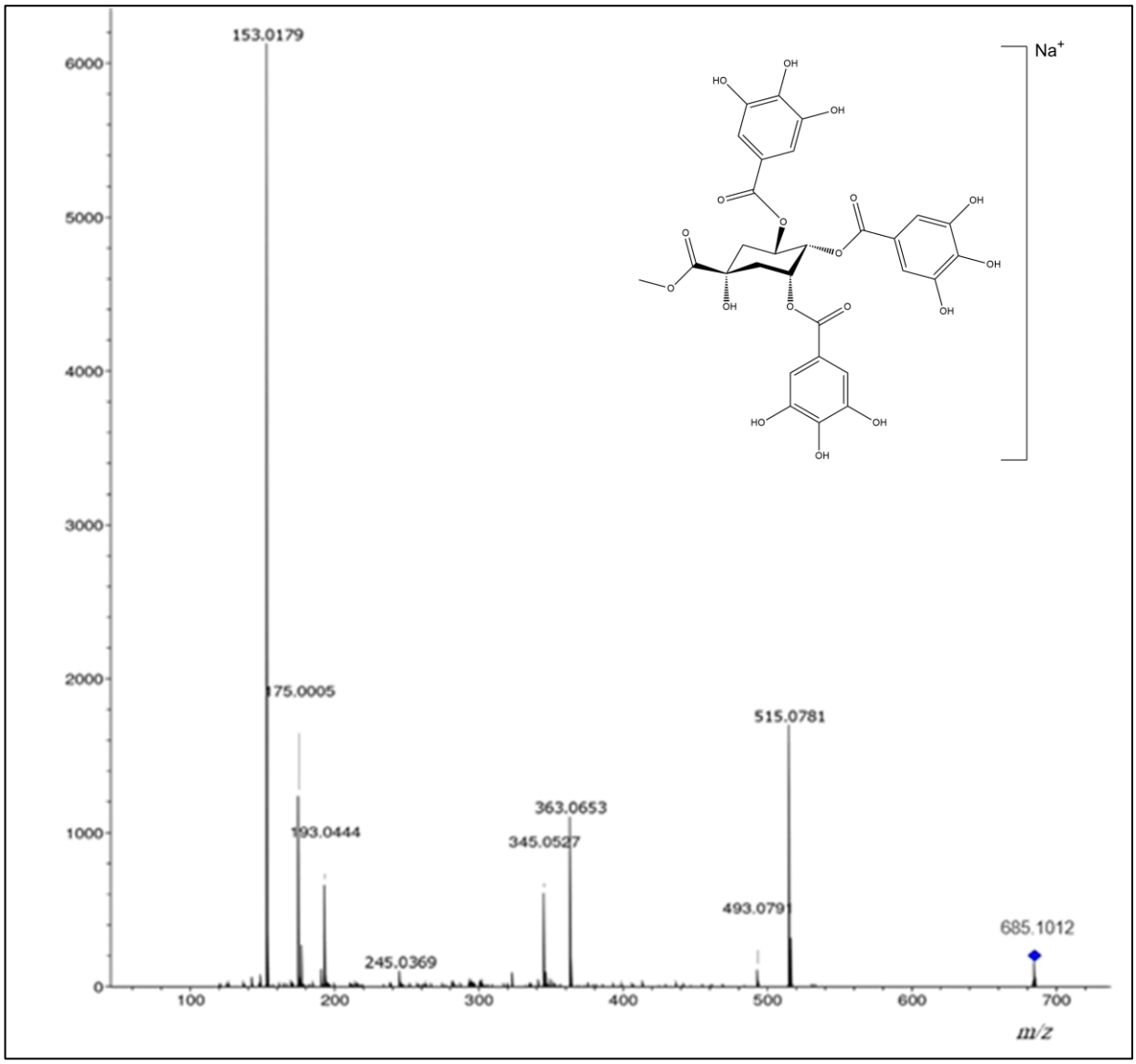

Figure 16. ESI-MS/MS spectrum of compound 6 in the positive ion mode $[M+Na]^+$.

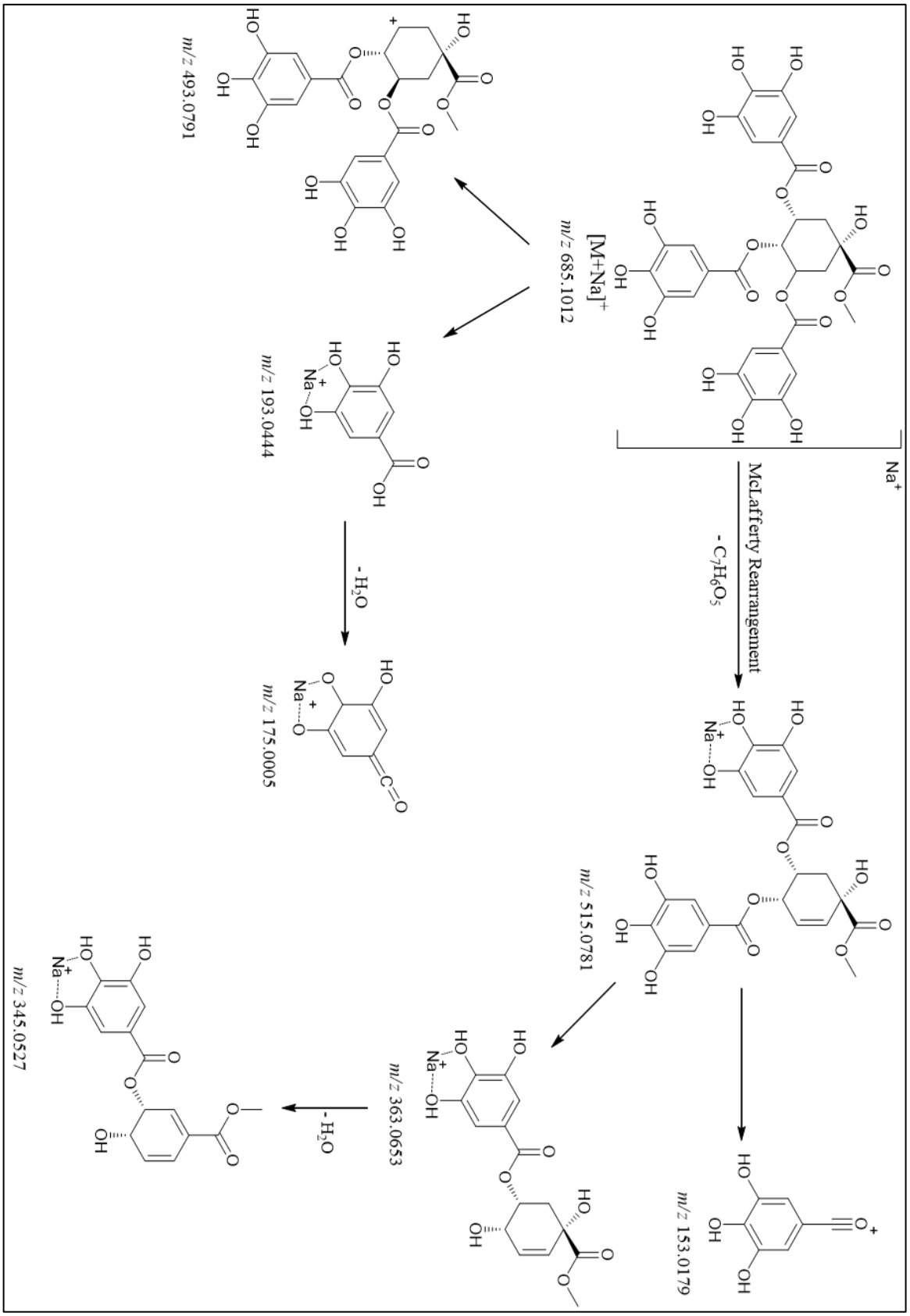

Scheme 5. ESI-MS/MS proposed fragmentation pattern of compound 6 in the positive ion mode, m/z $[M+Na]^+$ measured 685.0860, calculated $[M+Na]^+$ 685.1012.

The ESI-MS/MS analysis of the important synthetic intermediate 5 (Figures 17-19), a precursor of the final compound, revealed the following molecular ions: *m/z* $[M+H]^+$ 1473.5239, MS $[M+Na]^+$ 1496.5005, MS $[M+K]^+$ 1511.4664.

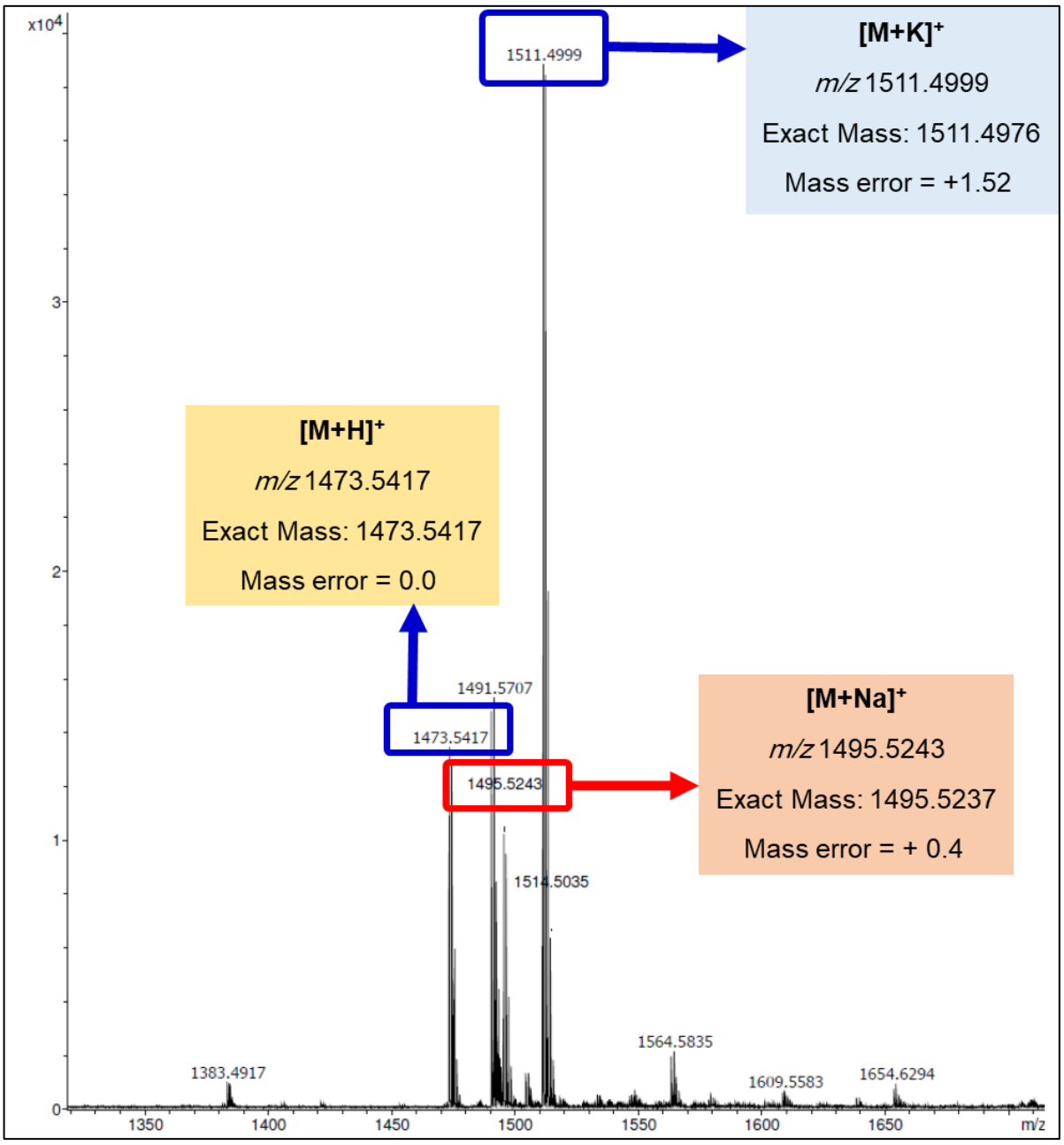

Figure 17. ESI-MS spectrum of the synthetic intermediate compound 5.

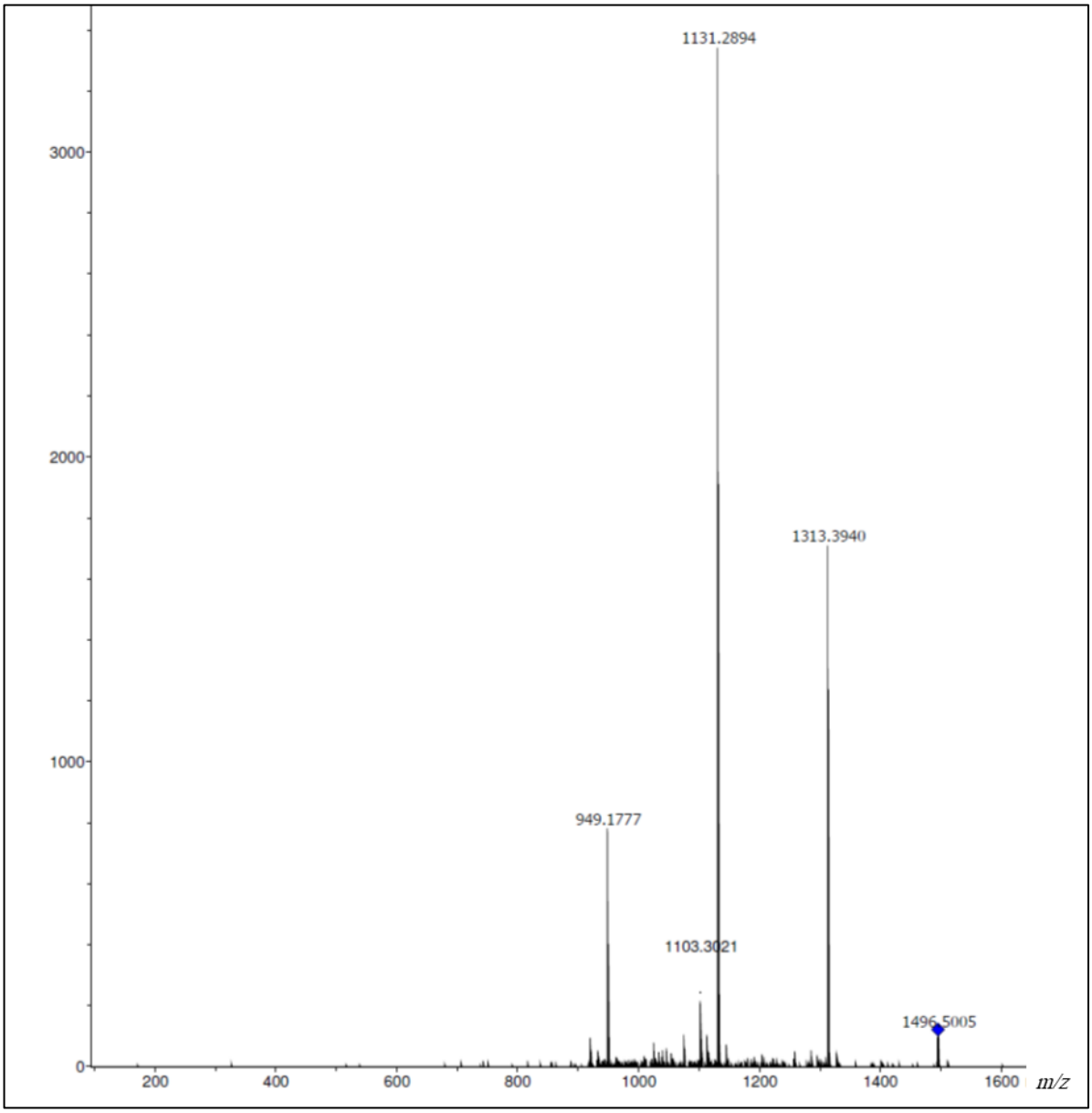

Figure 18. ESI-MS/MS spectrum of compound 5 in the positive ion mode, $[M+H+Na]^+$ 1496.5005.

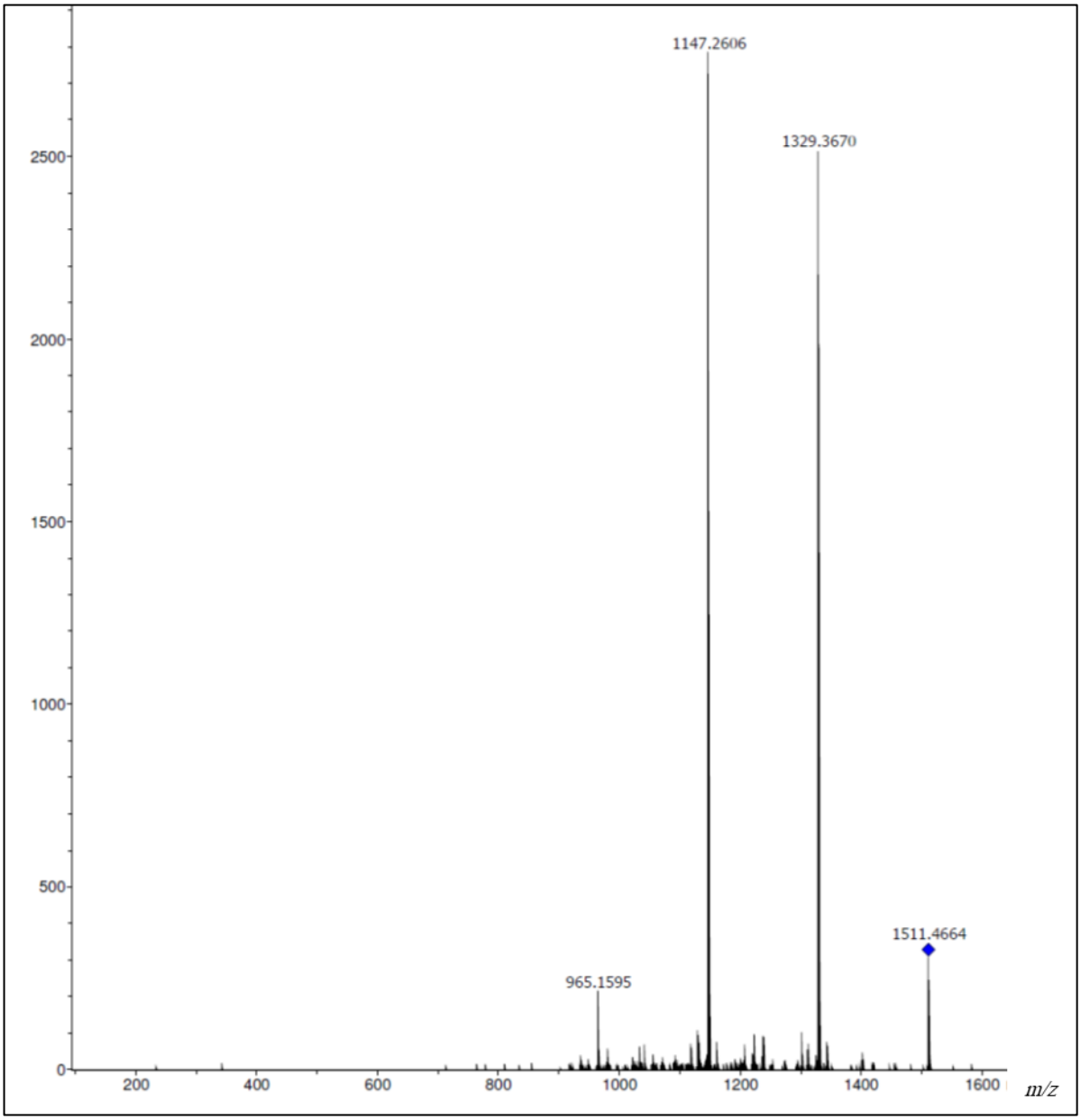

Figure 19. ESI-MS/MS spectrum of compound 5 in the positive ion mode, $[M+K]^+$ 1511.4664.

Chapter 2

Biotransformation of gallic and galloylquinic acids from Copaifera lucens by filamentous fungi

4 Chapter 2

4.1 Background

Biotransformation is a chemical reaction catalyzed by enzymes, cells or whole organs. It explores the unique properties of biocatalysts, namely their stereo-and regio-specificity and their potential to perform reactions at non-extreme pH values and temperatures. Biotransformation may be used to carry out specific conversions of complex substrates by the use of animals, plants (164), algae, filamentous fungi, yeast, actinomycetes, bacteria, as well as enzymes produced by these cells during the generation of products of interest. The use of microorganisms is a valuable tool in the identification of possible mammalian metabolites and could shed some light on the metabolic pathways of phytochemicals. *Copaifera* is a genus of flowering plants belonging to the family Fabaceae. Different species of these plants, such as *Copaifera langsdorffii* and *Copaifera lucens*, are widely distributed in Brazil (150) and they possess promising pharmacological and biological activities, (147, 156) mainly their use in modulating urolithiasis. We previously showed that *C. langsdorffii* leaf extract increased urinary magnesium and decreased uric acid excretion in rats (165). Moreover, treated rats had a higher urinary citrate excretion, lower urinary oxalate and reduced intratubular calcification as well as decreased the expression of osteopontin (OPN) expression (114, 166). The major secondary metabolites existing in *Copaifera* leaves are mainly galloylquinic acid derivatives (149), and flavonoids (149, 167), which might be attributed to its antiurolithic bioactivity. However, there is very little information on the metabolism of such compounds present in *Copaifera* extracts. Therefore, studies on the metabolism of *Copaifera* extracts by filamentous fungi are important for obtaining a better understanding of the metabolism and biological effects, especially the antiurolithic activity of this herb. In this study, the butanolic fraction of *C. lucens* (BF) and gallic acid were cultured aerobically with three filamentous fungi *Aspergillus alliaceus* (ATCC 10060) (Graphical abstract), *Cunninghamella elegans* (ATCC 10028b) and *Aspergillus brasiliensis* (ATCC 16404) for 60 h and 120 h. A highly sensitive and selective Ultra Performance Liquid Chromatography-Mass Spectrometry (UPLC-MS/MS) technique was employed to identify and characterize the resulting metabolites. On one hand, there was no change observed in case of *Cunninghamella elegans* and *A. brasiliensis*, but on the other hand, one major metabolite (M1) was detected and characterized in case of *A. alliaceus* ATCC 10060, which was tested for its potential to inhibit the adherence of calcium oxalate monohydrate crystals (COM) to the surface of Madin-Darby Canine Kidney type I (MDCKI) cells (see Part III of the thesis). The compound was also investigated for its antioxidant activity

in a DPPH free radicals scavenging assay (*see* Flowchart I). Based on the results using microorganisms as a model of mammalian metabolism, we obtained preliminary knowledge of a possible metabolic pathway for these extracts of *Copaifera* using filamentous *in vitro* in order to provide a foundation for further exploring the efficacy and toxicity of *C. lucens*. Moreover, this study also shows that galloylquinic acid compounds contribute to the antiurolithic activities of plant extracts containing them.

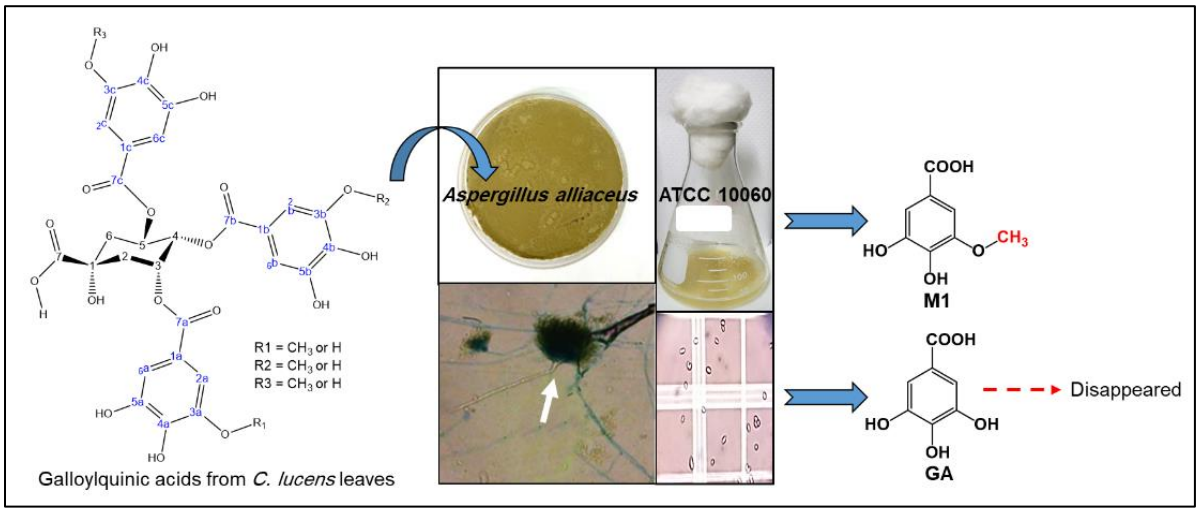

Graphical abstract 1. Biotransformation of galloylquinic acids from *C. lucens n*-butanolic fraction (BF) by *A. alliaceus*.

4.2 Materials and methods

<table>
<tr><th colspan="2">Materials</th></tr>
<tr><td>Biological
(filamentous fungi)</td><td>Cunninghamella elegans ATCC 10028b
Aspergillus brasiliensis ATCC 16404
Aspergillus alliaceus ATCC 100060</td></tr>
<tr><td rowspan="3">Chemicals

(culture media composition)</td><td>Culture media for Cunninghamella elegans ATCC 10028b

➢ Media for the production of spores: Potato Dextrose Agar (PDA) (Oxoid, UK): 39 g PDA in 1000 mL distilled water
➢ Pre-fermentation media: Caldo PDB (KASVI, Italy)
➢ Fermentation media: Czapek modified 1: 1.0% glucose (Synth, Brazil), 0.2% $NaNO_3$ (Vetec, Brazil), 0.1% K_2HPO_4 (Vetec), 0.05% $MgSO_4$. $7H_2O$ (Vetec, Brazil), 0.05% KCl (Vetec, Brazil) and 0.001% $FeSO_4$. $7H_2O$ (Vetec, Brazil), pH 7.0</td></tr>
<tr><td>Culture media for Aspergillus brasiliensis ATCC 16404

➢ For the production of spores: Sabouraud media
➢ Pre-fermentation medium: Jackson: 0.25% corn powder (Veranita, Brazil), 1.0% glucose (Synth, Brazil), 1.0% oatmeal (Quaker, Brazil), 4.0% tomato paste, 1.0% $CaCl_2$. $2H_2O$ (Vetec) and trace elements solution: (0.1% $FeSO_4$. $7H_2O$ (Vetec), 0.1% $MnCl_2$. $4H_2O$ (Vetec, Brazil), 0.0025% $CuCl_2$. $2H_2O$ (Vetec, Brazil), 0.01% $CaCl_2$. $2H_2O$ (Vetec, Brazil), 0.056% H_3BO_3 (Vetec, Brazil), 0.0019% (NH_4) 6.MoO_2. $4H_2O$ (Vetec, Brazil) and 0.02% $ZnSO_4$. $7H_2O$ (Vetec, Brazil), all in distilled water
➢ Fermentation medium: Koch's K1: 0.18% glucose (Synth, Brazil), 0.06% bacterial peptone (Himedia, India) and 0.04% yeast extract (Himedia, India)</td></tr>
<tr><td>Culture media for Aspergillus alliaceus ATCC 100060

➢ For the production of spores: Agar malt extract (2% malt extract, 2 % glucose, 0.1 % bacterial peptone, 1.8% agar-agar, distilled water)
➢ Pre-fermentation medium Jackson (as described above)
➢ Fermentative medium: Koch's K1 (as described above)</td></tr>
<tr><td>Biotransformation substrates</td><td>➢ n-Butanolic fraction (BF) obtained by the fractionation of Copaifera lucens leaves crude extract (see next page)
➢ Gallic acid (Sigma Aldrich, USA)</td></tr>
</table>

4.2.1 Conditions of chromatographic analysis

The analytical HPLC analysis was performed on a Shimadzu LC-10ADvp (Japan) operated with multisolvent delivery system, equipped with a Shimadzu SPD-MICAvp photodiode array detector (PDA). Analyses were performed using analytical reversed phase column (Polar-RP C 80 A) with dimensions: 150 mm × 4.6 mm (Shimadzu) and a particle diameter of 4 μm; the mobile phase consisted of acidified water (A) (0.1% formic acid in water) and methanol (B) in gradient conditions as follows: 15-50% of B (45 min), 50-90% of B (45-65 min) and 90-15% of B up to 75 min; flow rate, 1 mL/min. The injection volume was 20 μL. The sample was dissolved in methanol HPLC grade (2 mg/mL), filtered through 0.45 μm filter prior to automatic injection.

Ultra-Performance Liquid Chromatography-Mass Spectrometry (UPLC-MS/MS) analysis was performed on a Waters ACQUITY UPLC H-Class system coupled to the Xevo® TQ-S tandem quadrupole (Waters Corporation, Milford, MA, USA) mass spectrometer with a Z-spray source operating in the negative mode. The source and operating parameters were optimized as follows: capillary voltage = -2.5 kV, cone voltage = -40 V, source temperature = 150°C, desolvation temperature (N2) = 300°C, desolvation gas flow = 600 L/h (mass range from m/z 150 to 1,000). Tandem mass spectrometry experiments (MS/MS) with collision-induced dissociation (CID) were conducted by using argon as collision gas on selected precursor ions ([M-H]-). Mass data were processed by the MassLynx V4.1 software. Solvents used for extraction were of analytical grade and others were of HPLC grade.

4.2.2 Preparation of the crude extract of *Copaifera lucens* dried leaves

The leaves of *Copaifera lucens* Dwyer were collected from the field of the botanical garden of Rio de Janeiro, Brazil (Figure 19), which was identified by the botanist Haroldo Cavalcante de Lima, where a voucher sample was kept (RB 474303). The leaves were dried in a dark, dry and well-ventilated area. The dried leaves were exposed to pulverization and 0.5 Kg of the pulverized leaves were macerated (Figure 20) in 4.0 L of a hydroalcoholic solution (ethanol: water; 7:3). The ethanolic extract was obtained by filtration every three days and a fresh 70% ethanol was added each time. The process was repeated three times and finally the total collected extracts were subjected to evaporation using rotary evaporator (Rotavap: Model R210 Buchi ™ with Vacuum Pump V-700, Vacuum Controller V-855 and Recirculating Chiller F-105). The dried extracts (88.58 g) were lyophilized and kept aside at – 20°C upon use.

Figure 20. *Copaifera lucens* tree and leaves.

Figure 21. (A) *Copaifera lucens* dried leaves. (B) Pulverized leaves macerated in 70% ethyl alcohol.

4.2.3 Soxhlet extraction for calculating the remained part of the crude extract of *C. lucens*

Soxhlet extraction was performed for calculating the remained non-extracted part of the plant materials. For that, 10 g of the exhausted dried plant material was re-extracted in a Soxhlet apparatus using 100% ethanol. The net yield was 46 g per 500 g of the plant material weight (approximately 9.2% w/w of plant materials) in comparison with the first extracted crop using 70 % ethanol.

4.2.4 Liquid / liquid partitioning of the crude extract of *C. lucnes*

The crude extract (50 g) was dissolved in 600 mL of methanol: water (6:4). Then the solution was shaken in a separating funnel with ethylacetate (3 X 300 mL), followed by n-butanol (4 X 200 mL), in sequence (Figure 22). The solvent of each partition phase was evaporated using rotary evaporator, then the resulting crude fractions were lyophilized. The yields were 14.4, 14.9 and 17.6 g for *n*-butanolic, ethylacetate and water fractions, respectively. The *n*-butanolic fraction of *C. lucens* was named (BF) and was selected for the biotransformation experiments.

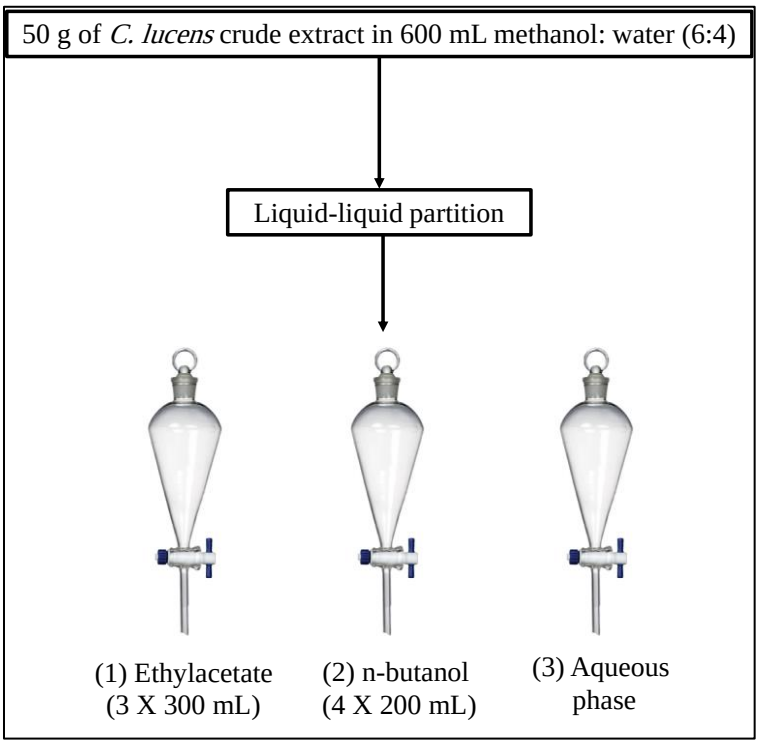

Figure 22. Liquid/liquid partitioning of the *C. lucens* crude extract.

4.2.5 HPLC analysis of the crude extract and its partition fractions

All samples were dissolved in 50% methanol (HPLC grade) and filtered through 0.45 μm using Millipore filter prior to injection into the analytical HPLC.

4.2.6 Preliminary stability study of galloylquinic acids in the *n*-butanolic fraction under extreme pH values similar to that produced during the metabolism of fungi

Two solutions of BF (3 mg/mL) in distilled water were separately adjusted into different pH values; 4.5 (similar to that of the bacteria) and 7.5-8.0 (similar to that of the fungi) using 0.1

M HCl and 0.1 M NaOH, respectively. The solutions were incubated in a gyratory shaker at 30-37°C, and 100 rpm for 28 h, and then analyzed by TLC.

4.2.7 Biotransformation procedures

A. alliaceus was grown in sterile test tubes containing agar malt extract for seven days in biochemical oxygen demand (BOD) incubator at 30°C. After this period, 4 x 10^6 spores / mL Erlenmeyer flasks were transferred to 125 mL containing 15 mL of pre-fermentation Jackson medium (Figure 23). Cultures were maintained under constant stirring at 120 rpm and 30°C for 24 h. After this period, the mycelial biomasses were aseptically filtered and transferred to 250 mL Erlenmeyer flasks containing 30 mL Kock's fermentative K1 media. At this point the substance BF was added at a concentration of 1 mg/mL. Control media cultures with or without the substance or the fungus were also performed. Cultures were maintained under constant stirring of 120 rpm and a temperature of 30°C, and biotransformation was evaluated after 60 and 120 h. After completion of the process, cultures were filtered and the culture broth was subjected to liquid-liquid partition process with *n*-butanol (100 mL). The separated fungal biomass was dried, sonicated and triturated with 30 mL of *n*-butanol followed by filtration. The obtained *n*-butanol filtrates were dried using rotary evaporator, lyophilized and the obtained masses were weighted. One mg of each sample was taken and dissolved in 1 mL of methanol (HPLC grade), filtrate through 0.45 μm bacterial filtrate, and then subjected to HPLC-UV and HPLC-MS/MS analyses.

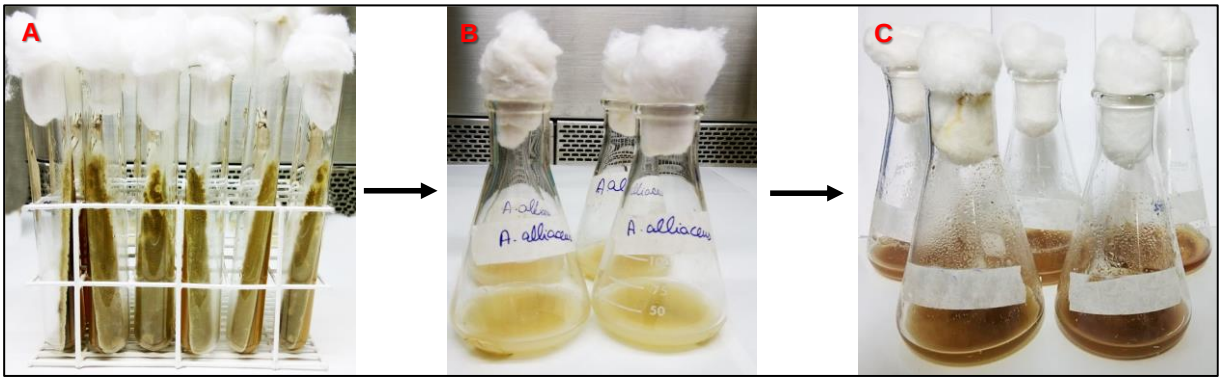

Figure 23. Culture of *A. alliaceus*. (A) Spore formation. (B) Pre-fermentation stage. (C) Fermentation stage and addition of BF substrate.

Cunninghamella elegans was cultured in Petri dishes containing PDA agar for seven days in BOD incubator at 30°C. After this period, three-agar mycelia discs of approximately 6 mm diameter, obtained with the aid of a sterilized transfer tube (Sigma®), were transferred to Erlenmeyer flasks of 250 mL containing 50 mL of PDB broth. Cultures were maintained under

a constant stirring at 120 rpm / 30°C for six days. After this period, the mycelial masses were filtered aseptically and transferred to separate 500 mL Erlenmeyer flasks of 100 mL containing modified Czapek fermentative medium. At this time BF substrate was added at a concentration of 1 mg/mL in water. Cultures were maintained under constant agitation of 120 rpm and a temperature of 30°C, and the biotransformation was monitored after 60 and 120 h. Control cultures were also kept in considerations. At the end of the experiment, cultures were filtered and the fungal biomasses were separated out and treated as previously mentioned.

A. brasiliensis was grown in Petri dishes containing agar Sabouraud for seven days in BOD at 30°C. After this period, 4 x 10^6 spores/mL Erlenmeyer flasks were transferred to 125 mL containing 15 mL of Jackson pre-fermentation medium. Cultures were maintained under constant stirring at 120 rpm and 30°C for 24 h. After this period, the mycelial masses were aseptically filtered and transferred to 250 mL Erlenmeyer flasks containing 30 mL Kock's fermentative K1 media. At this point, the substance BF was added at a concentration of 1 mg/mL. Control cultures were also performed. Cultures were maintained under constant stirring of 120 rpm and a temperature of 30°C, and biotransformation was evaluated after 60 and 120 h. After completion of the process, cultures were filtered and the culture broth was subjected to liquid-liquid partition process with *n*-butanol as explained before.

4.2.8 Hydrolysis of the *n*-butanolic fraction (BF) using NaOH

To a stirred solution of NaOH (10 mg) in 100 mL water, 100 mg of BF was added and the mixture was refluxed for 2 h. The reaction mixture was poured into 0.6 M HCl and the solution was extracted with *n*-butanol (2 X 100 mL) using a separating funnel. The organic layer was dried over anhydrous Na_2SO_4, filtered and concentrated under vacuum using rotary evaporator to give a red residue (0.05 g). The residue was analyzed using HPLC-UV.

4.3 Results and discussion

The preliminary stability study of galloylquinic acids of *C. lucens* BF showed no change in the number of spots, indicting the stability of the compounds under the aforementioned extreme pH conditions. It was interesting that the pH of the naive aqueous solution of SB was 4.8. The masses obtained by organic extraction of both the filtrate and the mycelia in the biotransformation experiment of BF are summarized in (Table 8).

Table 8. The masses obtained by organic extraction of both the filtrate and the mycelia in the biotransformation experiment of BF.

Aspergillus alliaceus ATCC 100060 (AA)					
	n-Butanolic partition of the fungal filtrate (wt in mg)		Separated fungal biomass + sonication + *n*-butanol (wt in mg)		pH
	60 h	120 h	60 h	120 h	
AA60-MF	15.0	-	-	-	-
AA60-MSB	75.0	-	7.9	-	7
AA60-MFSB	37.0	-	32.6	-	5
AA120-MF	-	7.0	-	-	-
AA120-MSB	-	9.0	-	4.6	8
AA120-MFSB	-	14.0	-	15.6	2
Aspergillus brasiliensis ATCC 16404 (AB)					
AB60-MF	35.0	-	-	-	7 ~ 8
AB60-MSB	16.0	-	11.5	-	7
AB60-MFSB	35.0	-	13.0	-	3
AB120-MF	-	17.0	-	-	7 ~ 8
AB120-MSB	-	95.0	-	7.2	7
AB120-MFSB	-	128.0	-	14.3	6 ~ 7
Cunninghamella elegans ATCC 10028b (CE)					
CE60-MF	6.3	-	-	-	1~2
CE60-MSB	51.4	-	54.9	-	7
CE60-MFSB	38.3	-	146.0	-	6~7
CE120-MF	-	10.9	-	-	2
CE120-MSB	-	73.1	-	15.1	5
CE120-MFSB	-	17.5	-	101.8	8

**MF = control media with fungus, MSB = control media with substrate, MFSB = substrate incubated with the fungus*

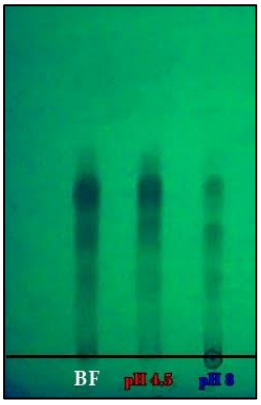

Figure 24. TLC screening of BF in acidic and basic pH.

Due to the similarities between the microbial system and human metabolic pathways, biotransformation using filamentous fungi or bacteria can be a useful tool in predicting the metabolic profiles of plant extracts (Hegazy et al. 2015). He et al. studied the biotransformation and *in vitro* metabolic profile of *Polygonum capitatum* bioactive extract (He et al. 2014). Gallic and quinic acids are the basic constructing units of galloylquinic acids. The phenolic group of gallic acid at position 3 can be found free or substituted with a methyl group. The HPLC-UV analysis of the BF revealed several peaks identified as galloylquinic acid derivatives by comparing their UV spectra (Figure 25) with that of our previously published data (Nogueira et al. 2015).

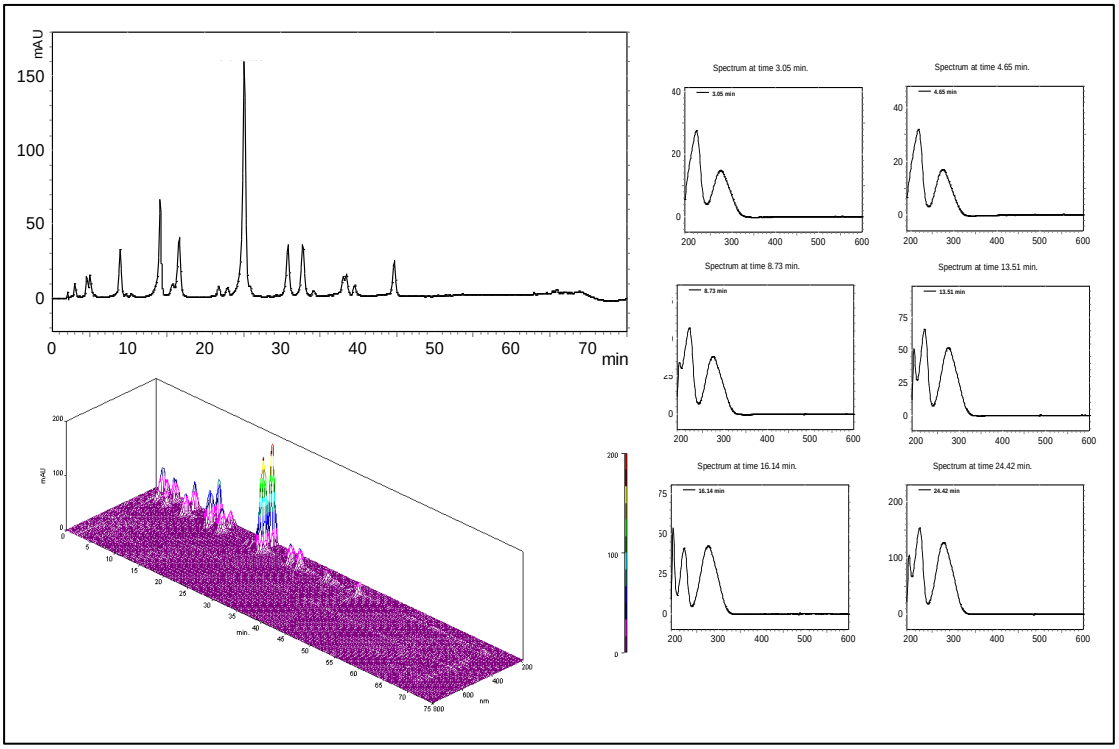

Figure 25. HPLC-UV spectrum of *C. lucens* BF at 280 nm. The major peaks represent galloylquinic acids according to their characteristic UV spectra.

There was no biotransformation observed in case of *A. brasiliensisATC 16404* and *Cunninghamella elegans* ATCC 10028b. Our biotransformation results showed that *A. alliaceus* 10060 hydrolyzed the non-methylated and methylated galloylquinic acids derivatives after 120 h into gallic acid (GA), and one major metabolite M1, respectively (Figure 26). However, the resulting GA disappeared as it was not detected in the HPLC chromatograph.

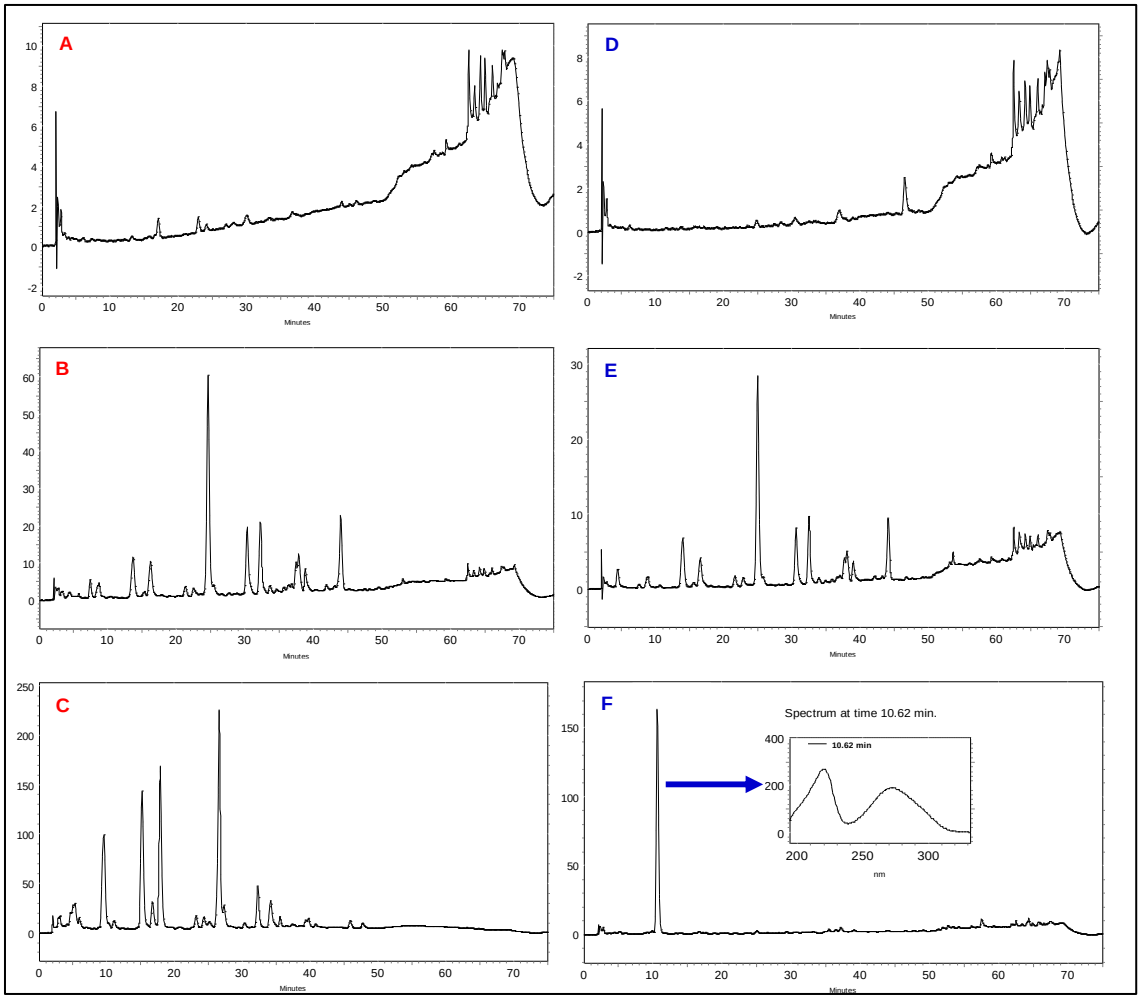

Figure 26. HPLC-UV analysis of the biotransformation of BF using *A. alliaceous*. (A) Control media after 60 h. (B) Substrate BF + media after 60 h. (C) Substrate BF incubated with the fungus after 60 h. (D) Control media after 120 h. (E) Substrate BF + media after 120 h. (F) Substrate BF incubated with the fungus after 120 h, furnishing the biotransformed metabolite M1.

The HPLC-UV and UPLC-DAD-MS/MS analysis of M1 showed the presence of a single peak with a retention time at 10.6 min and 18.5 min, respectively (Figure 27). It exhibited a similar UV spectral behavior to galloylquinic acids (149).

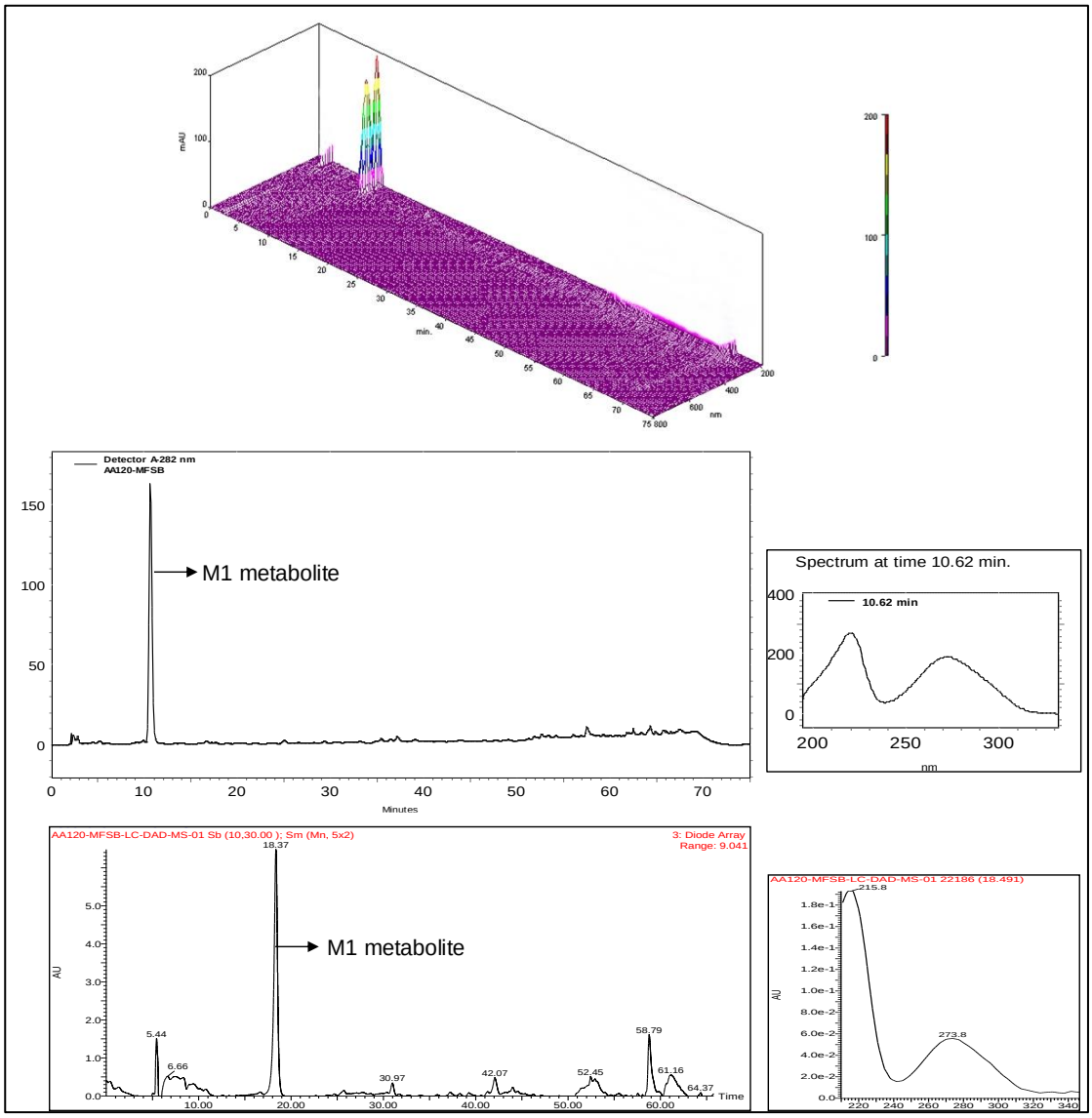

Figure 27. HPLC-UV and UPLC-DAD-MS/MS chromatograms of M1 metabolite.

The MS/MS analysis (Figure 28) in the negative ion mode showed a molecular ion peak $[M-H]^-$ at *m/z* 182.9. The fragmentation pattern of this molecular ion peak showed two molecular ion radicals at *m/z* 167.9 and *m/z* 123.9 that were formed by the loss of $-^{\bullet}CH_3$ radical and CO_2 respectively.

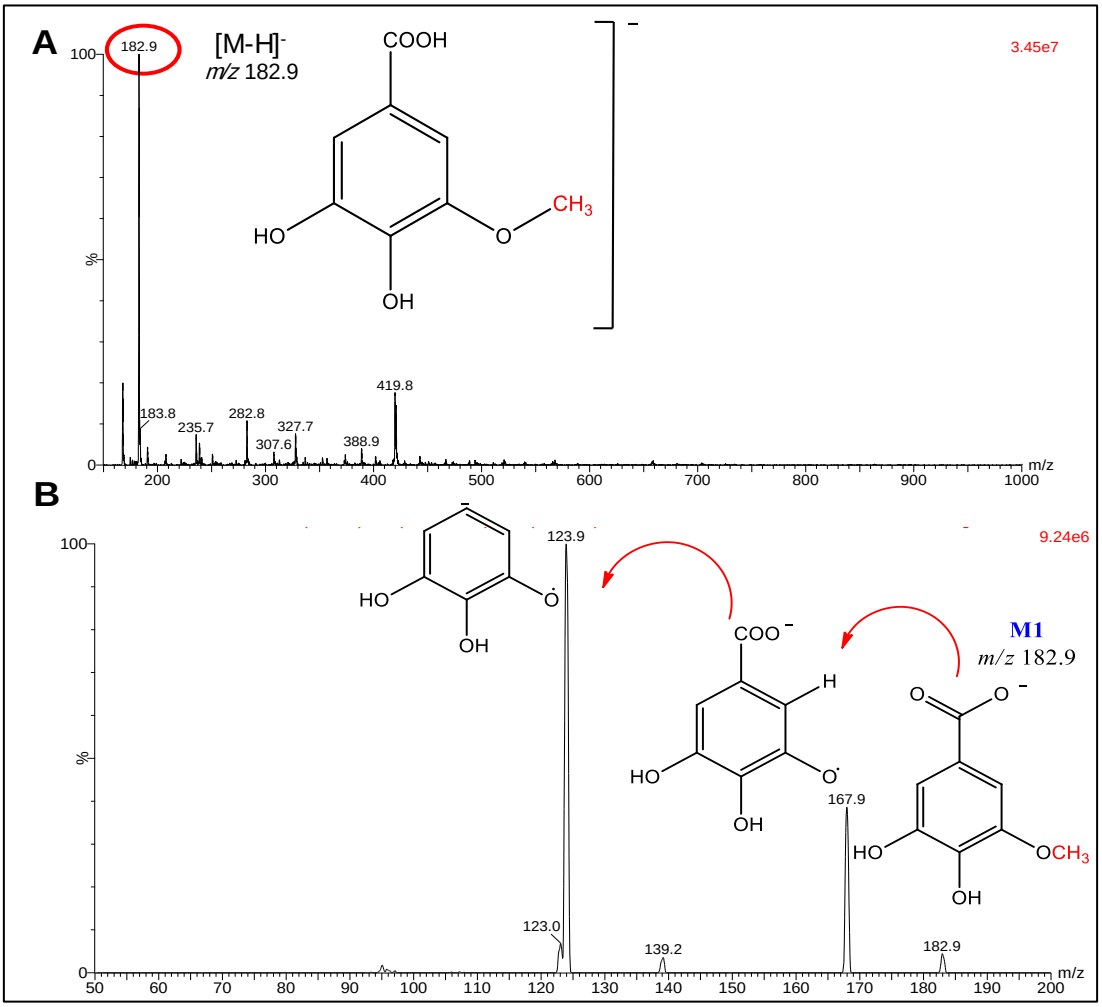

Figure 28. MS/MS spectrum of the biotransformed metabolite M1 by *A. alliaceus*. (A) MS spectrum of M1. (B) MS/MS spectrum of M1.

The ^{1}HNMR spectral data of M1 (Table 9) showed the presence of two signals in the aromatic range at (7.18-7.19) ppm referring to two aromatic hydrogen. A singlet peak at 3.35 ppm integrated to three hydrogen was also observed indicating the presence of a methyl group.

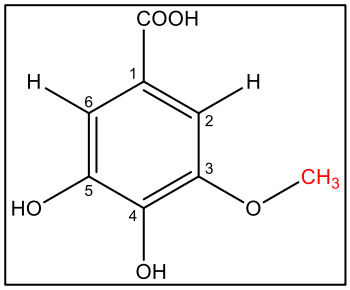

3-*O*-methyl gallic acid (M1)

Table 9. ^{1}H NMR data of M1 in CD_3OD.

Position	δ_H (ppm)
1	-
2	7.19 (s, 1H)
3	-
4	-
5	-
6	7.18 (s, 1H)
-OCH_3	3.35 (s, 3H)

From the previous NMR and MS data, M1 was identified as 3-*O*-methyl gallic acid. This metabolite is one of gallic acid metabolites produced in humans (Hsu et al. 2007). The proposed biotransformation pathway was further confirmed by the disappearance of GA standard after 24 h of incubation with *A. alliaceus* (Figure 29).

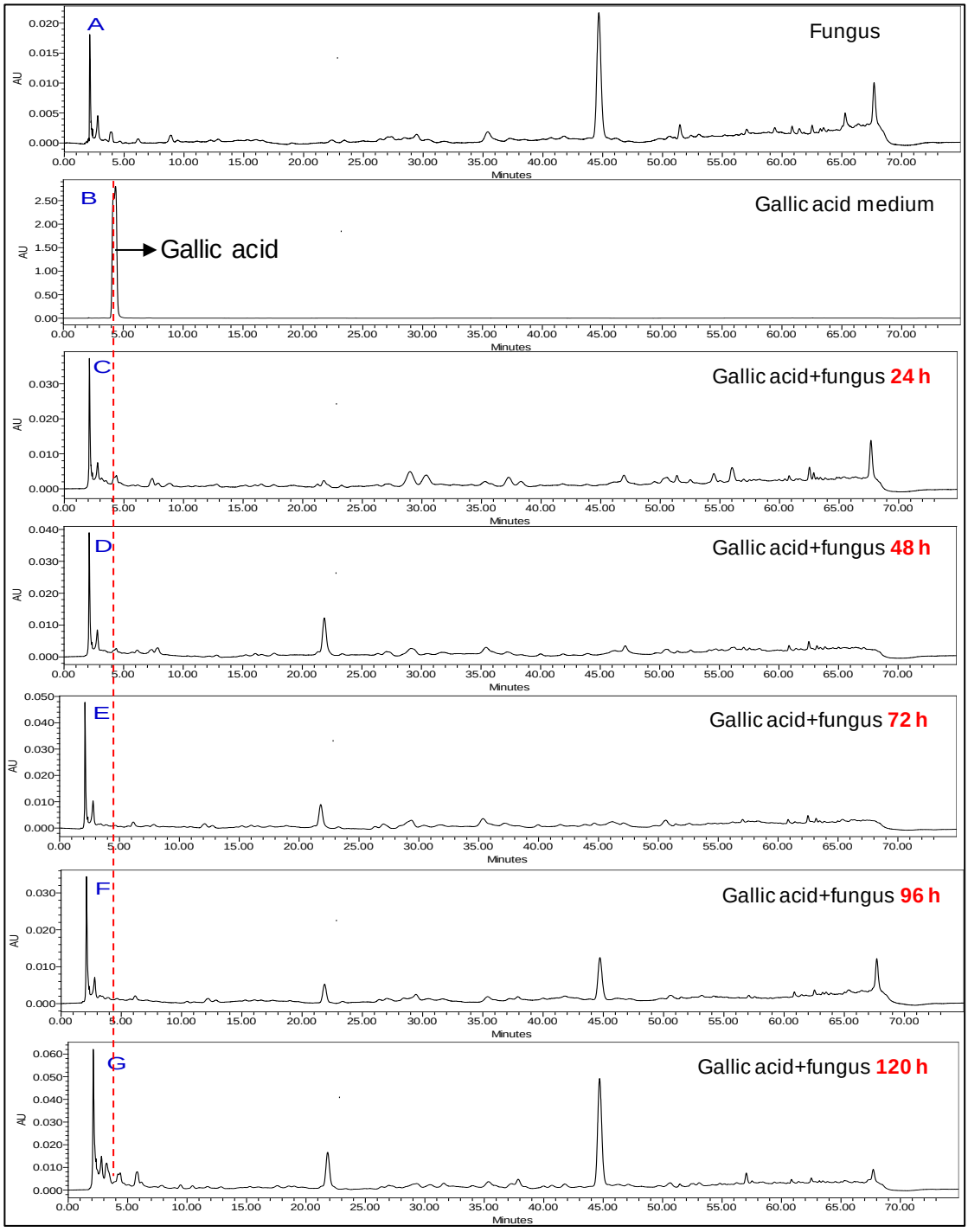

Figure 29. HPLC-UV analysis of the biotransformation of gallic acid by *A. allieaceus*. (A) Control. (B) Gallic acid standard. (C) Gallic acid + fungus after 24 h. (D) Gallic acid + fungus after 48 h. (E) Gallic acid + fungus after 72 h. (F) Gallic acid + fungus after 96 h. (G) Gallic acid + fungus after 120 h.

Our study clarifies that the *A. alliaceus* consumed GA as a sole carbon source and the fungus was not able to utilize the methylated GA resulting from the hydrolysis of the galloylquinic acid derivatives with methyl groups. These results are in agreement with the previously published data on *Aspergillus niger*, in which the fungus also utilized tannic acid as a source of carbon like our case and degraded it into GA and pyrogallol. Moreover, both of the metabolic products disappeared within 96 h of incubation (Sharma et al. 1998). To further confirm the hydrolytic specificity of the fungal catalytic enzymes, we performed a chemical hydrolysis of the BF in a basic medium. The HPLC-UV analysis of the resulting hydrolytic products showed different peaks from that of the metabolite M1 (Figure 30).

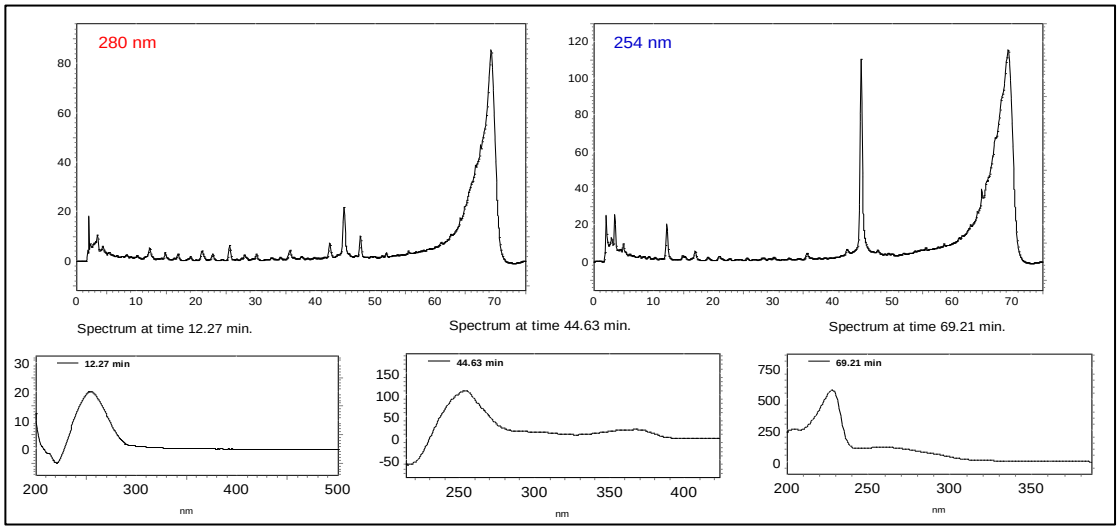

Figure 30. HPLC-UV analysis of the hydrolytic product resulting from the induced hydrolysis of galloylquinic acid in basic medium.

Most of previous biotransformation studies of flavonoids using *A. alliaceus* ATCC 10060 revealed that the fungus performs hydroxylation reactions (formation of hydroxylated metabolites) (168, 169). There is also one study showed that *A. alliaceus* ATCC 10060 opened ring C of 7-hydroxyflavanone (170). This may clarify the ability of the fungal catalytic enzymes to hydrolyze galoylquinic acids by a similar or related mechanism.

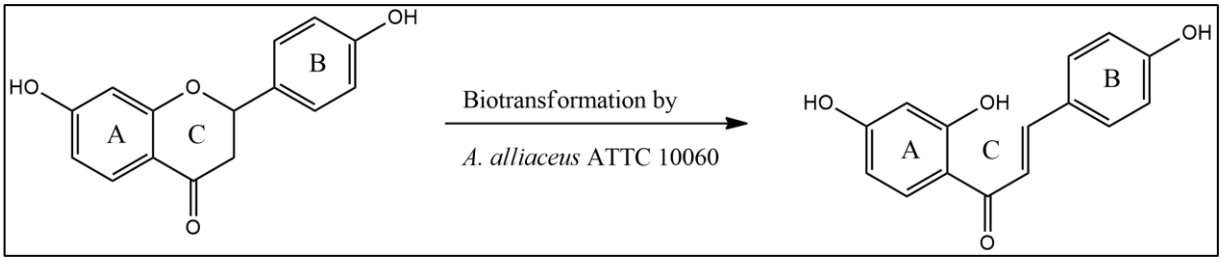

Chapter 3

Antiurolithic activities

5 Chapter 3

5.1 Background

COM crystal adhesion can lead to many downstream cascades of renal cellular responses (171, 172). Moreover, crystal adhesion can also enhance the adhesion of additional crystals, leading to crystal aggregation and retention inside renal tubules, and finally stone formation (173, 174).

In a human study, kidney tissues were obtained from patients with calcium oxalate nephrolithiasis. From these, approximately 50% of the specimens had crystals adhered on renal tubular epithelial cells and some of them were seen inside the cells (175). These findings strengthen the crucial role of crystal adhesion in kidney stone disease.

The mechanisms underlying COM crystal adhesion on the cell surface are quite complicated. Surface charge is an important factor mediating crystal adhesion as the data obtained from previous studies revealed that COM crystals adhered to the cell surface at anionic sites and could be blocked by specific cations (176). Adhesive property, electrostatic binding and specific interactions are also believed to be other important factors mediating crystal adhesion.

During the past decade, several studies had attempted to identify surface molecules on renal tubular cells that might serve as the receptors for COM crystal adhesion with the ultimate goal to inhibit or block these bindings for disease prevention. Indeed, the apical membrane of renal tubular cells comprises various types of membrane proteins (177). Many of these apical membrane proteins are expected to play a role in facilitating COM crystal-cell adhesion, including annexin A1, annexin II, (178), α-enolase, heat shock protein 90 (HSP90), sialic acid-containing proteins, nucleolin-related protein,(179) osteopontin, and surface receptor CD44 (180).

Interestingly, expression of these potential COM crystal receptors could be altered by stone modulators or risk factors. For example, high-calcium state increased surface annexin A1, whereas high-oxalate condition increased surface α-enolase on apical membranes of renal tubular epithelial cells (181, 182).

Even though the prevalence of nephrolithiasis is increasing, our understanding of the pathophysiology has not kept pace and new therapeutic approaches have not emerged. The development of new animal models of stone disease may allow for a better understanding of the pathophysiology underlying urolithiasis and open opportunities for new therapeutic approaches. The potential of a new physiological model such as *Drosophila melanogaster* is

exciting. *Drosophila* is a species of fly belongs to the taxonomic order Diptera, family Drosophilidae. It is also known as common fruit fly or vinegar fly. Charles William Woodworth, an American entomologist was the first person to breed the model organism *Drosophila* (April 28, 1865 – November 19, 1940) and to suggest to early genetic researchers at Harvard its use for scientific research. Drosophila system has many advantages among them: the low cost of maintaining flies; the rapid deployment of new transgenic lines, and the ability to test hypotheses in lower-species *in vivo* systems before embarking on studies in more complex higher-order animals. The fly is a good model for researching human disease such as Cancer, neurological disorders, genetics, diabetes and drug addiction. All multicellular organisms have a specialized organ for concentrating and excreting wastes from the body. The kidneys in vertebrates and the Malpighian tubules in *Drosophila* accomplish these functions. Mammals and Drosophila have similar features during renal tubular development. The major excretory epithelia in insects are the Malpighian tubules and the hindgut, and both of them act in concert to form the functional kidney. Malpighian tubules act as a system in the regulation of ions and epithelial fluid transport. Secretion of fluid and ions by Malpighian tubules may be followed by reabsorption of water, ions, or useful metabolites. They have the capability to actively excrete a very broad range of organic solutes such as xenobiotics and insecticides.

Drosophila has 4 tubules: the anterior pair and the posterior pair. The two tubules in each pair merge together at ureter and connect to the gut at the midgut/hindgut boundary. Each tubule had distinct morphologic regions: lower segment, main segment, transitional segment and the initial enlarged segment (the first 600 μm is of interest in female flies as they contain calcium stores). The presence of calcium inside the lumen of the initial enlarged segment is the concept of Ca-oxalate induction using oxalate as a model of urolithiasis.

In the present study, we investigated the potential effect of the synthesized plant metabolite TGAME (6), its hydrolytic metabolites, *C. lucens n*-butanolic fraction (BF), the biotransformed metabolite M1 and compound 16 (in which the –COOH of quinic acid is not methylated), the later was provided by our group (150), on COM crystal binding to the surface of Madin-Darby Canine Kidney Cells type I (MDCKI) and crystal growth in a *Drosophila melanogaster* Malpighian tubule models. Membrane, cytosolic and total Annexin A1 (ANXA1), α-enolase and HSP90 amounts were examined by Western blot analysis after subcellular fractionation, then confirmed by immunofluorescence staining of cultured cells and confocal microscopy. All compounds also were tested for their antioxidant activities using DPPH assay.

5.2 Materials and methods

Cell lines	⊙ Madin-Darby Canine Kidney Cells type I (MDCKI) ATTC®, USA, cloned from distal nephron of female dog ⊙ John Lieske cells (JL), human renal cells
Cell culture media, chemicals and reagents	► Dulbecco's Modified Eagle's Medium (DMEM) (Life Technologies-Gibco®, USA) ► Fetal bovine serum (FBS) (Life Technologies-Gibco®, USA) ► Hams F-12 culture medium (Life Technologies-Gibco®, USA) ► Penicillin (100 U/mL) (Life Technologies-Gibco®, USA) ► Streptomycin (100 μg/mL) (Life Technologies-Gibco®, USA) ► Amphotericin (1.25 μg/mL) (Life Technologies-Gibco®, USA) ► Dulbecco's phosphate buffer saline (DPBS) 1X (Life Technologies-Gibco®, USA) ► Trypsin, Tryple Express - Gibco®, [-] Phenol red (Life Technologies-Gibco®, USA) ► MTT (3-(4,5-Dimethylthiazol-2-yl)-2,5-Diphenyltetrazolium Bromide) kit (ThermoFisher Scientific, USA) ► Trypan blue 0.4% (Life Technologies-Gibco®, USA)
Reagents, chemicals, kits for subcellular proteins fractionation and quantification	► Cytosolic extraction buffer (10 mM PIPES pH 6.8, 0.02% digitonin, 0.3 mM sucrose, 15 mM NaCl, and 0.5 mM EDTA) ► Laemmli's buffer (60mM Tris-HCl, pH 6.8, 2% sodium dodecyl sulfate (SDS), 10% glycerol, 5% β-mercaptoethanol) ► Whole lysis buffer (20 mM Tris pH 7.5-8, 1% SDS) ► Pierce™ BCA Protein Assay Kit (ThermoFisher Scientific)

(Continue…)	► Protease inhibitor (cOmplete Mini Roche® Diagnosis GmbH, Germany): 1 tablet is mixed with each buffer separately; the solution can be used within 10 days, kept at 4ºC. ► Halt™ Phosphatase inhibitor (ThermoFisher Scientific) (100 x) ► Phenylmethylsulfonyl fluoride (PMSF) Protease Inhibitor (ThermoFisher Scientific) (100X) ► Ice cold Phosphate Buffer Saline (PBS)
Reagents, chemicals and buffers for Western blot	► Precision Plus Protein™ Standards Dual Protein Color Marker (BIO RAD) ► 2x loading dye: 9.5 mL 2x Laemmli sample buffer + 0.5 mL *β*-mercaptoethanol ► 1x running buffer (10x Tris/Glycine/SDS) (Bio Rad) ► 1x transfer buffer (10x Tris/Glycine) (Bio Rad) ► 10x Tris buffered saline (TBS) buffer (Bio Rad) ► Blocking buffer for primary antibodies (1xTBS, 0.1% tween 20 (Bio Rad), 0.1% sodium azide (Sigma Aldrich) and 5% bovine serum albumin (BSA) (Sigma Aldrich) ► Blocking buffer for secondary antibody (1xTBS, 0.1% tween 20 (Bio Rad), 5% milk (Blotting Grade Blcoker Non-fat Dry Milk) ► SuperSignal West Femto maximum sensitive chemiluminescence substrate solutions (Thermo Scientific, USA)
Antibodies for Western blot analysis	► Anti-α-enolase (enolase-1) polyclonal antibody (Cell Signaling) ► Anti-Annexin A1 polyclonal antibody (Cell Signaling) ► Ani-HSP90 polyclonal antibody (Cell Signaling) ► Anti-Actin polyclonal antibody (Santa Cruz) ► Rabbit IgG Horseradish Peroxidase (HRP) (Cell Signaling) ► Mouse IgG Horseradish Peroxidase (HRP) (Cell Signaling)

(Continue…)	► Rabbit (DA1E) mAb IgG XP® Isotype Control (Cell Signaling) ► Polyvinylidene difluoride (PVDF) membrane (Immobilon-P) Milipore ®, pore size of 0.45 μm, cut size 20 cm X 20 cm. ► Mini Trans-Blot® filter paper Bio Rad® ► 7.5% Mini-PROTEAN® TGX™ Precast Protein Gels, 10-well, 50 μl (Bio Rad) #4561024

Antibodies, reagents and chemicals for immunofluorescence staining	► Primary antibody: Annexin A1 (D5V2T)® XP Rabbit mAb: prepared by dilution in 1% FBS in PBS (1:400) for immunofluorescence staining ► Secondary antibody: Alexfluor 488 Donkey anti rabbit (1:200) in 1X PBS for immunofluorescence staining ► Collagen buffer (10 μg/mL) in plain DMEM: prepared by adding 167 μL to 50 mL plain DMEM. ► 4% P-Formaldehyde in saline ► 0.2% triton in PBS ► Blocking buffer (10% FBS in PBS) ► A counterstain (TOTO-3) with DAPI kit (Sigma Aldrich, USA): prepared by mixing 0.3 μl TOTO-3 with 1800 μL of PBS. ► Vectashield Mounting medium (one drop in each well of the chamber slide).
Reagents for the preparation of COM crystals	► Sodium oxalate ► Tris buffer saline ► NaCl ► Calcium chloride ► Methanol

Materials for *Drosophila melanogaster* experiments	— *Drosophila melanogaster* (wild type Oregon red flies) (Lab of Dr. Michael Romero, Mayo Clinic, MN, USA) — Flies vials (Sigma Aldrich™, USA) — Flies food (*see* Table 10) — Flies incubator — Insect phosphate buffer saline (iPBS) as fly physiological solution (*see* Table 10) — Schneider's solution for fly dissection — Stereomicroscope and bench set up for dissecting fruit flies and extracting Malpighian tubules (MTs) — Poly-L-lysine slides — Dissecting dish

Table 10. *Drosophila* food composition.

Ingredients	**Amount**
Tayo Agar, Agar-agar (Mooragar MA, Inc.)®	10 g
Sucrose (Sigma Aldrich)®	15 g
Glucose (Sigma Aldrich)®	33 g
Yeast (*Saccharomyces cerevisiae*)	35 g
Maize meal (Yellow corn Hodgson mill)®	15 g
What germ (Bob's red meal)®	10 g
Treacle (molasses) (Berer Rabbit)®	30 g
Soya flour (Hodgson mill)®	1 tablespoonful
Nipagin (10 mL)	25 g Methylparaben (Nipagin M) (Tegosept M™) (Sigma Aldrich)® in 250 mL ethanol
Propianic acid (Sigma Aldrich)®	5 mL
Water	Complete to 1 Liter

Table 11. Chemical composition of insect phosphate buffer saline (iPBS)

Chemicals	**Stock solution (M)**	**Final (mM)**	**Volume (mL) or amount (mg) For 1 Liter**
NaCl	2	121.5	60.75 mL
KCl	2	20	10 mL
Glucose	180.16	20	3.69 mL
(4-(2-hydroxyethyl)-1-piperazineethanesulfonic acid) (HEPES)	1	8.6	8.6 mL
$NaHCO_3$	84.01	10.24	860 mg
$NaH_2PO_4.H2O$	137.99	4.5	621 mg

**The pH of the final iPBS solution was adjusted to 6.8, with osmolarity of 350 +/- 5 mOsm, sterilized by filtration through bacterial filter and stored at 4°C upon use.*

5.2.1 Cell count and viability

The cell viability and count were determined using Trypan blue exclusion test, where 10 μL of each cell suspension was mixed with 10 μL of trypan blue dye (0.4%), and then 10 μL of the mixture was taken onto cell counting chamber slide (Countess ™). The cell count and viability were calculated using cell counter (Invitrogen Countess automated ™). The cell viability and counts for MDCKI and JL cells were 1.5 $X10^6$ / mL, 1.8 $X10^6$ / mL and 98% and 96%, respectively.

5.2.2 Cytotoxicity by MTT assay

The cytotoxicity of TGAME, compound 6, its synthetic intermediates, BF, M1 and compound 16 was evaluated by MTT colorimetric assay (MTT Kit ThermoFisher Scientific, USA). The cells of MDCKI or JL were seeded onto 96-well microplates at a density of 1×10^4 cells per well and treated with different amounts (0, 5, 10, 25, 50 μM or μg/mL in DMSO/ phosphate buffered saline (PBS)) of the tested substances for 24 h. The MTT (15 μL) working solution (5 mg/mL in PBS) was added to each well and incubated at 37°C for 3 h. After the addition of the stop solution (100 μL), the optical density (OD) was measured at 570 nm using a microplate reader (SpectraMax 190 Microplate Reader, USA).

Cell viability was calculated as a percentage of viable cells in tested substance-treated group *versus* untreated control by the following equation:

Cell viability (%) = [OD (tested subs) − OD (blank)] / [OD (control) − OD (blank)]×100

5.2.3 Cell-COM crystal binding assay

Preparation of COM crystals: Sodium oxalate (1 mM) in Tris buffer saline (50 mL) containing 90 mM NaCl (pH 7.4) was added to a gently stirred solution of 10 mM calcium chloride (50 mL). The mixture was incubated at RT overnight and then centrifuged at 3,000 rpm for 5 min. Crystals were re-suspended in methanol (1 mL) and centrifuged for 5 min at 3,000 rpm. The methanol supernatant was aspirated and the crystals were air-dried at RT, and then sterilized using UV radiation for 30 min before use in cell culture work. The dried crystals were examined under Zeiss Axiophot microscope using 10 X differential interference contrast (DIC) lens and appeared as six-sided prisms.

MDCKI cells (5×10^5 cells) were seeded into 6-well cell culture plate and incubated in a complete culture medium for 24 h. We excluded JL cells as they were not able to be polarized

upon adding COM crystals. Compound 6 was added (0, 1 μM, 10 μM, 25 μM, 50 μM) to the cells for 3 h (concentration-dependent study), whereas the cells kept in culture medium without compound represented as the control. The cells were pretreated with 0, 25 or 50 μM (the optimal two concentrations obtained in the previous study) of compound 6 for 1, 3 or 6 h (time-course study). The culture medium was aspirated and the cells were washed gently with PBS. Thereafter, cells were incubated for 30 min with COM crystals (100 μg crystals/mL culture medium), followed by washing 5 times with plain medium to remove non-adherent crystals. Bound crystals in each well were imaged and counted under a phase-contrast microscope (Zeiss) in 15 random high power fields (HPFs). The assay was also done for testing activity of the BF (50 μg/mL), M1 (with a concentration < IC_{50}) and compound 16 (50 μM) *versus* TGAME.

5.2.4 Annexin A1 neutralization by a specific anti-Annexin A1 antibody

The surface expression of Annexin A1 was blocked by pretreating the cells with rabbit polyclonal anti-Annexin A1 antibody (Cell Signaling, USA). Briefly, the confluent polarized cells were incubated for 15 min with bovine serum albumin (1%) in membrane preserving buffer (0.1mM $CaCl_2$ and 1mM $MgCl_2$ in PBS) to block non-specific bindings (Scheme 7). Cells were then washed with the same buffer (3X) followed by incubation anti-Annexin A1 antibody (0.2 μg/mL) or rabbit isotype-controlled IgG (0.2 μg/mL**)** at 37°C for 30 min. COM crystals (100 μg crystal/mL medium) were incubated for 1 h at 37°C, after washing the cells with the buffer. Unbound crystals were removed by washing with PBS (5X). Bound COM crystals were counted under a phase-contrast microscope by assessing 15 random HPFs.

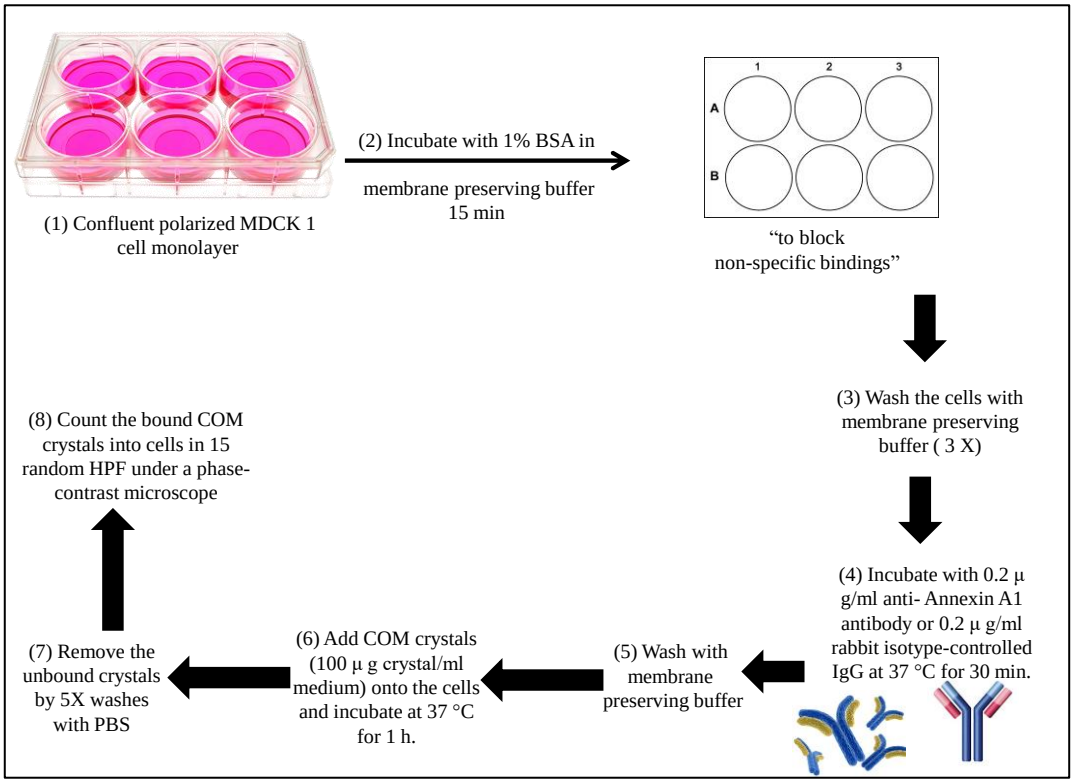

Figure 31. Schematic steps for Annexin A1 protein neutralization on the surface of MDCKI cells by anti-Annexin A1 antibody.

5.2.5 Analysis of Annexin A1, α-enolase and HSP90 by Western blot

Subcellular fractionations of MDCKI cell protein and subsequent Western blot were used to measure the concentrations of cytosolic, membrane and whole Annexin A1, α-enolase and HSP90. MDCKI cells (5×10^5 cells) were seeded into each well of 6-well plate and cultured in a complete medium overnight. After treatment with the appropriate concentration for each tested compound for 3 h, the cells were washed with cold PBS and incubated for 10 min at 4°C with cytosolic extracting buffer containing mainly 10 mM piperazine-N, N′-bis (PIPES), 0.5 mM EDTA and 0.02% digitonin, with gentle shaking. The cells were scrapped with the buffer, collected and centrifuged for 10 min at 10,000 rpm. The supernatant containing cytosolic proteins was next collected. The remaining cell pellet was mixed with membrane extracting buffer (60 mM Tris-HCl of pH = 6.8, 2% sodium dodecyl sulfate (SDS), 10% glycerol and 5% *β*-mercaptoethanol) and incubated for 30 min in ice bath with gentle shaking every 10 min, and named as "membrane fraction". Whole cell lysate was extracted from using whole lysate buffer. The protein concentrations were determined by Bradford's method (183) using Pierce BCA Protein Assay Kit (Thermo Scientific).

Each protein fraction (30 μg/lane) was mixed with Laemmli sample buffer (1:1), 2x (Bio Rad) and separated by 7.5% ready gel (BioRad), where all samples were boiled at 99ºC for 5 min prior to loading onto gel. The gel was run for 90 min at 100 V then transferred onto a nitrocellulose membrane using 1x transfer buffer. The membrane was probed by incubation at 4°C overnight with rabbit polyclonal anti-Annexin A1 (1:1000), rabbit polyclonal anti-HSP90 (1:1000), rabbit polyclonal anti-α enolase (1:1000) and mouse monoclonal anti-Actin (1:1000) antibodies (Cell Signaling ®, USA) in blocking buffer, separately. After washing with TBS/0.1% tween three times for 5 min each, the membrane was incubated with the corresponding secondary antibody conjugated with horseradish peroxidase (Rabbit IgG for all primary antibodies or mouse IgG Horseradish Peroxidase for β-actin) (1:5000) (Cell Signaling ®) in 1x Tris-buffered saline /0.1% tween 20 and 5% milk for 1 h at RT. The immunoreactive bands were detected by developing in SuperSignal West Femto maximum sensitive chemiluminescence substrate solutions, and then visualized by autoradiogram. The intensity corresponding to each band was measured by AEase FC software (Mayo Clinic).

5.2.6 COM crystals bound-Annexin A1 protein immunofluorescence staining and confocal microscopy

Collagen buffer (200 µL) was added to a chamber slide and incubated for 15-20 min at 37ºC followed by washing with 1X PBS. MDCKI cells (12,000/well) were seeded in each chamber, and incubated at 37ºC overnight. The media was removed and cells were treated with/without compound 6 (50 µM) for 3 h. Cells were then gently washed with PBS followed by fixation with 4% P-formaldehyde in saline (200 µL) for 15 min at RT, and finally washed twice with cold 1X PBS. Triton (0.2%) in PBS for 5 min was used for cell permeabilization, and then the cells were washed three times with PBS. A blocking buffer (200 µL) was added for one hour at RT, then replaced by the primary antibody with incubation overnight at 4ºC. The next day, the cells were washed with PBS (3X) for 5 min. The 1º antibody was replaced with the 2º antibody and incubated in the dark for 60 min, followed by washing with PBS (3X). The counterstain (TOTO-3) was added and incubated for 20 min at RT, and then washed one time with 1XPBS. The chamber frames were removed. The slide was mounted with Vectashield Mounting medium, and then the cells were examined using Zeiss confocal microscope (Axiovert 100 M) with 63 X oil immersion lens.

5.2.7 *Drosophila* assays as a physiological model for urolithiasis diseases

Oregon R (red) *Drosophila melanogaster* female flies were used as wild type for these experiments, where the female flies have Ca^{++} stores at the first 600 μM of their anterior pair of Malpighian tubules. There is a characteristic morphological difference between female and male insect. The female abdomen is long and pointed, but male abdomen is darker, short and blunt (Figure 32) (184).

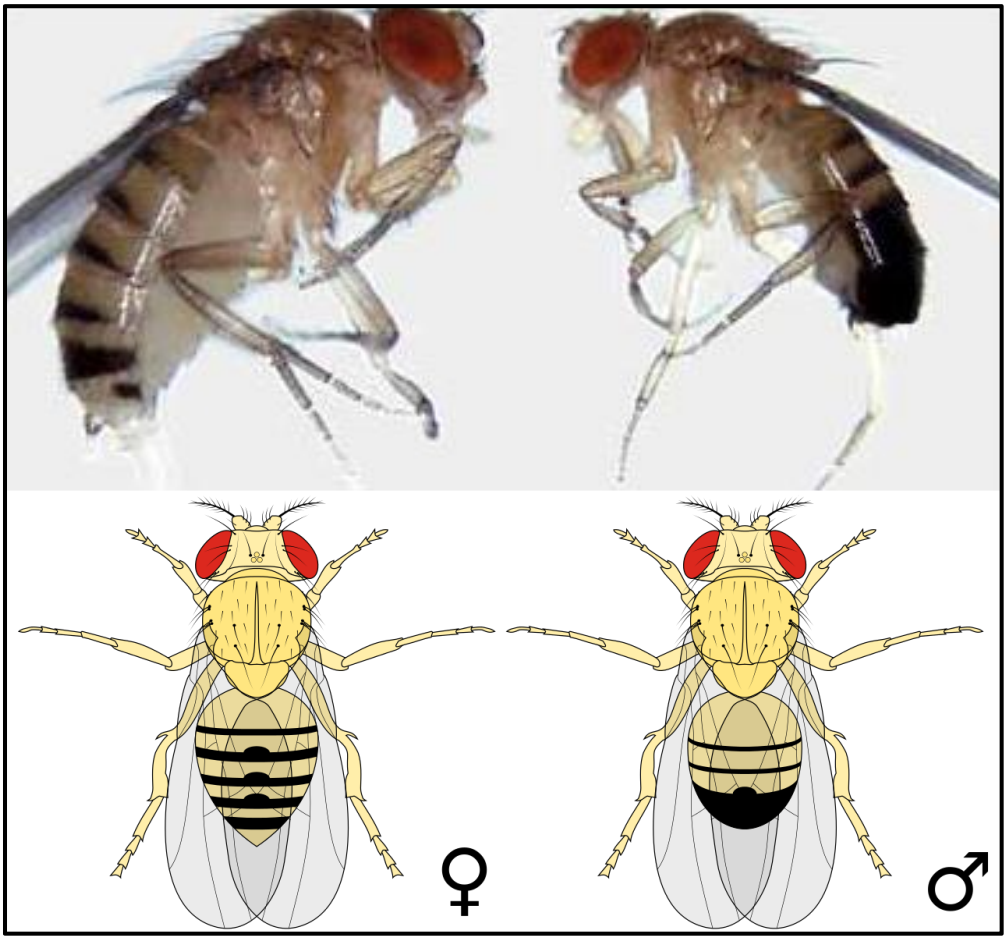

Figure 32. Morphological differences between adult female and male *Drosophila*.

The male and female flies were grown inside vials containing fly food and kept inside incubator at 28-28.5 °C (Figure 33).

Flies incubator (28 - 28.5 ˚C) Fly Food vials

Figure 33. *Drosophila* culture conditions.

The life cycle of the flies involves several stages. After egg fertilization, the embryo developed after one day. Then, the egg hatches to give the larvae that eats and grow through three molts over five days. The larvae pupates and undergoes metamorphosis over a period of four days to give the adult fly (Figure 34). The flies

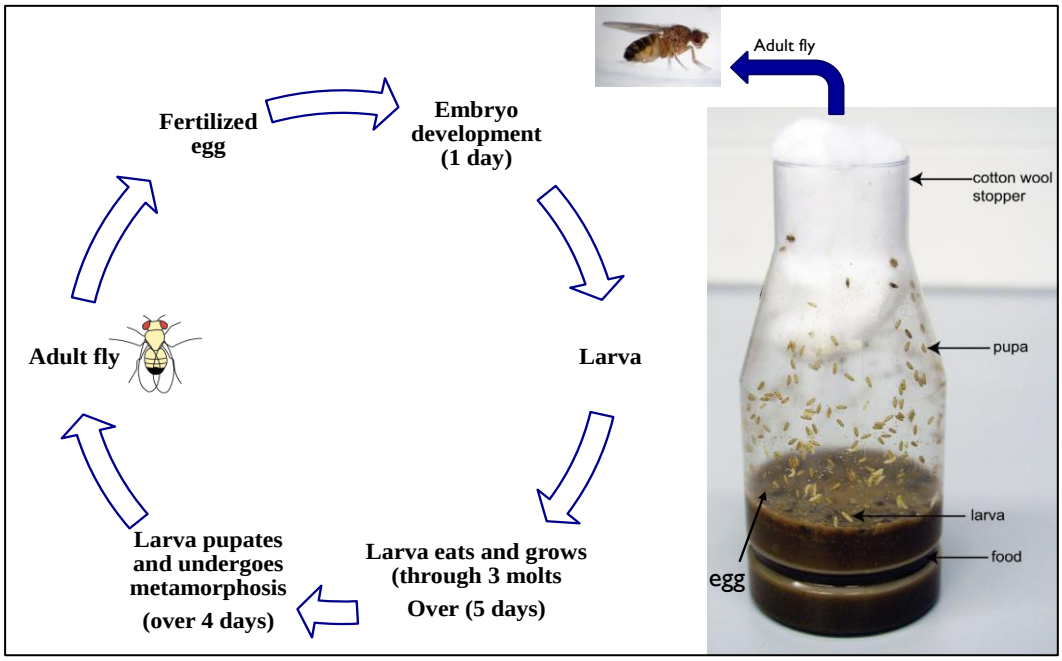

Figure 34. *Drosophila* life cycle.

5.2.7.1 Drosophila dissection for Malpighian tubules (MTs) extraction

A cold Schneider's solution was poured into a dissecting dish and a single anesthetized female fly (by passing CO_2 gas current inside the fly vials for few seconds) was transferred by the use of fine forceps into the dish under a dissecting stereoscope (Figure 35).

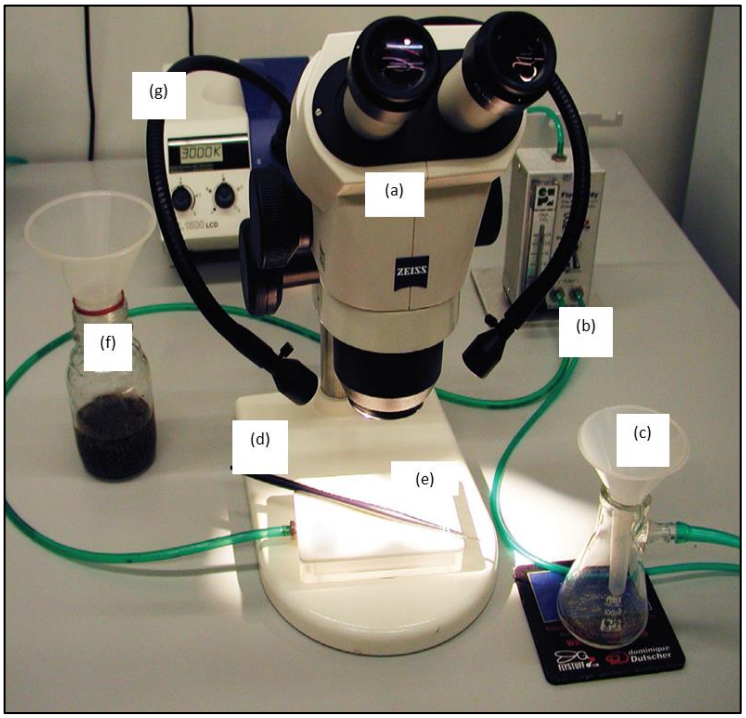

Figure 35. Bench set up for work with *Drosophila*: (a) stereomicroscope, (b) CO_2 regulator, (c) chamber for anesthesia, (d) paint brush, (e) porous pad connected to CO_2, (f) a fly morgue: a bottle containing methanol, and (g) a cold light source.

The fly was handled using a set of forceps, one is to hold it by the thorax region and the other one to gently grip the posterior of the abdomen. The posterior of the fly was opened. Once the hindgut is visible, the distal end was gripped, and the gut as well as the MTs system (Figure 36) (185) were freed from the underlying tracheoles by pulling the hindgut away from the body through repetitive, brief tugs. The anterior and posterior MTs were visible where they meet the junction of the midgut and hindgut through the ureter. The first pair of MTs to be free will likely be the posterior tubules as they encircle the hindgut. The anterior MTs were pinched at the ureter with fine forceps once the second set of MTs is free of the abdomen. This will separate the anterior MTs from the gut and close the ureter. The free anterior MTs were picked up with a fin glass rod by sliding it under the ureter such that the tubules fall to either side. MTs were lifted straight up out of the solution.

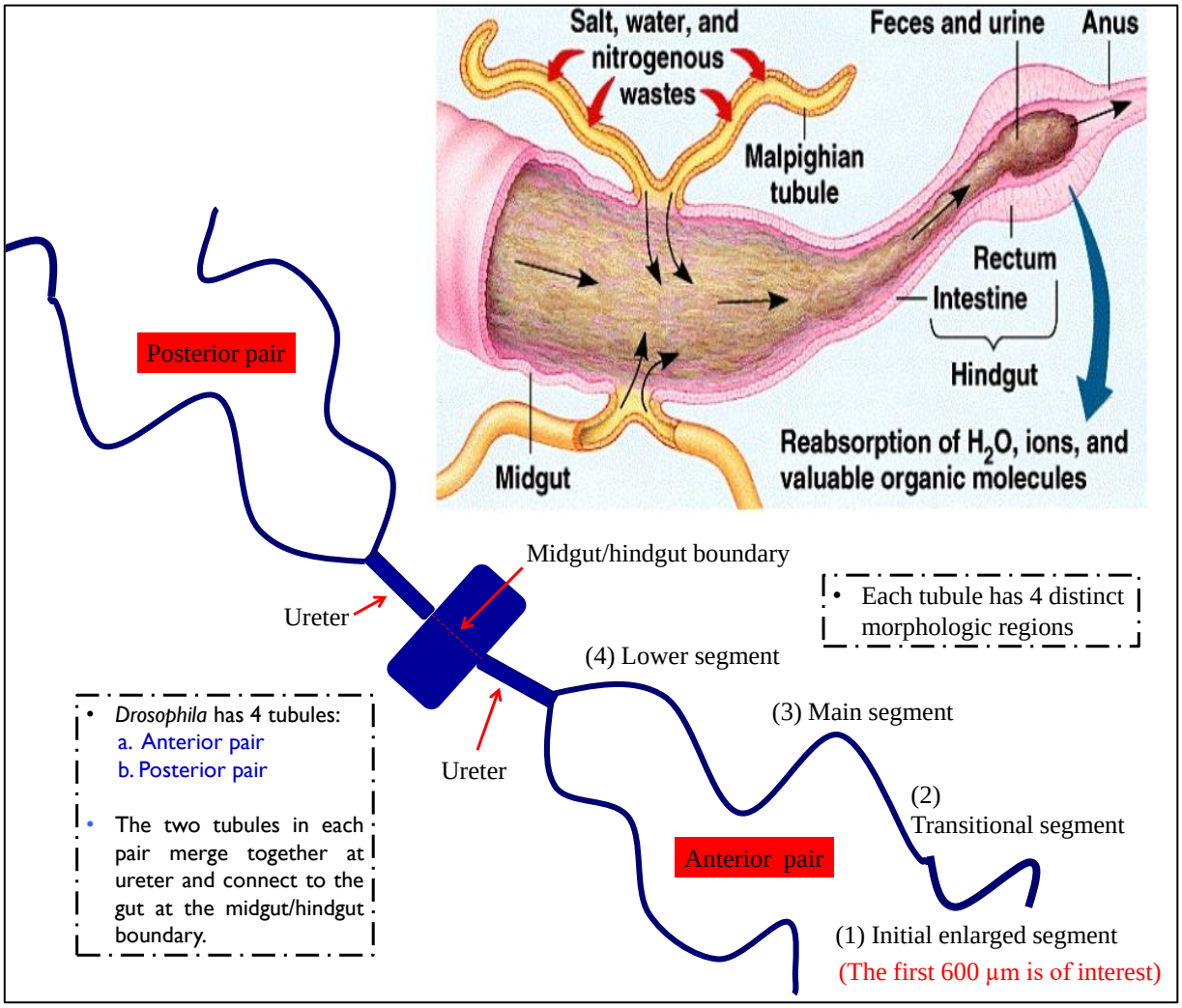

Figure 36. Anatomy of *Drosophila melanogaster* Malpighian tubules system.

The glass rod was turned up in such that the MTs and ureter are adhered to the underside of the rod and the ureter was lowered straight down onto the poly-L-lysine coated slide (Figure 37). The ureter was affixed and the distal ends of the MTs were sealed by pressing the ureter down onto the glass slide. Now, the MTs should be floating up in the solution with the ureter anchored to the slide. By using the fine end of the glass rod, each tubule was swapped across the slide surface. The glass rod was braced against the slide to avoid crushing the tubule and the rod had to be passed gently over the top of the tubule by distal to proximal movement to attach the full length of each tubule to the surface of the poly-L-lysine-coated slide.

Figure 37. The preparation of poly-L-lysine slides. (A) Liquind blocker marker. (B) Slides (Fisher brand™). (C) Poly-L-lysine. (D) Slides divided into champers having iPBS.

5.2.7.2 *Drosophila* crystallization assay: *Ex vivo* oxalate ± TGAME

Twenty four female flies (7 days age) were used in the experiment. Subsequently, twenty four Malpighian tubules (MT) were obtained by dissecting the flies in Schneider's solution and transferred to poly-L-lysine coated slides with iPBS (insect phosphate buffer saline).

The tubules were divided into two main groups (control and treated group; n=12 each). The treated group was pretreated with 100 μM of TGAME in iPBS for 20 min, followed by incubation with 100 μM of compound 6 and 10 mM Na-oxalate (Figure 38). Control group was incubated only with 10 mM Na-oxalate in iPBS. MTs were incubated for 1 h with fresh solutions, which was replaced every 15 min. Crystallization of CaOx was monitored by imaging the initial 600 μm of the anterior MTs using a Zeiss Observer® using DIC microscopy. Crystallization was quantified using ImageJ as previously (186).

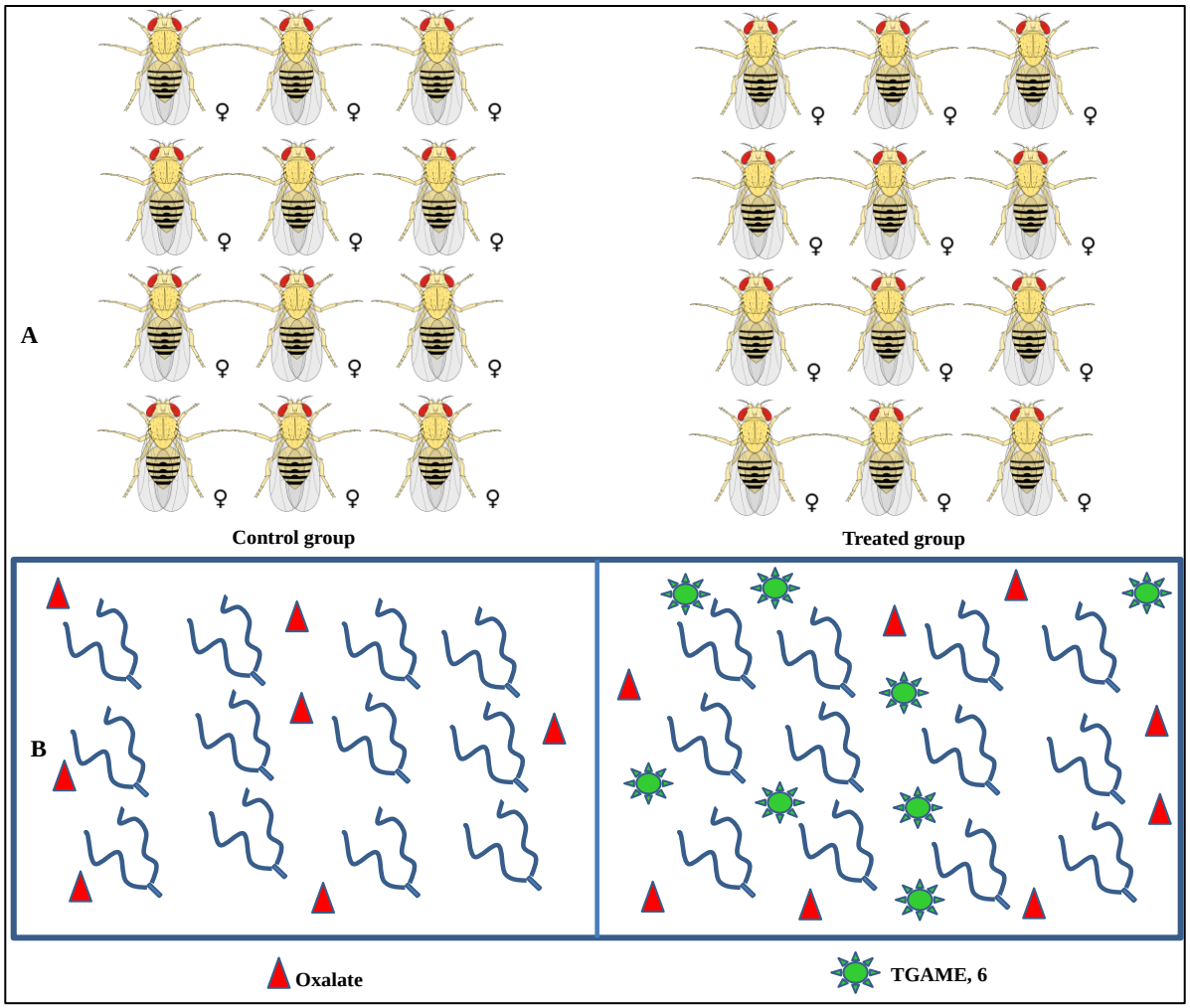

Figure 38. Schematic representation of the *ex vivo* experiment using *Drosophila* model. (A) Adult female flies (n = 12 for control and treated groups). (B) MTs tubules isolated from the dissected flies and kept on a pol-L-lysine covered slide. Treated group with TGAME 100 μM + oxalate 10 mM *versus* control with oxalate only (10 mM).

5.2.7.3 *Drosophila* feeding experiment: *In vivo* oxalate ± TGAME

Twenty two female flies were used in the experiment (11 control and 11 treatment) and then kept for 24 h on feeding with fly food mixed either with sodium oxalate (10 mM) or a mixture of TGMAE (50 μM) and sodium oxalate (10 mM) (Figure 39). After 24 h, the flies were dissected in Schneider's medium and transferred immediately to poly-L-lysine coated slides with iPBS. Crystallization was monitored by imaging the anterior MTs as above.

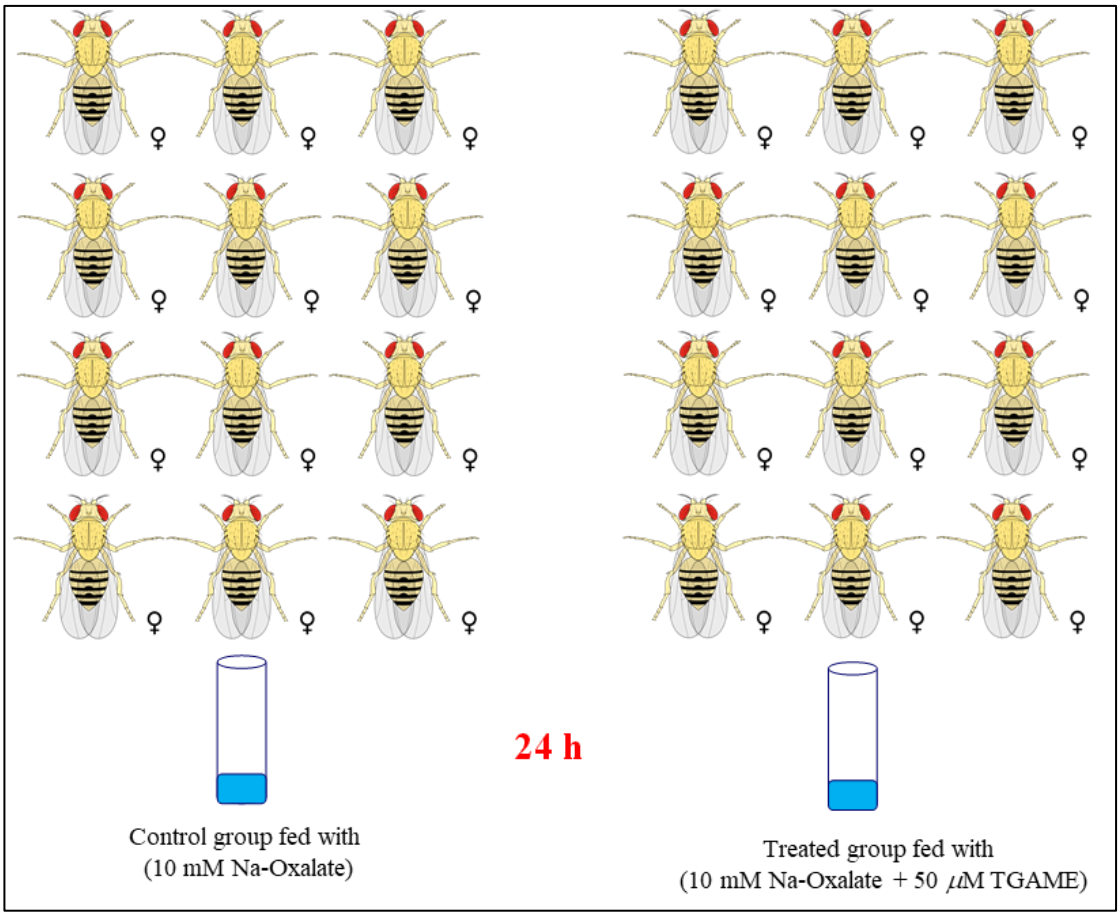

Figure 39. Schematic representation of the *in vivo* experiment using *Drosophila* model.

5.2.8 DPPH assay for antioxidant activity

To 1.96 mL of DPPH (0.1 mM) solution, different volumes (2 – 20 μL) of the tested compound (1 mM in DMSO), made up to 40 μL with DMSO were added. The reacted mixtures were incubated for 20 min at RT in the dark, and the absorbance was measured at 517 nm. Two mL of DPPH was served as control. The percentage of radical scavenging activity of tested compounds was calculated using the following formula:

$$\%\ RSA\ = \frac{\text{Absorbance of control} - \text{Absorbance of test}}{\text{Absorbance of control}}\ X\ 100$$

Principle of DPPH assay

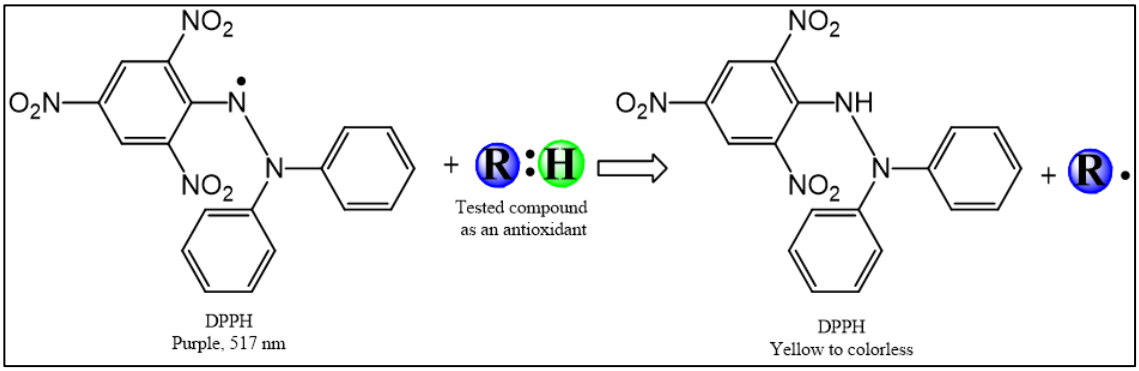

Figure 40. DPPH assay reaction.

5.3 Results and discussion

MDCKI cell cytotoxicity of TGAME and its hydrolytic metabolites.

To determine the safe *in vitro* concentration, cytotoxicity was assessed by the MTT assay after exposing MDCKI cells to increasing concentrations of BF, M1, TGAME, and compound 16 (0, 5, 10, 25, 50) (μg/mL for BF and μM for rest of compounds) for 24 h. Gallic acid and methyl quinate, which are products of the galloylquinic acid hydrolysis, were also tested. TGAME did not exert any apparent MDCKI and JL cells cytotoxicity in concentrations up to 154.8 ± 3.5 and 200.8 ± 10.2 μM, respectively. The inhibitory concentration 50% (IC_{50}) on MDCKI cells of the hydrolytic products of the compound, methyl quinate and gallic acid, were 119.7 ± 7.2 μM and 34.1 ± 6.1 μM, respectively. The IC_{50} of BF, M1 and compound 16 on MDCKI cells was 772.7 ± 10.2 μg/mL, 8.7 ± 0.3 μM and 166.3 ± 4.1 μM, respectively (Figure 41-44) (Table 12). Therefore, the nontoxic concentrations below the IC_{50} values were used in subsequent experiments for all compounds.

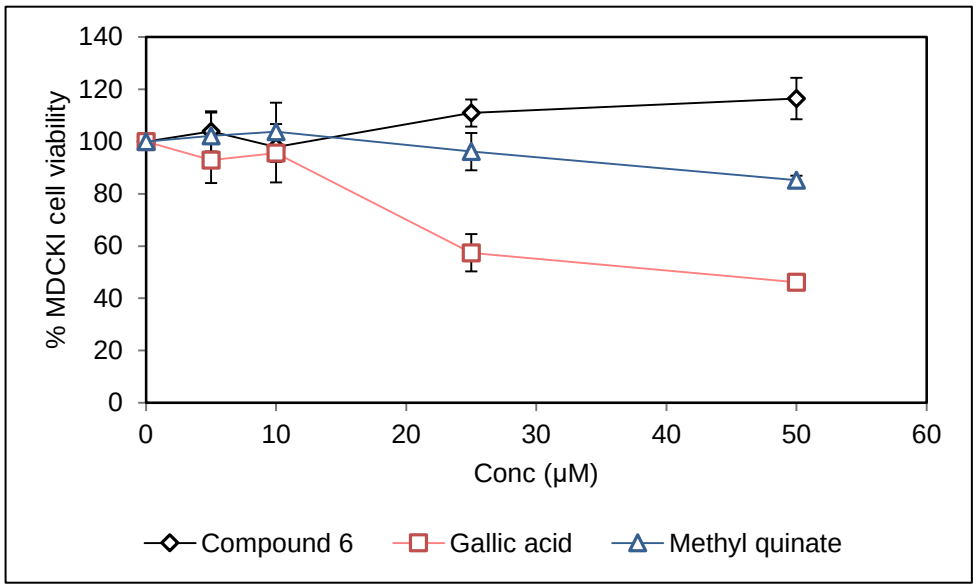

Figure 41. Cytotoxic effects of TGAME (6) and its synthetic intermediates in MDCKI Cells. The assay of cytotoxicity was evaluated by MTT assay. Cells were plated onto 96-well microplates (1×10^4 cells/well) and treated with various concentrations of each tested compound (0, 5, 10, 25, 50 μM in DMSO/PBS) for 24 h. Data were expressed as means ± S.D. of three independent experiments.

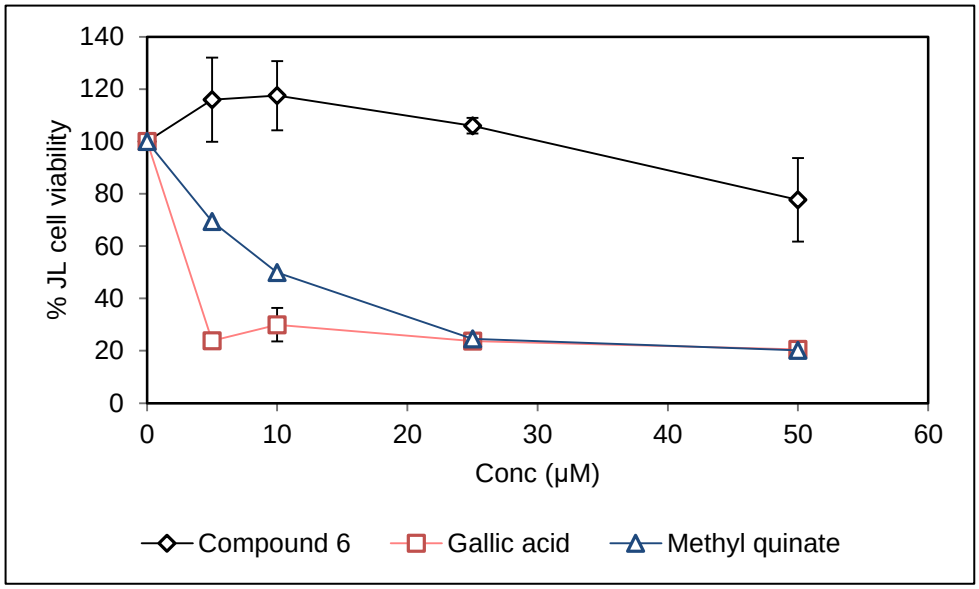

Figure 42. Cytotoxic effects of TGAME (6) and its synthetic intermediates in JL cells. The assay of cytotoxicity was evaluated by MTT assay. Cells were plated onto 96-well microplates (1×10^4 cells/well) and treated with various concentrations of each tested compound (0, 5, 10, 25, 50 μM in DMSO/PBS) for 24 h. Data were expressed as means ± S.D. of three independent experiments.

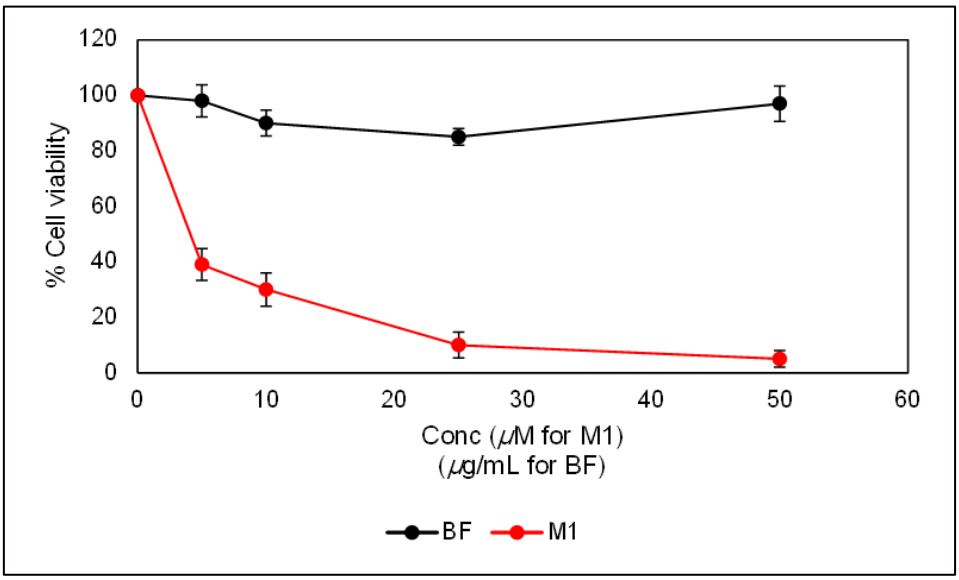

Figure 43. Cytotoxic effects of *n*-butanolic fraction (BF) of *C. lucens* and its biotransformed compound (M1) by *A. aliaceus* in MDCKI Cells. The assay of cytotoxicity was evaluated by MTT assay. Cells were plated onto 96-well microplates (1×10^4 cells/well) and treated with various amounts of the tested substances (0, 5, 10, 25, 50 μM for M1 and μg/mL for BF) in DMSO/PBS) for 24 h. Data were expressed as means ± S.D. of three independent experiments.

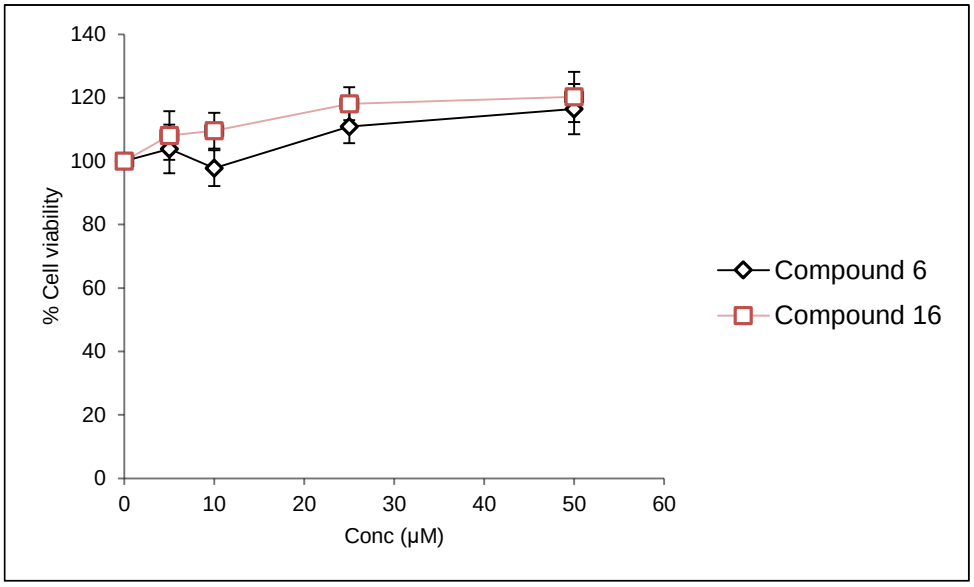

Figure 44. Cytotoxic effects of TGAME (compound 6) and compound 16 in MDCKI Cells. The assay of cytotoxicity was evaluated in renal epithelial cells MDCKI by MTT assay. Cells were plated onto 96-well microplates (1×10^4 cells/well) and treated with various concentrations of each tested compound (0, 5, 10, 25, 50 μM in DMSO/PBS) for 24 h. Data were expressed as means ± S.D. of three independent experiments.

Table 12. IC_{50} of compound 6, its hydrolytic products, BF, M1 and compound 16 on MDCKI and JL cells. The values are expressed in μM for all tested compounds except BF in μg/mL.

#	**IC_{50}**	
Cell line	MDCKI	JL
Compound 6	154.8 ± 3.5	200.9 ± 10.2
Gallic acid	34.1 ± 6.1	20.0 ± 2.5
Methyl quinate	119.7 ± 7.2	20.1 ± 1.5
BF	772.7 ± 10.2	-
M1	8.7 ± 0.3	-
Compound 16	166.3 ± 4.1	-

COM crystal-adherence assay. Microscopic examination of COM crystals revealed their appearance as six-sided prisms (Figure 45).

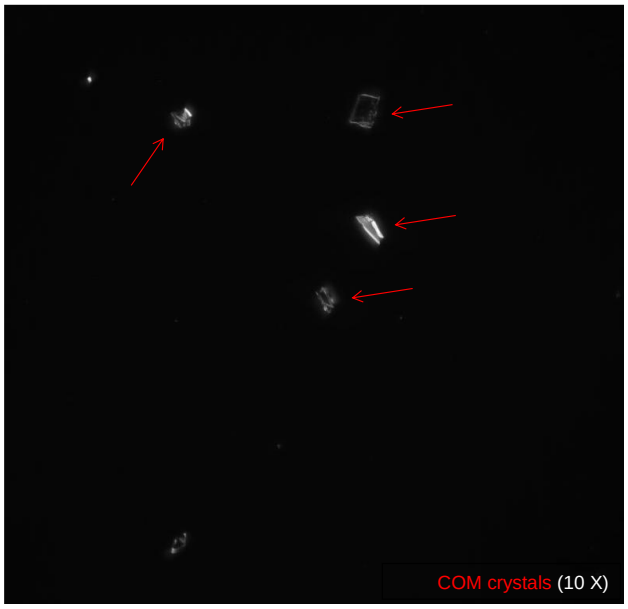

Figure 45. Microscopical examination using DIC filter of Calcium oxalate monohydrate crystals (COM) crystals. They appears as six-

MDCKI cells (originally derived from the distal nephron of a female dog), were used as an *in vitro* model since the initial site of nephrolithiasis has been proposed to be in the distal nephron, as supported by histopathological analysis (187, 188). MDCKI cells were incubated with COM crystals (100 μg/mL of culture medium) after pretreatment with 50 μM TGAME for up to 6 h. The amount of TGAME used in this study were based upon concertation-response and cytotoxicity studies along with the results from the crystal binding assay (concentration-dependence study) that demonstrated TGAME significantly decreased the number of crystals control (Figure 46) bound to the cell surface at both 25 μM and 50 μM *versus* the, while the concentration of 50 μM was more inhibitory in comparison with 25 μM (p <0.05).

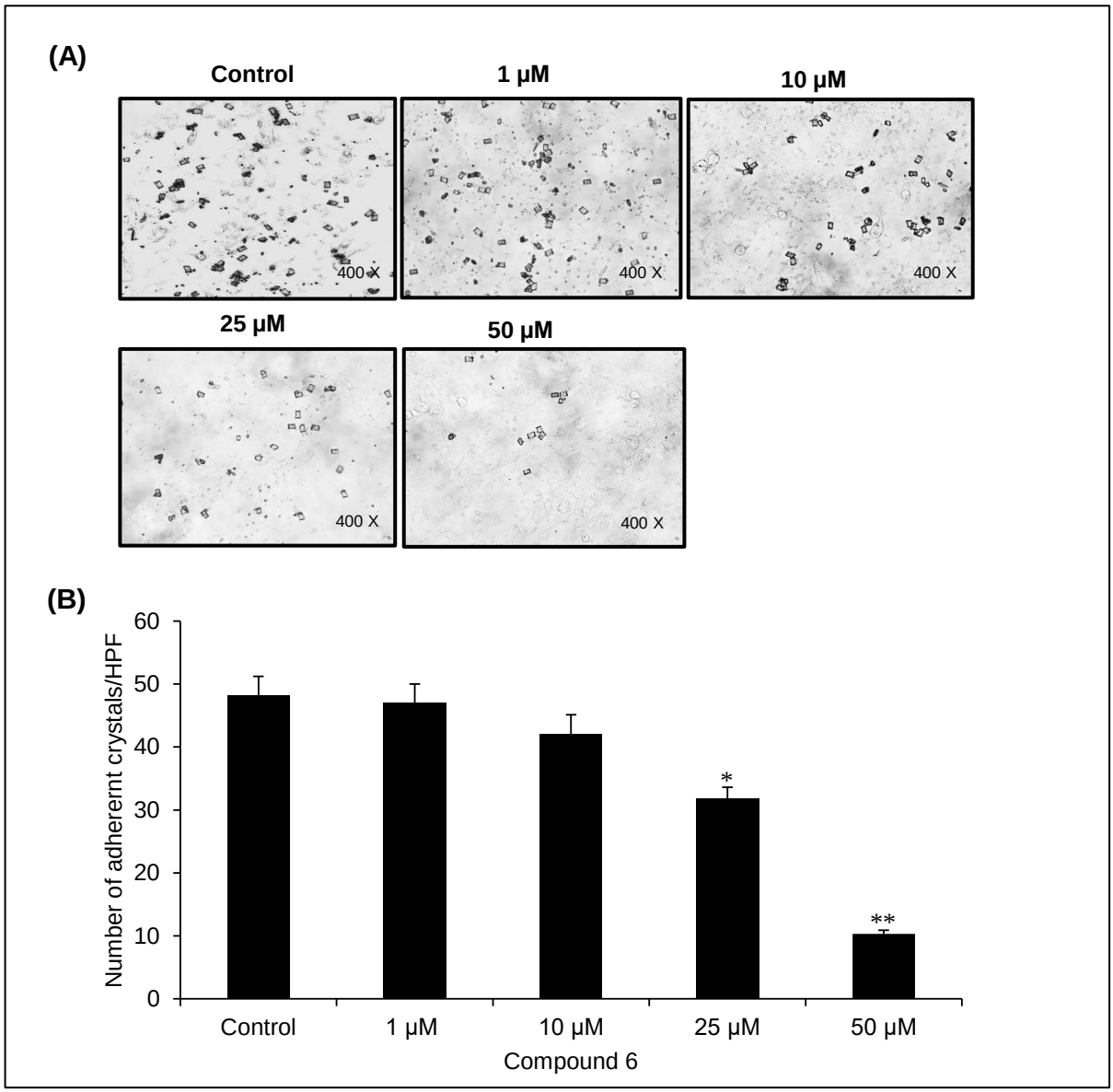

Figure 46. Effect of TGAME (6) on COM crystal-binding capability of the cells was dose dependent. MDCKI cells were pretreated with various concentrations of compound 6 (0, 1, 10, 25, and 50 μM) for 3 h followed by incubation with COM crystals (100 μg/ mL of culture medium) for 30 min. **(A)** After washing with plain DMEM culture media, images of the remaining crystals were captured under a phase-contrast microscope for at least 15 high-power fields (HPF) in each well. The original magnification power was ×400. **(B)** The remaining crystals that adhered on the cell surface were then counted. *$p < 0.05$ vs. control and **$p < 0.05$ for the effect of the concentration 50 μM *vs.* 25μM of compound 6.

Results from the crystal-binding assay (time-coarse study) demonstrated that pretreatment with TGAME (50 μM) significantly (p <0.05) decreased the number of cell surface associated-COM crystals by approximately 50% at 3 h and 6 h in comparison with the control (Figure 47). Assays were done at early time points (not exceeding 6 h) to focus on the crystal-binding stage and largely avoiding subsequent COM crystal phagocytosis (117, 189). A 3 h pretreatment time was selected to determine concentration-dependent effects (0-50 μM), since effects were measureable and a longer time of 6 h did not increase the magnitude. TGAME decreased crystal-binding in a concentration-dependent manner across this range with maximal effects at 50 μM.

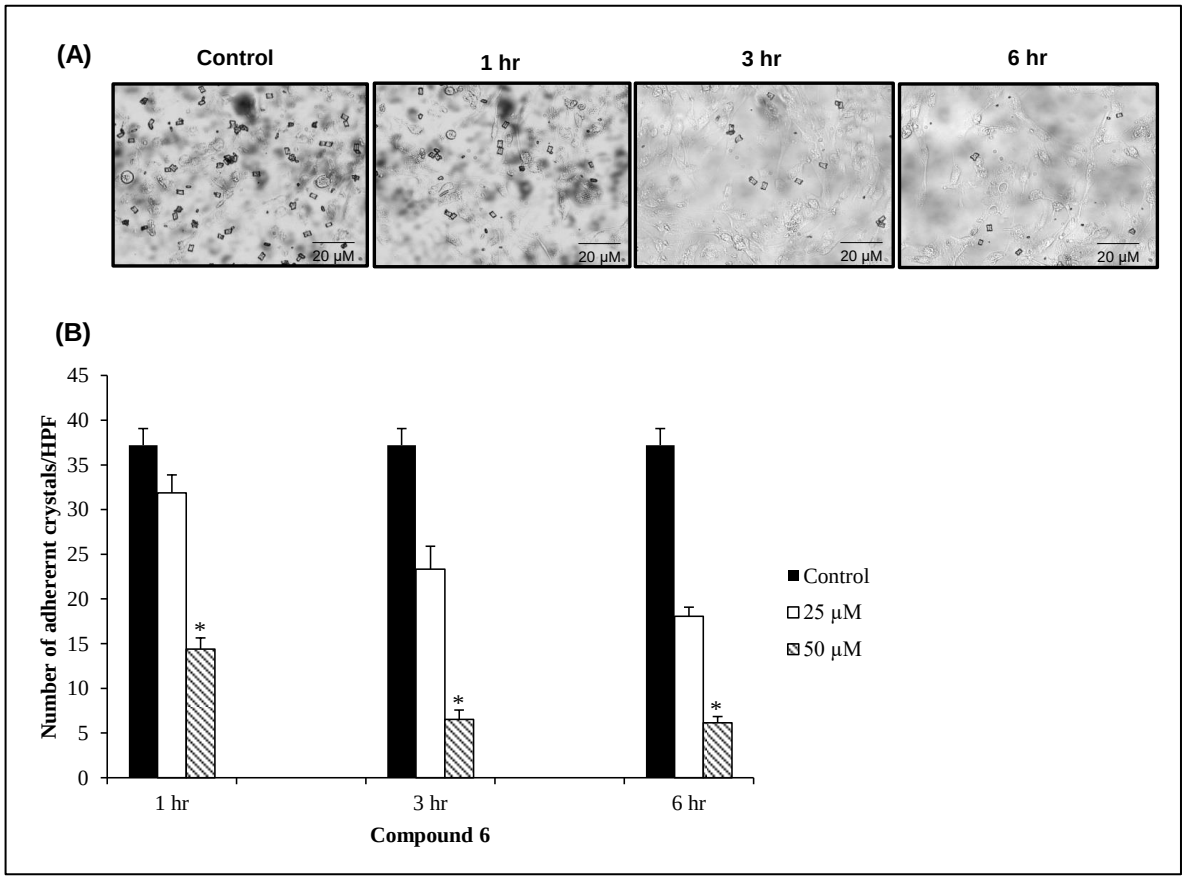

Figure 47. Pretreatment of TGAME (6) reduced COM crystal binding onto the cell surface. MDCKI cells were treated with 0, 25 or 50 μM compound 6 for 1, 3 or 6 h prior to incubation with COM crystals (100 μg/mL of culture medium) for 30 min. **(A)** After washing with plain DMEM culture media, images of the remaining crystals were captured under a phase-contrast microscope for at least 15 high-power fields (HPF) in each well. **(B)** Crystals remaining on the cell surface were then counted. *p < 0.05 vs. control.

Of note, one of the hydrolytic metabolites (gallic acid) of the compound significantly (p <0.05) decreased the crystal binding at a lower concentration (10 μM) after 3 h *versus* the control (Figure 48). Thus, further experiments used exposure to 50 μM of TGAME for 3 h.

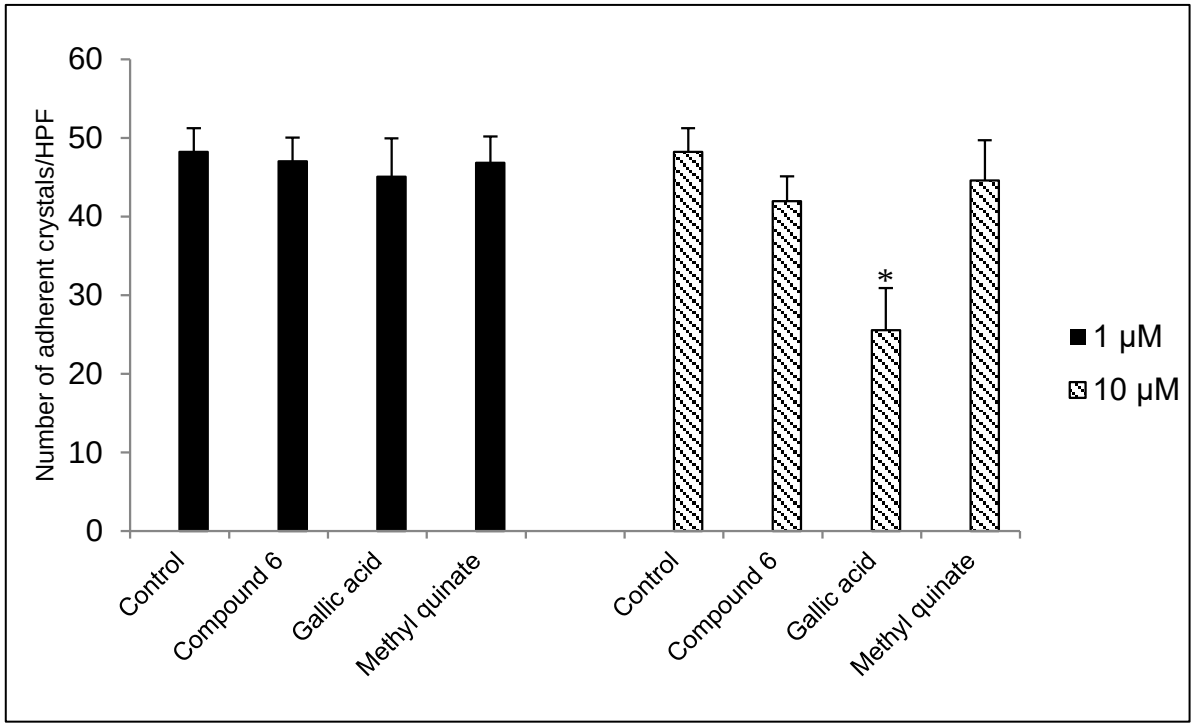

Figure 48. Effects of TGAME (6) and its synthetic intermediates on COM crystal binding to MDCKI cells. The cells were treated with 0, 1 or 10 μM of each compound for 3 h prior to incubation with COM crystals (100 μg/mL of culture medium) for 30 min. After washing with plain DMEM culture media, images of the remaining crystals were captured under a phase-contrast microscope for at least 15 high-power fields (HPF) in each well. Crystals remaining on the cell surface were then counted. *$p < 0.05$ vs. control.

Neutralization by a specific anti-ANXA1 (Figure 49), followed by COM incubation with MDCKI, showed a significant decrease in the bonded COM to the cells, which further confirms the hypothesis that AnAx1 protein is involved in COM adherence to the surface of renal cells.

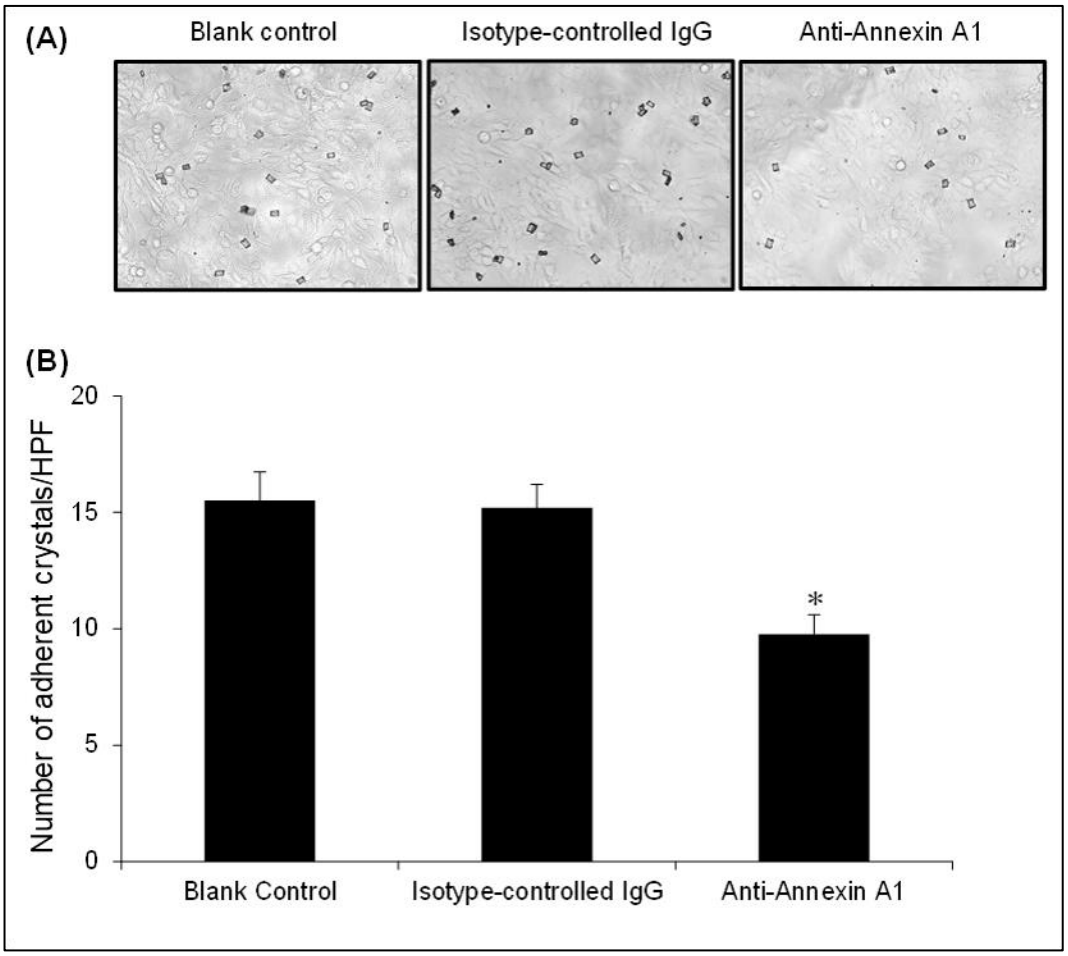

Figure 49. Cell-COM crystal adhesion assay and neutralization by a specific anti-Annexin A1. The confluent polarized MDCKI cell monolayer was incubated with 0.2 μg/mL anti-Annexin A1 antibody or 0.2 μg/mL rabbit isotype-controlled IgG prior to cell-crystals adhesion assay, whereas the cells without antibody treatment served as the blank control. **(A)** After removal of unbound crystals, crystals adherent on the cell surface were imaged by phase-contrast microscopy. **(B)** The adherent crystals were counted from 15 random high power fields (HPFs). Data were expressed as means ± SEM of three independent experiments. *$p < 0.05$ vs. controls.

We also interested in testing the inhibitory potential of the natural compound 16 (3,4,5-tri-*O*-galloylquinic acid), that was previously isolated from *C. langsdorffii* by our group, on COM adherence, and it was observed that this compound also inhibited COM crystal binding, but to a lower extent in comparison with compound 6 (Figure 50) versus the control. This explains that the presence of $–CH_3$ in compound 6 plays a role in its significant activity compared to compound 16 that lacks this group at –COOH.

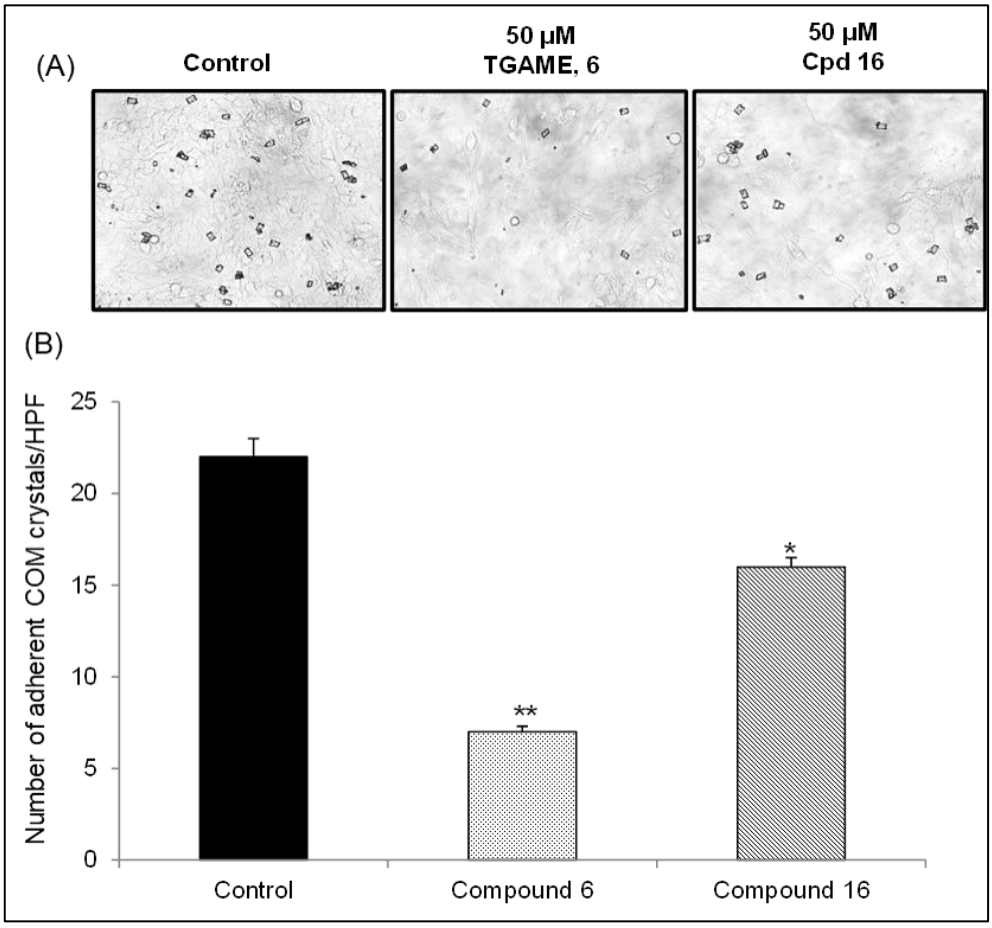

Figure 50. Effect of 3,4,5-tri-*O*-galloylquinic acid (compound 16) and 3,4,5-tri-*O*-galloylquinic methyl ester (TGAME, 6) on COM crystal-binding capability of the cells. MDCKI cells were pretreated with of each compound separately for 3 h followed by incubation with COM crystals (100 μg/ mL of culture medium) for 30 min. **(A)** After washing with plain DMEM culture media, images of the remaining crystals were captured under a phase-contrast microscope for 15 HPFs in each well. The original magnification power was ×400. **(B)** The remaining crystals that adhered on the cell surface were then counted. *$p < 0.05$ vs. control, **$p < 0.05$ TGAME vs. compound 16.

It is also interesting that both BF of *C. lucens* and the biotransformed metabolite M1 inhibited COM binding to the surface of MDCKI (Figure 51). However, M1 metabolite was more potent (p <0.05).

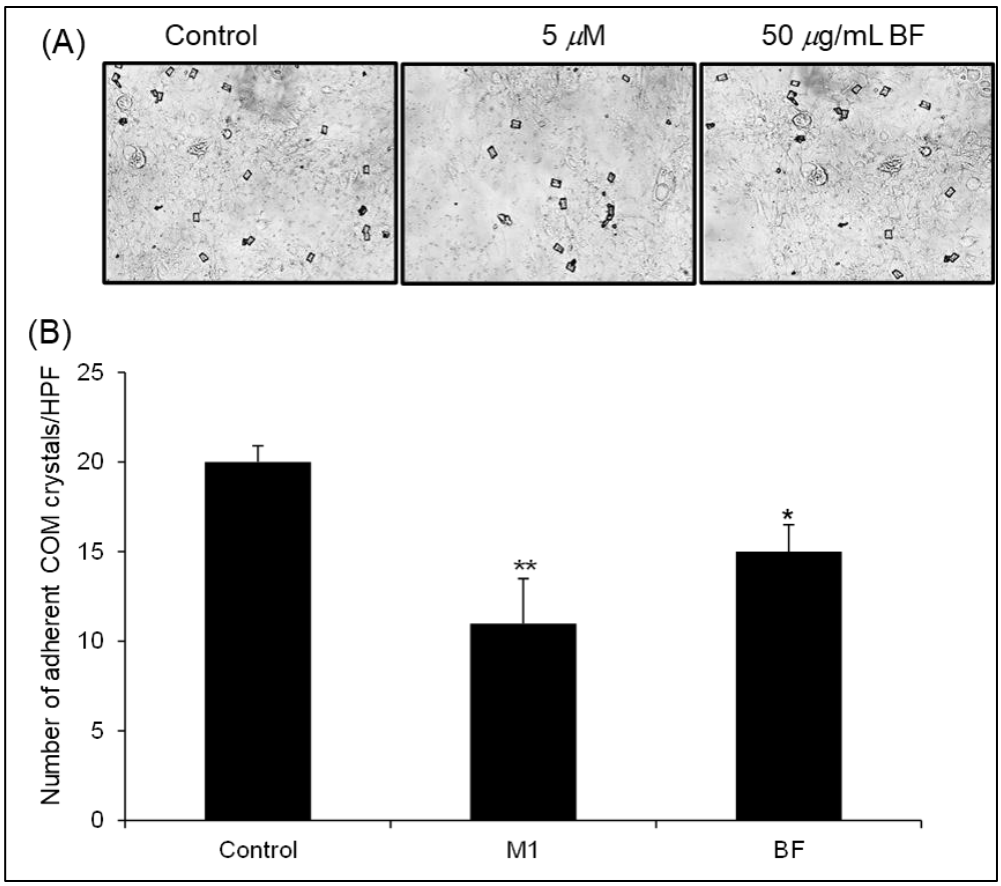

Figure 51. Effect of *C. lucens* BF and its biotransformed compound (M1) by *A. aliaceus* on COM crystal-binding capability of the cells. MDCKI cells were pretreated with 50 μg/mL BF or 5 μM M1 metabolite for 3 h followed by incubation with COM crystals (100 μg/ mL of culture medium) for 30 min. **(A)** After washing with plain DMEM culture media, images of the remaining crystals were captured under a phase-contrast microscope for at least 15 high-power fields (HPF) in each well. The original magnification power was ×400. **(B)** The remaining crystals that adhered on the cell surface were then counted. *p < 0.05 vs. control, **P <0.05 M1 versus BF.

Analysis of COM-binding proteins (Annexin A1, α-enolase and HSP90) by Western blot. We reported previously that when COM crystals were pre-coated with gallotannin (in green tea), their subsequent adhesion to renal tubular cells was reduced (121). A similar study demonstrated that aluminum citrate decreased COM crystal binding to the same cells, when the crystals were pre-coated with it (190). Moreover, it was reported that an aqueous extract of *Costus arabicus,* a plant used in Brazilian folk medicine to treat urolithiasis, inhibited the growth of COM crystals and their adhesion to renal epithelial cells (122). The inhibitory effect on the binding of crystals to the cell was only significant when pre-coated COM crystals were investigated. Pretreatment of cells with this extract had no effect on crystal adhesion. Unlike the previous studies, we found that TGAME exerted effects when added directly to renal cells followed by treatment with uncoated COM crystals. We propose that the observed biological activities might be related to cellular effects of TGAME and reduction of COM crystal-binding protein expression on the surface of renal cells. One of these proteins is ANXA1, (191) in addition to α-enolase and HSP90 (192, 193).

A previous publication documented that epigallocatechin gallate strongly interacts with phospholipid bilayers due to hydrogen bond formation, and it inhibits COM crystal adhesion to renal tubular cells by decreasing α-enolase surface expression (117). It is noteworthy that ANXA1, α-enolase, and HSP90 are all in the database of the lipid raft proteome (http://lipid-raft-database.di.uq.edu.au/). ANXA1 is present in the basolateral cell membrane, cytoplasm, cell projection and nucleus. We studied surface expression of these three putative COM crystal receptors on MDCKI cells pretreated with TGAME, BF, M1 and compound 16 by immunofluorescence microscopy and confirmed the results by Western blot analysis of whole cell lysate and subcellular fractions.

Proteins quantification results are presented in (Tables 13-18) and (Figures 52-55).

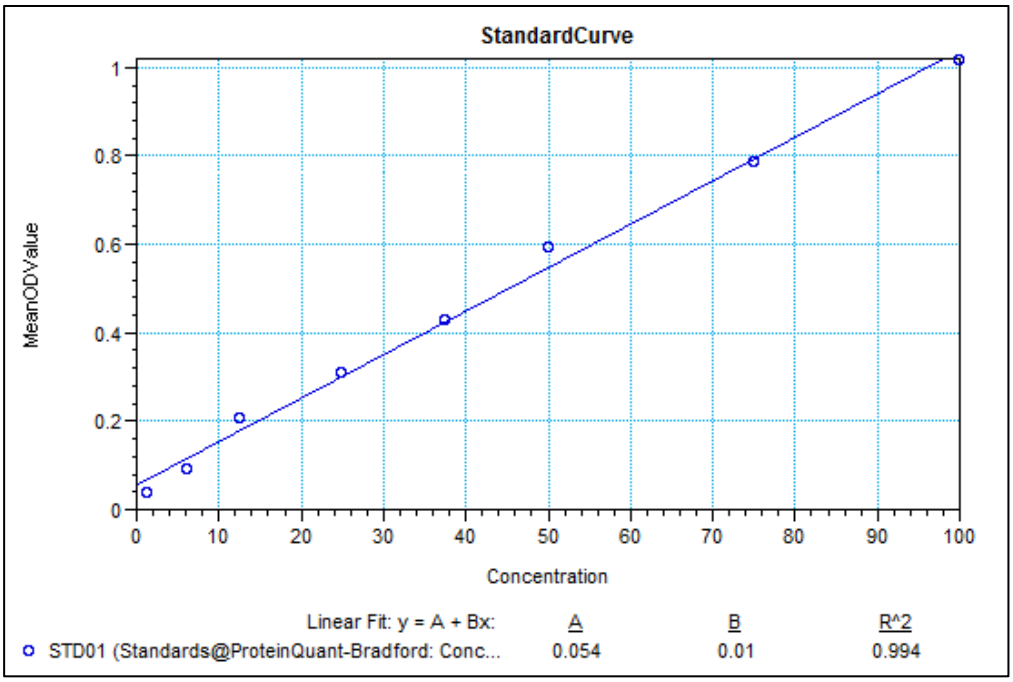

Figure 52. Color response curve of different concentrations (25, 125, 250, 500, 750, 1500 and 2000 μg/mL) of standard bovine serum albumin (BSA). The absorbance was measured at 562 nm. Data were expressed as means ± S.D. of two concentration replicates. The curve was for proteins quantification obtained from MDCKI cells after their incubation with compound 6.

Table 13. Absorbance and concentration values of standard bovine serum albumin (BSA) (μg/mL) used for cell proteins quantification of MDCKI treated with TGAME.

Sample	Concentration (μg/mL)	Back calculated concentration (μg/mL)	Optical density (OD) values	Mean OD value	Standard deviation (SD)
St 1	2000	1941.898	0.533	0.532	0.001
		1938.399	0.532		
St 2	1500	1532.993	0.428	0.423	0.006
		1499.565	0.490		
St 3	100	1027.304	0.298	0.305	0.011
		1085.219	0.312		
St 4	750	726.455	0.220	0.227	0.009
		776.208	0.233		
St 5	500	508.787	0.164	0.172	0.011
		569.424	0.180		
St 6	250	200.943	0.085	0.125	0.056
		508.787	0.164		
St 7	125	60.625	0.049	0.056	0.010
		113.487	0.062		
St 8	25	103.404	0.007	0.009	0.003
		86.690	0.011		

Table 14. Concentration of proteins extracted from MDCKI cells (cytosol, membrane and whole lysate fractions) treated with 50 μM TGAME for 3 h.

Sample #cpd 6	Optical density (OD) values	Concentration (μg/mL)	Mean concentration (μg/mL)	Standard deviation (SD)	Dilution factor	Adjunct concentration (μg/mL)
MW	0.400	1511.053	1527.354	23.053	20	30.547.079
control	0.408	1543.655				
MW	0.393	1482.526	1491.899	13.255	20	29837.989
Treatment	0.397	1501.272				
MS control	0.216	763.248	780.161	23.917	20	15603.213
	0.225	797.073				
MS	0.240	858.201	863.092	6.916	20	17261.831
treatment	0.242	867.982				
MM	0.049	316.280	328.098	16.713	20	6561.959
control	0.054	339.916				
MM	0.060	363.552	363.552	0.000	20	363.552
treatment	0.056	362.550				

Table 15. Concentration of proteins extracted from JL cells (cytosol, membrane and whole lysate fractions) treated with 50 μM TGAME (6) for 3 h.

Sample #cpd 6	Optical density (OD) values	Concentration (μg/mL)	Mean concentration (μg/mL)	Standard deviation (SD)	Dilution factor	Adjunct concentration (μg/mL)
JW	0.337	1392.916	1404.339	16.153	20	28086.772
control	0.342	1415.761				
JW	0.357	1481.096	1486.122	7.108	20	29722.432
Treatment	0.59	1491.147				
JS control	0.182	685.197	721.748	513691	20	14434.953
	0.198	758.299				
JS	0.221	862.926	878.460	21.969	20	17569.206
treatment	0.228	893.994				
JM	0.059	466.361	411.335	7.108	20	8226.703
control	0.057	406.309				
JM	0.058	414.990	414.990	0.000	20	414.990
treatment	0.060	422.300				

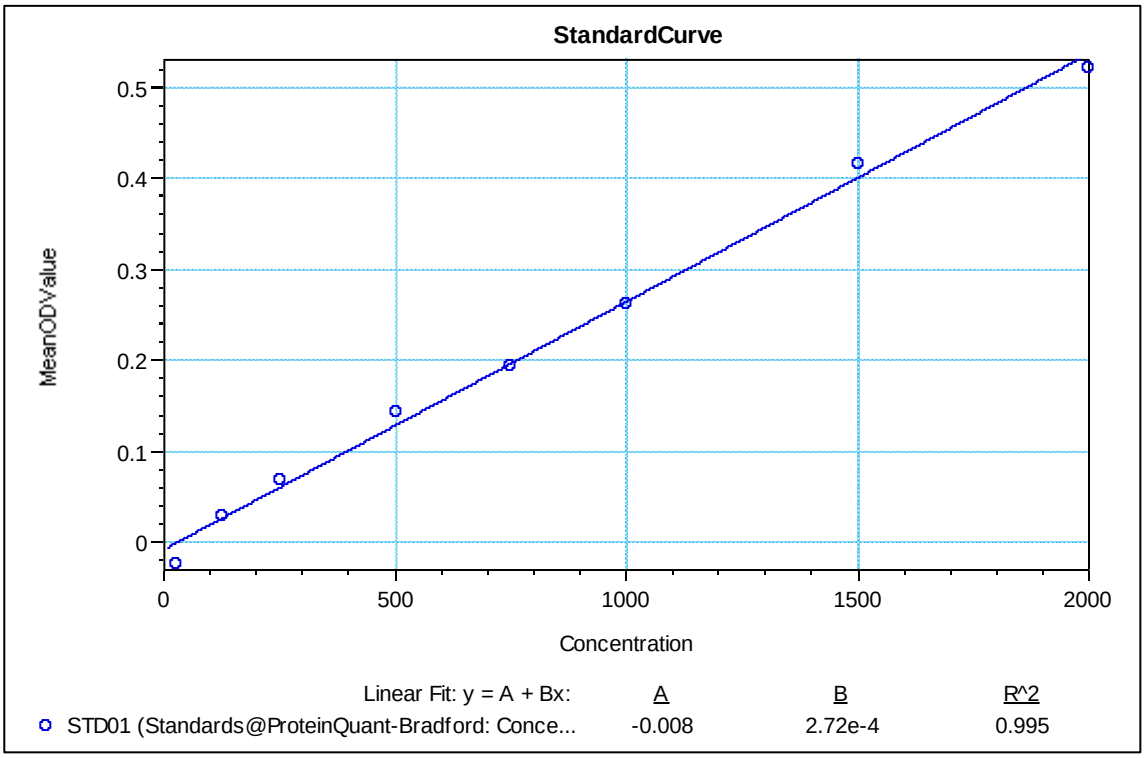

Figure 53. Color response curve of different concentrations (25, 125, 250, 500, 750, 1500 and 2000 μg/mL) of standard bovine serum albumin (BSA). The absorbance was measured at 562 nm. Data were expressed as means ± S.D. of two concentration replicates. The curve was for proteins quantification obtained from MDCKI cells after their incubation with *C. lucens* BF.

Table 16. Concentration of proteins extracted from MDCKI cells (cytosol, membrane and whole lysate fractions) treated with 50 μg/mL BF for 3 h.

Sample #BF	Optical density (OD) values	Concentration (μg/mL)	Mean concentration (μg/mL)	Standard deviation (SD)	Dilution factor	Adjunct concentration (μg/mL)
MW control	0.402	1402.202	1382.868	27.342	20	27657.369
	0.392	1363.535				
MW Treatment	0.427	1497.325	1490.945	9.023	20	29818.904
	0.424	1484.565				
MS control	0.236	759.929	821.604	87.22	20	16432.083
	0.268	883.279				
MS treatment	0.256	835.718	905.127	98.159	20	218102.5360
	0.292	974.536				
MM control	0.064	400.494	401.654	1.641	20	8033.086
	0.064	102.814				
MM treatment	0.056	369.560	385.414	22.421	20	27708.2760
	0.064	401.268				

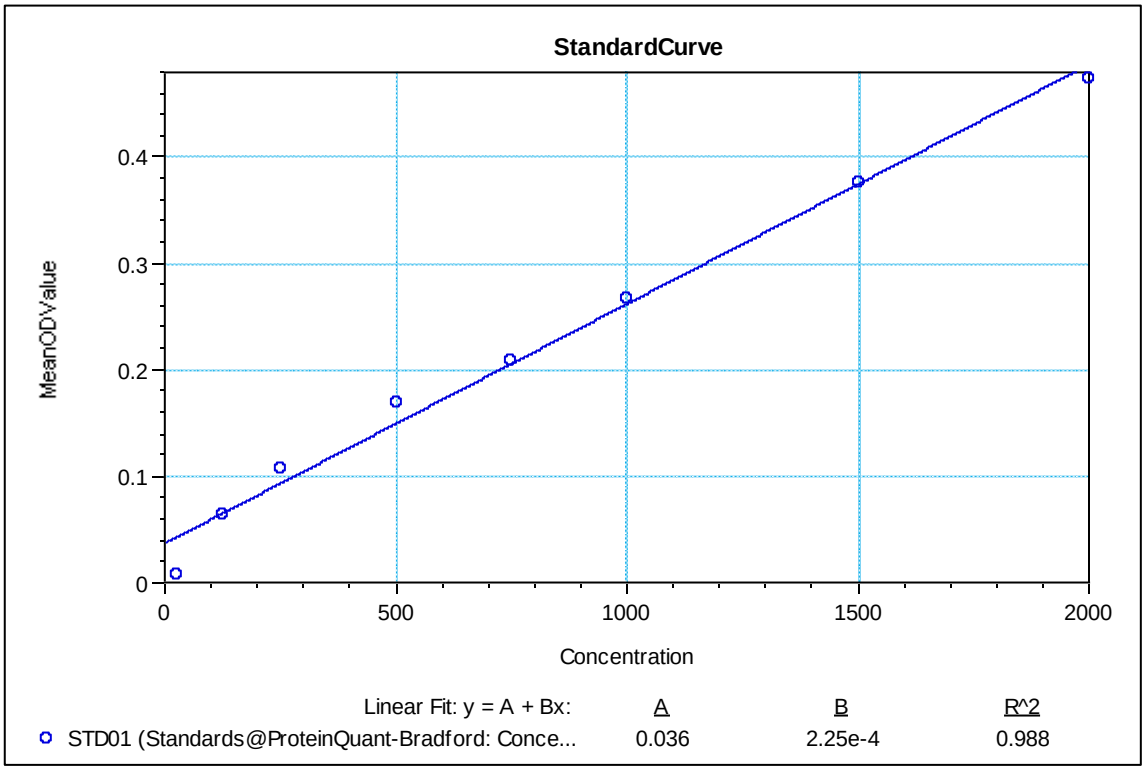

Figure 54. Color response curve of different concentrations (25, 125, 250, 500, 750, 1500 and 2000 μg/mL) of standard bovine serum albumin (BSA). The absorbance was measured at 562 nm. Data were expressed as means ± S.D. of two concentration replicates. The curve was for proteins quantification obtained from MDCKI cells after their incubation with compound (M1).

Table 17. Concentration of proteins extracted from MDCKI cells (cytosol, membrane and whole lysate fractions) treated with 5 μM M1 for 3 h.

Sample #M1	Optical density (OD) values	Concentration (μg/mL)	Mean concentration (μg/mL)	Standard deviation (SD)	Dilution factor	Adjunct concentration (μg/mL)
MW control	0.392	1577.336	1561.578	22.285	20	31231.569
	0.385	1545.821				
MW Treatment	0.400	1613.735	1629.270	21.971	20	32585.409
	0.407	1644.806				
MS control	0.225	838.273	849.814	16.321	20	16996.278
	0.231	861.355				
MS treatment	0.239	899.973	904.855	6.905	20	18097.105
	0.241	909.738				
MM control	0.020	248.350	259.669	16.007	20	5193.375
	0.025	270.988				
MM treatment	0.026	278.978	264.995	15.002	20	5579.552
	0.020	251.013				

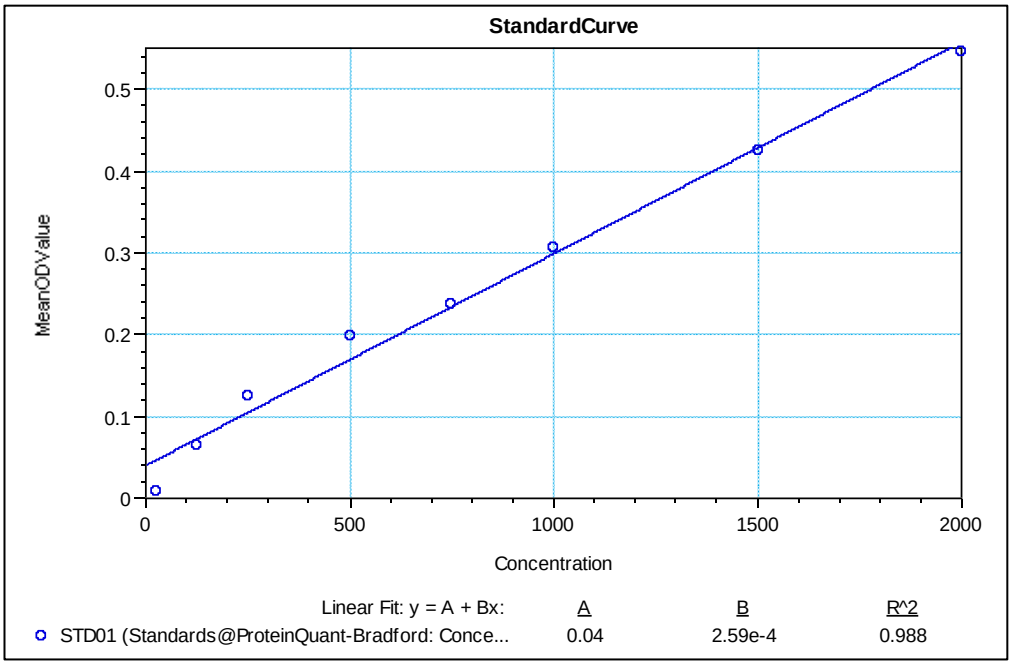

Figure 55. Response curve of different concentrations (25, 125, 250, 500, 750, 1500 and 2000 μg/mL) of standard bovine serum albumin (BSA). The absorbance was measured at 562 nm. Data were expressed as means ± S.D. of two concentration replicates. The curve was for proteins quantification obtained from MDCKI cells after their incubation with compound (16).

Table 18. Concentration of proteins extracted from MDCKI cells (cytosol, membrane and whole lysate fractions) treated with 50 μM compound 16 for 3 h.

Sample #cpd 16	Optical density (OD) values	Concentration (μg/mL)	Mean concentration (μg/mL)	Standard deviation (SD)	Dilution factor	Adjunct concentration (μg/mL)
MW control	0.426	1492.99	1498.679	90.023	20	29973.576
	0.429	1505.059				
MW Treatment	0.406	1415.736	1413.966	2.461	20	28279.922
	0.405	1412.256				
MS control	0.222	704.634	701.734	4.101	20	14034.675
	0.221	698.834				
MS treatment	0.274	906.867	897.973	12.55	20	17959.465
	0.270	889.080				
MM control	0.066	407.841	411.901	5.742	20	8238.026
	0.068	415.961				
MM treatment	0.070	423.695	426.788	4.375	20	8535.768
	0.071	429.882				

The Western blot analysis revealed that TGAME significantly reduced the presence of ANXA1 and the other two proteins α-enolase and HSP90 in the membrane fractions (P <0.05), whereas their concentrations in cytosolic fractions was greater (Figure 56). Overall, the total amount of protein in the whole cell lysate was the same. Interestingly, the inhibitory effect of TGAME on ANXA1 in the membrane fraction was more significant in comparison with its effect on α-enolase and HSP90 proteins (p <0.05).

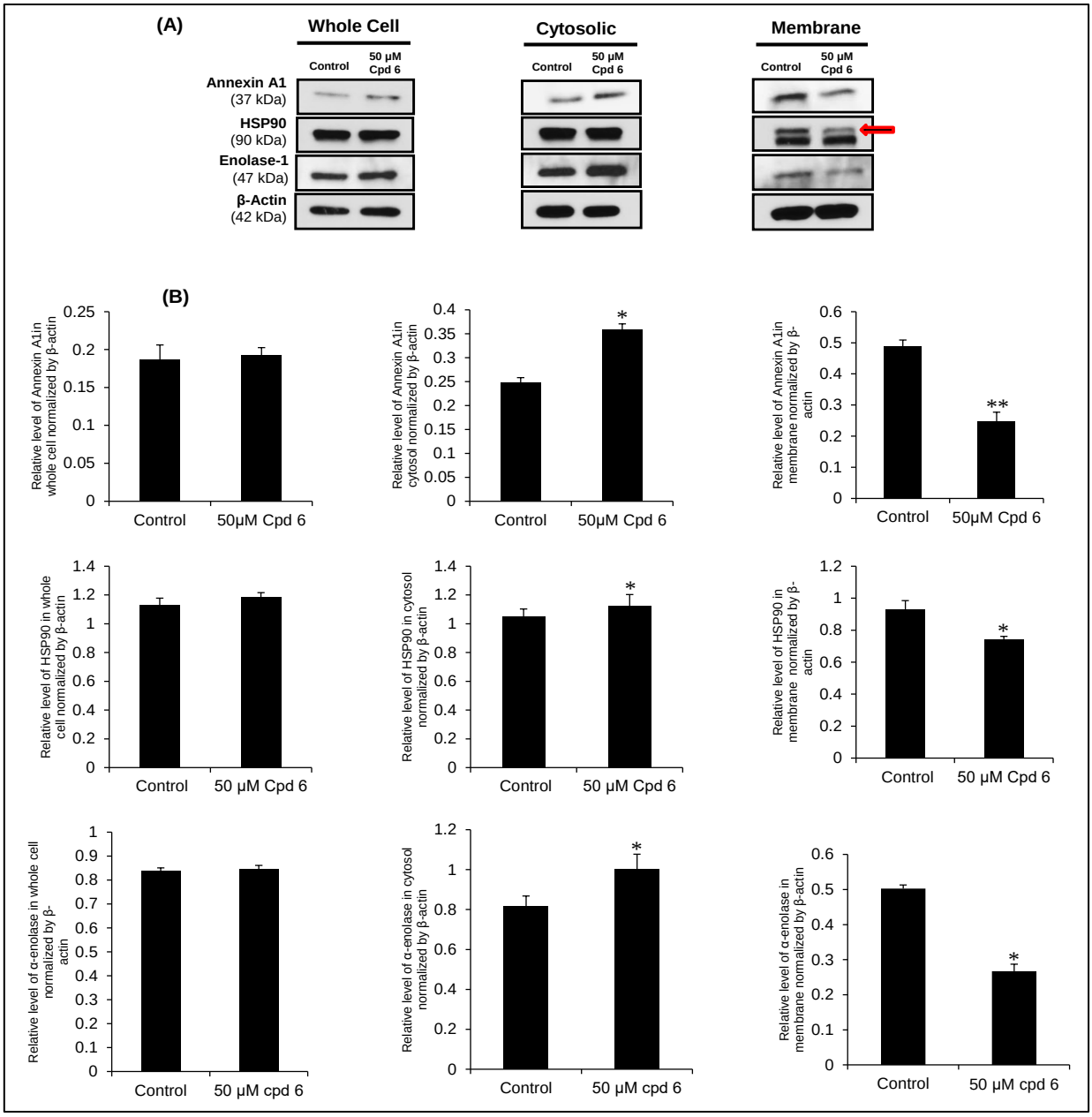

Figure 56. (A) Western blot analysis of COM crystal-binding proteins. Proteins obtained from whole cell lysate, cytosolic fraction and membrane fraction of MDCKI with or without 50 µM TGAME (6) treatment, were subjected to Western blotting for annexin A1, α-enolase, HSP90. *β*-actin served as the loading control. **(B)** Bands intensity was quantitated using AlphaEase FC software (Mayo Clinic). Each bar represents mean ± SEM from 3 independent experiments. * $p < 0.05$ vs. control. ** $p < 0.05$ for the effect of TGAME on Annexin A1 vs. α-enolase and HSP90.

Thus TGAME could decrease cell surface expression of these proteins through transcriptional suppression, alter molecular shuttling, or trafficking from the cytoplasm to the cell surface, since the compound is polyphenolic and could interact with lipid bilayers through hydrogen bond formation (Figure 57).

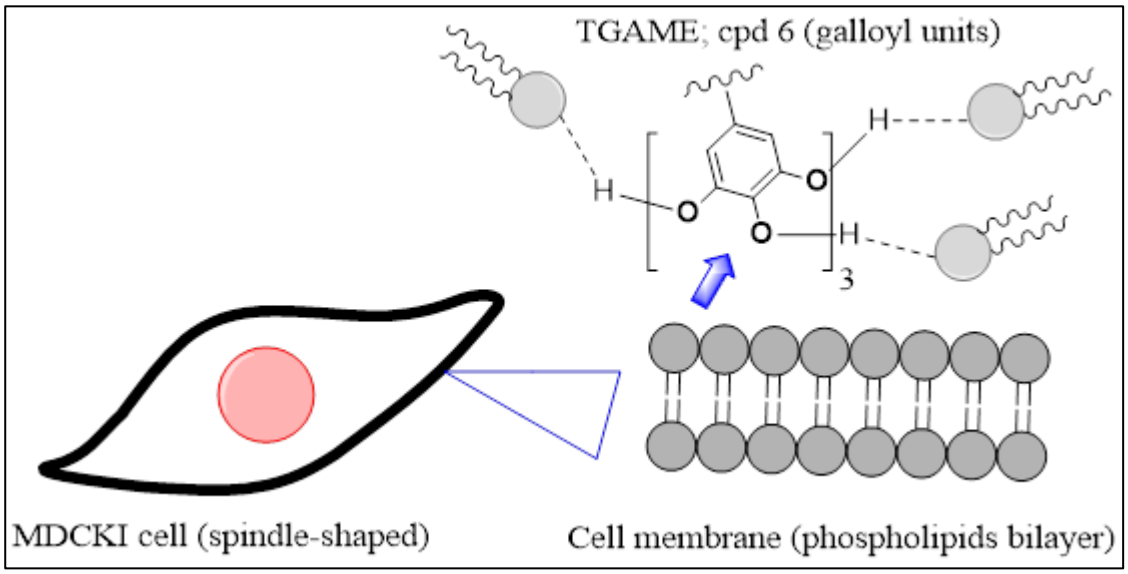

Figure 57. Proposed interaction of the galloyl units of TGAME; compound 6 with the cell membrane of MDCKI cells through H-bond formation.

These data suggested that TGAME decreased ANXA1 cell surface expression by inhibiting or re-localizing its shuttling from cytoplasm to the cell membrane. Annexins are Ca^{2+}-regulated membrane binding proteins found throughout the animal and plant kingdoms. The Annexin core (Ca^{2+}/membrane binding unit) is thought to be one essential element that facilitates membrane interactions. Thus Annexins can organize and assemble phospholipids into specific membrane domains (194). ANXA1 protein also plays important roles by controlling cellular Ca^{2+} storage and thus Ca^{2+}-dependent signal transduction. Overall, ANXA1 localizes to many cellular structures including the plasma, cytoplasm and organelle membranes (194).

A-enolase is another COM crystal binding protein on the surface of MDCKI cells, and it was reported that expression of this protein on the MDCKI cell surface increased after exposure to oxalate (117). Another study confirmed a role of α-enolase in COM crystal binding by using a specific antibody to block α-enolase and demonstrating decreased adhesion to the cell surface (192).

Surface heat shock protein 90 (HSP90) is also found on the surface of renal cells as a putative crystal binding molecule. Downregulating HSP90 expression using specific anti-

HSP90 antibodies or small interfering RNA (siRNA) decreased COM crystal adhesion by 50% and 75%, respectively (195).

Western blot analysis of MDCKI proteins resulting from incubation of compound 16 with the cells reveled that compound 16 only inhibited HSP90 protein (Figure 61) in comparison with compound 6 which inhibited all COM binding proteins. This explains the weak inhibitory effect of compound 16 on COM crystal binding relative to compound 6.

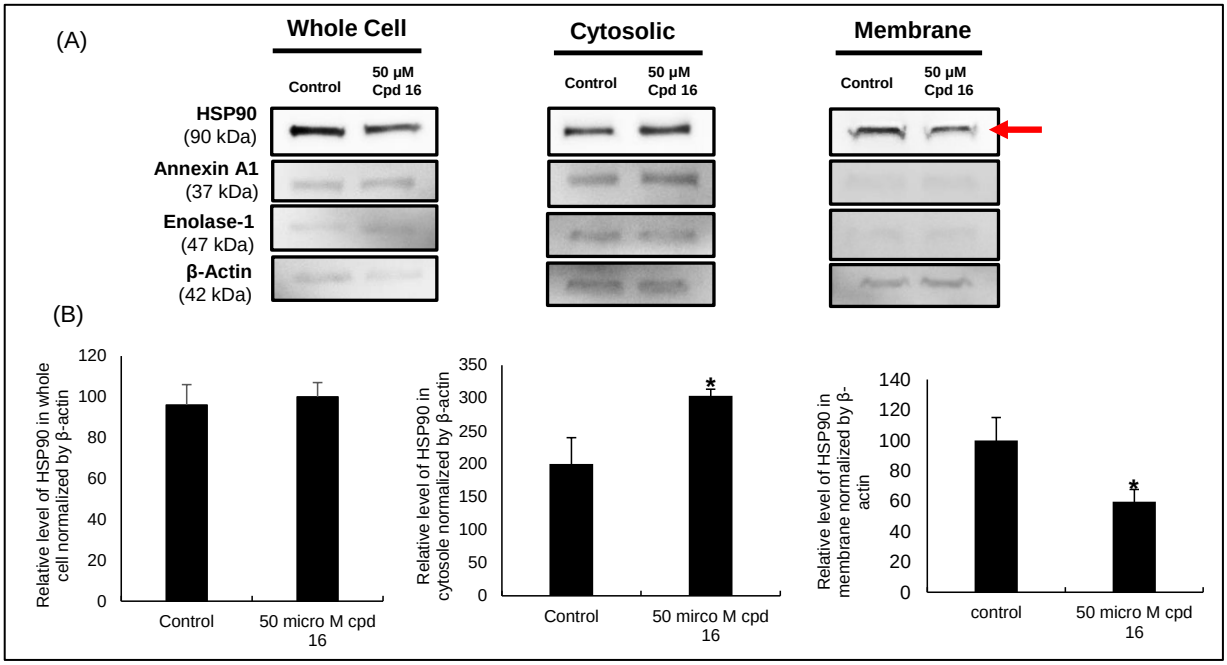

Figure 58. Western blot analysis of COM crystal-binding proteins. **(A)** Proteins obtained from whole cell lysate, cytosolic fraction and membrane fraction of MDCKI with or without compound 16 treatment (50 μM) each, were subjected to Western blotting of annexin A1, alpha-enolase and HSP90. β-actin served as the loading control. **(B)** Bands intensity of HSP90 was quantitated using ImagJ software. *$p < 0.05$ vs. control.

Interestingly, subcellular localization of COM-binding proteins by western blot analysis, showed that BF and M1 metabolite act on different targets COM binding proteins, where BF and M1 inhibited membrane HSP90 and (ANXA1), respectively (Figure 59 and 60). Therefore, our suggested mechanism underlying the observed biological effects might be related to cellular effects of BF and M1, and reduced the expression of COM crystal-binding proteins on the cell surfaces.

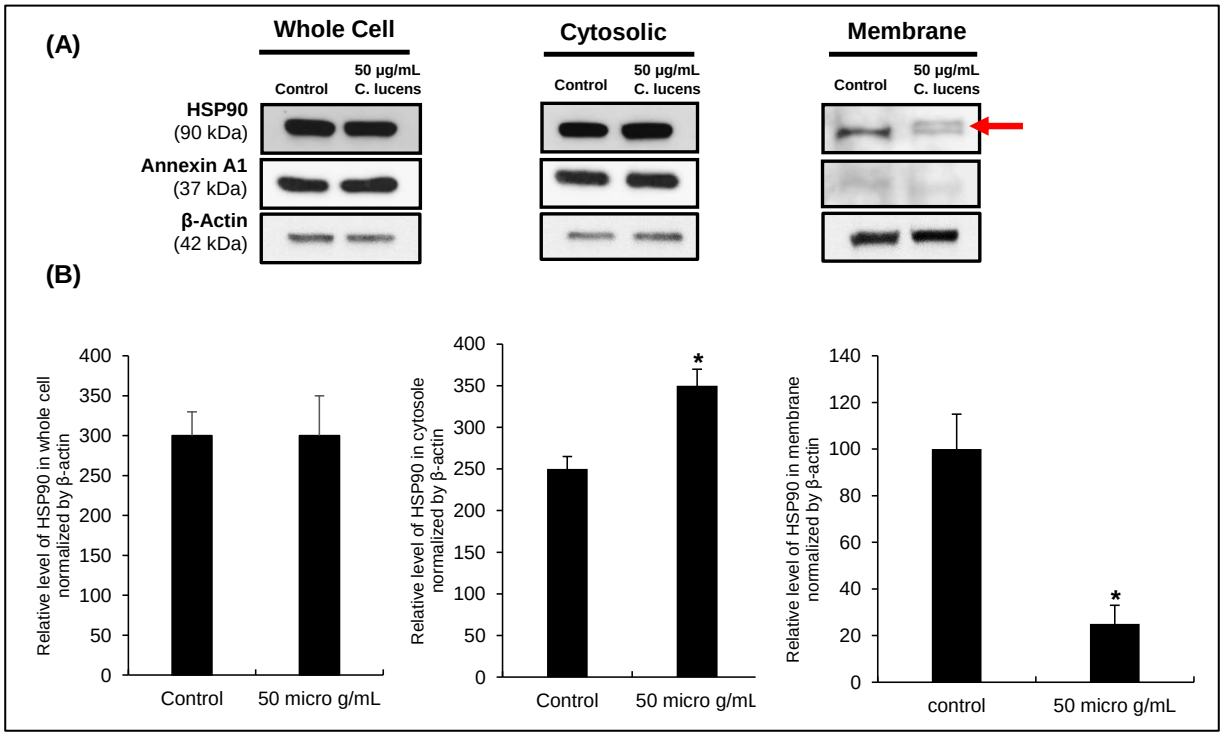

Figure 59. Western blot analysis of COM crystal-binding proteins. **(A)** Proteins obtained from whole cell lysate, cytosolic fraction and membrane fraction of MDCKI with or without or *C. lucens* BF (50 μg/mL) treatment, were subjected to Western blotting of Annexin A1 and HSP90. β-actin served as the loading control. **(B)** Bands intensity of HSP90 was quantitated using ImageJ software. Each bar represents mean ± SEM from 3 independent experiments. *$p < 0.05$ vs. control.

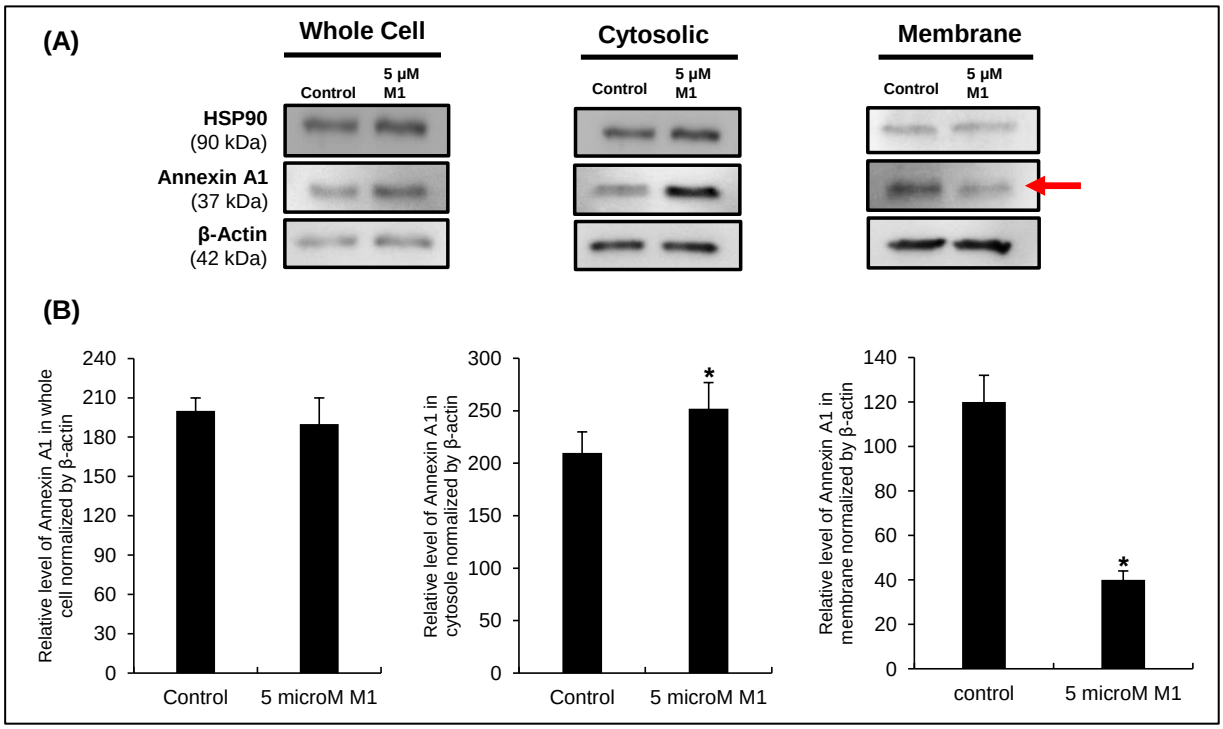

Figure 60. Western blot analysis of COM crystal-binding proteins. **(A)** Proteins obtained from whole cell lysate, cytosolic fraction and membrane fraction of MDCKI with or without or the transformed metabolite M1 (5 μM) treatment, were subjected to Western blotting of Annexin A1 and HSP90. β-actin served as the loading control. **(B)** Bands intensity of Annexin A1 was quantitated using ImageJ software. Each bar represents mean ± SEM from 3 independent experiments. *$p < 0.05$ vs. control.

Examining the expression of surface and intracellular Annexin A1 by immunofluorescence assay and laser-scanning confocal microscopy. Laser-scanning confocal microscopy showed that ANXA1 cell surface expression was dramatically inhibited by pretreatment with 50 μM of TGAME to approximately 50% of control (Figure 61). However, Annexin A1 expression inside cells increased after TGAME treatment.

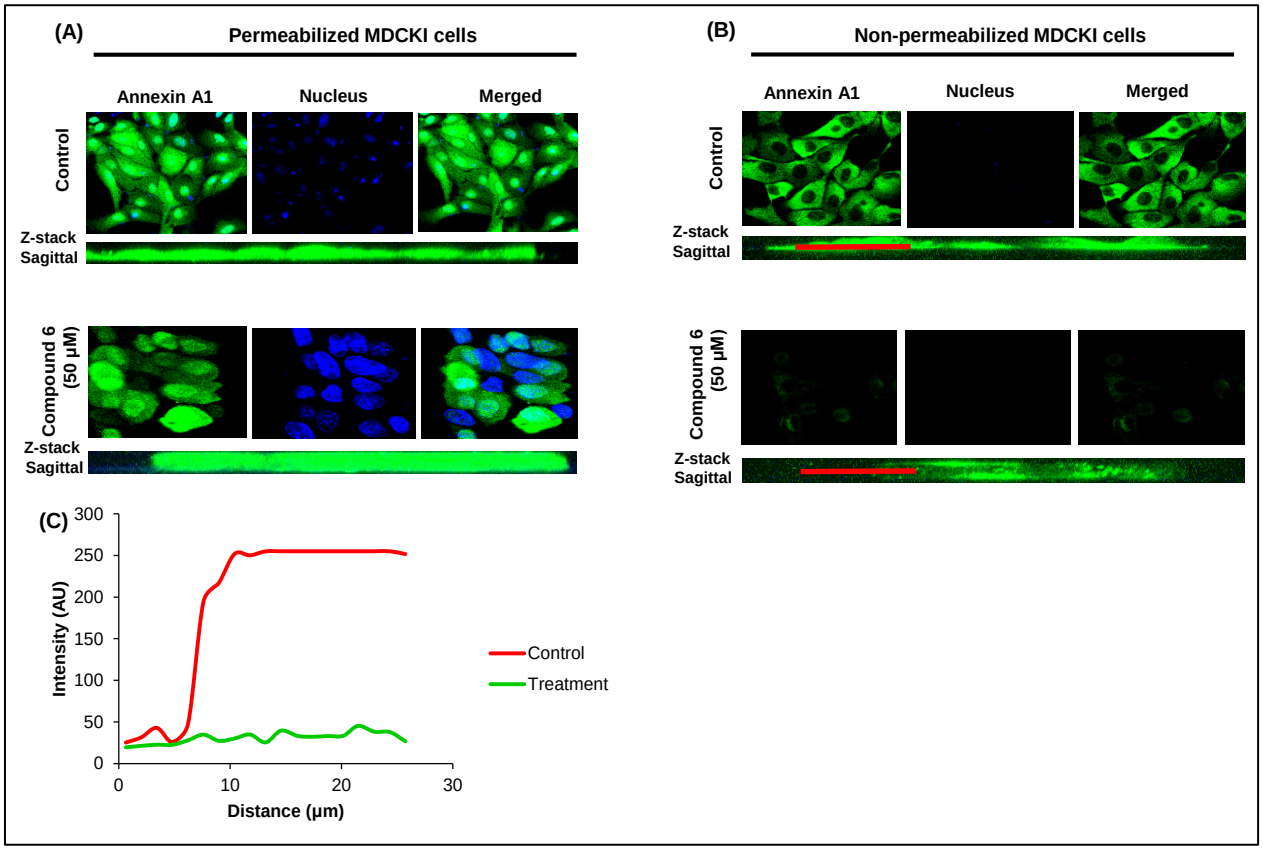

Figure 61. Confocal and laser scanning microscopy. TGAME (6) reduced the surface expression of Annexin A1, but increased its intracellular level. **(A)** Intracellular expression of Annexin A1 (with cell permeabilization). **(B)** Surface expression of Annexin A1 (without cell permeabilization). MDCKI cells were pretreated with 50 μM of compound 6 for 3 h and processed for immunofluorescence study using anti-Annexin A1 as a primary antibody and secondary antibody conjugated with Alexfluor 488 Donkey anti-rabbit (shown in green), whereas nuclei were counterstained with TOT-3 dye (shown in blue). Original magnification power was ×400. **(C)** The graph peaks represent the fluorescence intensities of the staining at the given distances (in micrometers) along the red bar.

We further studied surface expression of the two COM crystal receptors (ANXA1 and HSP90) on MDCKI cells pretreated with BF and M1 by immunofluorescence microscopy to confirm our findings by Western blot analysis. The analysis revealed that M1 significantly reduced ANXA1 in the membrane fraction, whereas its level in the cytosolic fraction was increased (Figure 62). However, the total level of ANXA1 in whole cell lysate remained unchanged. The same behavior was observed with BF but it acted on HSP90.

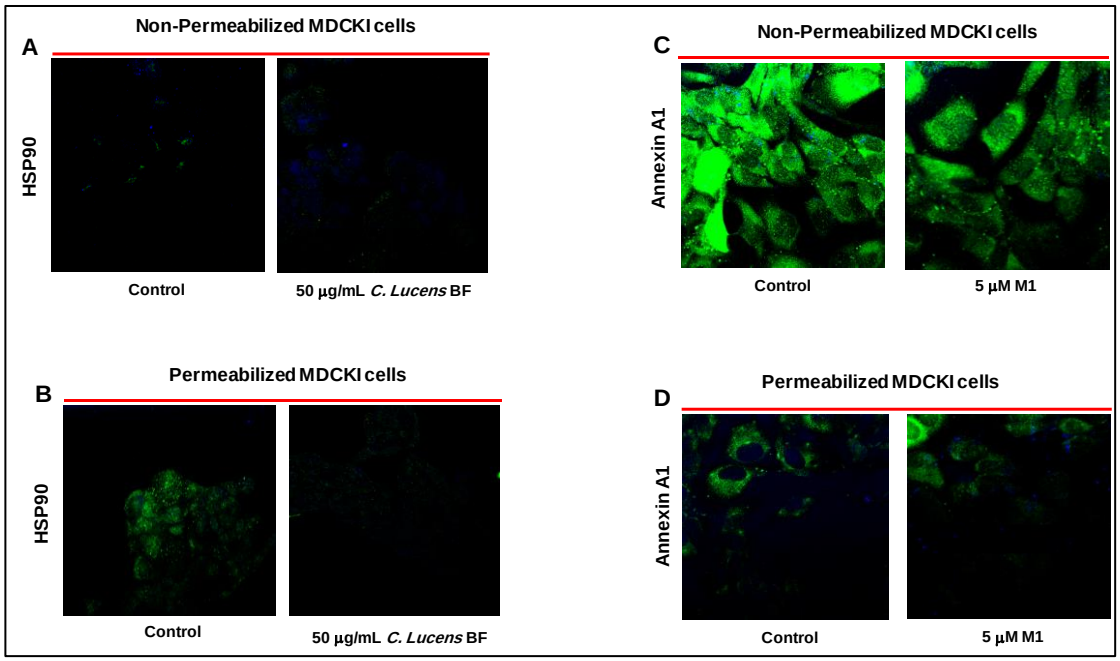

Figure 62. Confocal and laser scanning microscopy. BF and M1 inhibited HSP90 and annexin A1 surface expressions, respectively, but increased their intracellular levels. **(A)** and **(C)** Intracellular expression of HSP90 and annexin A1 (without cell permeabilization). **(B)** and **(D)** Surface expression of HSP90 and annexin A1 (with cell permeabilization). MDCKI cells were pretreated with 50 μg/mL BF or 5 μM for 3 h and processed for immunofluorescence study using anti-HSP90 and anti-annexin A1, respectively, as primary antibodies and secondary antibody conjugated with Alexfluor 488 donkey anti-rabbit (shown in green), whereas nuclei were counterstained with TOT-3 dye (shown in blue). Original magnification power was ×400.

In vivo feeding and ex vivo oxalate ± TGAME birefringence experiment in Drosophila (fruit fly) model. Our group previously studied the effect of thiosulfate and sulfate on Malpighian tubule calcium oxalate crystallization in a fruit fly model. (186) Chen et al. fed fruit flies lithogenic agents such as sodium oxalate (NaOx). Their analysis used polarized light microscopy of dissected tubules to show that NaOx feeding resulted in the formation of crystals within the Malpighian tubule lumen in a dose-dependent manner. These crystals were identified as CaOx using scanning electron microscopy and energy-dispersive X-ray spectroscopy. The study also demonstrated that crystal formation decreased lifespan of the flies and that the use of potassium citrate (KCit) as an antiurolithic agent, reduced crystallization inside MT and decreased mortality. Thus, *Drosophila* appears to be a useful model to study CaOx renal stones, before the use of higher order experimental animals. (196) Thus, we investigated the effect of TGAME on the formation of CaOx crystals within Malpighian tubule in feeding experiments and after *ex vivo* exposure of the tubules to oxalate.

The *ex vivo Drosophila* model experiment showed that TGAME (100 μM) manifested a significant decrease ($p < 0.05$) in CaOx crystal number, size and total crystal area within Malpighian tubules lumen (Figure 63).

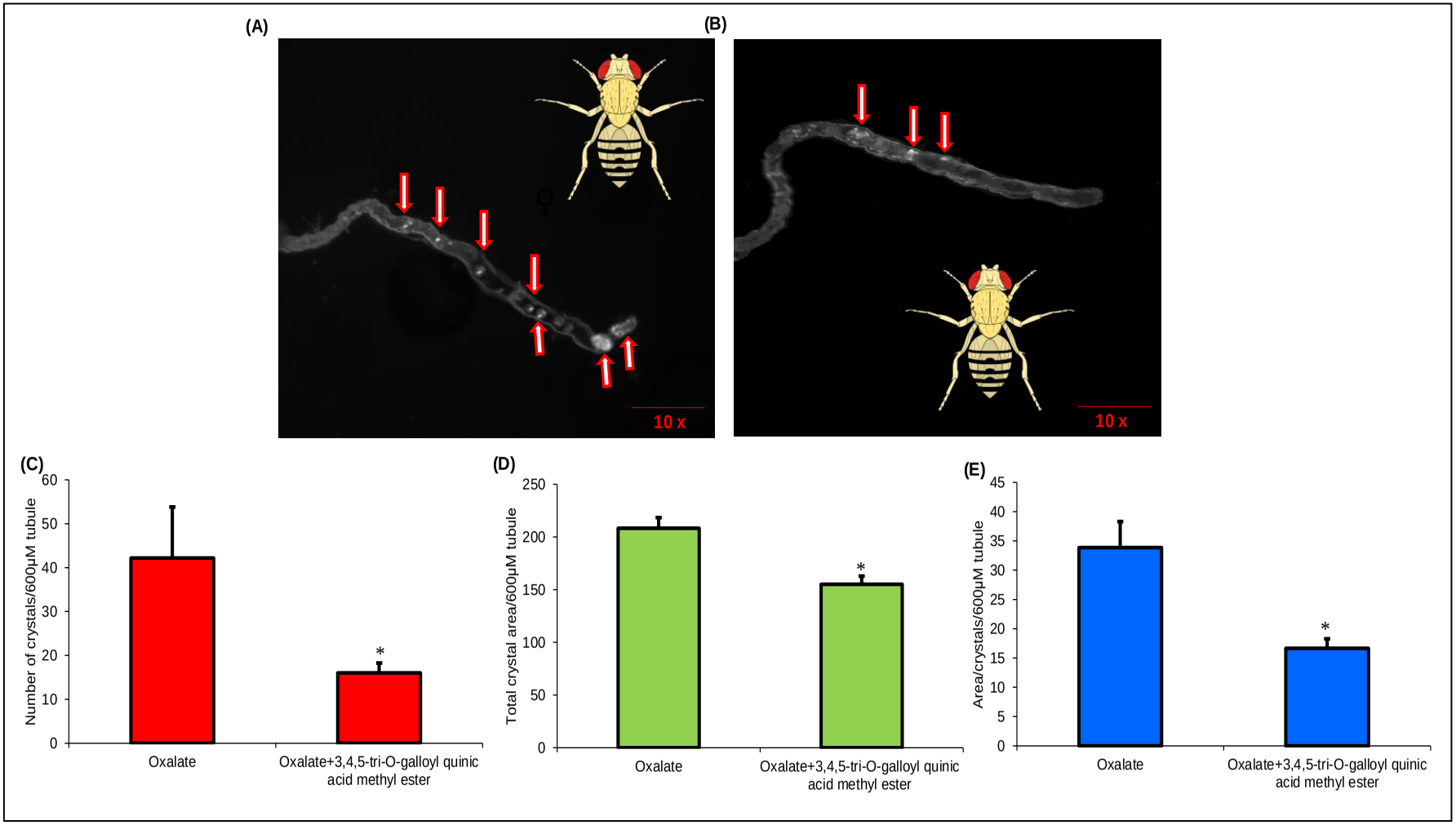

Figure 63. Malpighian tubule (MT) images from wild type female fruit flies incubated *ex vivo* with **(A)** Oxalate (10 mM) or **(B)** Oxalate (10 mM) and TGAME (6) (100 µM) for 1 h. The arrows indicate CaOx crystals within the lumen of the MT. **(C)** CaOx crystal number, **(D)** Total crystal area, and **(E)** Average area/crystal per 600 μm of tubule were determined using ImageJ. TGAME significantly decreased crystal number, total crystal area and average area/crystal. Values are means ± SE (n = 12 for both oxalate control group and compound 6-treated group). (*$P < 0.05$).

Flies fed oxalate (10 mM) + TGAME also exhibited a decrease in CaOx crystal number, size and total crystal area within Malpighian tubules after 24 h exposure in comparison to those fed oxalate alone, but these findings were not significant (p >0.05) (Figure 64). However, in the factors such as absorption parameters affecting delivery of TGAME to the blood stream or the need for doses greater than 50 μM *in vivo* to deliver sufficient amounts to Malpighian tubules to alter CaOx crystallization.

Annexin b11 (Axb11) is also found in *Drosophila* (197) as a Ca^{2+}-dependent phospholipids binding protein (http://flybase.org/reports/FBgn0030749.html) that is known to play important role in cell adhesion, involved in several functions such as differentiation, cell signaling and membrane fusions. In this case, we speculate that the effect of our compound TGAME in the fly model might be of its action on Axb11, where the decrease in cell surface Axb11 might decrease nucleation on the cell surface.

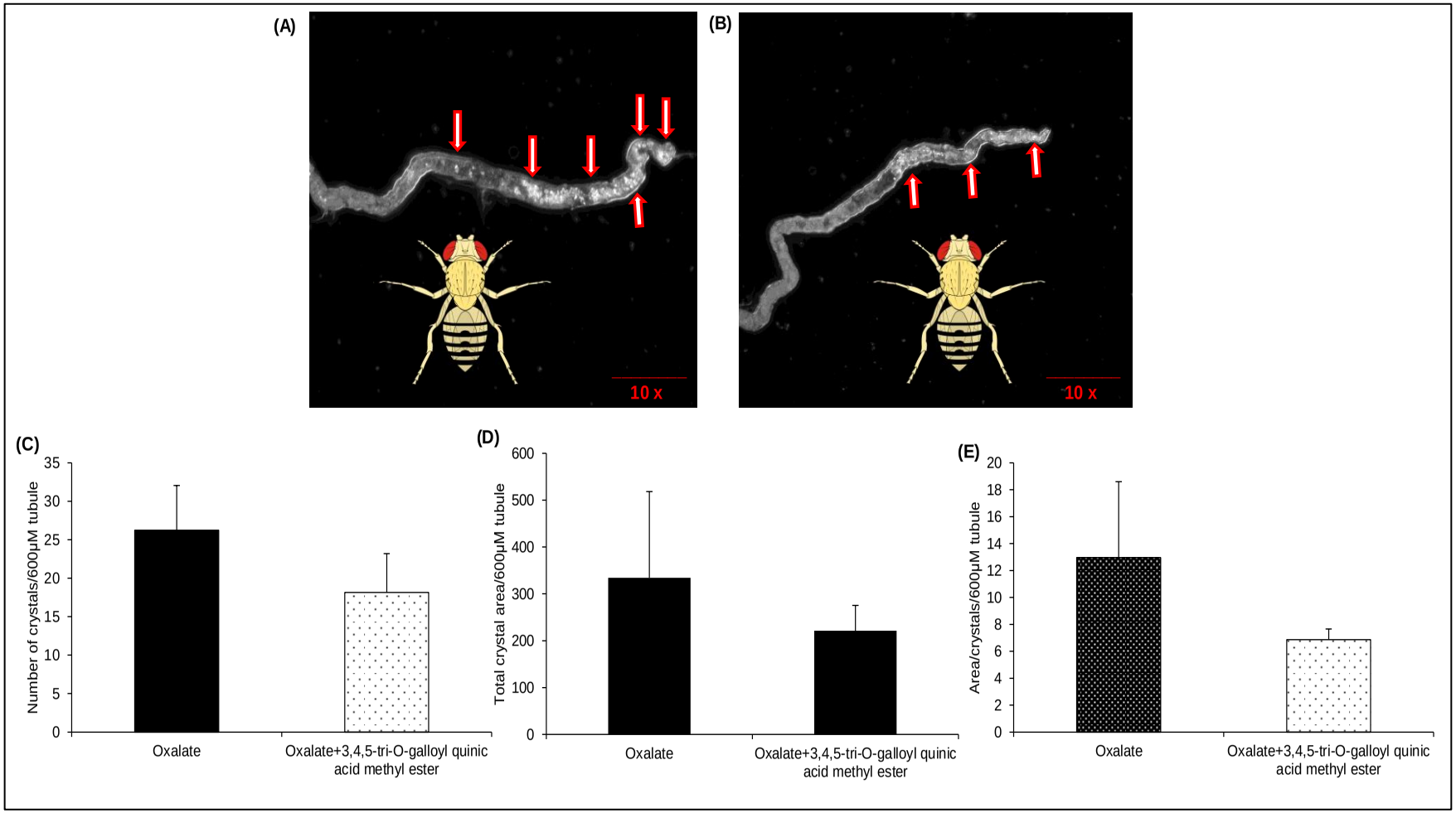

Figure 64. Malpighian tubule (MT) images from wild type female fruit flies fed **(A)** Oxalate (10 mM) or **(B)** Oxalate (10 mM) and TGAME (6) (50 µM) for 24 h. The arrows indicate CaOx crystals within the lumen of the MT. **(C)** CaOx crystal number, **(D)** Total crystal area, and **(E)** Average area/crystal per 600 µm of tubule were determined using ImageJ. Values are means ± SE (n = 11 for both oxalate control group and compound 6-treated group). $P > 0.05$.

Antioxidant and DPPH assay. Studies suggest that renal epithelial cell exposure to CaOx crystals, CaP crystals, and oxalate ions can lead to the generation of reactive oxygen species (ROS), potential cause of injury and/or promote inflammation. Further, the urine of stone formers and hyperoxaluric rats is enriched with markers of inflammation and oxidative stress (OS). (198) Stone formers also have been reported to have reduced peripheral concentrations of antioxidants including α- and beta-carotenes. There are many reported mechanisms whereby ROS can increase stone risk including decreased function of macromolecular inhibitors and/or cellular injury that promotes increased crystal adhesion. (199) Antioxidant treatments have also been shown to reduce pathological injury of crystal deposition in hyperoxaluria animal models.

In this study, the DPPH assay used to gauge OS, revealed that TGAME and its metabolite gallic acid could scavenge free radicals to a similar extent as the standard antioxidant vitamin C with an EC_{50} 10.6 +/- 0.3, 2.6 and 45.0 +/- 2.4 (Figure 65), respectively. Therefore, the compound is considered to be a potent antioxidant. Methyl quinate did not show any radical scavenging activity as expected, since it is a sugar and not a phenolic compound. The EC_{50} of compound 16, BF and M1 was 5.5 μM, 9.7 μg/mL and 39.3 μM, respectively (Figure 66-67) (Table 19).

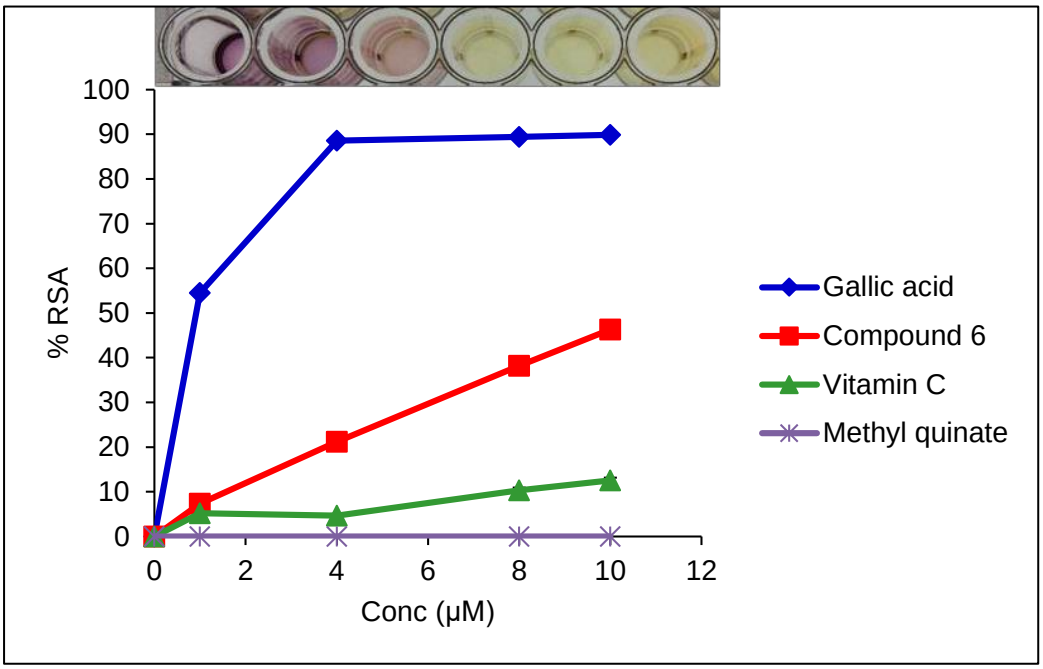

Figure 65. Antiradical efficiency (AE) of TGAME (6) and its synthetic intermediates gallic acid and methyl quinate in DPPH assay. Different volumes (2 – 20 μL) of the compounds and vitamin C (2-20 μM in DMSO) were made up to 40 μL with DMSO and 1.96 mL DPPH (0.1 mM) solution was added. The reaction mixture was incubated in dark condition at room temperature for 20 min. Then, the absorbance of the mixture was read at 517 nm. DPPH solution was taken as control. The percentage of radical scavenging activity of each compound was calculated.

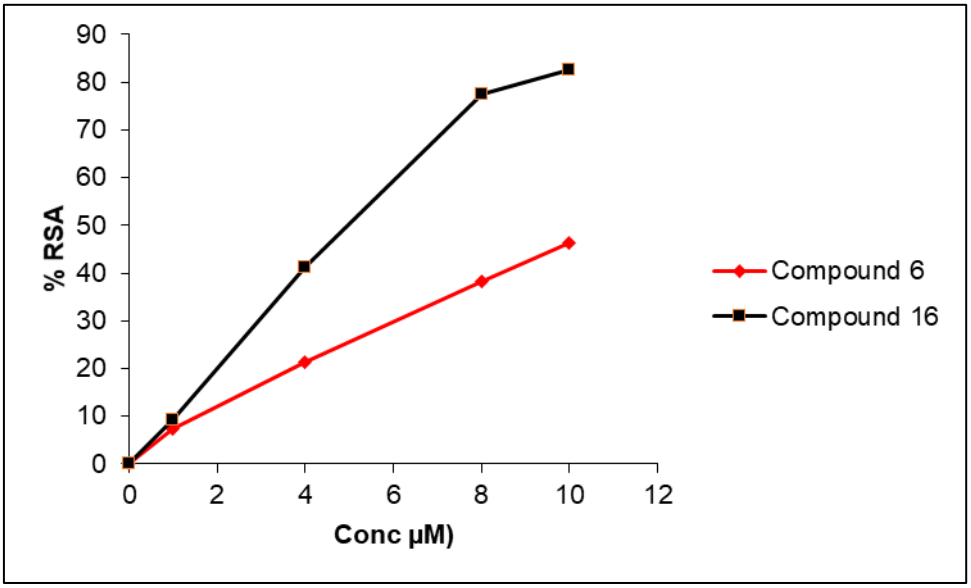

Figure 66. Antiradical efficiency (AE) of TGAME (6) and compound 16 in DPPH assay. Different volumes (2 – 20 μL) of the compounds (2-20 μM in DMSO) were made up to 40 μL with DMSO and 1.96 mL DPPH (0.1 mM) solution was added. The reaction mixture was incubated in dark condition at room temperature for 20 min. Then, the absorbance of the mixture was read at 517 nm. DPPH solution was taken as control and the percentage radical scavenging activity of each compound was calculated.

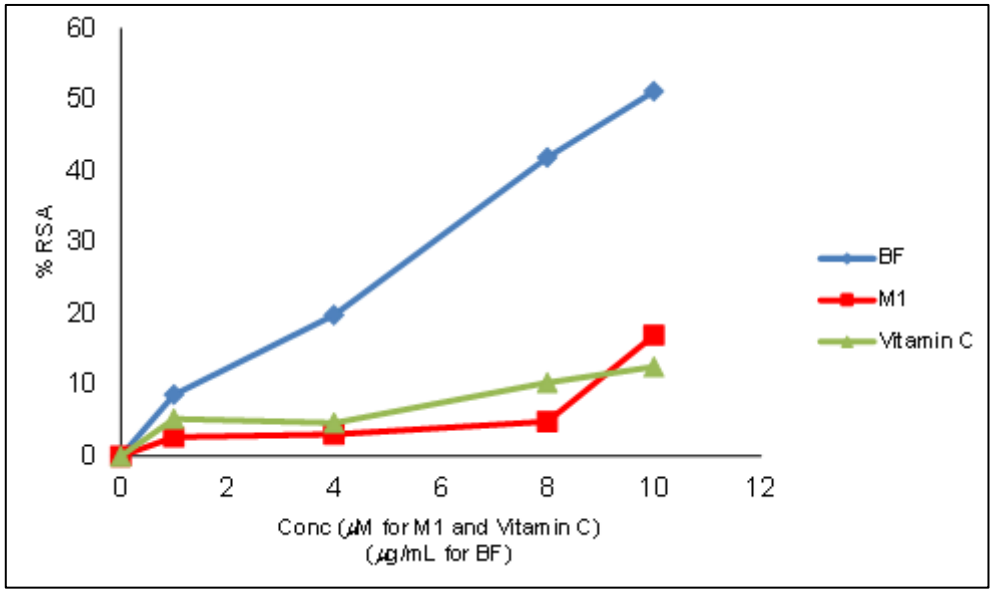

Figure 67. Antiradical efficiency (AE) of *n*-butanolic fraction of *C. lucens* (BF) or M1 metabolite in DPPH assay. Different volumes (2 – 20 μL) of compound 6, vitamin C or gallic acid (2-20 μM in DMSO) were made up to 40 μL with DMSO and 1.96 mL DPPH (0.1 mM) solution was added. The reaction mixture was incubated in dark condition at room temperature for 20 min. Then, the absorbance of the mixture was read at 517 nm. DPPH solution was taken as control.

Table 19. EC_{50} of TGAME (6) and its synthetic intermediates, *C. lucens* BF and its biotransformed metabolite M1 in DPPH free radicals assay. Data were expressed as means ± S.D. of three independent experiments.

Compound	EC_{50} (μM)
Compound 6	10.6 ± 0.3
Gallic acid	2.6 ± 0.0
Methyl quinate	—
Compound 16	5.5
C. lucens BF	9.7 μg/mL
M1	39.3
Vitamin C	45.0 ± 2.4

Overall, our study supports the hypothesis of Verkoelen and Verhulst (200) that crystal binding is preceded by pathologic alterations in cell surface binding molecules. Nonetheless, TGAME-treatment could not entirely prevent COM adhesion to cells, suggesting that these interactions involve multiple processes and many molecules, perhaps including annexin II, osteopontin and hyaluronan. (178, 193) Therefore, other unknown cell surface molecules might mediate the inhibitory effect of TGAME on COM crystal-binding to MDCKI cells.

Conclusion

6 Conclusion

In summary, we report that the plant 3,4,5-tri-*O*-galloylquinic acid methyl ester (TGAME, 6) inhibited COM crystal adhesion to renal cells and this effect is mediated by decreased expression of ANXA1 on cell surface. Thus, cell surface expression of ANXA1 might be a key pathogenic factor in crystal retention and urinary stone formation *in vivo*. Both M1 metabolite and BF as well as compound 16 also inhibited COM crystals binding to MDCKI cells with two different mechanisms of actions.

TGAME also significantly decreased CaOx crystal number, size and total crystal area within MTs of *Drosophila* models, as well as showing a potential antioxidant activity by free radicals scavenging capability. Our findings may also be relevant for the observed decrease of crystal deposition in urolithiasis animal models-treated with *Copaifera* leaf extracts. In addition to, our findings support a promising role for TGAME in the prevention and modulation of new or recurrent renal stone formation. Moreover, our results support the hypothesis of Verkoelen and Verhulst that crystal binding is preceded by pathologic alterations in cell surface binding molecules, therefore further preclinical and clinical studies should be performed for the use of this compound in urolithiasis.

We also reported that galloylquinic acids from *Copaifera lucens* leaves (*n*-butanolic fraction, BF) were all transformed by *Aspergillus alliaceus* into one major metabolite 3-*O*-methyl gallic acid (M1), which is one of the known metabolites of gallic acid studied in humans. These data can provide a tool for predicting the metabolic profile of galloylquinic acids or related compounds *in vivo*.

Both BF and its transformed product (M1) significantly diminished COM crystal-binding to MDCKI cells in concentrations of 50 μg/mL and 5 μM, respectively. The compounds also exhibited antioxidant activities.

Appendices

7 Appendices

Figure S 1. ^{1}H NMR (500 MHz) and ^{13}C NMR (125 MHz) spectra of compound 1 in DMSO-*d*6.

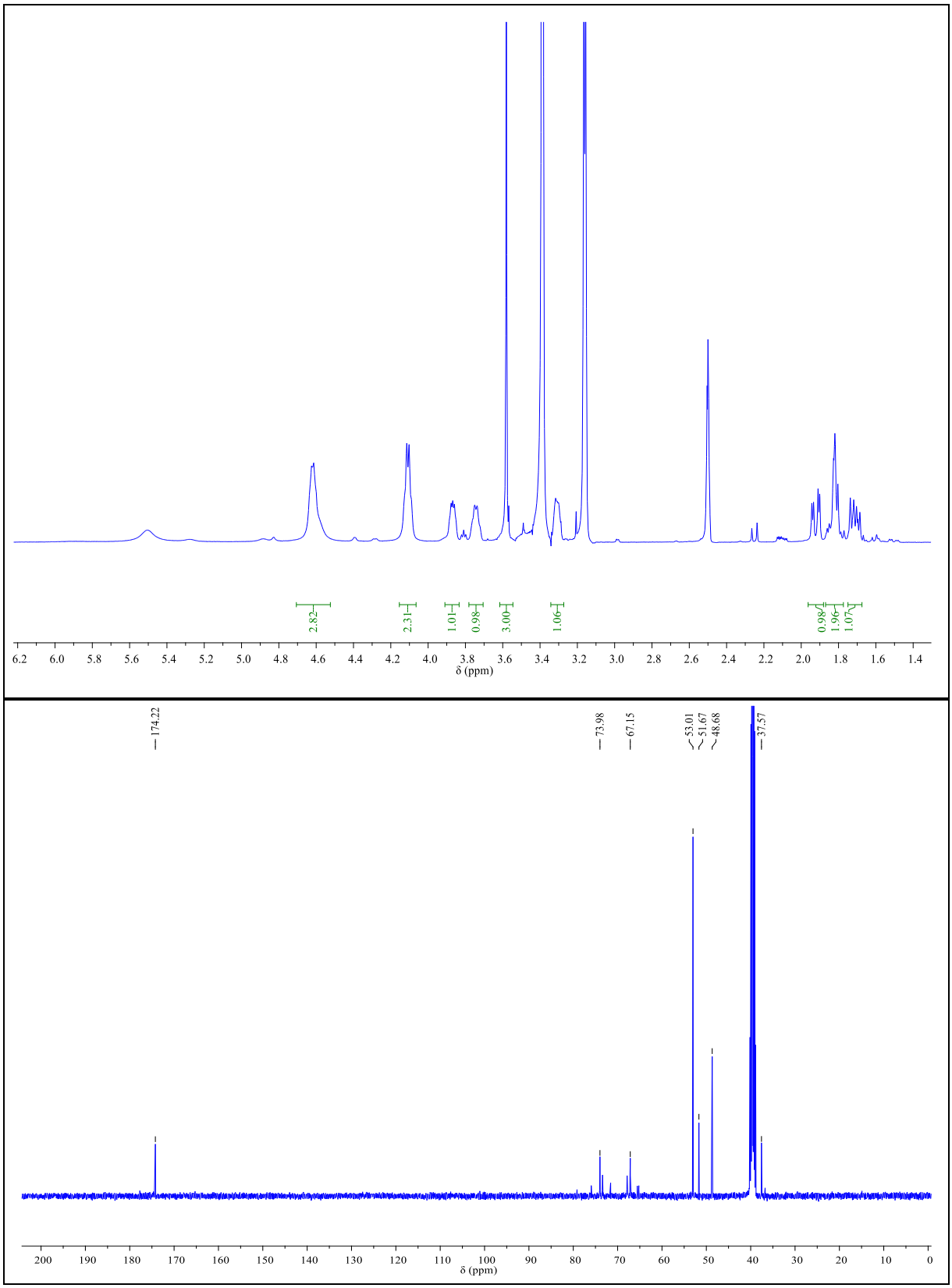

Figure S 2. DEPT 135 (125 MHz) of compound 1 in DMSO-*d*6.

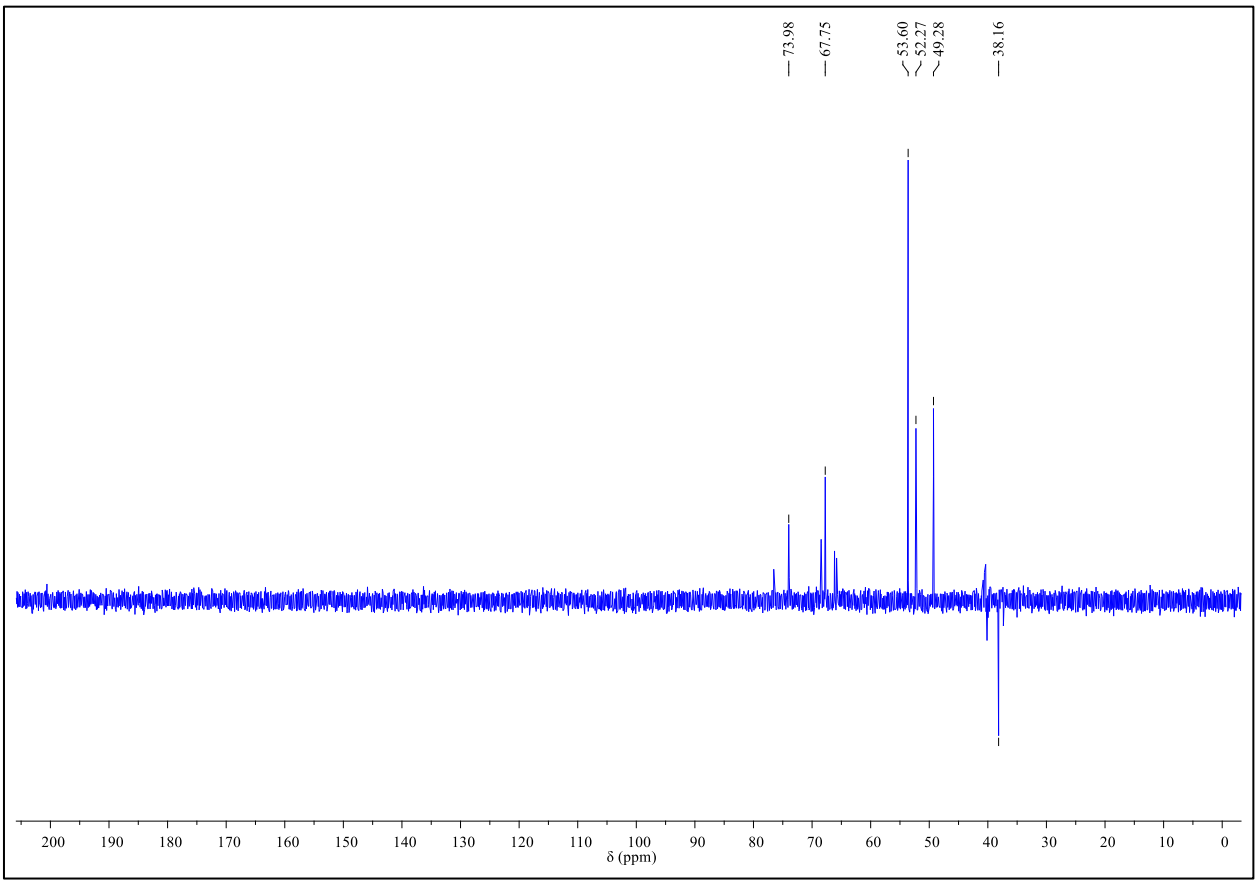

Figure S 3. ^{1}H NMR (500 MHz) and ^{13}C NMR (125 MHz) spectra of compound 2 in DMSO-*d*6.

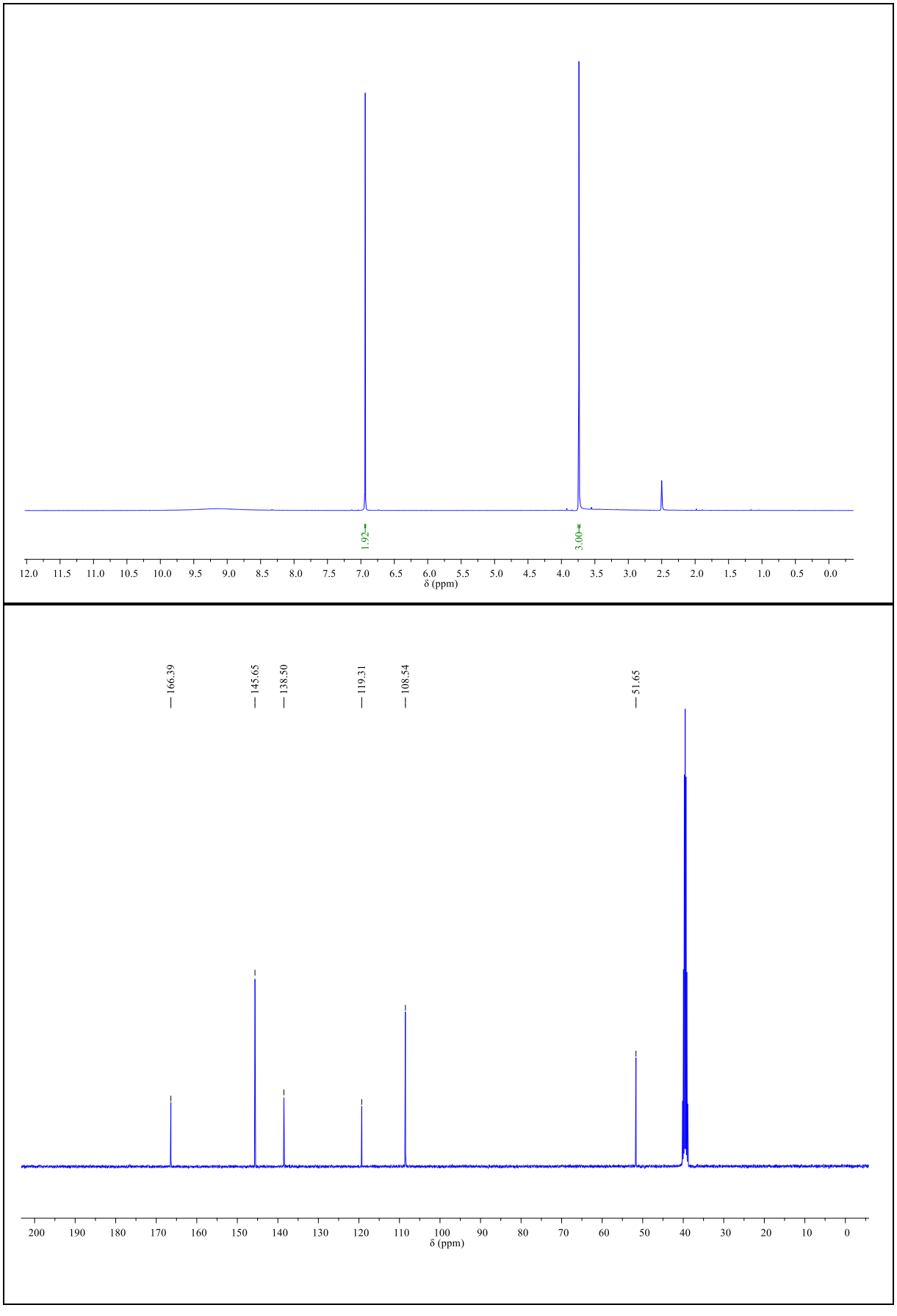

Figure S 4. DEPT 135 (125 MHz) of compound 2 in DMSO-*d*6.

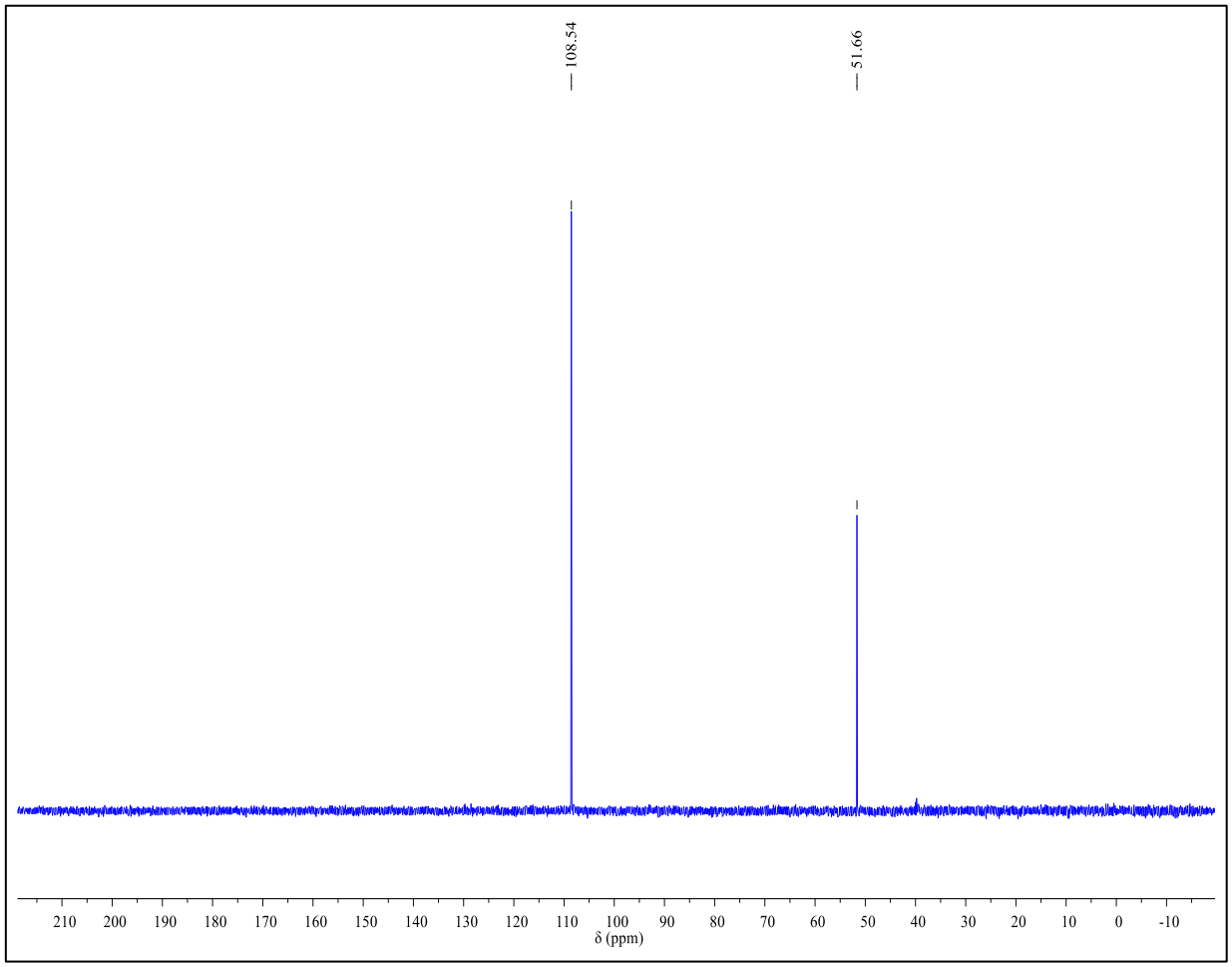

Figure S 5. ^{1}H NMR (500 MHz) and ^{13}C NMR (125 MHz) spectra of compound 3 in DMSO-*d*6.

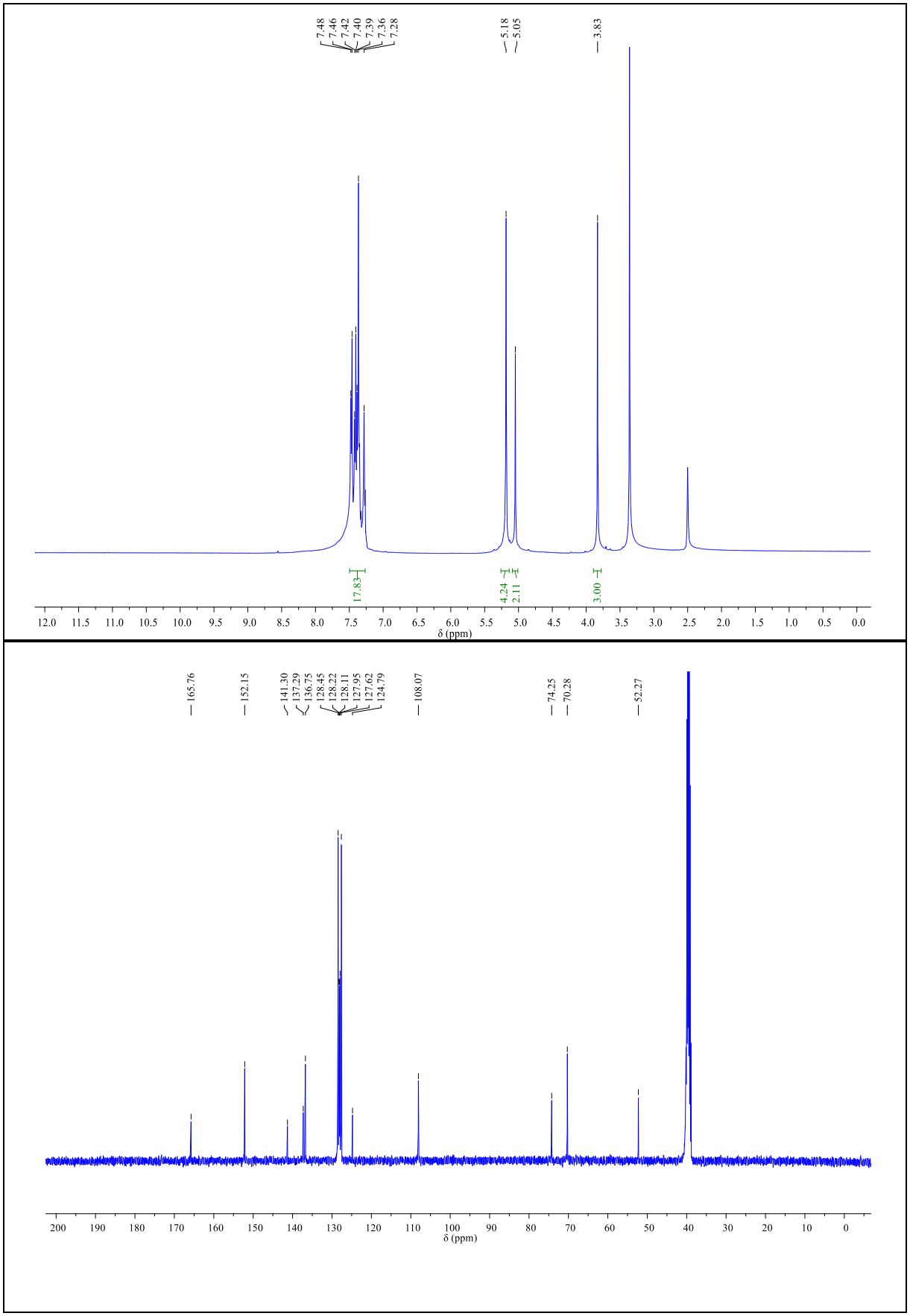

Figure S 6. DEPT 135 (125 MHz) of compound 3 in DMSO-*d*6.

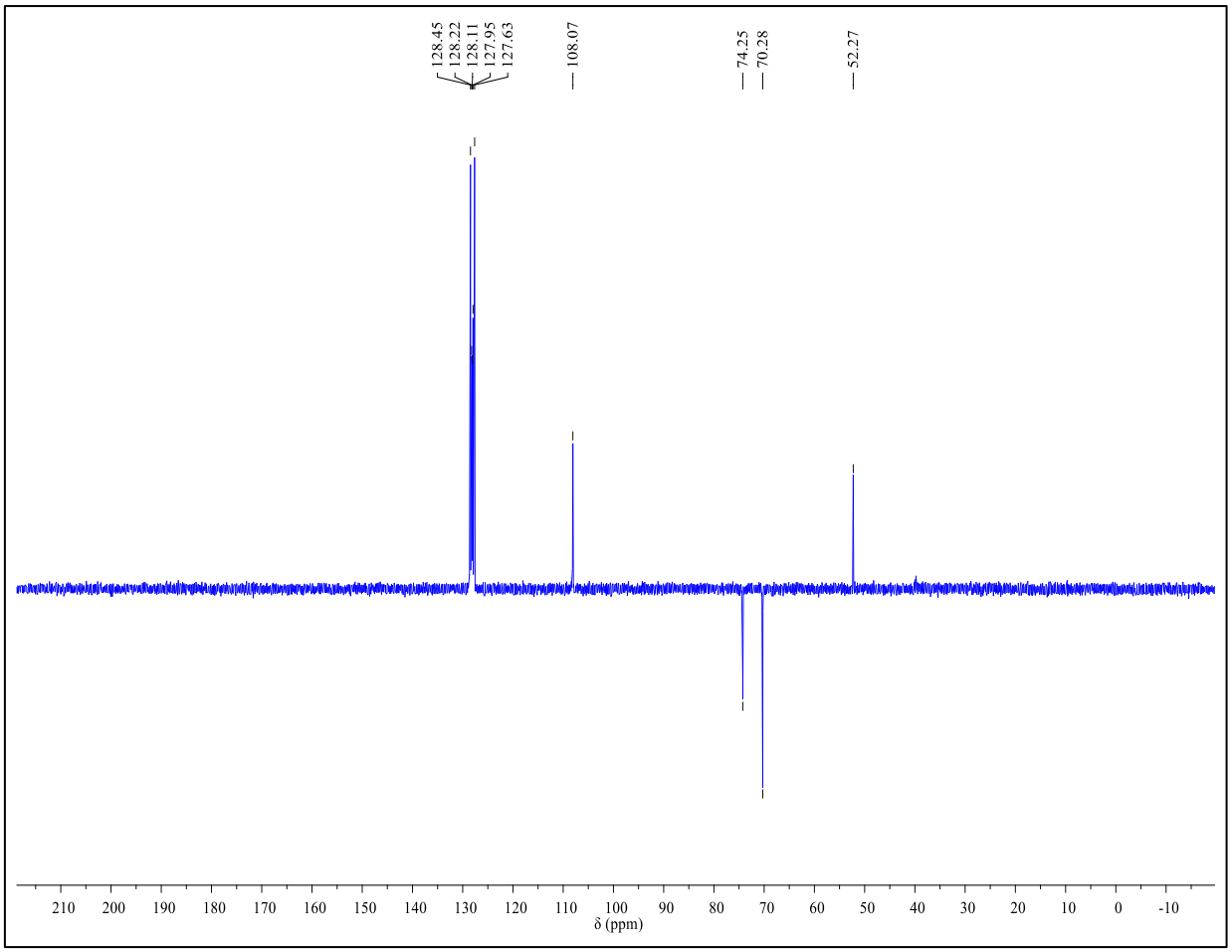

Figure S 7. ^{1}H NMR (500 MHz) and ^{13}C NMR (125MHz) spectra of compound 4 in DMSO-*d*6.

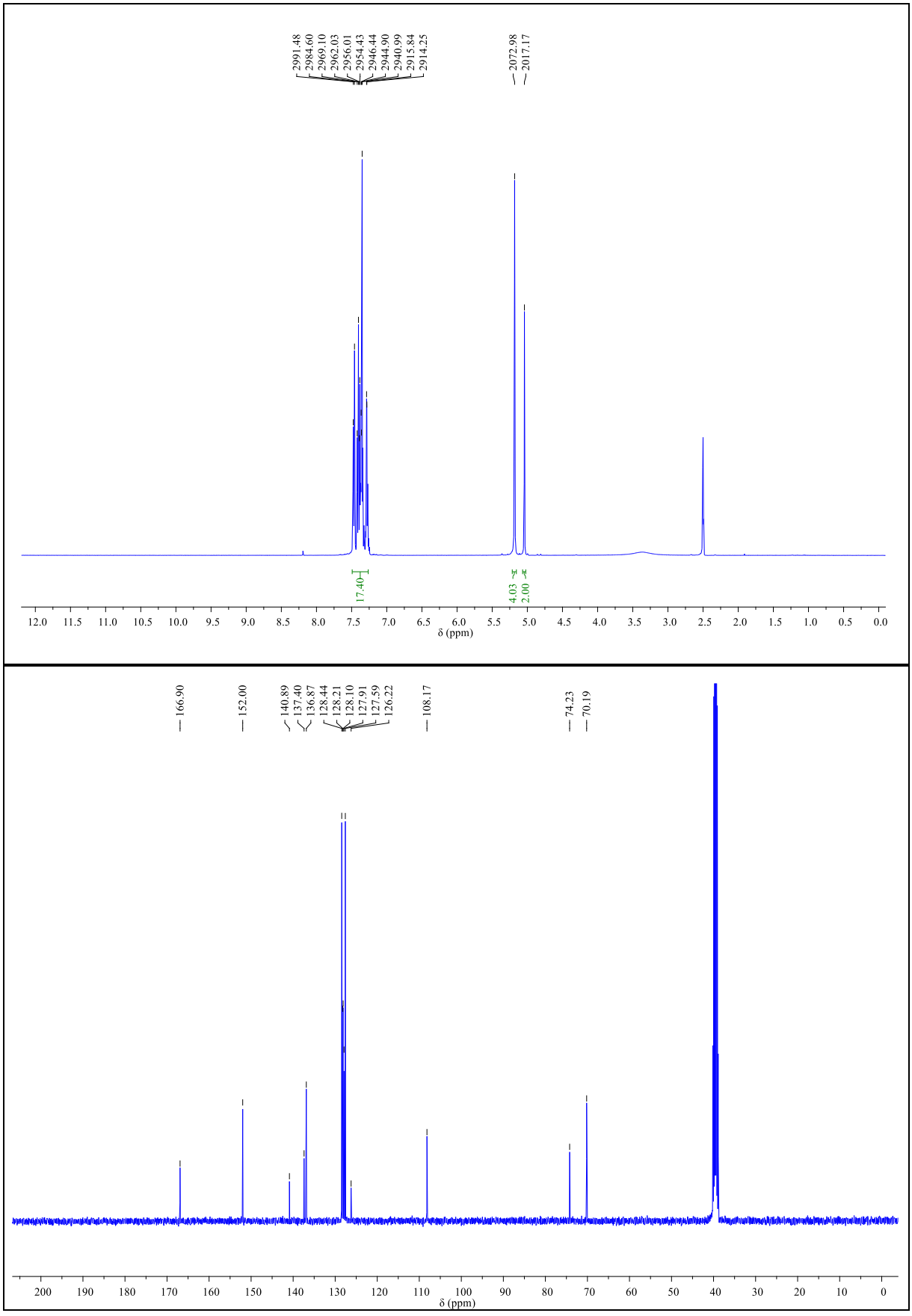

Figure S 8. DEPT 135 at (125 MHz) of compound 4 in DMSO-*d*6.

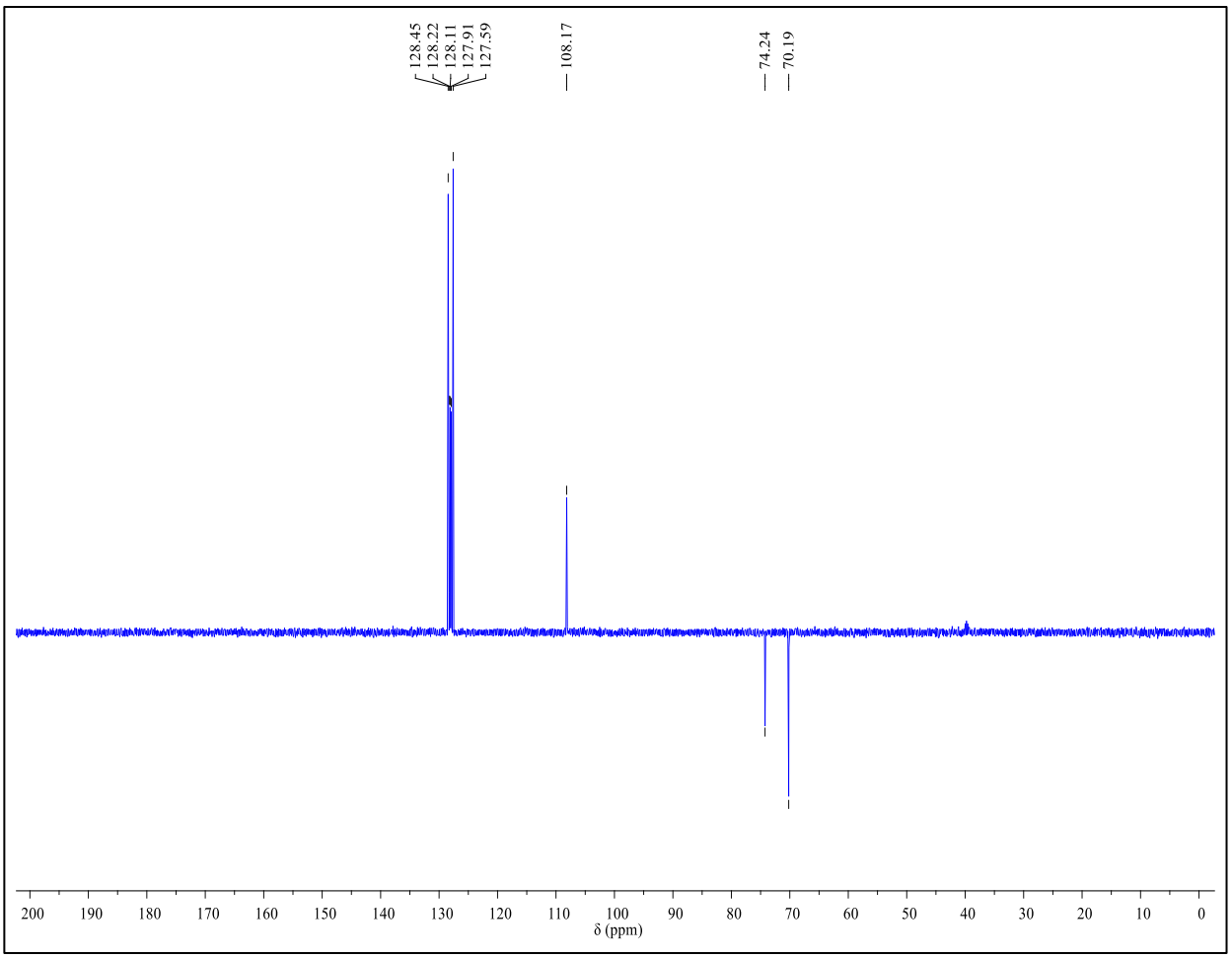

Figure S 9. ^{1} H NMR (500 MHz) and ^{13} C NMR (125 MHz) of compound 5 in $CDCl_3$.

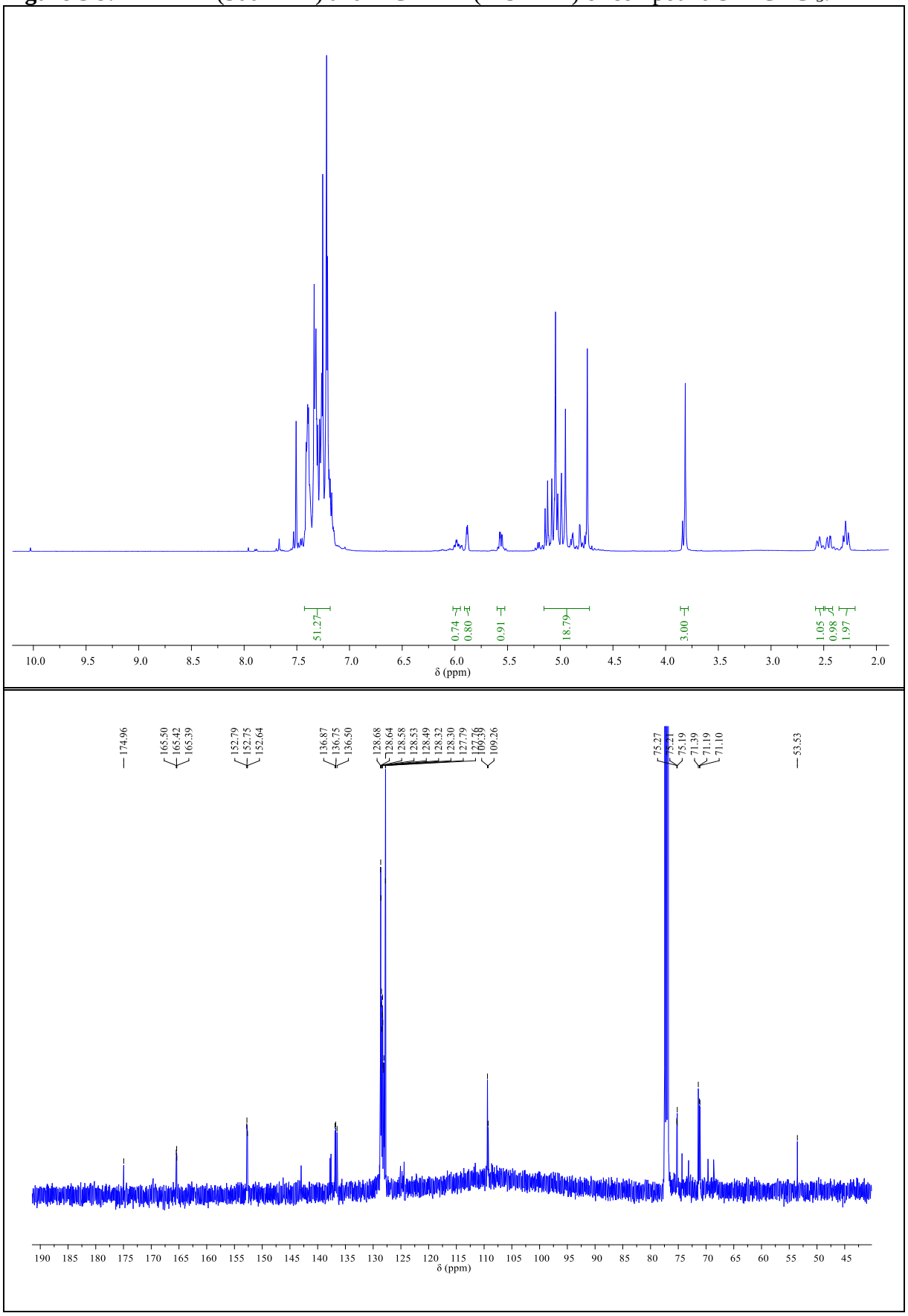

Figure S 10. HMBC and HSQC (500 MHz) of compound 5 in $CDCl_3$.

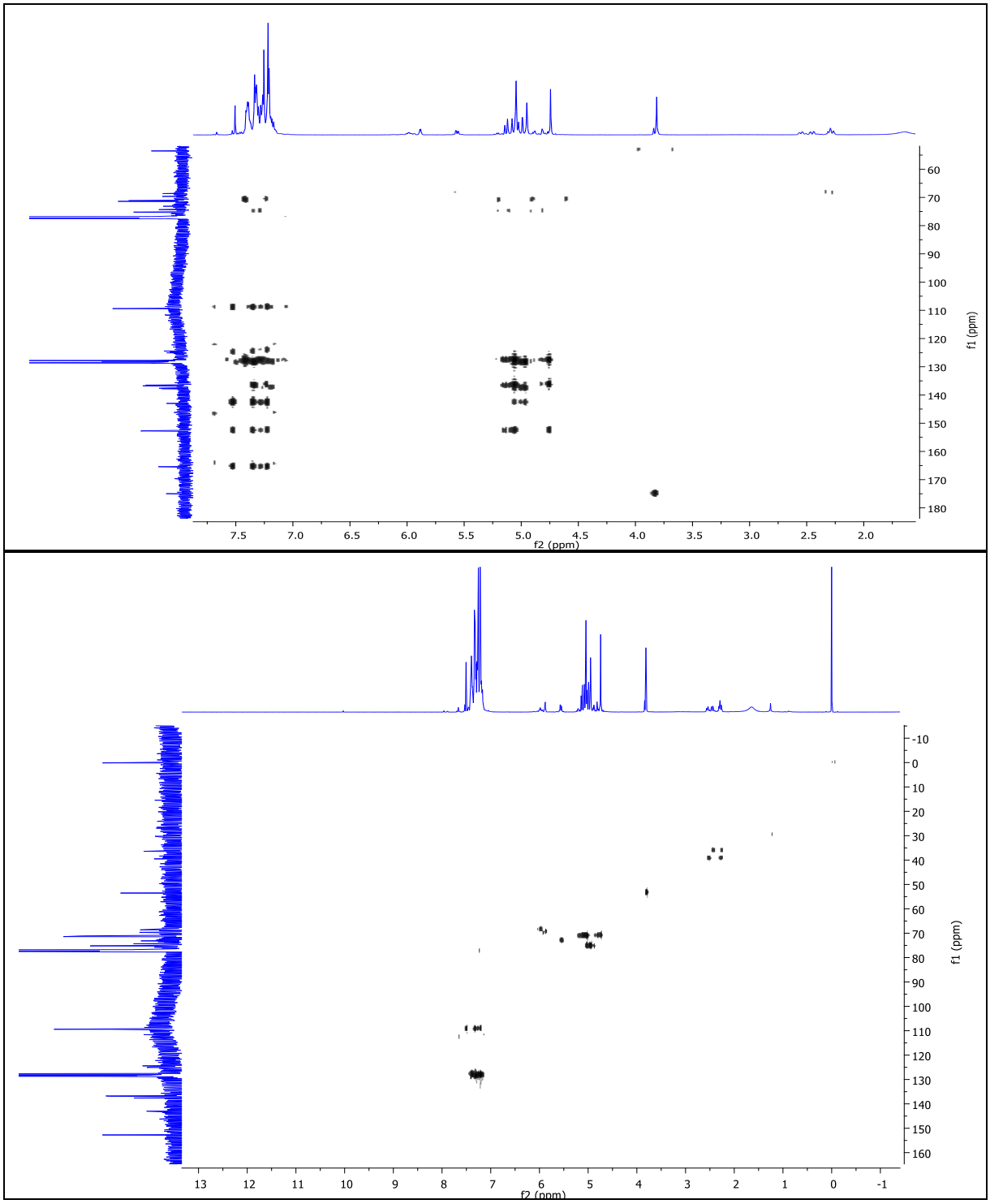

Figure S 11. ^{1}H-^{1}H (COSY) spectrum (125 and 500 MHz) of compound 5 in $CDCl_3$.

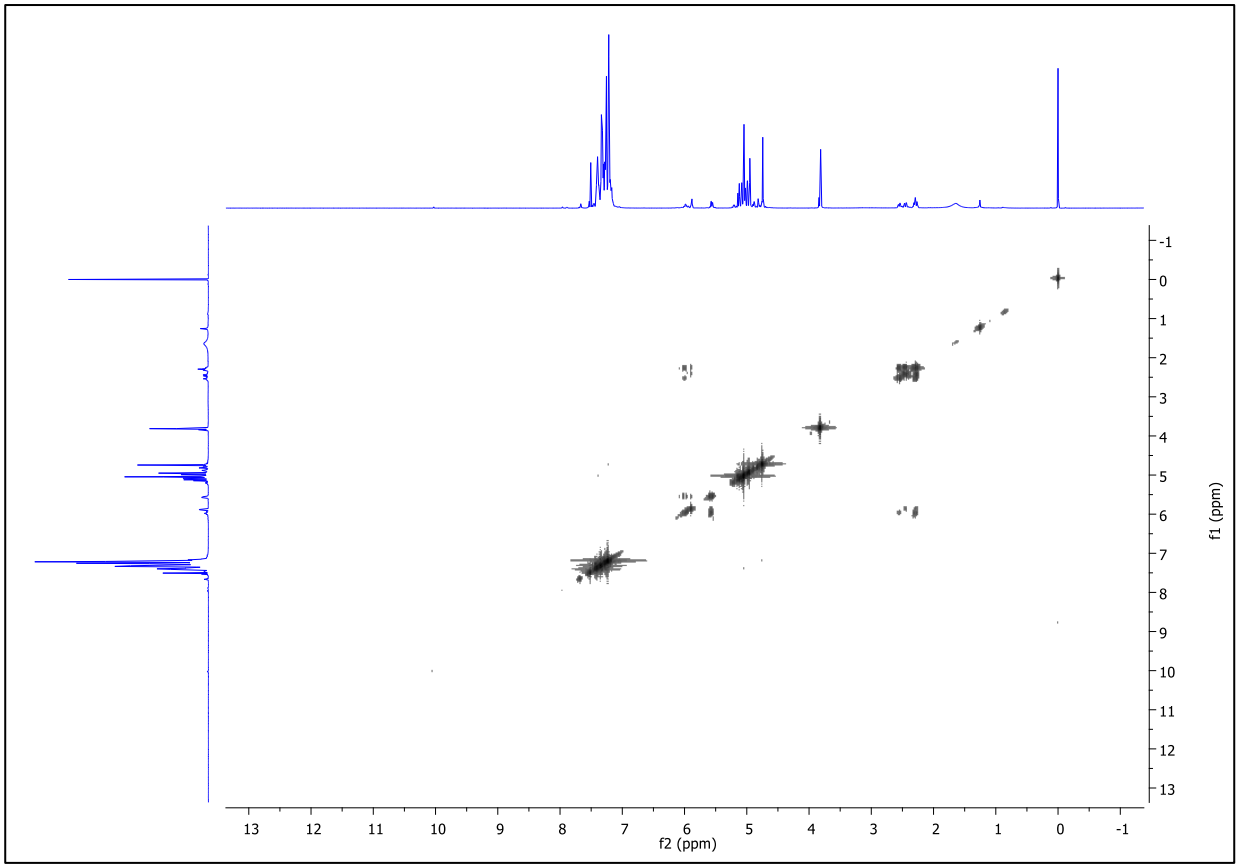

Figure S 12. ^{1}H NMR (500 MHz) and ^{13}C NMR (125 MHz) of compound 6 in DMSO-*d*6.

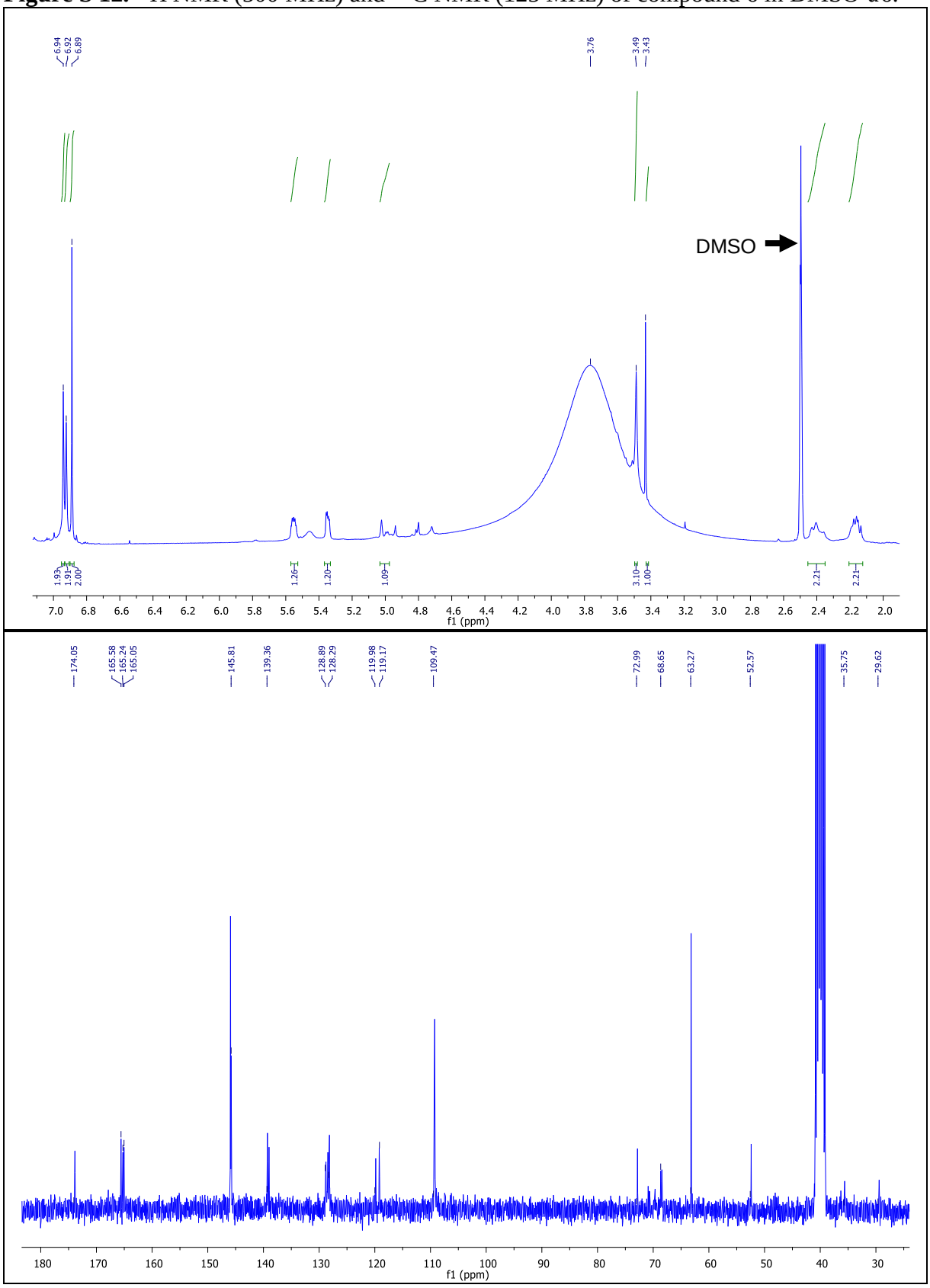

Figure S 13. [1] H NMR spectrum (500 MHz) of metabolite M1 CH_3OH-*d4*.

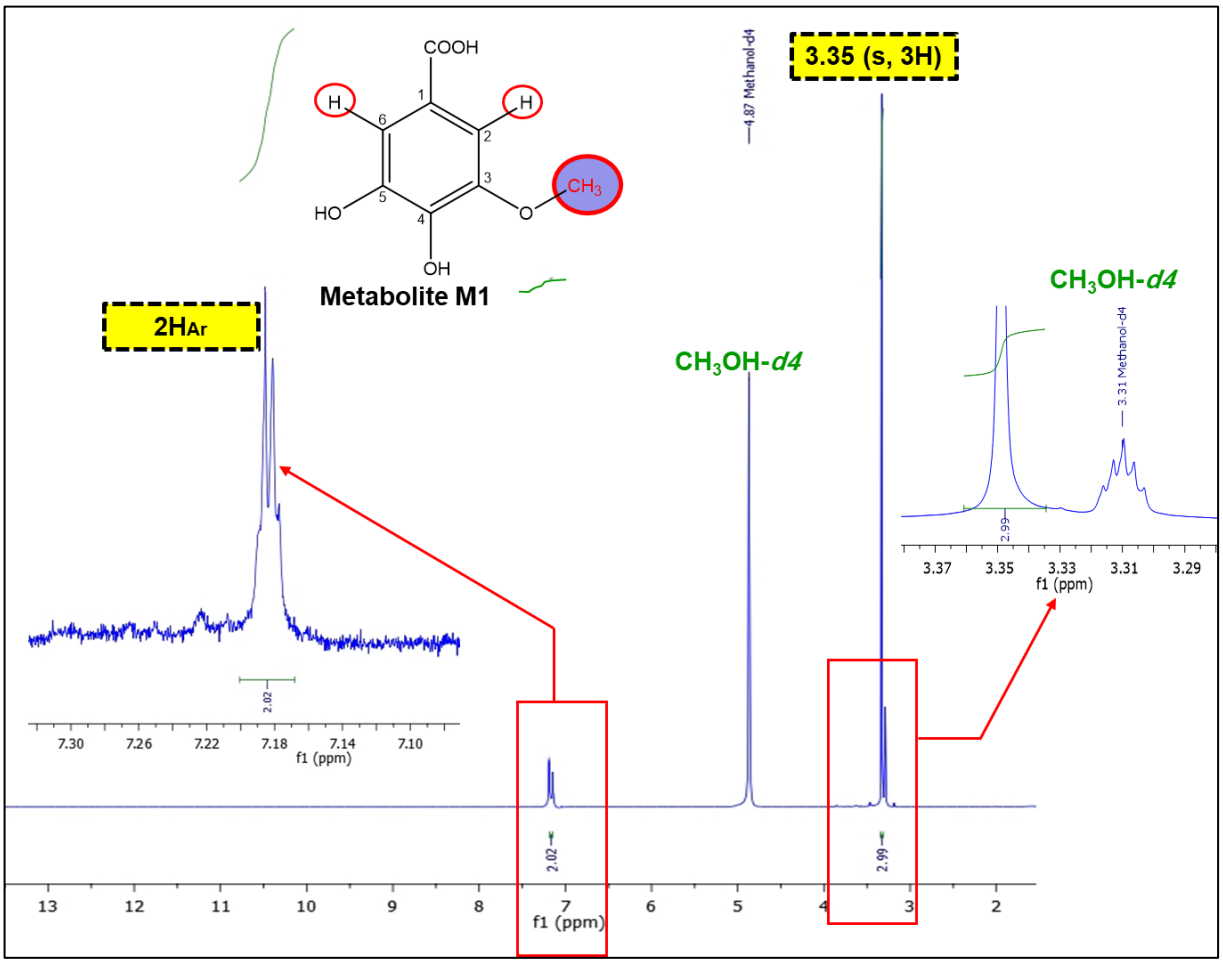

References

8 References

1. Finlayson B. Physicochemical aspects of urolithiasis. Kidney International. 1978;13(5):344-60.

2. Shattock S. A prehistoric or predynastic Egyptian calculus. Trans Pathol Soc (London). 1905;61:275-90.

3. Williams G. An ancient bladder stone. J Am Med Assoc 1926;87:941.

4. Beck C, Mulvaney W. Apatitic urinary calculi from early American Indians. JAMA. 1966;195:168-9.

5. Butt A. Etiologic factors in renal lithiasis. Thomas, Springfield, Illinois. 1956.

6. Desnos M. Pousson A, Desnos E (eds) Encyclopedie Francaise d'Urologie. Octane Doin et Fils, Paris. 1914:1-294.

7. Adams F. The genuine works of Hippocrates. Williams & Wilkins, Baltimore. 1939.

8. Blacklock N. Epidemiology of urolithiasis. In: Williams DI, Chisholm GD, (eds) Scientific foundations of urology Heinemann, London. I1976. p. 235-43.

9. Anderson C. Renal histological changes in stone-formers and non-stone-formers. In: Hodgkinson A, Nordin BEC (eds). Proceedings of the renal stone research symposium Churchill London. 1969:113-36.

10. Andersen D. Environmental factors in the aetiology of urolithiasis. In: Cifuentes Delatte L, Rapado A, Hodgkinson A (eds) Urinary calculi, Karger, Basel. 1973:130-44.

11. Blacklock N. Epidemiology of renal lithiasis. In: Wickham JEA (ed) Urinary calculous disease. Churchill Livingstone, Edinburgh. 1979:21-39.

12. Long LO, Park S. Update on nephrolithiasis management. Minerva Urol Nefrol. 2007;59(3):317-25.

13. Fink HA, Wilt TJ, Eidman KE, Garimella PS, MacDonald R, Rutks IR, et al. Medical management to prevent recurrent nephrolithiasis in adults: a systematic review for an American College of Physicians Clinical Guideline. Ann Intern Med. 2013;158(7):535-43.

14. Worcester EM, Coe FL. Calcium Kidney Stones. New England Journal of Medicine. 2010;363(10):954-63.

15. Department of Health and Human Services USA NIoHNIoDaDaKD. Urologic Diseases in America US Government Printing Office. 2012.

16. Scales CD, Jr., Smith AC, Hanley JM, Saigal CS. Prevalence of kidney stones in the United States. Eur Urol. 2012;62(1):160-5.

17. Obligado SH, Goldfarb DS. The association of nephrolithiasis with hypertension and obesity: a review. Am J Hypertens. 2008;21(3):257-64.

18. Taylor EN, Stampfer MJ, Curhan GC. Obesity, weight gain, and the risk of kidney stones. Jama. 2005;293(4):455-62.

19. Daudon M, Dore JC, Jungers P, Lacour B. Changes in stone composition according to age and gender of patients: a multivariate epidemiological approach. Urol Res. 2004;32(3):241-7.

20. Lieske JC, de la Vega LS, Gettman MT, Slezak JM, Bergstralh EJ, Melton LJ, 3rd, et al. Diabetes mellitus and the risk of urinary tract stones: a population-based case-control study. Am J Kidney Dis. 2006;48(6):897-904.

21. Strazzullo P, Barba G, Vuotto P, Farinaro E, Siani A, Nunziata V, et al. Past history of nephrolithiasis and incidence of hypertension in men: a reappraisal based on the results of the Olivetti Prospective Heart Study. Nephrol Dial Transplant. 2001;16(11):2232-5.

22. Johri N, Cooper B, Robertson W, Choong S, Rickards D, Unwin R. An update and practical guide to renal stone management. Nephron Clin Pract. 2010;116(3):c159-71.

23. Rule AD, Krambeck AE, Lieske JC. Chronic kidney disease in kidney stone formers. Clin J Am Soc Nephrol. 2011;6(8):2069-75.

24. El-Zoghby ZM, Lieske JC, Foley RN, Bergstralh EJ, Li X, Melton LJ, 3rd, et al. Urolithiasis and the risk of ESRD. Clin J Am Soc Nephrol. 2012;7(9):1409-15.

25. Shoag J, Halpern J, Goldfarb DS, Eisner BH. Risk of chronic and end stage kidney disease in patients with nephrolithiasis. J Urol. 2014;192(5):1440-5.

26. Keddis MT, Rule AD. Nephrolithiasis and loss of kidney function. Curr Opin Nephrol Hypertens. 2013;22(4):390-6.

27. Dontas IA, Khaldi L. Urolithiasis and transitional cell carcinoma of the bladder in a Wistar rat. J Am Assoc Lab Anim Sci. 2006;45(4):64-7.

28. Romero V, Akpinar H, Assimos DG. Kidney Stones: A Global Picture of Prevalence, Incidence, and Associated Risk Factors. Reviews in Urology. 2010;12(2-3):e86-e96.

29. Stamatelou KK, Francis ME, Jones CA, Nyberg LM, Curhan GC. Time trends in reported prevalence of kidney stones in the United States: 1976-1994. Kidney Int. 2003;63(5):1817-23.

30. Turney BW, Reynard JM, Noble JG, Keoghane SR. Trends in urological stone disease. BJU Int. 2012;109(7):1082-7.

31. Scales CD, Jr., Curtis LH, Norris RD, Springhart WP, Sur RL, Schulman KA, et al. Changing gender prevalence of stone disease. J Urol. 2007;177(3):979-82.

32. Lieske JC, Pena de la Vega LS, Slezak JM, Bergstralh EJ, Leibson CL, Ho KL, et al. Renal stone epidemiology in Rochester, Minnesota: an update. Kidney Int. 2006;69(4):760-4.

33. Strope SA, Wolf JS, Jr., Hollenbeck BK. Changes in gender distribution of urinary stone disease. Urology. 2010;75(3):543-6, 6.e1.

34. Ordon M, Urbach D, Mamdani M, Saskin R, Honey RJ, Pace KT. A population based study of the changing demographics of patients undergoing definitive treatment for kidney stone disease. J Urol. 2015;193(3):869-74.

35. Curhan GC, Rimm EB, Willett WC, Stampfer MJ. Regional variation in nephrolithiasis incidence and prevalence among United States men. J Urol. 1994;151(4):838-41.

36. Mandel NS, Mandel GS. Urinary tract stone disease in the United States veteran population. I. Geographical frequency of occurrence. J Urol. 1989;142(6):1513-5.

37. Soucie JM, Thun MJ, Coates RJ, McClellan W, Austin H. Demographic and geographic variability of kidney stones in the United States. Kidney Int. 1994;46(3):893-9.

38. Curhan GC, Willett WC, Rimm EB, Speizer FE, Stampfer MJ. Body size and risk of kidney stones. J Am Soc Nephrol. 1998;9(9):1645-52.

39. Sorensen MD, Chi T, Shara NM, Wang H, Hsi RS, Orchard T, et al. Activity, energy intake, obesity, and the risk of incident kidney stones in postmenopausal women: a report from the Women's Health Initiative. J Am Soc Nephrol. 2014;25(2):362-9.

40. Chung SD, Chen YK, Lin HC. Increased risk of diabetes in patients with urinary calculi: a 5-year followup study. J Urol. 2011;186(5):1888-93.

41. West B, Luke A, Durazo-Arvizu RA, Cao G, Shoham D, Kramer H. Metabolic syndrome and self-reported history of kidney stones: the National Health and Nutrition Examination Survey (NHANES III) 1988-1994. Am J Kidney Dis. 2008;51(5):741-7.

42. Jeong IG, Kang T, Bang JK, Park J, Kim W, Hwang SS, et al. Association between metabolic syndrome and the presence of kidney stones in a screened population. Am J Kidney Dis. 2011;58(3):383-8.

43. Ferraro PM, Taylor EN, Eisner BH, Gambaro G, Rimm EB, Mukamal KJ, et al. History of kidney stones and the risk of coronary heart disease. Jama. 2013;310(4):408-15.

44. Alexander RT, Hemmelgarn BR, Wiebe N, Bello A, Samuel S, Klarenbach SW, et al. Kidney stones and cardiovascular events: a cohort study. Clin J Am Soc Nephrol. 2014;9(3):506-12.

45. Rule AD, Roger VL, Melton LJ, Bergstralh EJ, Li X, Peyser PA, et al. Kidney Stones Associate with Increased Risk for Myocardial Infarction. Journal of the American Society of Nephrology : JASN. 2010;21(10):1641-4.

46. Evan AP. Physiopathology and etiology of stone formation in the kidney and the urinary tract. Pediatr Nephrol. 2010;25(5):831-41.

47. Ryall RL, Chauvet MC, Grover PK. Intracrystalline proteins and urolithiasis: a comparison of the protein content and ultrastructure of urinary calcium oxalate monohydrate and dihydrate crystals. BJU Int. 2005;96(4):654-63.

48. McKee MD, Nanci A, Khan SR. Ultrastructural immunodetection of osteopontin and osteocalcin as major matrix components of renal calculi. J Bone Miner Res. 1995;10(12):1913-29.

49. Khan SR, Hackett RL. Role of organic matrix in urinary stone formation: an ultrastructural study of crystal matrix interface of calcium oxalate monohydrate stones. J Urol. 1993;150(1):239-45.

50. Khan SR, Kok DJ. Modulators of urinary stone formation. Front Biosci. 2004;9:1450-82.

51. Atmani F, Khan SR. Role of urinary bikunin in the inhibition of calcium oxalate crystallization. J Am Soc Nephrol. 1999;10 Suppl 14:S385-8.

52. Ryall RL. Macromolecules and Urolithiasis: Parallels and Paradoxes. Nephron Physiology. 2004;98(2):p37-p42.

53. Khan SR, Atmani F, Glenton P, Hou Z, Talham DR, Khurshid M. Lipids and membranes in the organic matrix of urinary calcific crystals and stones. Calcif Tissue Int. 1996;59(5):357-65.

54. Khan SR, Shevock PN, Hackett RL. Membrane-associated crystallization of calcium oxalate in vitro. Calcif Tissue Int. 1990;46(2):116-20.

55. Hunter GK. Role of osteopontin in modulation of hydroxyapatite formation. Calcif Tissue Int. 2013;93(4):348-54.

56. Khan SR, Johnson JM, Peck AB, Cornelius JG, Glenton PA. Expression of osteopontin in rat kidneys: induction during ethylene glycol induced calcium oxalate nephrolithiasis. J Urol. 2002;168(3):1173-81.

57. Aihara K, Byer KJ, Khan SR. Calcium phosphate-induced renal epithelial injury and stone formation: involvement of reactive oxygen species. Kidney Int. 2003;64(4):1283-91.

58. Grases F, Villacampa AI, Costa-Bauza A, Sohnel O. Uric acid calculi: types, etiology and mechanisms of formation. Clin Chim Acta. 2000;302(1-2):89-104.

59. Khan SR, Hackett RL. Identification of urinary stone and sediment crystals by scanning electron microscopy and x-ray microanalysis. J Urol. 1986;135(4):818-25.

60. Siener R, Netzer L, Hesse A. Determinants of brushite stone formation: a case-control study. PLoS One. 2013;8(11):e78996.

61. Sakhaee K, Adams-Huet B, Moe OW, Pak CY. Pathophysiologic basis for normouricosuric uric acid nephrolithiasis. Kidney Int. 2002;62(3):971-9.

62. Fellstrom B, Danielson BG, Karlstrom B, Lithell H, Ljunghall S, Vessby B. The influence of a high dietary intake of purine-rich animal protein on urinary urate excretion and supersaturation in renal stone disease. Clin Sci (Lond). 1983;64(4):399-405.

63. Khan SR, Hackett RL, Finlayson B. Morphology of urinary stone particles resulting from ESWL treatment. J Urol. 1986;136(6):1367-72.

64. Griffith DP, Osborne CA. Infection (urease) stones. Miner Electrolyte Metab. 1987;13(4):278-85.

65. Biyani CS, Cartledge JJ. Cystinuria—Diagnosis and Management. EAU-EBU Update Series. 2006;4(5):175-83.

66. Tattevin P, Revest M, Chapplain JM, Ratajczak-Enselme M, Arvieux C, Michelet C. Increased risk of renal stones in patients treated with atazanavir. Clin Infect Dis. 2013;56(8):1186.

67. Izzedine H, Lescure FX, Bonnet F. HIV medication-based urolithiasis. Clinical Kidney Journal. 2014;7(2):121-6.

68. Raheem OA, Mirheydar HS, Palazzi K, Chenoweth M, Lakin C, Sur RL. Prevalence of nephrolithiasis in human immunodeficiency virus infected patients on the highly active antiretroviral therapy. J Endourol. 2012;26(8):1095-8.

69. Bischoff K, Rumbeiha WK. Pet food recalls and pet food contaminants in small animals. Vet Clin North Am Small Anim Pract. 2012;42(2):237-50, v.

70. Cianciolo RE, Bischoff K, Ebel JG, Van Winkle TJ, Goldstein RE, Serfilippi LM. Clinicopathologic, histologic, and toxicologic findings in 70 cats inadvertently exposed to pet food contaminated with melamine and cyanuric acid. J Am Vet Med Assoc. 2008;233(5):729-37.

71. Gabriels G, Lambert M, Smith P, Wiesner L, Hiss D. Melamine contamination in nutritional supplements--Is it an alarm bell for the general consumer, athletes, and 'Weekend Warriors'? Nutr J. 2015;14:69.

72. Ding J. Childhood urinary stones induced by melamine-tainted formula: how much we know, how much we don't know. Kidney International. 2009;75(8):780-2.

73. Robertson WG, Peacock M, Nordin BE. Calcium oxalate crystalluria and urine saturation in recurrent renal stone-formers. Clin Sci. 1971;40(5):365-74.

74. Finlayson B, Reid F. The expectation of free and fixed particles in urinary stone disease. Invest Urol. 1978;15(6):442-8.

75. Robertson WG. Factors affecting the precipitation of calcium phosphatein vitro. Calcified Tissue Research. 1973;11(4):311-22.

76. Khan SR, Hackett RL. Developmental morphology of calcium oxalate foreign body stones in rats. Calcified Tissue International. 1985;37(2):165-73.

77. Khan SR, Hackett RL. Urolithogenesis of mixed foreign body stones. J Urol. 1987;138(5):1321-8.

78. Linnes MP, Krambeck AE, Cornell L, Williams JC, Korinek M, Bergstralh EJ, et al. Phenotypic characterization of kidney stone formers by endoscopic and histological quantification of intrarenal calcification. Kidney International. 2013;84(4):818-25.

79. Wang X, Krambeck AE, Williams JC, Tang X, Rule AD, Zhao F, et al. Distinguishing Characteristics of Idiopathic Calcium Oxalate Kidney Stone Formers with Low Amounts of Randall's Plaque. Clinical Journal of the American Society of Nephrology : CJASN. 2014;9(10):1757-63.

80. Khan SR. Experimental calcium oxalate nephrolithiasis and the formation of human urinary stones. Scanning Microsc. 1995;9(1):89-100; discussion -1.

81. Khan SR, Canales BK. Unified theory on the pathogenesis of Randall's plaques and plugs. Urolithiasis. 2015;43 Suppl 1:109-23.

82. Hosking DH, Erickson SB, Van den Berg CJ, Wilson DM, Smith LH. The stone clinic effect in patients with idiopathic calcium urolithiasis. J Urol. 1983;130(6):1115-8.

83. Borghi L, Meschi T, Amato F, Briganti A, Novarini A, Giannini A. Urinary volume, water and recurrences in idiopathic calcium nephrolithiasis: a 5-year randomized prospective study. J Urol. 1996;155(3):839-43.

84. Borghi L, Schianchi T, Meschi T, Guerra A, Allegri F, Maggiore U, et al. Comparison of two diets for the prevention of recurrent stones in idiopathic hypercalciuria. N Engl J Med. 2002;346(2):77-84.

85. Meschi T, Maggiore U, Fiaccadori E, Schianchi T, Bosi S, Adorni G, et al. The effect of fruits and vegetables on urinary stone risk factors. Kidney International. 2004;66(6):2402-10.

86. Ferraro PM, Taylor EN, Gambaro G, Curhan GC. Soda and other beverages and the risk of kidney stones. Clin J Am Soc Nephrol. 2013;8(8):1389-95.

87. Bushinsky DA, Bashir MA, Riordon DR, Nakagawa Y, Coe FL, Grynpas MD. Increased dietary oxalate does not increase urinary calcium oxalate saturation in hypercalciuric rats. Kidney Int. 1999;55(2):602-12.

88. Pearle MS, Goldfarb DS, Assimos DG, Curhan G, Denu-Ciocca CJ, Matlaga BR, et al. Medical management of kidney stones: AUA guideline. J Urol. 2014;192(2):316-24.

89. Sakhaee K, Maalouf NM, Kumar R, Pasch A, Moe OW. Nephrolithiasis-associated bone disease: pathogenesis and treatment options. Kidney Int. 2011;79(4):393-403.

90. Yendt ER, Cohanim M. Prevention of calcium stones with thiazides. Kidney International. 1978;13(5):397-409.

91. Barnela SR, Soni SS, Saboo SS, Bhansali AS. Medical management of renal stone. Indian Journal of Endocrinology and Metabolism. 2012;16(2):236-9.

92. Arowojolu O, Goldfarb DS. Treatment of calcium nephrolithiasis in the patient with hyperuricosuria. J Nephrol. 2014;27(6):601-5.

93. Pak CY, Sakhaee K, Fuller CJ. Physiological and physiochemical correction and prevention of calcium stone formation by potassium citrate therapy. Trans Assoc Am Physicians. 1983;96:294-305.

94. Ettinger B, Pak CYC, Citron JT, Thomas C, Adams-Huet B, Vangessel A. POTASSIUM-MAGNESIUM CITRATE IS AN EFFECTIVE PROPHYLAXIS AGAINST RECURRENT CALCIUM OXALATE NEPHROLITHIASIS. The Journal of Urology. 1997;158(6):2069-73.

95. Sakhaee K, Nicar M, Hill K, Pak CYC, Sakhaee K. Contrasting effects of potassium citrate and sodium citrate therapies on urinary chemistries and crystallization of stone-forming salts. Kidney International. 1983;24(3):348-52.

96. Fabris A, Lupo A, Bernich P, Abaterusso C, Marchionna N, Nouvenne A, et al. Long-term treatment with potassium citrate and renal stones in medullary sponge kidney. Clin J Am Soc Nephrol. 2010;5(9):1663-8.

97. Skolarikos A, Straub M, Knoll T, Sarica K, Seitz C, Petrik A, et al. Metabolic evaluation and recurrence prevention for urinary stone patients: EAU guidelines. Eur Urol. 2015;67(4):750-63.

98. Holdgate A, Pollock T. Nonsteroidal anti-inflammatory drugs (NSAIDS) versus opioids for acute renal colic. Cochrane Database of Systematic Reviews. 2004(1).

99. Serinken M, Eken C, Turkcuer I, Elicabuk H, Uyanik E, Schultz CH. Intravenous paracetamol versus morphine for renal colic in the emergency department: a randomised double-blind controlled trial. Emerg Med J. 2012;29(11):902-5.

100. Papadopoulos G, Bourdoumis A, Kachrilas S, Bach C, Buchholz N, Masood J. Hyoscine N-butylbromide (Buscopan(R)) in the treatment of acute ureteral colic: what is the evidence? Urol Int. 2014;92(3):253-7.

101. Worster AS, Bhanich Supapol W. Fluids and diuretics for acute ureteric colic. Cochrane Database of Systematic Reviews. 2012(2).

102. Campschroer T, Zhu Y, Duijvesz D, Grobbee DE, Lock MT. Alpha-blockers as medical expulsive therapy for ureteral stones. Cochrane Database Syst Rev. 2014(4):Cd008509.

103. Pickard R, Starr K, MacLennan G, Lam T, Thomas R, Burr J, et al. Medical expulsive therapy in adults with ureteric colic: a multicentre, randomised, placebo-controlled trial. Lancet. 2015;386(9991):341-9.

104. Trinchieri A, Esposito N, Castelnuovo C. Dissolution of radiolucent renal stones by oral alkalinization with potassium citrate/potassium bicarbonate. Arch Ital Urol Androl. 2009;81(3):188-91.

105. Harvey AL, Edrada-Ebel R, Quinn RJ. The re-emergence of natural products for drug discovery in the genomics era. Nat Rev Drug Discov. 2015;14(2):111-29.

106. Mishra BB, Tiwari VK. Natural products: an evolving role in future drug discovery. Eur J Med Chem. 2011;46(10):4769-807.

107. Rey-Ladino J, Ross AG, Cripps AW, McManus DP, Quinn R. Natural products and the search for novel vaccine adjuvants. Vaccine. 2011;29(38):6464-71.

108. Butler MS. The Role of Natural Product Chemistry in Drug Discovery. Journal of Natural Products. 2004;67(12):2141-53.

109. Dias DA, Urban S, Roessner U. A historical overview of natural products in drug discovery. Metabolites. 2012;2(2):303-36.

110. Veiga Junior VF, Pinto AC. O gênero copaifera L. Química Nova. 2002;25:273-86.

111. do Nascimento ME, Zoghbi MdGB, Brasil Pereira Pinto JE, Vilela Bertolucci SK. Chemical variability of the volatiles of Copaifera langsdorffii growing wild in the Southeastern part of Brazil. Biochemical Systematics and Ecology. 2012;43(Supplement C):1-6.

112. Izumi E, Ueda-Nakamura T, Veiga-Júnior VF, Nakamura CV. Toxicity of Oleoresins from the Genus Copaifera in Trypanosoma cruzi: A Comparative Study. Planta Med. 2013;79(11):952-8.

113. Oliveira RBd, Coelho EB, Rodrigues MR, Costa-Machado ARdM, Sousa J, #xe3, et al. Effect of the Copaifera langsdorffii Desf. Leaf Extract on the Ethylene Glycol-Induced Nephrolithiasis in Rats. Evidence-Based Complementary and Alternative Medicine. 2013;2013:10.

114. Brancalion AP, Oliveira RB, Sousa JP, Groppo M, Berretta AA, Barros ME, et al. Effect of hydroalcoholic extract from Copaifera langsdorffii leaves on urolithiasis induced in rats. Urol Res. 2012;40(5):475-81.

115. Youn SH, Kwon JH, Yin J, Tam LT, Ahn HS, Myung SC, et al. Anti-Inflammatory and Anti-Urolithiasis Effects of Polyphenolic Compounds from Quercus gilva Blume. Molecules. 2017;22(7).

116. Jeong BC, Kim BS, Kim JI, Kim HH. Effects of green tea on urinary stone formation: an in vivo and in vitro study. J Endourol. 2006;20(5):356-61.

117. Kanlaya R, Singhto N, Thongboonkerd V. EGCG decreases binding of calcium oxalate monohydrate crystals onto renal tubular cells via decreased surface expression of alpha-enolase. JBIC Journal of Biological Inorganic Chemistry. 2016;21(3):339-46.

118. Hofmann AS, Gross GG. Biosynthesis of gallotannins: Formation of polygalloylglucoses by enzymatic acylation of 1,2,3,4,6-penta-O-galloylglucose. Archives of Biochemistry and Biophysics. 1990;283(2):530-2.

119. Lee J-H, Yehl M, Ahn KS, Kim S-H, Lieske JC. 1,2,3,4,6-penta-O-galloyl-beta-d-glucose attenuates renal cell migration, hyaluronan expression, and crystal adhesion. European Journal of Pharmacology. 2009;606(1):32-7.

120. Lee H-J, Jeong S-J, Lee H-J, Lee E-O, Bae H, Lieske JC, et al. 1,2,3,4,6-Penta-O-galloyl-beta-D-glucose reduces renal crystallization and oxidative stress in a hyperoxaluric rat model. Kidney International.79(5):538-45.

121. Lee H-J, Jeong S-J, Park MN, Linnes M, Han HJ, Kim JH, et al. Gallotannin Suppresses Calcium Oxalate Crystal Binding and Oxalate-Induced Oxidative Stress in Renal Epithelial Cells. Biological and Pharmaceutical Bulletin. 2012;35(4):539-44.

122. de Cógáin MR, Linnes MP, Lee HJ, Krambeck AE, de Mendonça Uchôa JC, Kim S-H, et al. Aqueous extract of Costus arabicus inhibits calcium oxalate crystal growth and adhesion to renal epithelial cells. Urolithiasis. 2015;43(2):119-24.

123. De Mello JF. Plants in traditional medicine in Brazil. Journal of Ethnopharmacology. 1980;2(1):49-55.

124. Paulino N, Cechinel-Filho V, Yunes RA, Calixto JB. The Relaxant Effect of Extract of Phyllanthus urinaria in the Guinea-pig Isolated Trachea. Evidence for Involvement of ATP-sensitive Potassium Channels. Journal of Pharmacy and Pharmacology. 1996;48(11):1158-63.

125. Freitas AM, Schor N, Boim MA. The effect of Phyllanthus niruri on urinary inhibitors of calcium oxalate crystallization and other factors associated with renal stone formation. BJU International. 2002;89(9):829-34.

126. Campos AH, Schor N. Phyllanthus niruri inhibits calcium oxalate endocytosis by renal tubular cells: its role in urolithiasis. Nephron. 1999;81(4):393-7.

127. Barros ME, Lima R, Mercuri LP, Matos JR, Schor N, Boim MA. Effect of extract of Phyllanthus niruri on crystal deposition in experimental urolithiasis. Urol Res. 2006;34(6):351-7.

128. Khan A, Khan SR, Gilani AH. Studies on the in vitro and in vivo antiurolithic activity of Holarrhena antidysenterica. Urol Res. 2012;40(6):671-81.

129. Winston D. Herbal and Nutritional Treatment of Kidney Stones. Journal of the American Herbalists Guild. 2011;10(2):61-71.

130. Bashir S, Gilani AH, Siddiqui AA, Pervez S, Khan SR, Sarfaraz NJ, et al. Berberis vulgaris root bark extract prevents hyperoxaluria induced urolithiasis in rats. Phytother Res. 2010;24(8):1250-5.

131. Hadjzadeh MA, Khoei A, Hadjzadeh Z, Parizady M. Ethanolic extract of nigella sativa L seeds on ethylene glycol-induced kidney calculi in rats. Urol J. 2007;4(2):86-90.

132. Freitas AM, Schor N, Boim MA. The effect of Phyllanthus niruri on urinary inhibitors of calcium oxalate crystallization and other factors associated with renal stone formation. BJU Int. 2002;89(9):829-34.

133. Rodgers A, Lewandowski S, Allie-Hamdulay S, Pinnock D, Baretta G, Gambaro G. Evening primrose oil supplementation increases citraturia and decreases other urinary risk factors for calcium oxalate urolithiasis. J Urol. 2009;182(6):2957-63.

134. Grases F, Prieto RM, Gomila I, Sanchis P, Costa-Bauza A. Phytotherapy and renal stones: the role of antioxidants. A pilot study in Wistar rats. Urol Res. 2009;37(1):35-40.

135. Mudhir S. Shekha ABQ, Haval H. Ali, Xebat E. Selim. Effect of Fenugreek (Trigonella foenum-graecum) on Ethylene Glycol Induced Kidney Stone in Rats. Jordan Journal of Biological Sciences. 1995;7(4):257-60.

136. Laroubi A, Touhami M, Farouk L, Zrara I, Aboufatima R, Benharref A, et al. Prophylaxis effect of Trigonella foenum graecum L. seeds on renal stone formation in rats. Phytother Res. 2007;21(10):921-5.

137. Aggarwal A, Tandon S, Singla SK, Tandon C. Diminution of oxalate induced renal tubular epithelial cell injury and inhibition of calcium oxalate crystallization in vitro by aqueous extract of Tribulus terrestris. Int Braz J Urol. 2010;36(4):480-8; discussion 8, 9.

138. Woottisin S, Hossain RZ, Yachantha C, Sriboonlue P, Ogawa Y, Saito S. Effects of Orthosiphon grandiflorus, Hibiscus sabdariffa and Phyllanthus amarus extracts on risk factors for urinary calcium oxalate stones in rats. J Urol. 2011;185(1):323-8.

139. Prasongwatana V, Woottisin S, Sriboonlue P, Kukongviriyapan V. Uricosuric effect of Roselle (Hibiscus sabdariffa) in normal and renal-stone former subjects. J Ethnopharmacol. 2008;117(3):491-5.

140. Hirayama H, Wang Z, Nishi K, Ogawa A, Ishimatu T, Ueda S, et al. Effect of Desmodium styracifolium-triterpenoid on calcium oxalate renal stones. Br J Urol. 1993;71(2):143-7.

141. Grases F, Masarova L, Costa-Bauza A, March JG, Prieto R, Tur JA. Effect of "Rosa Canina" infusion and magnesium on the urinary risk factors of calcium oxalate urolithiasis. Planta Med. 1992;58(6):509-12.

142. Atmani F, Slimani Y, Mimouni M, Aziz M, Hacht B, Ziyyat A. Effect of aqueous extract from Herniaria hirsuta L. on experimentally nephrolithiasic rats. J Ethnopharmacol. 2004;95(1):87-93.

143. Christina AJ, Ashok K, Packialakshmi M, Tobin GC, Preethi J, Murugesh N. Antilithiatic effect of Asparagus racemosus Willd on ethylene glycol-induced lithiasis in male albino Wistar rats. Methods Find Exp Clin Pharmacol. 2005;27(9):633-8.

144. Prasad KVSRG, Sujatha D, Bharathi K. Herbal drugs in urolithiasis - A review. Pharmacognosy Reviews. 2007;1(1):175-9.

145. Cao ZG, Liu JH, Radman AM, Wu JZ, Ying CP, Zhou SW. [An experimental study of effect of different extracts of Alisma orientalis on urinary calcium oxalate stones formation in rats]. Zhongguo Zhong Yao Za Zhi. 2003;28(11):1072-5.

146. Chen YC, Ho CY, Chen LD, Hsu SF, Chen WC. Wu-Ling-San formula inhibits the crystallization of calcium oxalate in vitro. Am J Chin Med. 2007;35(3):533-41.

147. Bouchet N, Levesque J, Bodo B, Pousset J-L. 3,4,5-Tri-O-Galloylquinic Acid Ethyl Ester from Guiera senegalensis. Pharmaceutical Biology. 1998;36(1):63-5.

148. Bokesch HR, McKee TC, Currens MJ, Gulakowski RJ, McMahon JB, Cardellina JH, et al. HIV-Inhibitory Gallotannins from Lepidobotrys staudtii. Natural Product Letters. 1996;8(2):133-6.

149. Nogueira MS, Furtado RA, Bastos JK. Flavonoids and Methoxy-galloylquinic Acid Derivatives from the Leaf Extract of Copaifera langsdorffii Desf. Journal of Agricultural and Food Chemistry. 2015;63(31):6939-45.

150. Motta EVS, Lemos M, Costa JC, Banderó-Filho VC, Sasse A, Sheridan H, et al. Galloylquinic acid derivatives from Copaifera langsdorffii leaves display gastroprotective activity. Chemico-Biological Interactions. 2017;261:145-55.

151. Neszmelyi A, Kreher B, Muller A, Dorsch W, Wagner H. Tetragalloylquinic acid, the major antiasthmatic principle of Galphimia glauca. Planta medica. 1993;59(2):164-7.

152. Lee K-H, Kashiwada Y, Nonaka G-i, Nishioka I, Nishizawa M, Yamagishi T, et al. Tannins and Related Compounds as Anti-HIV Agents 1. In: Chu CK, Cutler HG, editors. Natural Products as Antiviral Agents. Boston, MA: Springer US; 1992. p. 69-90.

153. Sousa LRFd, Ramalho SD, Fernandes JB, Silva MFdGFd, Iemma MRdC, Corrêa CJ, et al. Leishmanicidal galloylquinic acids are noncompetitive inhibitors of arginase. Journal of the Brazilian Chemical Society. 2014;25:1832-8.

154. Baratto MC, Tattini M, Galardi C, Pinelli P, Romani A, Visioli F, et al. Antioxidant activity of galloyl quinic derivatives isolated from P. lentiscus leaves. Free radical research. 2003;37(4):405-12.

155. Mahmood N, Moore P, De Tommasi N, De Simone F, Colman S, Hay A, et al. Inhibition of HIV infection by caffeoylquinic acid derivatives. Antiviral Chemistry and Chemotherapy. 1993;4(4):235-40.

156. Nishizawa M, Yamagishi T, Dutschman GE, Parker WB, Bodner AJ, Kilkuskie RE, et al. Anti-Aids Agents, 1. Isolation and Characterization of Four New Tetragalloylquinic Acids as a New Class of HIV Reverse Transcriptase Inhibitors from Tannic Acid. Journal of Natural Products. 1989;52(4):762-8.

157. Nishimura H, Nonaka G-I, Nishioka I. Seven quinic acid gallates from quercus stenophylla. Phytochemistry. 1984;23(11):2621-3.

158. Lewandowska U, Fichna J, Gorlach S. Enhancement of anticancer potential of polyphenols by covalent modifications. Biochemical Pharmacology. 2016;109:1-13.

159. Karas D, Ulrichová J, Valentová K. Galloylation of polyphenols alters their biological activity. Food and Chemical Toxicology. 2017;105:223-40.

160. Iglesias J, Pazos M, Lois S, Medina I. Contribution of galloylation and polymerization to the antioxidant activity of polyphenols in fish lipid systems. J Agric Food Chem. 2010;58(12):7423-31.

161. Pazos M, Torres JL, Andersen ML, Skibsted LH, Medina I. Galloylated polyphenols efficiently reduce alpha-tocopherol radicals in a phospholipid model system composed of sodium dodecyl sulfate (SDS) micelles. J Agric Food Chem. 2009;57(11):5042-8.

162. Wang Z. Steglich Catalyst. Comprehensive Organic Name Reactions and Reagents: John Wiley & Sons, Inc.; 2010.

163. Ren Y, Himmeldirk K, Chen X. Synthesis and Structure−Activity Relationship Study of Antidiabetic Penta-O-galloyl-d-glucopyranose and Its Analogues. Journal of Medicinal Chemistry. 2006;49(9):2829-37.

164. Abd El-Salam M, Mekky H, El-Naggar EMB, Ghareeb D, El-Demellawy M, El-Fiky F. Hepatoprotective properties and biotransformation of berberine and berberrubine by cell suspension cultures of Dodonaea viscosa and Ocimum basilicum. South African Journal of Botany. 2015;97:191-5.

165. Brancalion APS, Oliveira RB, Sousa JPB, Groppo M, Berretta AA, Barros ME, et al. Effect of hydroalcoholic extract from Copaifera langsdorffii leaves on urolithiasis induced in rats. Urological Research. 2012;40(5):475-81.

166. de Oliveira RB, Coelho EB, Rodrigues MR, Costa-Machado AR, de Sousa JP, Berretta AA, et al. Effect of the Copaifera langsdorffii Desf. Leaf Extract on the Ethylene Glycol-Induced Nephrolithiasis in Rats. Evidence-based complementary and alternative medicine : eCAM. 2013;2013:131372.

167. de Sousa JP, Brancalion AP, Junior MG, Bastos JK. A validated chromatographic method for the determination of flavonoids in Copaifera langsdorffii by HPLC. Natural product communications. 2012;7(1):25-8.

168. Herath W, Mikell JR, Hale AL, Ferreira D, Khan IA. Microbial Metabolism Part 9. Structure and Antioxidant Significance of the Metabolites of 5,7-Dihydroxyflavone (Chrysin), and 5- and 6-Hydroxyflavones. Chemical and Pharmaceutical Bulletin. 2008;56(4):418-22.

169. Herath W, Mikell JR, Hale AL, Ferreira D, Khan IA. Microbial Metabolism. Part 6. Metabolites of 3- and 7-Hydroxyflavones. Chemical and Pharmaceutical Bulletin. 2006;54(3):320-4.

170. Mikell JR, Khan IA. Bioconversion of 7-Hydroxyflavanone: Isolation, Characterization and Bioactivity Evaluation of Twenty-One Phase I and Phase II Microbial Metabolites. Chemical and Pharmaceutical Bulletin. 2012;60(9):1139-45.

171. Tsujihata M. Mechanism of calcium oxalate renal stone formation and renal tubular cell injury. Int J Urol. 2008;15(2):115-20.

172. Khan SR. Crystal-induced inflammation of the kidneys: results from human studies, animal models, and tissue-culture studies. Clin Exp Nephrol. 2004;8(2):75-88.

173. Lieske JC, Norris R, Swift H, Toback FG. Adhesion, internalization and metabolism of calcium oxalate monohydrate crystals by renal epithelial cells. Kidney Int. 1997;52(5):1291-301.

174. Kramer G, Steiner GE, Prinz-Kashani M, Bursa B, Marberger M. Cell-surface matrix proteins and sialic acids in cell-crystal adhesion; the effect of crystal binding on the viability of human CAKI-1 renal epithelial cells. BJU Int. 2003;91(6):554-9.

175. Ebisuno S, Kohjimoto Y, Tamura M, Inagaki T, Ohkawa T. Histological observations of the adhesion and endocytosis of calcium oxalate crystals in MDCK cells and in rat and human kidney. Urol Int. 1997;58(4):227-31.

176. Lieske JC, Leonard R, Swift H, Toback FG. Adhesion of calcium oxalate monohydrate crystals to anionic sites on the surface of renal epithelial cells. Am J Physiol. 1996;270(1 Pt 2):F192-9.

177. Fullekrug J, Simons K. Lipid rafts and apical membrane traffic. Ann N Y Acad Sci. 2004;1014:164-9.

178. Kumar V, Farell G, Deganello S, Lieske JC. Annexin II Is Present on Renal Epithelial Cells and Binds Calcium Oxalate Monohydrate Crystals. Journal of the American Society of Nephrology. 2003;14(2):289-97.

179. Sorokina EA, Kleinman JG. Cloning and preliminary characterization of a calcium-binding protein closely related to nucleolin on the apical surface of inner medullary collecting duct cells. J Biol Chem. 1999;274(39):27491-6.

180. Asselman M, Verhulst A, De Broe ME, Verkoelen CF. Calcium oxalate crystal adherence to hyaluronan-, osteopontin-, and CD44-expressing injured/regenerating tubular epithelial cells in rat kidneys. J Am Soc Nephrol. 2003;14(12):3155-66.

181. Chutipongtanate S, Fong-ngern K, Peerapen P, Thongboonkerd V. High Calcium Enhances Calcium Oxalate Crystal Binding Capacity of Renal Tubular Cells via Increased Surface Annexin A1 but Impairs Their Proliferation and Healing. Journal of Proteome Research. 2012;11(7):3650-63.

182. Kanlaya R, Fong-ngern K, Thongboonkerd V. Cellular adaptive response of distal renal tubular cells to high-oxalate environment highlights surface alpha-enolase as the enhancer of calcium oxalate monohydrate crystal adhesion. Journal of Proteomics. 2013;80:55-65.

183. Kruger NJ. The Bradford Method for Protein Quantitation. In: Walker JM, editor. The Protein Protocols Handbook. Totowa, NJ: Humana Press; 2002. p. 15-21.

184. Dedication UCPD. Drosophila melanogaster 2012. Available from: https://commons.wikimedia.org

185. Education P. Malpighian tubules system 2017. Publishing as Binjamin Cummings]. Available from: https://www.pearson.com.

186. Landry GM, Hirata T, Anderson JB, Cabrero P, Gallo CJR, Dow JAT, et al. Sulfate and thiosulfate inhibit oxalate transport via a dPrestin (Slc26a6)-dependent mechanism in an insect model of calcium oxalate nephrolithiasis. American Journal of Physiology - Renal Physiology. 2016;310(2):F152-F9.

187. Rindler MJ, Chuman LM, Shaffer L, Saier MH. Retention of differentiated properties in an established dog kidney epithelial cell line (MDCK). The Journal of Cell Biology. 1979;81(3):635-48.

188. Saier MHJ. Growth and differentiated properties of a kidney epithelial cell line (MDCK). Am J Physiol. 1981;240:106-9.

189. Sun X-Y, Gan Q-Z, Ouyang J-M. Size-dependent cellular uptake mechanism and cytotoxicity toward calcium oxalate on Vero cells. 2017;7:41949.

190. Guo C, Dugas T, Scates C, Garcia-Villarreal M, Ticich T, McMartin KE. Aluminum Citrate Blocks Toxicity of Calcium Oxalate Crystals by Preventing Binding with Cell Membrane Phospholipids. American Journal of Nephrology. 2013;37(1):41-9.

191. Peerapen P, Thongboonkerd V. Caffeine prevents kidney stone formation by translocation of apical surface annexin A1 crystal-binding protein into cytoplasm: In vitro evidence. 2016;6:38536.

192. Fong-ngern K, Thongboonkerd V. Alpha-enolase on apical surface of renal tubular epithelial cells serves as a calcium oxalate crystal receptor. Scientific Reports. 2016;6:36103.

193. Fong-ngern K, Peerapen P, Sinchaikul S, Chen S-T, Thongboonkerd V. Large-scale Identification of Calcium Oxalate Monohydrate Crystal-binding Proteins on Apical Membrane of Distal Renal Tubular Epithelial Cells. Journal of Proteome Research. 2011;10(10):4463-77.

194. Gerke V, Moss SE. Annexins: From Structure to Function. Physiological Reviews. 2002;82(2):331-71.

195. Fong-ngern K, Sueksakit K, Thongboonkerd V. Surface heat shock protein 90 serves as a potential receptor for calcium oxalate crystal on apical membrane of renal tubular epithelial cells. JBIC Journal of Biological Inorganic Chemistry. 2016;21(4):463-74.

196. Chen Y-H, Liu H-P, Chen H-Y, Tsai F-J, Chang C-H, Lee Y-J, et al. Ethylene glycol induces calcium oxalate crystal deposition in Malpighian tubules: a Drosophila model for nephrolithiasis/urolithiasis. Kidney International. 2011;80(4):369-77.

197. Kotsyfakis M, Ehret-Sabatier L, Siden-Kiamos I, Mendoza J, Sinden RE, Louis C. Plasmodium berghei ookinetes bind to Anopheles gambiae and Drosophila melanogaster annexins. Molecular microbiology. 2005;57(1):171-9.

198. Ozbek E. Induction of Oxidative Stress in Kidney. International Journal of Nephrology. 2012;2012:9.

199. Khan SR. Reactive oxygen species, inflammation and calcium oxalate nephrolithiasis. Translational Andrology and Urology. 2014;3(3):256-76.

200. Verkoelen CF, Verhulst A. Proposed mechanisms in renal tubular crystal retention. Kidney Int. 2007;72(1):13-8.

9 Publications

Abd El-Salam M. et al. J. Med. Chem., 2018, 61 (4), pp 1609–1621

DOI: 10.1021/acs.jmedchem.7b01566

Publication Date (Web): February 6, 2018

Copyright © 2018 American Chemical Society

Publications

Journal of Medicinal Chemistry

Article

Cite This: J. Med. Chem. 2018, 61, 1609−1621

pubs.acs.org/jmc

The Synthesized Plant Metabolite 3,4,5-Tri-*O*-Galloylquinic Acid Methyl Ester Inhibits Calcium Oxalate Crystal Growth in a *Drosophila* Model, Downregulates Renal Cell Surface Annexin A1 Expression, and Decreases Crystal Adhesion to Cells

Mohamed Abd El-Salam,[†,‡,⊥] Jairo Kenupp Bastos,[†] Jing Jing Han,[‡] Daniel Previdi,[§] Eduardo B. Coelho,[∥] Paulo M. Donate,[§] Michael F. Romero,[⊥] and John Lieske*[,‡]

[†]Department of Pharmaceutical Sciences, School of Pharmaceutical Sciences, University of São Paulo, Ribeirão Preto, São Paulo 14040-903, Brazil

[‡]Department of Internal Medicine, Division of Nephrology and Hypertension, Mayo Clinic College of Medicine, Rochester, Minnesota 55905, United States

[§]Department of Chemistry, Faculty of Philosophy, Arts and Sciences, University of São Paulo, Ribeirão Preto, São Paulo 14040-901, Brazil

[∥]Department of Clinical Medicine, School of Medicine of Ribeirão Preto, University of São Paulo, Ribeirão Preto, São Paulo 14040-900, Brazil

[⊥]Department of Physiology and Biomedical Engineering, Mayo Clinic College of Medicine, Rochester, Minnesota 55905, United States

Supporting Information

ABSTRACT: The plant metabolite 3,4,5-tri-*O*-galloylquinic acid methyl ester (TGAME, compound **6**) was synthesized, and its potential effect on calcium oxalate monohydrate (COM) crystal binding to the surface of Madin−Darby canine kidney cells type I (MDCKI) and crystal growth in a *Drosophila melanogaster* Malpighian tubule (MT) model were investigated. Membrane, cytosolic, and total annexin A1 (AxA1), α-enolase, and heat shock protein 90 (HSP90) amounts were examined by Western blot analysis after subcellular fractionation, then confirmed by immunofluorescence staining of cultured cells. Pretreatment of MDCKI cells with TGAME for up to 6 h significantly diminished COM crystal binding in a concentration-dependent manner. TGAME significantly inhibited AxA1 surface expression by immunofluorescence microscopy, whereas intracellular AxA1 increased. Western blot analysis confirmed AxA1 expression changes in the membrane and cytosolic fractions of compound-treated cells, whereas whole cell AxA1 remained unchanged. TGAME also significantly decreased the size, number, and growth of calcium oxalate (CaOx) crystals induced in a *Drosophila melanogaster* MT model and possessed a potent antioxidant activity in a DPPH assay.

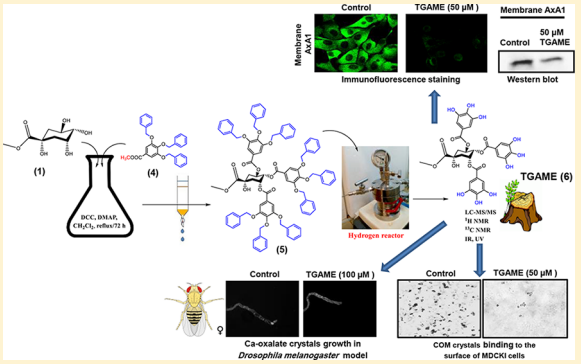

INTRODUCTION

Renal stone disease, also known as urolithiasis, is common with a recent overall estimated prevalence rate of 14.8% that appears to be rising, with a 5-year recurrence rate of up to 50%.[1,2] The first stages of stone formation include nucleation,[3] crystallization, and retention of these crystals within the kidney. Crystal nucleation is the first step in crystallization and can occur homogeneously or heterogeneously. Homogeneous nucleation demands a high degree of supersaturation with respect to the mineral concerned. By contrast, heterogeneous nucleation is the much more likely mechanism through which crystal initiation occurs in the urine[4] and this process can occur in the presence of particulate matters consisting of cell debris, proteins, or crystals of another mineral and is contained within receptacles lined with chemically active cell surfaces. Once a crystal nucleus is formed inside the kidneys,[4] exposure to the urine makes the stone able to grow by encrustation.[5] There are two basic pathways (free-particle and fixed-particle mechanisms) for the establishment of a stone nucleus, both of which can be active in any stone former. Crystallization in turn requires supersaturation of tubular and/or interstitial fluid with respect to ionic compounds such as calcium oxalate (CaOx) and calcium phosphate (CaP). If these processes occur in tubular fluid, the retention of crystals in the kidney may involve

Received: November 19, 2017
Published: February 6, 2018

ACS Publications © 2018 American Chemical Society

DOI: 10.1021/acs.jmedchem.7b01566
J. Med. Chem. 2018, 61, 1609−1621

aggregation of smaller crystals and/or adhesion to the tubular cell surface.[3,6]

Calcium oxalate monohydrate (COM) is found in up to 70−80% of stones.[7] Many studies have demonstrated that COM crystal binding to renal tubular cells triggers diverse cellular responses including proliferation, mitochondrial dysfunction, oxidative stress, cytotoxicity, and cell death.[8,9] One possible strategy to prevent stone formation is to arrest these early intrarenal events after COM crystal nucleation including crystal growth, crystal aggregation, and crystal adherence to renal epithelial cells.[10,11] Previous studies have suggested some possible COM crystal binding proteins on the apical surface of renal tubular cells (e.g., α-enolase, annexin A1, and heat shock protein 90 (HSP90)).[11−14]

Several studies have reported the role of natural products in the prevention of renal stones by inhibiting calcification and hyperoxaluria-induced oxidative stress in animal models of nephrolithiasis. We previously demonstrated that *Copaifera langsdorffii* Desf. (Fabaceae) leaf extract increased urinary magnesium and decreased urinary uric acid excretion in rats.[15] Moreover, treated rats had lower urinary oxalate and higher urinary citrate excretion, reduced intratubular calcification, and decreased osteopontin (OPN) expression.[16] Galloylquinic acid compounds are the major secondary metabolites found in *C. langsdorffii* leaf that might significantly contribute to its antiurolithic activity. It is interesting to note that the compounds have an affinity for the kidney. A high concentration (C_{max} = 15.84 μg/g tissue) was measured in renal tissue after an intravenous pharmacokinetic study performed in an animal model by our group.[17] This relatively high distribution of the compounds within the kidney might make them particularly effective for preventing kidney stone formation. Recently, we isolated 16 galloylquinic acid compounds from the aqueous fraction of the leaves, which displayed potential gastroprotective activity in a mouse model of gastric ulcer and cytotoxicity for gastric adenocarcinoma cells.[18] The methyl and ethyl 3,4,5-tri-*O*-galloylquinic acid were previously isolated from *Lepidobotrys staudtii* Egnl. stem bark and the leaves of *Guiera senegalensis* J.F. Gmel, respectively.[19,20]

Previous studies also reported chemically related compounds to galloyquinic acids, such as gallotannin, epigallocatechin-3-gallate, and 1,2,3,4,6-penta-*O*-galloyl-β-D-glucose in suppressing oxalate-induced oxidative stress and COM crystal binding to renal epithelial cells.[7,11,21] The present study involved the total synthesis of 3,4,5-tri-*O*-galloylquinic acid methyl ester (TGAME, **6**) (Figure 1) and its evaluation on renal cells and COM crystal adhesion, as well as investigating its effect on CaOx crystallization in a *Drosophila melanogaster* Malpighian tubule in vivo and ex vivo models. We also determined the antioxidant activity of the compound using DPPH assay.

RESULTS AND DISCUSSION

Chemistry. The promising diverse bioactivities of plant extracts[18,20,22] rich in galloylquinic acids prompted our interest to synthesize the trisubstituted 3,4,5-tri-*O*-galloylquinic acid methyl ester, with the goal of developing lead compounds for kidney stone prevention. The total synthesis included six steps starting from commercially available quinic and gallic acids. The key step in the synthetic pathway was the affordable Steglich esterification[23] of methyl quinate with 3,4,5-tribenzyloxybenzoic acid using dicyclohexylcarbodiimide (DCC) and *N*,*N*-(dimethylamino) pyridine (DMAP) as the coupling reagents. The chemical structures of the final compound and its synthetic

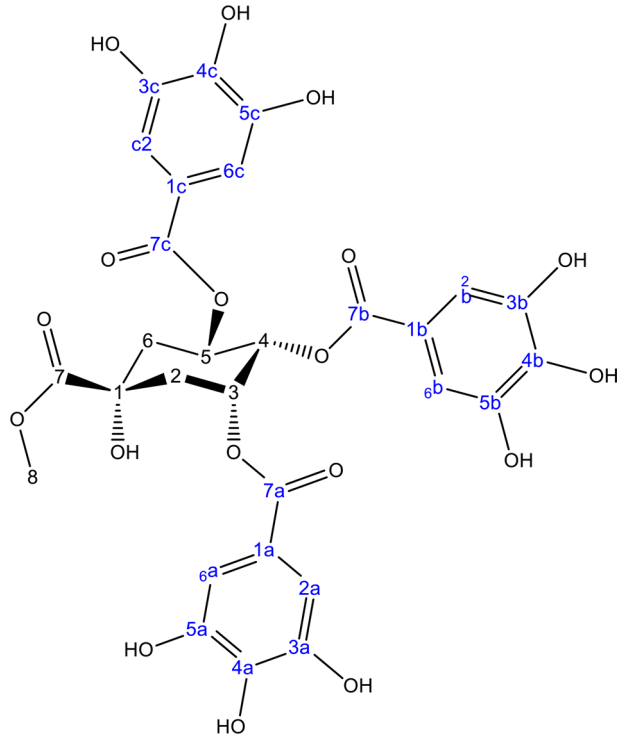

Figure 1. Chemical structure of 3,4,5-tri-*O*-galloylquinic acid methyl ester (TGAME, **6**).

intermediates were elucidated by all possible spectroscopic, spectrometric, and spectrophotometric methods of analyses.

The designed synthetic route of the target TGAME is summarized in Scheme 1. The type of esterification reaction used is a mild one, which allowed conversion of the sterically demanding and acid labile methyl quinate, a compound with complex stereochemistry, into the triester form. A protection protocol using benzyl chloride was applied for the hydroxyl groups of gallic acid to mask their reactivity and formation of undesired side products.

The proposed mechanism of the reaction is illustrated in Scheme 2. The chemical structure of TGAME and its intermediates were elucidated and confirmed by IR, ^{1}H NMR, ^{13}C NMR, and mass spectrometric data, which were in full agreement with their structures.[18] TGAME was obtained as a light-yellow amorphous solid with a specific rotation $[\alpha]_D^{25}$ of −42.6, which is levorotatory similar to the naturally occurring one in plants.[24] The HPLC-UV analysis of the compound at 280 and 254 nm revealed one single peak at 33.57 min. The UV spectrum of the peak showed two characteristic bands at 225 and 275 nm, indicating that the compound belongs to galloylquinic acids class.[18] The IR spectrum of TGAME showed a broad band at 3387 cm^{-1} referring to the presence of H-bonded hydroxyl groups. A characteristic carbonyl group of the ester appeared at 1707 cm^{-1}. The bands at 1216 and 1034 indicated the presence of a C−O functional group. Two bending bands of C−H appeared at 1475 and 1338 cm^{-1}, reflecting an aliphatic methyl group. Other characteristic IR bands of the compound are presented in the Supporting Information. The ESI-MS/MS analysis of the important synthetic intermediate **5** ($C_{92}H_{80}O_{18}$), a precursor of the final compound, manifested the following molecular ions: *m*/*z* [M + H]$^+$ 1473.5239, MS [M + Na]$^+$ 1496.5005, MS [M + K]$^+$ 1511.4664.

DOI: 10.1021/acs.jmedchem.7b01566
J. Med. Chem. 2018, 61, 1609−1621

Scheme 1. Synthesis of 3,4,5-Tri-*O*-galloylquinic Acid Methyl Ester (TGAME, 6)[a]

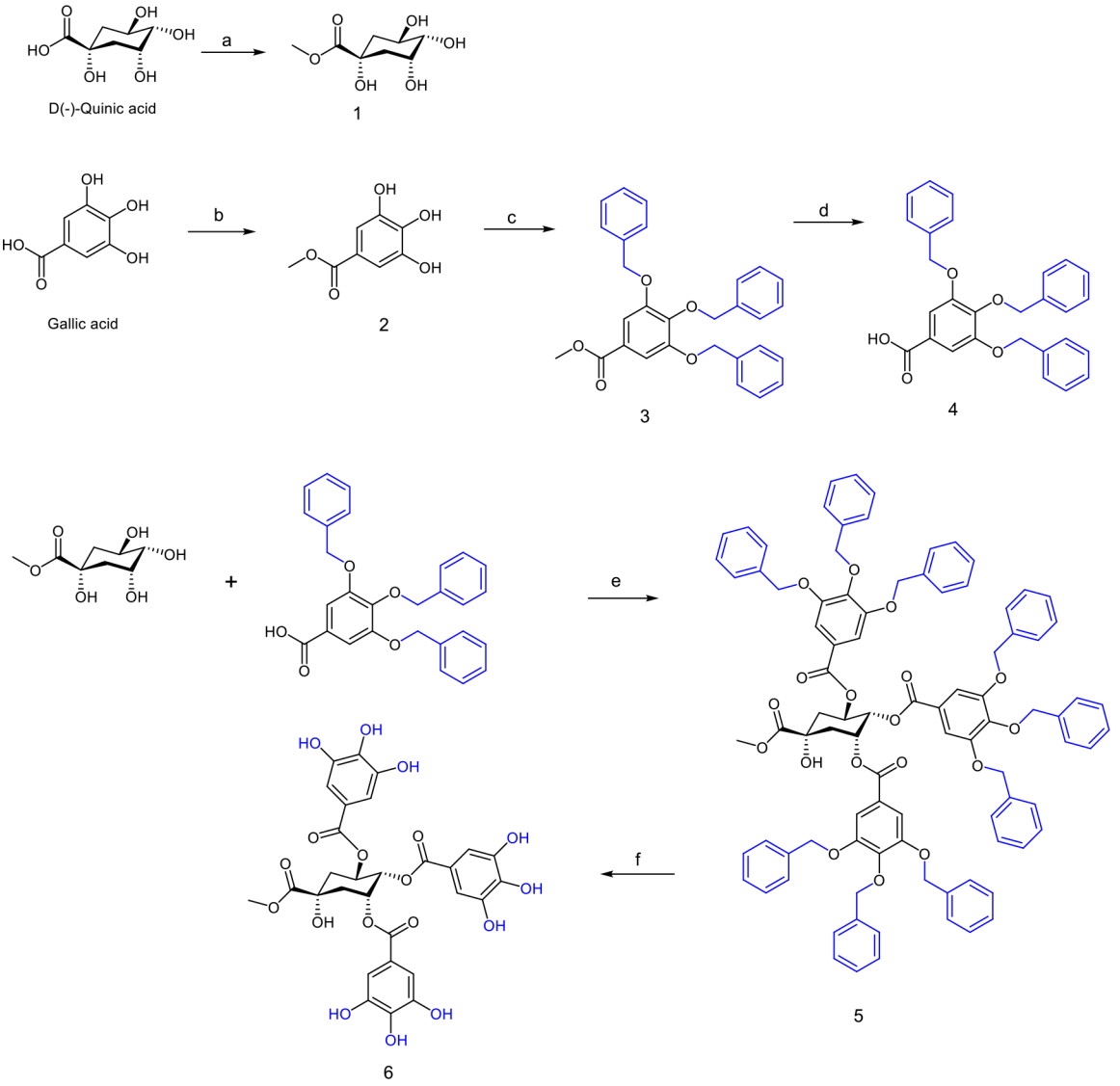

[a]Reagents and conditions: (a,b) H_2SO_4, methanol, reflux/18 h for (a) and 24 h for (b); (c) KI, K_2CO_3, benzyl chloride, acetone, reflux/21 h; (d) NaOH, ethanol, reflux/2 h then HCl; (e) DCC, DMAP, CH_2Cl_2, reflux/72 h followed by purification using silica gel column chromatography, $CHCl_3$/methanol (100:1); (f) H_2, pressure 80 psi equivalent to 6 kgf/cm^2, ethyl acetate, 10% Pd/C for 6 h.

The molecular weight of TGAME was determined by ESI-MS/MS in both the positive and negative ion modes. The experimental and calculated m/z of the protonated molecular ion $[M + H]^+$ were 663.1190 and 663.1200, respectively. The MS analysis in the negative ion mode revealed a molecular ion of m/z $[M - H]^-$ at 661.0878. The base peak at m/z 169.0089 was formed through McLafferty rearrangement pathway. Other fragments were formed through the loss of water and CO_2 as shown in the proposed fragmentation pathways in Supporting Information. The sodiated molecular $[M + Na]^+$ ion also was observed in the positive ion mode at m/z 685.1012 with an error of precision +1.75 ppm. The proposed fragmentation patterns of the protonated and sodiated molecular ion are further illustrated in Supporting Information. The NMR and 2D NMR (HMBC and HSQC) spectral data of compounds **5** and **6** agreed with our previously published data.[18]

MDCKI Cell Cytotoxicity of TGAME and Its Hydrolytic Products. To determine the safe in vitro concentration, cytotoxicity was assessed by the MTT assay after exposing Madin-Darby canine kidney type I (MDCKI) cells to increasing concentrations of TGAME (0, 5, 10, 25, 50 μM) for 24 h. Gallic acid and methyl quinate, which are products of TGAME hydrolysis, were also tested. TGAME did not exert any apparent MDCKI cell cytotoxicity in a concentration up to 155 $\pm$ 4 μM (Figure 2). The inhibitory concentration 50% (IC_{50}) of the hydrolytic products, methyl quinate and gallic acid, were 120 $\pm$ 7 and 34 $\pm$ 6 μM, respectively. Therefore, the nontoxic concentrations below this IC_{50} were used in subsequent experiments for the compounds.

COM Crystal-Adherence Assay. MDCKI cells (originally derived from the distal nephron of a female dog), were used as an in vitro model because the initial site of nephrolithiasis has been proposed to be in the distal nephron as supported by histopathological analysis.[25,26] MDCKI cells were incubated with COM crystals (100 μg/mL of culture medium) after pretreatment with 50 μM TGAME for up to 6 h. The concentrations of TGAME used in this study were based upon concentration–response and cytotoxicity studies together with

DOI: 10.1021/acs.jmedchem.7b01566
J. Med. Chem. 2018, 61, 1609–1621

Scheme 2. Proposed Mechanism of the Coupling Reaction between Compounds 1 and 4 for the Synthesis of 3,4,5-Tri-*O*-galloylquinic Acid Methyl Ester (TGAME, 6)

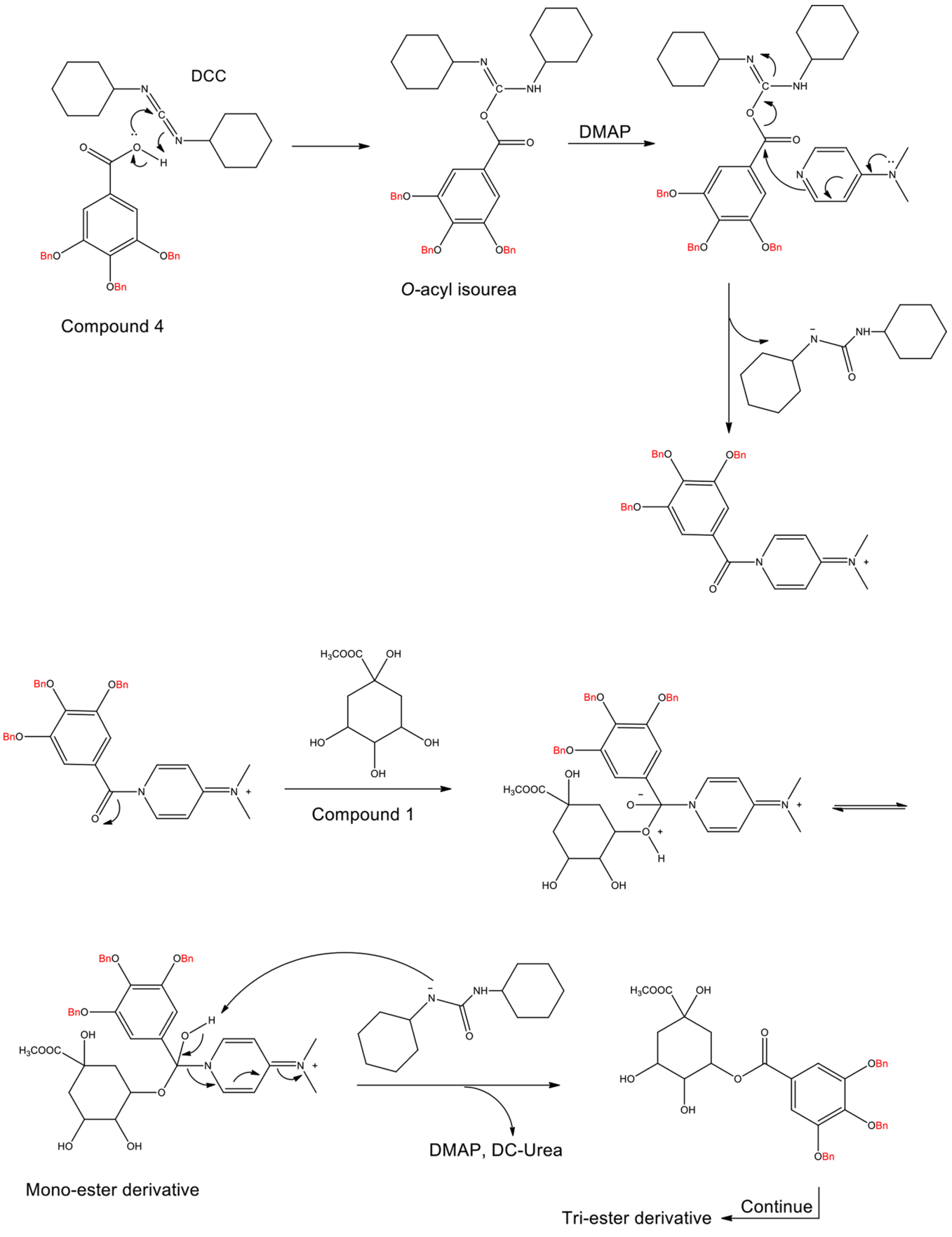

DOI: 10.1021/acs.jmedchem.7b01566
J. Med. Chem. 2018, 61, 1609−1621

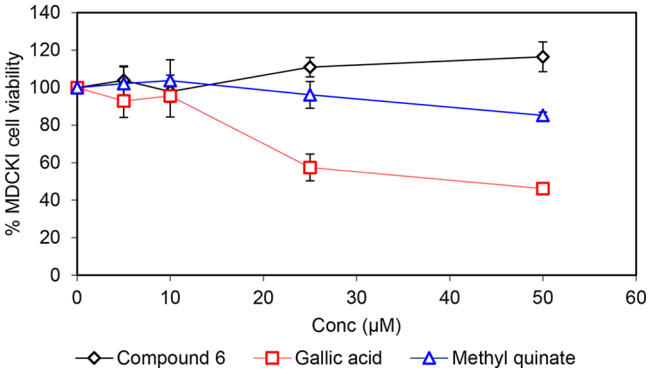

Figure 2. Cytotoxic effects of TGAME (**6**) and its hydrolytic products in MDCKI cells. The assay of cytotoxicity was evaluated by MTT assay. Cells were plated onto 96-well microplates (1×10^4 cells/well) and treated with various concentrations of each tested compound (0, 5, 10, 25, 50 μM in DMSO/PBS) for 24 h. Data were expressed as means ± SD of three independent experiments.

results from the crystal binding assay (concentration-dependence study) that demonstrated TGAME significantly decreased the number of crystals bound to the cell surface at both 25 and 50 μM versus the control (Figure 3), while the concentration of 50 μM was more inhibitory compared to 25 μM ($p < 0.05$). Results from the crystal-binding assay (time-course study) demonstrated that pretreatment with TGAME (50 μM) significantly ($p < 0.05$) decreased the number of cell surface associated-COM crystals by approximately 50% at 3 and 6 h compared to control (Figure 4). Assays were done at early time points (not exceeding 6 h) to focus on the crystal-binding stage and largely avoiding subsequent COM crystal phagocytosis.[11,27]

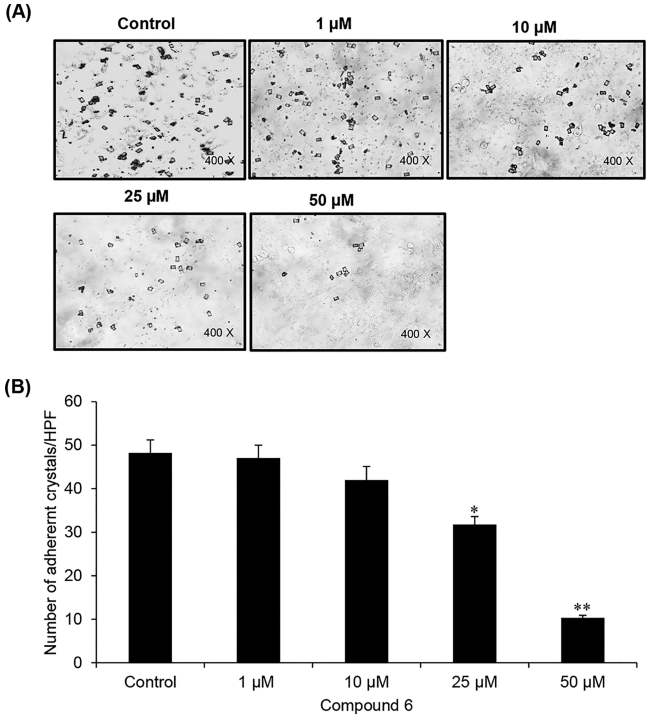

Figure 3. Effect of TGAME (6) on COM crystal-binding capability of the cells was dose dependent. MDCKI cells were pretreated with various doses of compound **6** (0, 1, 10, 25, and 50 μM) for 3 h followed by incubation with COM crystals (100 μg/mL of culture medium) for 30 min. (A) After washing with plain DMEM culture media, images of the remaining crystals were captured under a phase-contrast microscope for 15 high-power fields (HPF) in each well. The original magnification power was ×400. (B) The remaining crystals that adhered on the cell surface were then counted. *$p < 0.05$ vs control and **$p < 0.05$ for the effect of the concentration 50 vs 25 μM of compound **6**.

A 3 h pretreatment time was selected to determine concentration-dependent effects (0−50 μM) because effects were measurable and a longer time of 6 h did not increase the magnitude. TGAME decreased crystal binding in a concentration-dependent manner across this range with maximal effects at 50 μM. Thus, further experiments used exposure to 50 μM of TGAME for 3 h. Of note, gallic acid (one of the compound hydrolytic products) significantly ($p < 0.05$) decreased the crystal binding at a lower concentration (10 μM) after 3 h versus the control (Figure 5). This indicates that TGAME can still generate active metabolites if it undergoes in vivo metabolism by body esterases.

Analysis of COM-Binding Proteins (Annexin A1, α-Enolase, and HSP90) by Western Blot. We reported previously that when COM crystals were precoated with gallotannin (in green tea), their subsequent adhesion to renal tubular cells was reduced.[7] A similar study demonstrated that aluminum citrate decreased COM crystal binding to the same cells when the crystals were precoated with it.[28] Moreover, we recently showed that an aqueous extract of *Costus arabicus*, a plant used in Brazilian folk medicine to treat urolithiasis, inhibited the growth of COM crystals and their adhesion to renal epithelial cells.[29] The inhibitory effect on the binding of crystals to the cell was only significant when precoated COM crystals were investigated. Pretreatment of cells with this extract had no effect on crystal adhesion. Unlike the previous studies, we found that TGAME exerted effects when added directly to renal cells followed by treatment with uncoated COM crystals. We propose that the observed biological activities might be related to cellular effects of TGAME and reduction of COM crystal-binding protein expression on the surface of renal cells. One of these proteins is AxA1,[14] in addition to α-enolase and heat shock protein 90 (HSP90).[6,30]

A previous publication documented that epigallocatechin gallate strongly interacts with phospholipid bilayers due to hydrogen bond formation, and it inhibits COM crystal adhesion to renal tubular cells by decreasing α-enolase surface expression.[11] It is noteworthy that AxA1, α-enolase, and HSP90 are all in the database of the lipid raft proteome (http://lipid-raft-database.di.uq.edu.au/). AxA1 is present in the basolateral cell membrane, cytoplasm, cell projection, and nucleus. Thus TGAME could decrease cell surface expression of these proteins through transcriptional suppression, altered molecular shuttling, or trafficking from the cytoplasm to the cell surface because the compound is polyphenolic and could interact with lipid bilayers through hydrogen bond formation. We studied surface expression of these three putative COM crystal receptors on MDCKI cells pretreated with TGAME by immunofluorescence microscopy and confirmed results by Western blot analysis of whole cell lysate and subcellular fractions. The analysis revealed that TGAME significantly reduced the presence of AxA1 and the other two proteins in the membrane fractions ($P < 0.05$), whereas their concentrations in cytosolic fractions was greater (Figure 6). Overall, the total amount of protein in the whole cell lysate was the same. Interestingly, the inhibitory effect of TGAME on AxA1 in the

DOI: 10.1021/acs.jmedchem.7b01566
J. Med. Chem. 2018, 61, 1609−1621

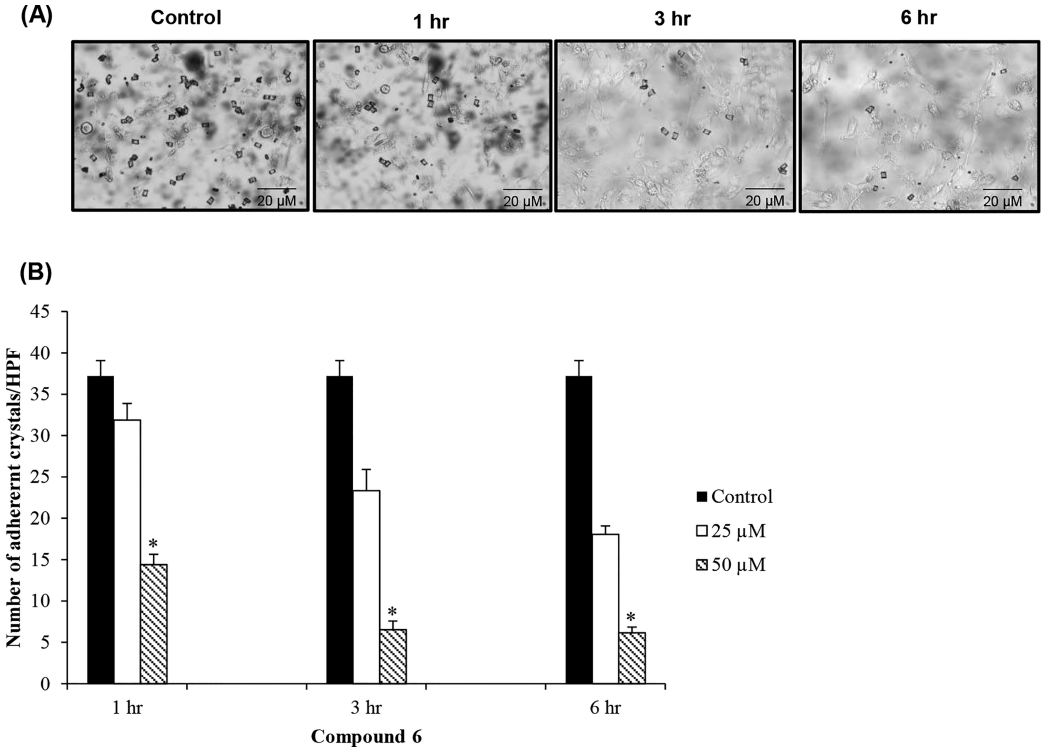

Figure 4. Pretreatment of TGAME (**6**) reduced COM crystal binding onto the cell surface. MDCKI cells were treated with 0, 25, or 50 μM compound **6** for 1, 3, or 6 h prior to incubation with COM crystals (100 μg/mL of culture medium) for 30 min. (A) After washing with plain DMEM culture media, images of the remaining crystals were captured under a phase-contrast microscope for at least 15 high-power fields (HPF) in each well. (B) Crystals remaining on the cell surface were then counted. *$p < 0.05$ vs control.

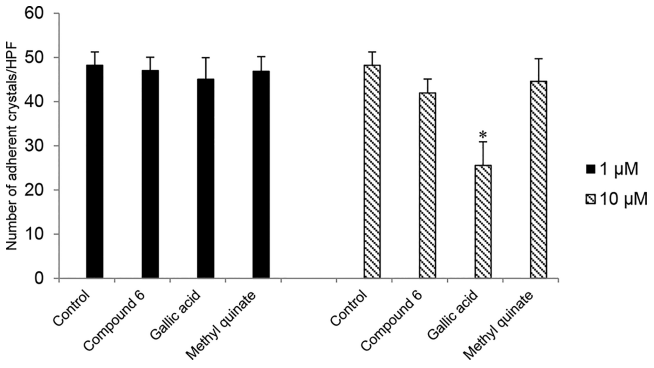

Figure 5. Effects of TGAME (**6**) and its hydrolytic products on COM crystal binding to MDCKI cells. The cells were treated with 0, 1, or 10 μM of each compound for 3 h prior to incubation with COM crystals (100 μg/mL of culture medium) for 30 min. After washing with plain DMEM culture media, images of the remaining crystals were captured under a phase-contrast microscope for 15 high-power fields (HPF) in each well. Crystals remaining on the cell surface were then counted. *$p < 0.05$ vs control.

membrane fraction was more significant in comparison with its effect on α-enolase and HSP90 proteins ($p < 0.05$).

These data suggested that TGAME decreased AxA1 cell surface expression by inhibiting or relocalizing its shuttling from cytoplasm to the cell membrane. Annexins are Ca^{2+}-regulated membrane binding proteins found throughout the animal and plant kingdoms. The annexin core (Ca^{2+}/membrane binding unit) is thought to be one essential element that facilitates membrane interactions. Thus annexins can organize and assemble phospholipids into specific membrane domains.[31] AxA1 protein also plays important roles by controlling cellular Ca^{2+} storage and thus Ca^{2+}-dependent signal transduction. Overall, AxA1 localizes to many cellular structures including the plasma, cytoplasm, and organelle membranes.[31]

α-Enolase is another COM crystal binding protein on the surface of MDCKI cells, and it was reported that expression of this protein on the MDCKI cell surface increased after exposure to oxalate.[11] Another study confirmed a role of α-enolase in COM crystal binding by using a specific antibody to block α-enolase and demonstrating decreased adhesion to the cell surface.[30]

HSP90 is also found on the surface of renal cells as a putative crystal binding molecule. Downregulating HSP90 expression using specific anti-HSP90 antibodies or small interfering RNA (siRNA) decreased COM crystal adhesion by 50% and 75%, respectively.[13]

To further support our hypothesis that the COM crystal adhesion inhibition by TGAME is mediated in part by surface AxA1, we used a specific anti-AxA1 antibody. As expected, COM crystal adhesion to the surface of renal cells was significantly reduced ($p < 0.05$) in comparison with the control and controlled isotypic-IgG treated cells (Figure 7).

Examining the Expression of Surface and Intracellular Annexin A1 by Immunofluorescence Assay and Laser-Scanning Confocal Microscopy. Laser-scanning confocal microscopy demonstrated that AxA1 cell surface expression was dramatically inhibited by pretreatment with 50 μM of TGAME to approximately 50% of control (Figure 8). However, annexin A1 expression inside cells increased after TGAME treatment.

In Vivo Feeding and Ex Vivo Oxalate ± TGAME Birefringence Experiment in *Drosophila melanogaster* Malpighian Tubule Model. Our group previously studied the

DOI: 10.1021/acs.jmedchem.7b01566
J. Med. Chem. 2018, 61, 1609−1621

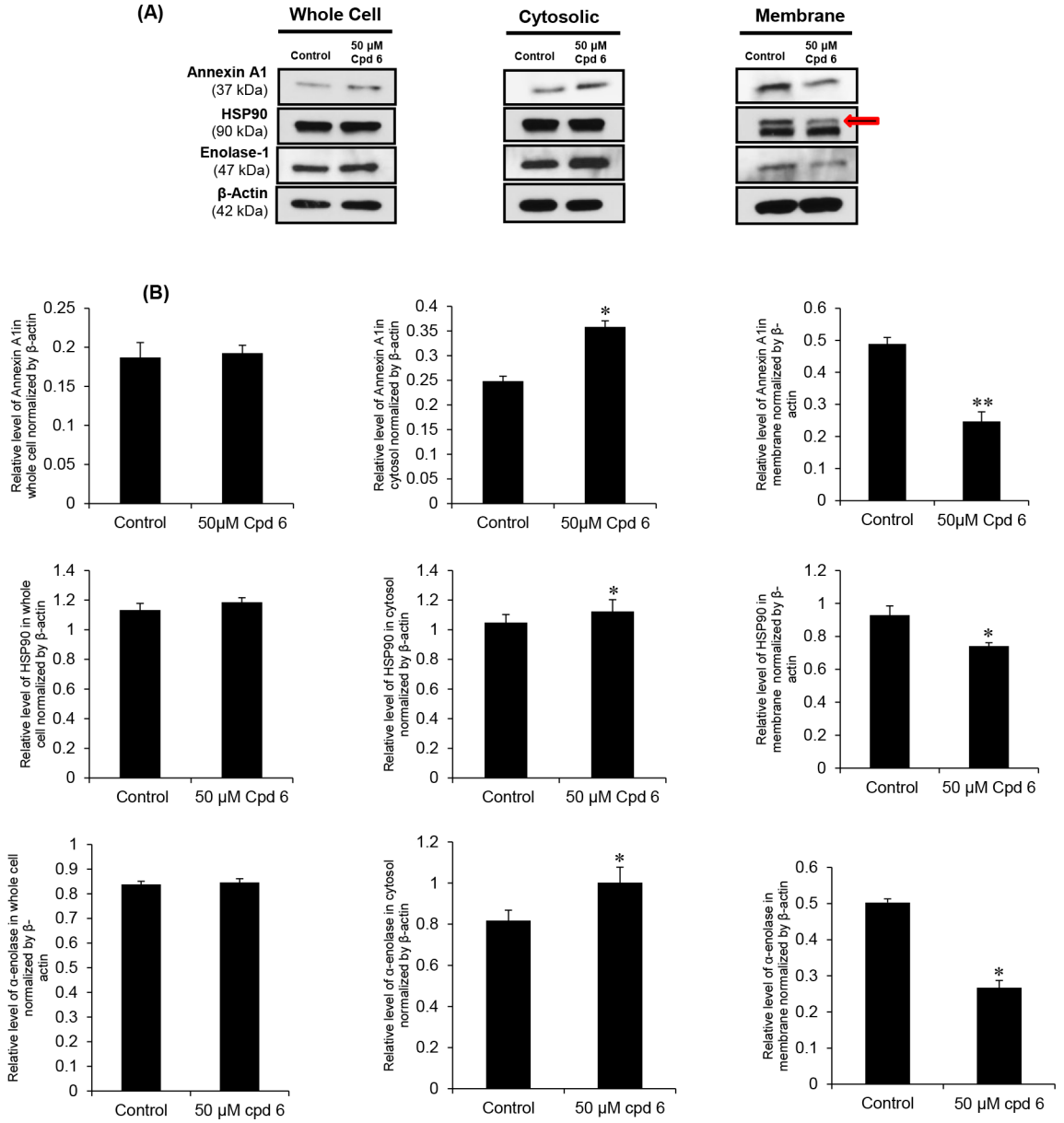

Figure 6. (A) Western blot analysis of COM crystal-binding proteins. Proteins obtained from whole cell lysate, cytosolic fraction, and membrane fraction of MDCKI, with or without 50 μM TGAME (**6**) treatment, were subjected to Western blotting for annexin A1, α-enolase, and HSP90. β-Actin served as the loading control. (B) Bands intensity was quantitated using AlphaEase FC software (Mayo Clinic). Each bar represents mean ± SEM from three independent experiments. *p < 0.05 vs control. **p < 0.05 for the effect of TGAME on annexin A1 vs α-enolase and HSP90.

effect of thiosulfate and sulfate on Malpighian tubule (MT) CaOx crystallization in a *Drosophila melanogaster* (fruit fly) model.[32] Chen et al. fed fruit flies lithogenic agents such as sodium oxalate (NaOx). Their analysis used polarized light microscopy of dissected tubules to show that NaOx feeding resulted in the formation of crystals within the Malpighian tubule lumen in a dose-dependent manner. These crystals were identified as CaOx using scanning electron microscopy and energy-dispersive X-ray spectroscopy. The study also demonstrated that crystal formation decreased lifespan of the flies and that the use of potassium citrate (KCit) as an antiurolithic agent reduced crystallization inside MT and decreased mortality. Thus, *Drosophila* appears to be a useful model to study CaOx renal stones before embarking on the use of higher-order experimental animals.[33] Therefore, we investigated the effect of TGAME on the formation of CaOx crystals within MT in feeding experiment and after ex vivo exposure of the tubules to oxalate.

The results of the ex vivo experiment (Figure 9) showed that TGAME (100 μM) significantly (p < 0.05) decreased CaOx crystallization, size, and total crystal area within Malpighian tubules. Flies fed oxalate (10 μM) + TGAME (50 μM) also manifested a decrease in CaOx crystal number, size, and total crystal area within MT after 24 h exposure in comparison to those fed oxalate alone, but these findings were not significant (p > 0.05) (Figure 10), however, in the factors such as pharmacokinetic parameters affecting TGAME absorption to reach the bloodstream or the need for doses greater than 50 μM in vivo to deliver sufficient amounts to MT in order to alter CaOx crystallization.

Annexin b11 (Axb11) is also found in *Drosophila*[34] as a Ca^{2+}-dependent phospholipids binding protein (http://flybase.org/

DOI: 10.1021/acs.jmedchem.7b01566
J. Med. Chem. 2018, 61, 1609−1621

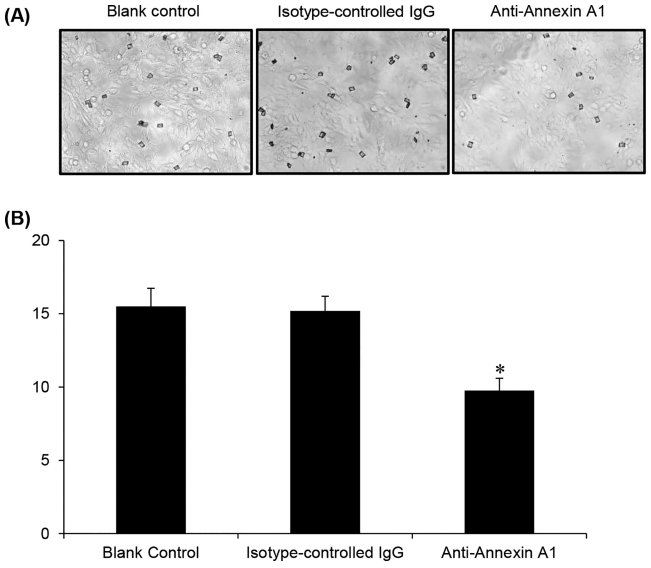

Figure 7. Cell-COM crystal adhesion assay and neutralization by a specific anti-annexin A1. The confluent polarized MDCKI cell monolayer was incubated with 0.2 μg/mL anti-annexin A1 antibody or 0.2 μg/mL rabbit isotype-controlled IgG prior to cell-crystals adhesion assay, whereas the cells without antibody treatment served as the blank control. (A) After removal of unbound crystals, crystals adherent on the cell surface were imaged by phase-contrast microscopy. (B) The adherent crystals were counted from 15 random high power fields (HPF). Data were expressed as means ± SEM of three independent experiments. $^*p < 0.05$ vs controls.

reports/FBgn0030749.html) that is known to play important role in cell adhesion, involved in several functions, among them differentiation, cell signaling, and membrane fusions. In this case, we speculate that the effect of our compound TGAME in the fly model might be of its action on Axb11, where the decrease in cell surface Axb11 might subsequently decrease nucleation on the cell surface.

Antioxidant Activity and DPPH Assay. Studies suggest that renal epithelial cell exposure to CaOx crystals, CaP crystals, and oxalate ions can lead to the generation of reactive oxygen species (ROS), potential cause of injury, and/or promote inflammation. Further, the urine of stone formers and hyperoxaluric rats is enriched with markers of inflammation and oxidative stress (OS).[35] Stone formers also have been reported to have reduced peripheral concentrations of antioxidants including α- and β-carotenes. There are many reported mechanisms whereby ROS can increase stone risk including decreased function of macromolecular inhibitors and/or cellular injury that promotes increased crystal adhesion.[36] Antioxidant treatments have also been shown to reduce pathological injury of crystal deposition in hyperoxaluria animal models.

In this study, the DPPH assay used to gauge OS revealed that TGAME and its metabolite gallic acid can scavenge free radicals to a similar extent as the standard antioxidant vitamin C with an EC_{50} 11 ± 0.3, 3, and 45 ± 2 (Figure 11), respectively. Therefore, the compound is considered to be a potent antioxidant. Methyl quinate did not show any radical scavenging activity as expected because it is a sugar with no phenolic properties.

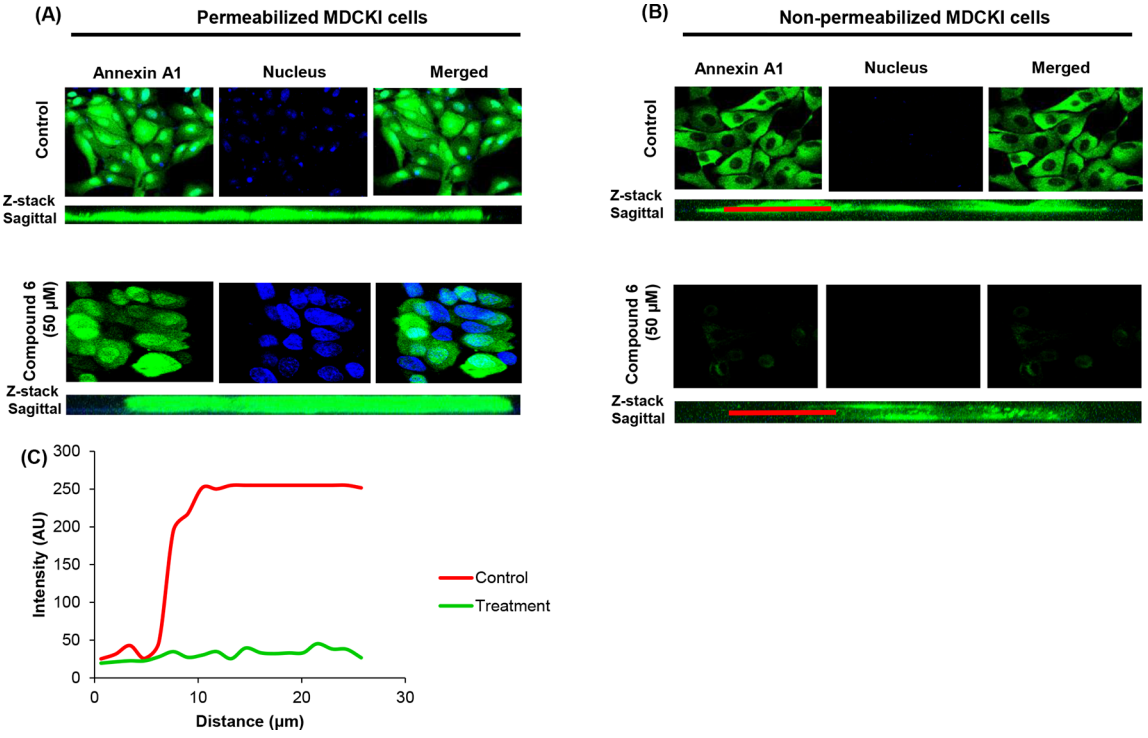

Figure 8. Confocal and laser scanning microscopy. TGAME (**6**) reduced the surface expression of annexin A1 but increased its intracellular level. (A) Intracellular expression of annexin A1 (with cell permeabilization). (B) Surface expression of annexin A1 (without cell permeabilization). MDCKI cells were pretreated with 50 μM compound **6** for 3 h and processed for immunofluorescence study using anti-annexin A1 as a primary antibody and secondary antibody conjugated with Alexfluor 488 donkey antirabbit (shown in green), whereas nuclei were counterstained with TOT-3 dye (shown in blue). Original magnification power was ×400. (C) The graph peaks represent the fluorescence intensities of the staining at the given distances (in μm) along the red bar.

DOI: 10.1021/acs.jmedchem.7b01566
J. Med. Chem. 2018, 61, 1609−1621

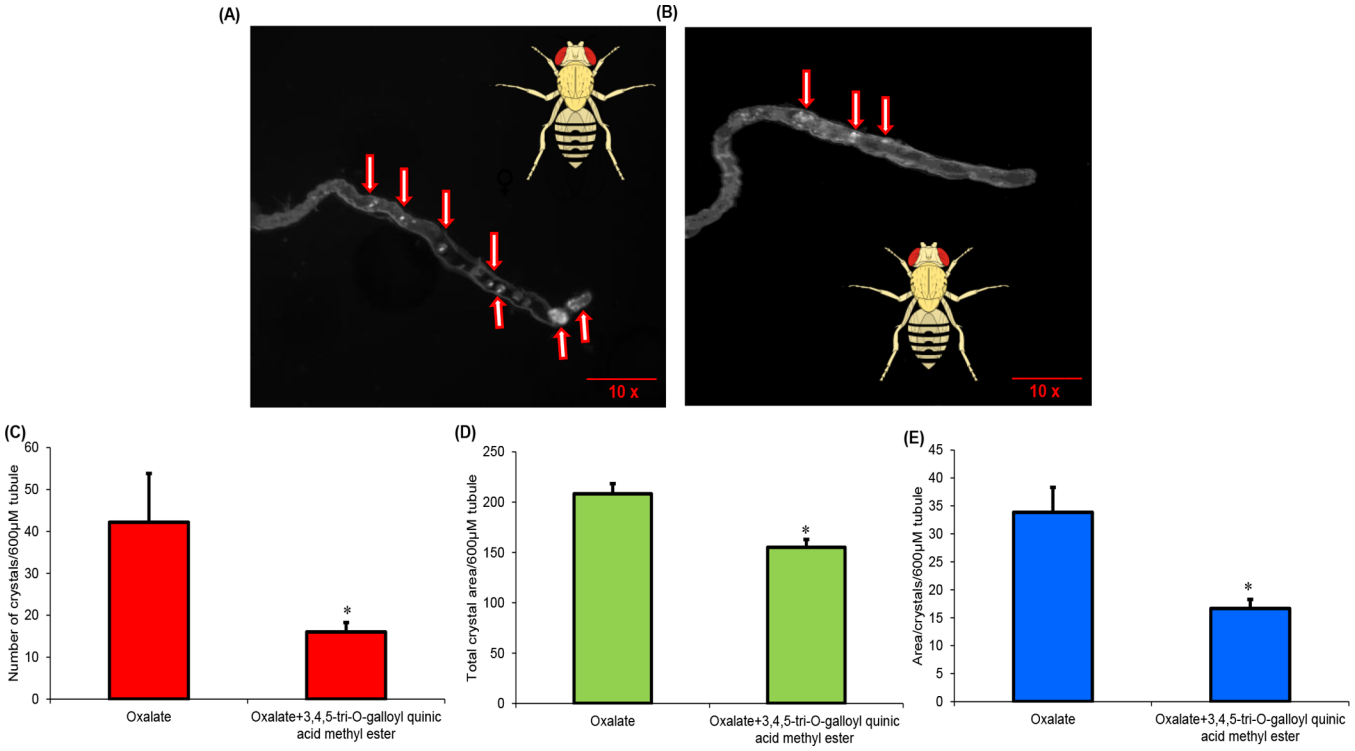

Figure 9. Malpighian tubule (MT) images from wild-type female fruit flies incubated ex vivo with (A) oxalate (10 mM) or (B) oxalate (10 mM) and 3,4,5-tri-*O*-galloylquinic acid methyl ester (TGAME) (100 μM) for 1 h. The arrows indicate CaOx crystals within the lumen of the MT. (C) CaOx crystal number, (D) total crystal area, and (E) average area/crystal per 600 μm of tubule were determined using ImageJ. TGAME significantly decreased crystal number, total crystal area, and average area/crystal. Values are means ± SE (n = 12 for both oxalate control group and compound **6**-treated group). *p < 0.05 vs control.

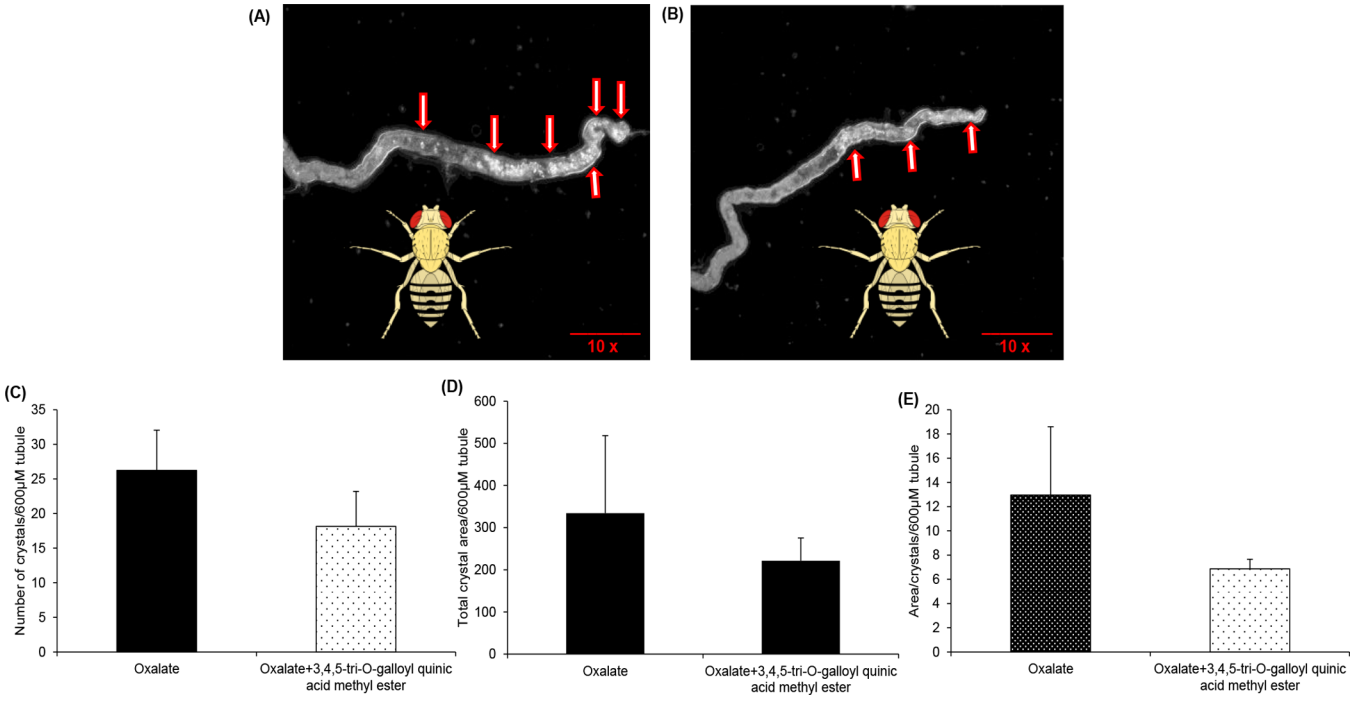

Figure 10. Malpighian tubule (MT) images from wild-type female fruit flies fed (A) oxalate (10 mM) or (B) oxalate (10 mM) and 3,4,5-tri-*O*-galloylquinic acid methyl ester (TGAME) (50 μM) for 24 h. The arrows indicate CaOx crystals within the lumen of the MT. (C) CaOx crystal number, (D) total crystal area, and (E) average area/crystal per 600 μm of tubule were determined using ImageJ. Values are means ± SE (n = 11 for both oxalate control group and compound **6**-treated group). p > 0.05.

In total, our study supports the hypothesis of Verkoelen and Verhulst[37] that crystal binding is preceded by pathologic alterations in cell surface binding molecules. Nonetheless, TGAME-treatment could not entirely prevent COM adhesion

DOI: 10.1021/acs.jmedchem.7b01566
J. Med. Chem. 2018, 61, 1609−1621

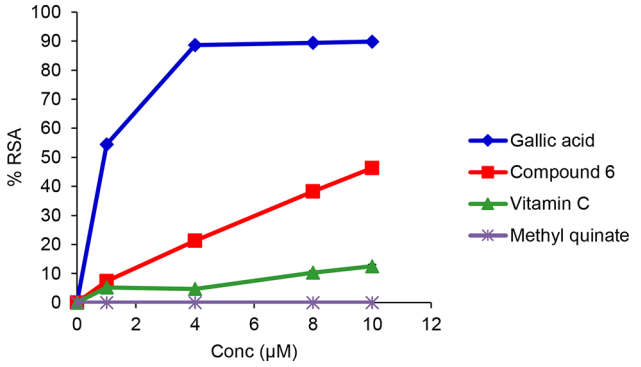

Figure 11. Antiradical efficiency (AE) of TGAME (**6**) and its hydrolytic products (gallic acid and methyl quinate) in DPPH assay using vitamin C as a standard. Different volumes (2−20 μL) of the compounds (2−20 μM in DMSO) were made up to 40 μL with DMSO, and 1.96 mL of DPPH (0.1 mM) solution was added. The reaction mixture was incubated in dark condition at room temperature for 20 min. Then, the absorbance of the mixture was read at 517 nm. DPPH solution was taken as control, and the % radical scavenging activity of each compound was calculated.

to cells, suggesting that these interactions involve multiple processes and many molecules, perhaps including annexin II, osteopontin, and hyaluronan.[6,38] Therefore, other unknown cell surface molecules might mediate the inhibitory effect of TGAME on COM crystal-binding to MDCKI cells.

CONCLUSIONS

We report that TGAME inhibited COM crystal adhesion to renal cells, and this effect is mediated by decreased expression of AxA1 on cell surface. Thus, cell surface expression of AxA1 might be a key pathogenic factor in crystal retention and urinary stone formation in vivo. Moreover, the compound significantly decreased CaOx crystal number, size, and total crystal area within MT of *Drosophila* models, as well as showing a potential antioxidant activity by free radicals scavenging capability. Our findings may also be relevant for the observed decrease of crystal deposition when hyperoxaluric animals treated with *C. langsdorffii* leaf extract. Finally, our findings support a promising role for TGAME in the prevention and modulation of new or recurrent renal stone formation. Further preclinical and clinical studies should be performed for the use of this compound in urolithiasis.

EXPERIMENTAL SECTION

Materials and Methods. The purity of the tested compounds was determined by HPLC analysis and MS error of precision data as being ≥98%. See the Supporting Information for full details. Biological assays were conducted at Department of Internal Medicine, Division of Nephrology and Hypertension, Mayo Clinic Medical School, USA.

All methods were performed using anhydrous solvents purchased from commercial vendors and used without further purification. Quinic and gallic acids were purchased from Sigma Adrich, Germany, in addition to all other reagents. Hydrogenolysis was performed using a hydrogen reactor system (FAMABRAS, IND. BRAS. 1/8, 255046, Brazil) supported with a pressure controller (CLASSE B ABNT). Melting points (°C, uncorrected) were determined in capillary tubes using a Fisatom melting point device (model 431, Brazil). Optical rotation $[\alpha]_D^{25}$was done using a polarimeter (Jasco P-2000, Japan) at 25 °C and a wavelength of 589 nm. Methanol and chloroform were used as solvents. Three readings of $[\alpha]_D^{25}$were recorded, and the average was taken. Chromatographic purification was performed based on flash chromatography using silica gel (pore size 60 A°, 40−63 μm, Sigma, batch no. MKBC6227), and the solvent systems are expressed as v/v percent ratios as indicated. All reactions were monitored by TLC using fluorescent precoated silica gel plates (Merck, Germany) at short wavelength. Molybdate/H_2SO_4 spray solution was used as the raveling reagent. The IR spectra were recorded using FT-IR spectrophotometer (PerkinElmer Spectrum Two) in the range of 400−4000 cm^{-1} by KBr pellet technique. The analytical HPLC analysis was performed on a Shimadzu LC-10ADvp (Japan) operated with multisolvent delivery system, equipped with a Shimadzu SPD-MICAvp photodiode array detector (PDA). Analyses were performed using analytical reversed phase column (Polar-RP C 80 A°) with dimensions of 150 mm × 4.6 mm (Shimadzu) and a particle diameter of 4 μm; the mobile phase consisted of acidified water (A) (0.1% formic acid in water) and methanol (B) in gradient conditions as follows: 15−50% of B (45 min), 50−90% of B (45−65 min), and 90−15% of B up to 75 min; flow rate, 1 mL/min, with injection volume of 20 μL. All samples were dissolved in HPLC grade methanol (2 mg/mL) 0.45 μm filtered prior to automatic injection. Mass spectra were acquired on a high resolution MicroTOF II-Q mass spectrometer (Bruker Daltonics, Billerica, MA, US) fitted with an electrospray ionization (ESI) operating system in the positive and negative ion modes. Accurate masses were obtained using TFA-Na^+ (sodiated trifluoroacetic acid, 10 mg/mL) as the internal standard; end plate, −500 V; capillary, 3500 V; dry gas temperature, 180 °C with flow rate 4L/min; nebulizer gas pressure, 0.4 bar of N_2 gas; infusion bomb model, Cole Parmer with a flow rate of 300 μL/h. ^{1}H NMR, ^{13}C NMR, and two-dimensional (2D) spectroscopic techniques were recorded on a Bruker-Avance DRX500 spectrometer operating at a frequency of 500 MHz. Samples were dissolved in Aldrich deuterated dimethyl sulfoxide (DMSO-d_6) for compounds **1**−**4**, **6**, and chloroform ($CHCl_3$-*d*) for compound **5**. Data for ^{1}H NMR are reported as follows: chemical shift (δ, ppm), multiplicity (s = singlet, d = doublet, t = triplet, m = multiplet, coupling constant (s) in Hz, integration). Data for ^{13}C NMR are recorded in terms of chemical shift (δ, ppm).

Synthetic Steps of TGAME. *Synthesis of Quinic Acid Methyl Ester. Methyl-(1S,3R,4S,5R)-1,3,4,5-tetrahydroxycyclohexanecarboxylate (1).* To a stirred solution of methanol (160 mL) and sulfuric acid (2 mL), quinic acid (4 g) was added. The mixture was refluxed at 79−80 °C for 18 h. TLC analysis demonstrated a whole conversion of quinic acid into a single product spot (R_f = 0.56; ethyl acetate/methanol/water/formic acid = 6:3:3:0.2). The reaction mixture then was poured over solid $NaHCO_3$ until no effervescence (neutralization was detected by litmus paper) and was filtered. The filtrate was evaporated to give a solid crude hygroscopic residue (8.67 g) that was recrystallized in methanol to give rosette crystals (4.60 g, 91%) with undefined melting point, molecular formula $C_8H_{14}O_6$.

Synthesis of Methyl 3,4,5-Trihydroxybenzoate (2). Sulfuric acid (1 mL) was added dropwise to a stirred solution of gallic acid in methanol (10 g dissolved in 100 mL). The resulting reaction mixture was refluxed for 24 h. The solvent was evaporated, and an off-white precipitate was obtained which was dissolved in ethyl acetate (150 mL). The organic phase was washed with distilled water (3 × 20 mL) and sodium bicarbonate solution (3 × 20 mL), successively. The organic phase was dried over anhydrous sodium sulfate then evaporated to furnish 8 g of a yellowish-white precipitate (R_f = 6.3; ethyl acetate/formic acid = 8:2). The product was purified by recrystallization in methanol, and clusters of plate-like crystals were formed (6 g, 60%), mp 200−202 °C, molecular formula $C_8H_8O_5$.

Synthesis of Methyl 3,4,5-Tribenzyloxybenzoic Acid (3). Compound **2** (5 g (27.15 mmol)), 2 g (12 mmol) of KI, and 22 g (159 mmol) of dry K_2CO_3 were mixed in 250 mL of acetone and stirred for 20 min at room temperature (RT). Next, 11 g (87 mmol) of benzyl chloride in 50 mL of acetone was added portionwise. The suspension was refluxed for 21 h. TLC screening revealed a single spot of the formed product (R_f = 0.30; hexane/ethyl acetate = 8:2). The reaction mixture was filtered, and then the filtrate was concentrated under a vacuum. The resulting residue was resuspended in 200 mL of CH_2Cl_2 then filtered through Celite and was concentrated under a vacuum. The product was obtained as off-white solid (12 g, 97%), molecular formula $C_{29}H_{26}O_5$.

DOI: 10.1021/acs.jmedchem.7b01566
J. Med. Chem. 2018, 61, 1609−1621

Synthesis of 3,4,5-Tribenzyloxybenzoic Acid (4). Compound **3** (10 g) was mixed with a solution of 1.77 g (44.25 mmol) of sodium hydroxide in 250 mL of 95% ethanol. The resulting mixture was heated up for 2 h with reflux, followed by immediate pouring into 260 mL of 0.6 M HCl and stirred for 10 min, and finally filtered under vacuum. The resulting product was washed with a 1:1 mixture of 95% ethanol and water (50 mL), followed by pure water (50 mL), 95% ethanol (50 mL), methanol (2 × 25 mL), and diethyl ether (25 mL). The yield was dried under vacuum overnight to give a white solid (8.9 g, 94%), mp 192−195 °C, $C_{28}H_{24}O_5$.

Synthesis of (1S,3R,4S,5R)-5-Hydroxy-5-(methoxycarbonyl)-cyclohexane-1,2,3-triyl Tris(3,4,5-tris(benzyloxy)benzoate) (5). A suspension of 7 g (16 mmol) of 3,4,5-tribenzyloxybenzoic acid, 0.82 g (4 mmol) of methyl quinate, 4 g (20 mmol) of dicyclohexylcarbodiimide (DCC), and 12.24 g (18.4 mmol) of *N,N*-(dimethylamino) pyridine (DMAP) in 500 mL of dry dichloromethane was refluxed for 72 h. After cooling to RT, the mixture was filtered and then concentrated using a rotary evaporator. The resulting crude residue (14.5 g) was purified by flash chromatography (two times, 97 fractions of 20 mL each were collected/per one time) using a mixture of chloroform/methanol (100:1). Both the reaction and the column fractions were monitored by TLC (dichloromethane/toluene/ethyl acetate = 7.5:2.5:0.1), and the desired product fractions (*f* 71−81 and *f* 82−91) were combined and concentrated to give (1.74 g, 29%) of a faint yellowish-white glassy material (R_f = 0.2); mp 129−130 °C; molecular formula $C_{92}H_{80}O_{18}$; $[\alpha]_D^{25}$ −49.2 (*c* 0.15; $CHCl_3$); *m/z* [M + H]$^+$ 1473.5239; MS [M + Na]$^+$ 1496.5005; MS [M + K]$^+$ 1511.4664.

Synthesis of TGAME, (1S,3R,4S,5R)-1-Hydroxy-3,4,5-Tris((3,4,5-trihydroxybenzoyl)oxy)cyclohexanecarboxylic Acid (6). A suspension of 44 mg of palladium (10 wt % on activated carbon) and 200 mg of compound **5** in 15 mL of dry ethyl acetate was stirred at RT for 6 h inside a cell of a hydrogen reactor system at RT under a hydrogen gas atmosphere with a pressure of 80 psi, equivalent to 6 kgf/cm^2. Next, the reaction mixture was filtered through Celite filter aid using a mixture of ethyl acetate and methanol. The filtrate was concentrated under vacuum, and the obtained residue was lyophilized and recrystallized in ethyl acetate to give a light-yellow amorphous solid (93 mg, 99%); mp 137−140 °C. UV λ_{max} (methanol): 280 and 254 nm. Molecular formula $C_{29}H_{26}O_{18}$; MS: *m/z* 663.1190 [M + H]$^+$, 661.0878 [M − H]$^-$, 685.1012 [M + Na]$^+$; $[\alpha]_D^{25}$ −42.6 (*c* 0.50; CH_3OH). IR υ_{max} (KBr): (3387 cm^{-1}, O−H "H-bonded"), (2953 cm^{-1}, C−H aliphatic "stretch"), (1707 cm^{-1}, C═O), (1616 cm^{-1}, C−C aromatics), (1475 and 1338 cm^{-1}, C−H (−CH_3) "bend"), (1216 and 1034 cm^{-1}, C−O), (764 cm^{-1}, C−H aromatics "out-of-plane bend"). ^{1}HNMR (DMSO/TMS): δ (ppm) 2.30 (m, 2H), 2.40 (m, 2H), 3.43 (s, 1H), 3.49 (s, 3H), 3.75 (s, 9H), 4.90 (m, 1H), 5.40 (dd, 1H), 5.60 (m, 1H), 6.89 (s, 2H), 6.92 (s, 2H), 6.94 (s, 2H). ^{13}C NMR (DMSO/TMS): δ (ppm) 29.2, 35.5, 52.4 (−CH_3), 63.3, 68.4, 72.8, 109.2, 119.2, 119.8, 128.1, 128.2, 128.4, 128.7, 139.0, 139.3, 145.8, 145.9, 165.0, 165.2, 165.6, 173.9.

For more details on ^{1}H, ^{13}C NMR, 2D NMR, *DEPT*, and FT-IR spectral data of all synthetic compounds, see Supporting Information.

Cytotoxicity by MTT Assay. The cytotoxicity of TGAME, gallic acid, and methyl quinate was evaluated by MTT colorimetric assay (MTT Kit ThermoFisher Scientific, USA). The cells of MDCKI (ATCC CRL-2935, USA, provided by Dr John Lieske, Mayo Clinic Medical School, MN, USA) were seeded onto 96-well microplates at a density of 1 × 10^4 cells per well and treated with different concentrations (0, 5, 10, 25, 50 μM in DMSO/phosphate buffered saline (PBS)) of the compounds for 24 h. The MTT (15 μL) working solution (5 mg/mL in PBS) was added to each well and incubated at 37 °C for 3 h. After the addition of the stop solution (100 μL), the optical density (OD) was measured at 570 nm using a microplate reader (SpectraMax 190 microplate reader, USA). Cell viability was calculated as a percentage of viable cells in compound-treated group versus untreated control by the following equation:

$$\text{cell viability (\%)} = \frac{[\text{OD(compound)} - \text{OD(blank)}]}{[\text{OD(control)} - \text{OD(blank)}]} \times 100$$

Cell-COM Crystal Binding Assay and Neutralization by a Specific Anti-Annexin A1 Antibody. *Preparation of COM Crystals.* NaOx (1 mM) in Tris buffer saline (50 mL) containing 90 mM sodium chloride (pH 7.4) was added to a gently stirred solution of 10 mM calcium chloride (50 mL). The mixture was incubated at RT overnight and then centrifuged at 3000 rpm for 5 min. Crystals were resuspended in methanol (1 mL) and centrifuged for 5 min at 3000 rpm. The methanol supernatant was aspirated, and the crystals were air-dried at RT then sterilized using UV radiation for 30 min before use in cell culture work. The dried crystals were examined under a Zeiss Axiophot microscope using a 10× differential interference contrast (DIC) lens and appeared as six-sided prisms.

MDCKI cells (5 × 10^5 cells) were seeded into 6-well cell culture plate and incubated in a complete culture medium for 24 h. Compound **6** was added (0, 1, 10, 25, and 50 μM) to the cells for 3 h (concentration-dependent study), whereas the cells kept in culture medium without compound represented as the control. The cells were pretreated with 0, 25, or 50 μM (the optimal two concentrations obtained in the previous study) of compound **6** for 1, 3, or 6 h (time-course study). The culture medium was aspirated, and the cells were washed gently with PBS. Thereafter, cells were incubated for 30 min with COM crystals (100 μg of crystals/mL culture medium), followed by washing 5 times with plain medium to remove nonadherent crystals. Bound crystals in each well were imaged and counted under a phase-contrast microscope (Zeiss) in 15 random high power fields (HPF).

The surface expression of AxA1 was blocked by pretreating the cells with rabbit polyclonal anti-AxA1 antibody (Cell Signaling, USA). Briefly, the confluent polarized cells were incubated for 15 min with bovine serum albumin (1%) in membrane preserving buffer (0.1 mM $CaCl_2$ and 1 mM $MgCl_2$ in PBS) to block nonspecific binding. Cells were then washed with the same buffer (3×) followed by incubation anti-AxA1 antibody (0.2 μg/mL) or rabbit isotype-controlled IgG (0.2 μg/mL) at 37 °C for 30 min. COM crystals (100 μg of crystal/mL medium) were incubated for 1 h at 37 °C, after washing the cells with the buffer. Unbound COM crystals were removed by washing with PBS (5×). Bound crystals were counted under a phase-contrast microscope by assessing 15 random HPF.

Analysis of Annexin A1, α-Enolase, and HSP90 by Western blot. Subcellular fractionations of MDCKI cell protein and subsequent Western blot were used to measure the concentrations of cytosolic, membrane, and whole AxA1, α-enolase, and HSP90. MDCKI cells (5 × 10^5 cells) were seeded into each well of a 6-well plate and cultured in a complete medium overnight. After treatment with 50 μM TGAME for 3 h, the cells were washed with cold PBS and incubated for 10 min at 4 °C with cytosolic extracting buffer containing mainly 10 mM piperazine-*N*,*N*′-bis (PIPES), 0.5 mM EDTA, and 0.02% digitonin, with gentle shaking. The cells were scrapped with the buffer, collected, and centrifuged for 10 min at 10000 rpm. The supernatant containing cytosolic proteins was next collected. The remaining cell pellet was mixed with membrane extracting buffer (60 mM Tris-HCl of pH = 6.8, 2% sodium dodecyl sulfate (SDS), 10% glycerol, and 5% 2-mercaptoethanol) and incubated for 30 min in an ice bath with gentle shaking every 10 min and named as "membrane fraction". Whole cell lysate was extracted by using whole lysate buffer. The protein concentrations were determined by Bradford's method[39] using Pierce BCA Protein Assay Kit (Thermo Scientific).

Each protein fraction (30 μg/lane) was mixed with laemmli sample buffer (1:1), 2× (Bio Rad), and separated by 7.5% ready gel (BioRad), where all samples were boiled at 99 °C for 5 min prior to loading onto gel. The gel was run for 90 min at 100 V then transferred onto a nitrocellulose membrane using 1× transfer buffer. The membrane was probed by incubation at 4 °C overnight with rabbit polyclonal anti-AxA1 (1:1000), rabbit polyclonal anti-HSP90 (1:1000), rabbit polyclonal anti-α-enolase (1:1000), and mouse monoclonal anti-β-actin (1:1000) antibodies (Cell Signaling , USA) in blocking buffer, separately. After washing with TBS/0.1% Tween three times for 5 min each, the membrane was incubated with the corresponding secondary antibody conjugated with horseradish peroxidase (Rabbit IgG for all primary antibodies or mouse IgG horseradish peroxidase for β-actin)

DOI: 10.1021/acs.jmedchem.7b01566
J. Med. Chem. 2018, 61, 1609−1621

(1:5000) (Cell Signaling) in 1× Tris-buffered saline/0.1% Tween 20 and 5% milk for 1 h at RT. The immunoreactive bands were detected by developing in SuperSignal West Femto maximum sensitive chemiluminescence substrate solutions (Thermo Scientific, USA) and then visualized by autoradiogram. The intensity corresponding to each band was measured by AlphaEase FC software (Mayo Clinic, USA).

COM Crystals Bound Annexin A1 Protein Immunofluorescence Staining and Confocal Microscopy. Collagen buffer (200 μL) was added to a chamber slide and incubated for 15−20 min at 37 °C followed by washing with 1× PBS. MDCKI cells (12000/well) were seeded in each chamber and incubated at 37 °C overnight. The media was removed, and cells were treated with/without compound **6** (50 μM) for 3 h. Cells then were gently washed with PBS followed by fixation with 4% *p*-formaldehyde in saline (200 μL) for 15 min at RT and finally washed twice with cold 1× PBS. Triton (0.2%) in PBS for 5 min was used for cell permeabilization, and then the cells were washed three times with PBS. A blocking buffer (200 μL) was added for 1 h at RT, then replaced by the primary antibody with incubation overnight at 4 °C. The next day cells were washed with PBS (3×) for 5 min. The primary antibody was replaced with the secondary antibody and incubated in the dark for 60 min, followed by washing with PBS (3×). The counterstain (TOTO-3) was added and incubated for 20 min at RT, then washed one time with 1× PBS. The slide was mounted with Vectashield mounting medium, and then the cells were examined using Zeiss confocal microscope (Axiovert 100 M) with 63× oil immersion lens.

DPPH Assay for Antioxidant Activity. To 1.96 mL of DPPH (0.1 mM) solution, different volumes (2−20 μL) of compound **6**, gallic acid, or methyl quinate (1 mM in DMSO), made up to 40 μL with DMSO, were added. The reacted mixtures were incubated for 20 min at RT in the dark, and the absorbance was measured at 517 nm. DPPH solution (2 mL) was served as control. The percentage radical scavenging activity (%RSA) of tested compounds was calculated using the following formula:

$$\%\mathrm{RSA} = \frac{\text{absorbance of control} - \text{absorbance of test}}{\text{absorbance of control}} \times 100$$

***Drosophila* Crystallization Assay: Ex Vivo Oxalate ± TGAME.** Oregon R (red) *Drosophila melanogaster* flies were used as wild type for these experiments and CaOx crystallization monitored as birefringence using DIC optics.[24] Flies were raised on standard *Drosophila* media (fly food) at 25 °C. There were 24 female flies (7 days age) that were used in the experiment. Subsequently, 24 MT were obtained by dissecting the flies in Schneider's solution and transferred to poly-L-lysine coated slides with iPBS (insect phosphate buffer saline). The tubules were divided into two main groups (control and treated group; n = 12 each). The MTs of the treated group were preincubated with 100 μM of TGAME in iPBS for 20 min, followed by incubation with a mixture of 100 μM TGAME and 10 μM NaOx in iPBS for 1 h, with fresh solutions replaced every 15 min. Control group was incubated only with 10 μM NaOx in iPBS. Crystallization of CaOx was monitored by imaging the initial 600 μm of the anterior MTs using a Zeiss Observer using DIC microscopy. Crystallization was quantified using ImageJ as previously.[32]

***Drosophila* Feeding Experiment: In Vivo Oxalate ± TGAME.** There were 22 female flies that were used in the experiment (11 control and 11 treatment) and then kept for 24 h on feeding with fly food mixed either with NaOx (10 μM) or a mixture of TGMAE (50 μM) and NaOx (10 μM). After 24 h, the flies were dissected in Schneider's medium and MTs were transferred immediately to poly-L-lysine coated slides with iPBS. Crystallization was monitored by imaging the anterior MTs as above.

■ ASSOCIATED CONTENT

Supporting Information

The Supporting Information is available free of charge on the ACS Publications website at DOI: 10.1021/acs.jmedchem.7b01566.

Supplemental spectroscopic and spectrophotometric data for compound **6** (TGAME) and its synthetic intermediates: FTIR, ^{1}H NMR, ^{13}C NMR spectra of compounds **1**−**6** and two-dimensional NMR (HMBC and HSQC) correlations necessary for identifying the positions of galloyl subunits and the methyl group linked to quinic acid in compound **5**; HPLC-UV spectrum of compound **6**; ESI-MS/MS spectra and the proposed fragmentation pattern of compounds **5** and **6** (PDF)

■ AUTHOR INFORMATION

Corresponding Author

*Phone: (507) 284-2511. E-mail: Lieske.John@mayo.edu.

ORCID

Mohamed Abd El-Salam: 0000-0001-9920-1520

Paulo M. Donate: 0000-0002-1404-5328

Notes

The authors declare no competing financial interest.

■ ACKNOWLEDGMENTS

Mohamed Abd El-Salam is a recipient of a TWAS-CNPq full Ph.D. Fellowship (190066/2014-8), The Academy of Sciences for the Developing World (TWAS), Italy, and the National Council for Scientific and Technological Development (CNPq), Brazil, and he is a visiting Pre-Doctoral Fellow at Mayo Clinic College of Medicine, USA (P-3-04976). He also is on a study leave from Faculty of Pharmacy, Delta University for Science and Technology, Egypt. We are thankful to the State of São Paulo Research Foundation (FAPESP) for financial support, grant number 2011/13630-7. Biological studies were partially supported by the Mayo Clinic O'Brien Urology Research Center (NIH DK100227) and the Mayo Foundation for Medical Research. We thank Antonio E. M. Crotti for helpful suggestions of the interpretation of MS results, Jacob Anderson for teaching the *Drosophila* assays, and Giuliano Cesar Clososki for his advice.

■ ABBREVIATIONS USED

AxA1, annexin A1; COM, calcium oxalate monohydrate; CaOx, calcium oxalate; CaP, calcium phosphate; HSP90, heat shock protein 90; DIC, differential interference contrast; DCC, *N*,*N*′-dicyclohexylcarbodiimide; DMAP, 4-(dimethylamino) pyridine; DPPH, 2,2-diphenyl-1-picrylhydrazyl; HPF, high power field; IC_{50}, inhibitory concentration 50%; iPBS, insect phosphate buffer solution; MDCKI, Madin−Darby canine kidney type I; MT, Malpighian tubules; OPN, osteopontin; OS, oxidative stress; OD, optical density; ROS, reactive oxygen species; NaOx, sodium oxalate; TGAME, 3,4,5-tri-*O*-galloylquinic acid methyl ester

■ REFERENCES

(1) Sohgaura, A.; Bigoniya, P. A review on epidemiology and etiology of renal stone. *Am. J. Drug Discovery Dev.* **2017**, *7*, 54−62.

(2) Khan, S. R.; Pearle, M. S.; Robertson, W. G.; Gambaro, G.; Canales, B. K.; Doizi, S.; Traxer, O.; Tiselius, H. G. Kidney stones. *Nat. Rev. Dis. Primers.* **2017**, *3*, 17001.

(3) Lieske, J. C.; Toback, F. G.; Deganello, S. Direct nucleation of calcium oxalate dihydrate crystals onto the surface of living renal epithelial cells in culture. *Kidney Int.* **1998**, *54*, 796−803.

(4) Finlayson, B.; Reid, F. The expectation of free and fixed particles in urinary stone disease. *Invest. Urol* **1978**, *15*, 442−448.

(5) Khan, S. R.; Hackett, R. L. Urolithogenesis of mixed foreign body stones. *J. Urol.* **1987**, *138*, 1321−1328.

DOI: 10.1021/acs.jmedchem.7b01566
J. Med. Chem. 2018, 61, 1609−1621

(6) Fong-ngern, K.; Peerapen, P.; Sinchaikul, S.; Chen, S. T.; Thongboonkerd, V. Large-scale identification of calcium oxalate monohydrate crystal-binding proteins on apical membrane of distal renal tubular epithelial cells. *J. Proteome Res.* **2011**, *10*, 4463−4477.
(7) Lee, H. J.; Jeong, S. J.; Park, M. N.; Linnes, M.; Han, H. J.; Kim, J. H.; Lieske, J. C.; Kim, S. H. Gallotannin suppresses calcium oxalate crystal binding and oxalate-induced oxidative stress in renal epithelial cells. *Biol. Pharm. Bull.* **2012**, *35*, 539−544.
(8) Du, C.; Wang, X.; Chen, H. Oxidative Stress to Renal Tubular Epithelial Cells − A common Pathway in Renal Pathologies. In *Systems Biology of Free Radicals and Antioxidants*; Laher, I., Ed.; Springer: Berlin, Heidelberg, 2014; pp 2605−2624.
(9) Peerapen, P.; Thongboonkerd, V. p38 MAPK mediates calcium oxalate crystal-induced tight junction disruption in distal renal tubular epithelial cells. *Sci. Rep.* **2013**, *3*, 1041.
(10) Finkielstein, V. A.; Goldfarb, D. S. Strategies for preventing calcium oxalate stones. *Canadian Med. Assoc. J.* **2006**, *174*, 1407−1409.
(11) Kanlaya, R.; Singhto, N.; Thongboonkerd, V. EGCG decreases binding of calcium oxalate monohydrate crystals onto renal tubular cells *via* decreased surface expression of alpha-enolase. *JBIC, J. Biol. Inorg. Chem.* **2016**, *21*, 339−346.
(12) Chutipongtanate, S.; Fong-ngern, K.; Peerapen, P.; Thongboonkerd, V. High calcium enhances calcium oxalate crystal binding capacity of renal tubular cells *via* increased surface annexin A1 but impairs their proliferation and healing. *J. Proteome Res.* **2012**, *11*, 3650−3663.
(13) Fong-ngern, K.; Sueksakit, K.; Thongboonkerd, V. Surface heat shock protein 90 serves as a potential receptor for calcium oxalate crystal on apical membrane of renal tubular epithelial cells. *JBIC, J. Biol. Inorg. Chem.* **2016**, *21*, 463−474.
(14) Peerapen, P.; Thongboonkerd, V. Caffeine prevents kidney stone formation by translocation of apical surface annexin A1 crystal-binding protein into cytoplasm: in vitro evidence. *Sci. Rep.* **2016**, *6*, 38536.
(15) Brancalion, A. P. S.; Oliveira, R. B.; Sousa, J. P. B.; Groppo, M.; Berretta, A. A.; Barros, M. E.; Boim, M. A.; Bastos, J. K. Effect of hydroalcoholic extract from *Copaifera langsdorffii* leaves on urolithiasis induced in rats. *Urol. Res.* **2012**, *40*, 475−481.
(16) Barbosa de Oliveira, R.; Barbosa Coelho, E.; Rezende Rodrigues, M.; de Mello Costa-Machado, A. R.; Barreto de Sousa, J. P. B.; Berretta, A. A.; Bastos, J. K. Effect of the *Copaifera langsdorffii* Desf. leaf extract on the ethylene glycol-induced nephrolithiasis in rats. *eCAM* **2013**, *2013*, 131372.
(17) de Carvalho da Costa, J.; da Silva Motta, E. V.; Barreto, F.; Verlindo de Araujo, B.; Bastos, J. K. Pharmacokinetic study of a galloylquinic acid isolated from *Copaifera langsdorffii* Desf. leaves. *Planta Med.* **2016**, *82*, S1−S381.
(18) Motta, E. V. S.; Lemos, M.; Costa, J. C.; Banderó-Filho, V. C.; Sasse, A.; Sheridan, H.; Bastos, J. K. Galloylquinic acid derivatives from *Copaifera langsdorffii* leaves display gastroprotective activity. *Chem.-Biol. Interact.* **2017**, *261*, 145−155.
(19) Bouchet, N.; Levesque, J.; Bodo, B.; Pousset, J.-L. 3,4,5-tri-*O*-galloylquinic acid ethyl ester from *Guiera senegalensis*. *Pharm. Biol.* **1998**, *36*, 63−65.
(20) Bokesch, H. R.; McKee, T. C.; Currens, M. J.; Gulakowski, R. J.; McMahon, J. B.; Cardellina, J. H.; Boyd, M. R. HIV-inhibitory gallotannins from *Lepidobotrys staudtii*. *Nat. Prod. Lett.* **1996**, *8*, 133−136.
(21) Lee, J.-H.; Yehl, M.; Ahn, K. S.; Kim, S.-H.; Lieske, J. C. 1,2,3,4,6-penta-*O*-galloyl-beta-d-glucose attenuates renal cell migration, hyaluronan expression, and crystal adhesion. *Eur. J. Pharmacol.* **2009**, *606*, 32−37.
(22) Nogueira, M. S.; Furtado, R. A.; Bastos, J. K. Flavonoids and methoxy-galloylquinic acid derivatives from the leaf extract of *Copaifera langsdorffii* Desf. *J. Agric. Food Chem.* **2015**, *63*, 6939−6945.
(23) Wang, Z. Steglich Catalyst. In *Comprehensive Organic Name Reactions and Reagents*; John Wiley & Sons, Inc.: Houston, TX, 2010; Vol. *576*, pp 2651−2655.
(24) Nishizawa, M.; Yamagishi, T.; Dutschman, G. E.; Parker, W. B.; Bodner, A. J.; Kilkuskie, R. E.; Cheng, Y.-C.; Lee, K.-H. Anti-aids agents, isolation and characterization of four new tetragalloylquinic acids as a new class of HIV reverse transcriptase inhibitors from tannic acid. *J. Nat. Prod.* **1989**, *52*, 762−768.
(25) Rindler, M. J.; Chuman, L. M.; Shaffer, L.; Saier, M. H. Retention of differentiated properties in an established dog kidney epithelial cell line (MDCK). *J. Cell Biol.* **1979**, *81*, 635−648.
(26) Saier, M. H. J. Growth and differentiated properties of a kidney epithelial cell line (MDCK). *Am. J. Physiol.* **1981**, *240*, C106−C109.
(27) Sun, X.-Y.; Gan, Q.-Z.; Ouyang, J.-M. Size-dependent cellular uptake mechanism and cytotoxicity toward calcium oxalate on Vero cells. *Sci. Rep.* **2017**, *7*, 41949.
(28) Guo, C.; Dugas, T.; Scates, C.; Garcia-Villarreal, M.; Ticich, T.; McMartin, K. E. Aluminum citrate blocks toxicity of calcium oxalate crystals by preventing binding with cell membrane phospholipids. *Am. J. Nephrol.* **2013**, *37*, 41−49.
(29) de Cógáin, M. R.; Linnes, M. P.; Lee, H. J.; Krambeck, A. E.; de Mendonça Uchôa, J. C.; Kim, S.-H.; Lieske, J. C. Aqueous extract of *Costus arabicus* inhibits calcium oxalate crystal growth and adhesion to renal epithelial cells. *Urolithiasis* **2015**, *43*, 119−124.
(30) Fong-ngern, K.; Thongboonkerd, V. Alpha-enolase on apical surface of renal tubular epithelial cells serves as a calcium oxalate crystal receptor. *Sci. Rep.* **2016**, *6*, 36103.
(31) Gerke, V.; Moss, S. E. Annexins: from structure to function. *Physiol. Rev.* **2002**, *82*, 331−371.
(32) Landry, G. M.; Hirata, T.; Anderson, J. B.; Cabrero, P.; Gallo, C. J. R.; Dow, J. A. T.; Romero, M. F. Sulfate and thiosulfate inhibit oxalate transport via a dPrestin (Slc26a6)-dependent mechanism in an insect model of calcium oxalate nephrolithiasis. *Am. J. Physiol. Renal Physiol.* **2016**, *310*, F152−F159.
(33) Chen, Y. H.; Liu, H. P.; Chen, H. Y.; Tsai, F. J.; Chang, C. H.; Lee, Y. J.; Lin, W. Y.; Chen, W. C. Ethylene glycol induces calcium oxalate crystal deposition in Malpighian tubules: a *Drosophila* model for nephrolithiasis/urolithiasis. *Kidney Int.* **2011**, *80*, 369−377.
(34) Kotsyfakis, M.; Ehret-Sabatier, L.; Siden-Kiamos, I.; Mendoza, J.; Sinden, R. E.; Louis, C. *Plasmodium berghei* ookinetes bind to *Anopheles gambiae* and *Drosophila melanogaster* annexins. *Mol. Microbiol.* **2005**, *57*, 171−179.
(35) Ozbek, E. Induction of oxidative stress in kidney. *Int. J. Nephrol.* **2012**, *2012*, 465897.
(36) Khan, S. R. Reactive oxygen species, inflammation and calcium oxalate nephrolithiasis. *Transl. Androl. Urol.* **2014**, *3*, 256−276.
(37) Verkoelen, C. F.; Verhulst, A. Proposed mechanisms in renal tubular crystal retention. *Kidney Int.* **2007**, *72*, 13−18.
(38) Kumar, V.; Farell, G.; Deganello, S.; Lieske, J. Annexin II is present on renal epithelial cells and binds calcium oxalate monohydrate crystals. *J. Am. Soc. Nephrol.* **2003**, *14*, 289−297.
(39) Kruger, N. J. The Bradford Method for Protein Quantitation. In *The Protein Protocols Handbook*; Walker, J. M., Ed.; Humana Press: Totowa, NJ, 2002; pp 15−21.

DOI: 10.1021/acs.jmedchem.7b01566
J. Med. Chem. 2018, 61, 1609−1621

Copyright Clearance Center RightsLink®

Home Account Info Help

ACS Publications Most Trusted. Most Cited. Most Read.

Title: The Synthesized Plant Metabolite 3,4,5-Tri-O-Galloylquinic Acid Methyl Ester Inhibits Calcium Oxalate Crystal Growth in a Drosophila Model, Downregulates Renal Cell Surface Annexin A1 Expression, and Decreases Crystal Adhesion to Cells

Author: Mohamed Abd El-Salam, Jairo Kenupp Bastos, Jing Jing Han, et al

Publication: Journal of Medicinal Chemistry

Publisher: American Chemical Society

Date: Feb 1, 2018

Copyright © 2018, American Chemical Society

Logged in as:
Mohamed Abd El-Salam
University of Sao Paulo
Account #: 3001250458

LOGOUT

PERMISSION/LICENSE IS GRANTED FOR YOUR ORDER AT NO CHARGE

This type of permission/license, instead of the standard Terms & Conditions, is sent to you because no fee is being charged for your order. Please note the following:

- Permission is granted for your request in both print and electronic formats, and translations.
- If figures and/or tables were requested, they may be adapted or used in part.
- Please print this page for your records and send a copy of it to your publisher/graduate school.
- Appropriate credit for the requested material should be given as follows: "Reprinted (adapted) with permission from (COMPLETE REFERENCE CITATION). Copyright (YEAR) American Chemical Society." Insert appropriate information in place of the capitalized words.
- One-time permission is granted only for the use specified in your request. No additional uses are granted (such as derivative works or other editions). For any other uses, please submit a new request.

BACK CLOSE WINDOW

Copyright © 2018 Copyright Clearance Center, Inc. All Rights Reserved. Privacy statement. Terms and Conditions.
Comments? We would like to hear from you. E-mail us at customercare@copyright.com


UNIVERSIDADE DE SÃO PAULO
SCIENTIA VINCES